

Self-assembling tyrosine kinase inhibitors for localised targeted delivery

Mohammed Al-Ameedee (M.Sc.)

Thesis submitted to the University of Nottingham for the degree of Doctor of Philosophy

November 2017

Declaration

The work presented in this thesis is submitted to the University of Nottingham in support of my application for the degree of Doctor of Philosophy. No part has been submitted for any other degree at The University of Nottingham or any other institution. The work presented in this thesis has been carried out by myself, except for:

- The TEM images in Chapter 3 and 5 was acquired with Dr. Mike Fay of the University of Nottingham.
- The solid state NMR in chapter 5 was carried out by Susana Ramalhete from the University of East Anglia
- The plasma stability study was done by Edward Browne from Sygnature Discovery Centre

The data presented in Chapters 3 is based upon a previous publication:

- Linifanib–a multi-targeted receptor tyrosine kinase inhibitor and a low molecular weight gelator. Marlow, M., **Al-Ameedee, M**., Smith, T., Wheeler, S. and Stocks, M.J. (2015). *Chemical Communications*, 51(29), 6384-6387.

Mohammed Al-Ameedee

Abstract

Localised delivery of cancer therapy is an approach used to overcome the serious side effects associated with the systemic treatment of many anticancer drugs which is the main route of administration. Low molecular weight gelators have received great attention in recent years as a drug delivery strategy for localised targeted therapy. These are small molecules, which self-assemble into a 3D network fibre *via* non-covalent interactions to create macroscopically a gel. Studies on this drug delivery platform provide an alternative to the extensively investigated gel delivery systems based on polymers.

One of the approaches of low molecular weight gelators is the development of gelators based on anticancer drugs, i.e. self-assembled anticancer prodrug gelators that form a gel. Indeed, there are only a limited number of studies which investigate the gelation ability of anticancer drugs.

Therefore, this project intends to search for an anticancer agent which demonstrates gelation. This has been achieved by preliminary screening of selected members of two categories of cancer treatments which are five benzothiazole-based quinols and four tyrosine kinase inhibitors (sorafenib, linifanib, semaxanib and orantinib). These anticancer drugs have significant anticancer activity but suffer from systemic toxicity. Therefore, the development of LMWGs based on these drugs is a useful approach for localised drug delivery helping improve the toxicity profile.

Preliminary screening showed that only linifanib out of the compounds investigated formed gels. Therefore, it was decided to focus on this potent tyrosine kinase inhibitor as the main part in this project. Further characterisation and analysis showed that the urea functional group and the fluorine substitution on the adjacent aromatic ring are key elements in promoting self-assembly. Also, oscillatory rheology showed that linifanib has superior mechanical strength to gels of structurally related analogues.

The prodrug approach was then progressed with linifanib to provide more controlled delivery of the drug. The first library of potential linifanib prodrugs were carbamate derivatives. Unfortunately, all of these compounds failed in inducing gel formation in the preliminary screening regardless of the length and nature of side chain.

The second linkage used for creating linifanib prodrugs was the amide conjugation with aliphatic carboxylic acids, single amino acid and dipeptides. With regard to the derivatives with aliphatic carboxylic acid side chain, gels were formed for compounds with clog P between 3.98 and 4.72 which means that there is a correlation between hydrophobicity and gel formation.

Preliminary screening of dipeptide derivatives of linifanib were negative for all compounds except the proline-proline derivative which formed a gel after 7 days. Stability study in DMSO – water mixtures of these compounds showed that proline-containing dipeptides degraded to linifanib, at a quicker cleavage rate than other compounds, with the highest cleavage rate for the proline-proline analogue. This has led to the conclusion that the gel observed for this analogue was due to the gelation of linifanib.

Finally, the single amino acid derivatives gelation screening revealed that the serine analogue of linifanib was the most stable gel. Further characterisation of this compound showed that the formation of gel and its mechanical strength are affected mainly by changes in pH and possibly the buffer composition. The highest mechanical strength was observed with the concentration of 0.5% w/v serine analogue in 5% v/v DMSO/phosphate buffer pH 7.4.

Overall, the serine analogue of linifanib can be considered as the best gelator prodrug of linifanib for two main reasons. This derivative exhibited stable gels with good mechanical strength (> 4 kPa) at physiologic pH. In addition, the serine derivative of linifanib demonstrated a cleavage rate half-life of 7 days in phosphate buffer pH 7.4. These findings suggest that it is a promising linifanib prodrug gelator for targeted delivery.

Acknowledgements

I would like to thank my supervisors Dr. Michael Stocks and Dr. Maria Marlow for their support throughout the whole of my PhD and for contribution to my scientific and professional experience.

I would like also to thank Dr. Tracey Bradshaw for her scientific advice which contributed to the project.

This work would not be possible without the technical help provided by Lee Hibbett, Paul Cooling and Dr. Michael Fay for their guidance on the techniques and procedures used in this project.

Additional appreciation goes to all members of C25 and C30 who accompanied me through the whole period of my PhD. Special thanks to Dr. Francesca Citossi, Dr. Kathryn Skilling and Masar Mohamed for sharing advice about this work. Also, thanks to my laboratory colleagues especially Dr. Nickolas Kindon, Dr. Fadi Soukareih and Sean Conroy.

The last four years would not have been possible without my close friends: Ali Hasson, Akeel Abolard and Wathiq Al-Hachami for their continuous support during hard times.

Finally, my grateful thanks to my parents and my brothers and sisters for their constant help in all the times and for my wife Maha for her encouragement all the time.

This project has been funded by the Ministry of Higher Education of Iraq.

Abbreviations

3D	Three-dimensional
5-FU	5-fluorouracil
AFM	Atomic force microscopy
ATP	Adenosine triphosphate
Boc	*tert*-butyloxycarbonyl
CBZ	Carboxybenzyl
CD	Circular dichroism
CDCl3	Deuterated chloroform
DCM	Dichloromethane
DIPEA	*N*,*N*-diisopropylethylamine
DKP	Diketopiperazine
DMF	Dimethyl formamide
DMSO	Dimethyl sulfoxide
DNA	Deoxyribonucleic acid
DSC	Differential scan calorimetry
EGF	Epidermal growth factor
FDA	Food and drug administration
FGFR	Fibroblast growth factor receptor
Fmoc	Fluorenylmethyloxycarbonyl
FTIR	Fourier transmission infrared
G'	Storage modulus
G"	Loss modulus
GABA	γ-aminobutyric acid
HATU	(1-[*bis* (dimethylamino) methylene] -1H- 1,2,3- triazolo [4,5-b] pyridinium 3-oxid hexafluorophosphate)
HCl	Hydrochloric acid
HIF-1	Hypoxia-inducible factor-1
HRMS	High resolution mass spectroscopy
hPepT1	Human peptide transporter1
HPLC	High performance liquid chromatography
IC_{50}	Inhibitory concentration of 50%
kPa	Kilo pascal

LC-MS	Liquid chromatography mass spectroscopy
LMWGs	Low molecular weight gelators
LVER	Linear viscoelastic region
MGC	Minimum gelator concentration
MMP-2	Matrix metalloproteinase-2
MS	Mass spectrum
NADPH	Nicotinamide adenine dinucleotide phosphate
Nap	Naphthalene
nM	Nanomolar
NMR	Nuclear magnetic resonance
PBS	Phosphate buffered saline
PDGF	Platelet-derived growth factor
pH	Power of hydrogen
ppm	Part per million
Raf	Rapidly accelerated fibrosarcoma
Ras	Rapidly accelerated sarcoma
RTK	Receptor tyrosine kinase
SAXS	X-ray scattering
SEM	Scanning electron microscope
TEM	Transmission electron microscope
TFA	Trifluoroacetic acid
T_{gel}	Gel – sol transition temperature
TIAB	*bis*(trifluoroacetoxy)iodo] benzene
TLC	Thin layer chromatography
VEGF	Vascular endothelial growth factor
μM	Micromolar

Table of Contents

Declaration ..... **ii**
Abstract ..... **iii**
Acknowledgements ..... **v**
Abbreviations ..... **vi**
Table of Contents ..... **viii**
List of Figures ..... **xii**
List of Tables ..... **xviii**
List of Schemes ..... **xx**
Chapter One: Introduction **1**
1.1. Cancer: Current status 1
1.1.1. Pathogenesis of cancer 1
1.1.2. Current treatments of solid tumours 3
1.2. Low molecular weight gelators in drug delivery 5
1.2.1. Principle of gelation by LMWGs 6
1.2.2. Design of stimuli – responsive LMWGs 7
1.2.2.1. Temperature – sensitive gelators 8
1.2.2.2. pH – sensitive gelators 9
1.2.2.3. Enzyme – sensitive gelators 10
1.2.3. Classification of LMWGs 11
1.2.3.1. Hydrogelators 12
1.2.3.2. Organogelators 14
1.2.4. Characterisation of LMWGs 14
1.2.4.1. Table-top rheology 15
1.2.4.2. Oscillatory rheology 16
1.2.4.3. Microscopy 18
1.2.4.4. Spectroscopy 20
1.3. The role of LMWGs in localised drug delivery 20
1.3.1. LMWGs using inert matrix intended for drug delivery 21
1.3.2. Self-assembling LMWGs prodrugs 24
1.3.3. Therapeutic LMWGs 28
1.4. Benzothiazole-quinols: A cytotoxic cancer treatment 30
1.5. Tyrosine kinase inhibitors 32
1.5.1. Tumour targeting 32

1.5.2. Tyrosine kinases 32
1.5.3. Mechanism of action 33
1.5.4. Vascular endothelial growth factor receptor (VEGFR) 34
1.5.5. Platelet-derived growth factor receptor (PDGFR) 35
1.5.6. Epidermal growth factor receptor (EGFR) 36
1.6. Aims and Objectives of the PhD 37
Chapter Two: Preliminary gelation screening of selected anticancer agents 39
2.1. Introduction 39
2.1.1. Sorafenib 41
2.1.2. Linifanib 41
2.1.3. Semaxanib 41
2.1.4. Orantinib 42
2.1.5. Benzothiazole-substituted quinols 42
2.2. Results and Discussion 43
2.2.1. Synthesis 44
2.2.1.1. Semaxanib 44
2.2.1.2. Orantinib 45
2.2.1.3. Benzothiazole-derived quinols 47
2.2.2. Preliminary gelation screening 48
2.3. Conclusions 52
Chapter Three: Linifanib as A Multitargeted Tyrosine Kinase Inhibitor and a Low Molecular Weight Gelator 53
3.1. Introduction 53
3.2. Linifanib 59
3.1.1. Chemistry and rational drug design 59
3.1.2. Mechanism of action and related toxicity 60
3.3. Results and Discussion 62
3.3.1. General mechanism of synthesis of linifanib and its analogues: 62
3.3.2. Iodoindazole synthesis 63
3.3.3. Urea boronate synthesis 63
3.3.4. Suzuki reaction 64
3.3.4.1. Oxidative addition 64
3.3.4.2. Transmetallation 64

3.3.4.3. Reductive elimination 65
3.3.5. Synthesis of amide analogue (compound 3.25) 66
3.3.6. Structural Analysis of Gels 67
3.3.6.1. Vial Inversion Test 67
3.3.6.2. Rheology characterisation 70
3.3.6.3. Transmission electron microscopy (TEM) imaging 74
3.4. Conclusions 75
Chapter Four: Carbamate Analogues of Linifanib as Candidates for Self-Assembly 76
4.1. Introduction 76
4.1.1. Carbamate group as a gelator motif 76
4.1.2. Carbamate-based Prodrugs 79
4.2. Results and Discussion 82
4.2.1. Design and synthesis of linifanib carbamate derivatives 82
4.2.2. Gelation tests of carbamate prodrugs of linifanib 83
4.3. Conclusions 85
Chapter Five: Self-assembling amide derivatives of linifanib 86
5.1. Introduction 86
5.1.1. Amide gelators 87
5.1.2. Amino acids as moieties in prodrug design 89
5.1.3. LMWGs based on amino acids 92
5.2. Results and discussion 98
5.2.1. Amide derivatives of linifanib with aliphatic carboxylic acid side chain 98
5.2.1.1. Synthesis 99
5.2.1.2. Vial inversion screening 100
5.2.1.3. Rheology characterisation of compound 5.36 102
5.2.2. Dipeptide derivatives of linifanib 103
5.2.2.1. Synthesis 104
5.2.2.2. Vial inversion screening 105
5.2.2.3. Chemical stability study 106
5.2.3. Amino acid analogues of linifanib 107
5.2.3.1. Synthesis 107
5.2.3.2. Vial inversion screening 108

5.2.3.3. Chemical stability study 111
5.2.3.4. Rheology 113
5.2.3.5. Vial inversion test using DMSO/phosphate buffer mixtures 115
5.2.3.6. Rheological measurements 116
5.2.3.7. Solid State NMR 118
5.2.3.8. FT-IR spectroscopy 120
5.2.3.9. Transmission electron microscopy 122
5.2.3.10. Plasma stability 124
Chapter Six: General Conclusions and Future Work 128
6.1. Conclusions 128
6.2. Future Work 131
Chapter Seven: Experimental 133
7.1. General Procedures 133
7.1.1. Materials 133
7.1.2. General Methods 133
7.1.3. Instrumentation 133
7.2. Preparation of gels 134
7.3. Preparation of phosphate buffers 136
7.4. Experimental Data 137
References 181

List of Figures

Figure 1.1. The mitotic cycle of cell division and their specificity of some cytotoxic anticancer drug classes. 3
Figure 1.2. Different stages of assembly causing gelation. There are three different molecular packing which lead to formation of the nanostructure and finally the macrostructure. 7
Figure 1.3. Classification of different stimuli which trigger gelation: physical (red) and chemical (black). 7
Figure 1.4. Thermally triggered phase transition of the gel of compound 1.5. 9
Figure 1.5. General mechanism of formation of enzyme-triggered gelators. (a) formation of gels through hydrolysis, (b) formation of gels through condensation. 10
Figure 1.6. Dephosphoprylation of the tripeptide phosphate (1.7) to tripeptide (1.8) by phosphatase enzyme 11
Figure 1.7. Reversed hydrolysis of hydrogelator (1.11) 11
Figure 1.8. Structural features of saccharide-based gelator 1.12 12
Figure 1.9. Schematic representation of gel formation assessment by tube inversion method. 16
Figure 1.10. Oscillatory rheology analysis of an enzyme-induced gelator. A. Strain sweep, B. frequency sweep. 17
Figure 1.11. Different morphologies detected for some amide, urea and carbamate molecular gels using SEM on the xerogel status. 18
Figure 1.12. Transmission electron microscopy (TEM) of an enzyme-triggered hydrogelator based on nucleobases, amino acids, and saccharide. Scale bar = 100 nm. 19
Figure 1.13. Inert matrix drug delivery approach: incorporation of the drug within a gel network followed by diffusion of the drug. 22
Figure 1.14. Self-assembled prodrugs. Synthesis of amphiphilic prodrugs that could self-assemble to form hydrogels and the enzyme-triggered release of drug. 24
Figure 1.15. Molecular structure of paclitaxel (red), the linker (blue) and the self-assembling protected tetrapeptide (black).....26

Figure 1.16. a. Mechanism of cancer cell death triggered by enzyme-stimulated gelator. b. Molecular structure of the gelator precursor (ER-C16), the gelator (G-C16) and the peptide fragment. 27
Figure 1.17. Prodrugs of 5-FU. 28
Figure 1.18. Self-assembly of N-acetyl cysteine hydrogels. 29
Figure 1.19. Structure-activity relationship of benzothiazole scaffold. 30
Figure 1.20. Mechanism of action of tyrosine kinases. 33
Figure 1.21. Different classes of anti-VEGF therapy with examples of drugs of each class. 34
Figure 1.22. Tumour-associated process which are stimulated by PDGF. Purple: tumour cells, red: endothelial cells, green: fibroblasts, smooth muscle cells and pericytes, brown: extracellular matrix. 35
Figure 1.23. Mechanism of activation of EGFR showing possible sites for anti-EGF therapy. 36
Figure 2.1. Molecular structures of (A) benzothiazole scaffold and (B) benzothiazole substituted quinols.....40
Figure 3.1. Urea hydrogen bond urea α-tape. 53
Figure 3.2. Schematic representation of primary, secondary and tertiary structure of self-assembly process of urea-based gelator. 54
Figure 3.3. Library of *bis*(urea) derivatives 3.1-3.6 56
Figure 3.4. Inter- and intra-molecular hydrogen interactions between molecules of gelator 3.12. 58
Figure 3.5. Chemical structure of linifanib. 59
Figure 3.6. Rational design of 3-aminoindazole urea RTK inhibitors. 60
Figure 3.7. Binding of linifanib to catalytic site of VEGF2 receptor. 61
Figure 3.8. Storage modulus (G') (black circle) and loss modulus (G'') (red square) versus linifanib concentration (% (w/v)) in 5% (v/v) DMSO/water at 1% strain and angular frequency of 10 rad s and 37 °C. All measurements were carried out in triplicate and the mean calculated. Error bars represent standard deviation. 71
Figure 3.9. Amplitude sweep of linifanib gels at different concentrations (0.0625-1.25 w/v) in 5% w/v DMSO/water at angular frequency of 10 rad/s and

37 °C. Only storage modulus G' shown. Gels were formed instantly and measurements were taken after 3 hours. 72
Figure 3.10. Storage modulus (G') versus linifanib concentration (% (w/v) in 0.5% (v/v) DMSO/water at 37 °C. All measurements were carried out at 1% strain and angular frequency of 10 rad s in triplicate and the mean calculated. Slope = 1.86 to 2 decimal places. Gels were formed instantly and measurements were taken after 3 hours. 73
Figure 3.11. Amplitude sweep of difluoro analogue of linifanib (3.23) at 0.25 % (w/w) at 37 °C. All measurements were carried out at 1% strain and angular frequency of 10 rad s in triplicate and the mean calculated. Error bars represent standard deviation. Gels were formed instantly and measurements were taken after 3 hours.....73
Figure 3.12. Transmission electron micrograph (TEM): 0.5% (w/v) linifanib in 5% (v/v) DMSO–water; scale bar = 1 μm using JEOL JEM –2000FXII transmission electron microscope and accelerating voltage of 100 kV 74
Figure 4.1. Structure of carbamate prodrug of amine-containing drug.....76
Figure 4.2. Structures of 4,6-O-benzylidene methyl-R-D-glucopyranoside carbamate and ester derivatives.....77
Figure 4.3. Chemical structure of O- and N-linked glucopyranose carbamates 77
Figure 5.1. General structures of aliphatic and mono- and di-amino acid amides of linifanib 87
Figure 5.2. Enzymatic conversion of brivanib alaninate to brivanib 90
Figure 5.3. Enzymatic conversion of valacyclovir to its parent drug and then to its triphosphate active form 90
Figure 5.4. 5'-L-isoleucyl gemcitabine mechanism of resistance to deamination by cytidine deaminase. 91
Figure 5.5. Hydrolysis of proline prodrug of methotrexate. 91
Figure 5.6. Mechanism of diketopiperazine formation 92
Figure 5.7. Hydrolysis of paracetamol dipeptide esters to paracetamol 92
Figure 5.8. Library of lysine-based organogelators 93
Figure 5.9. The lysine-based hydrogelators 5.21 and 5.22 94

Figure 5.10. Molecular dynamic simulation showing the distribution of β-sheet distances between the Fmoc-protected amino acids molecules and π–π stacking distances between Fmoc residues described in reference 95
Figure 5.11. Amplitude sweep of 0.5% w/v acetoxyacetate derivative of linifanib (5.36) using 5% v/v DMSO/water mixture at 37 °C. The measurements were performed at strains of 0.01% to 100% strain at 10 rad s and were carried out in triplicate and the mean calculated. Error bars represent standard deviation. Gels were formed instantly and measurements were taken after 3 hours. 102
Figure 5.12. Vial inversion test 0.5 % (w/v) Pro-Pro derivative of linifanib (5.48) in 5-25 % (v/v) DMSO/water. 105
Figure 5.13. Stability study of dipeptide analogues of linifanib (5.44-5.50) using 0.5 % (w/v) of compound in 20% (v/v) DMSO/water at pH 4.0 and 37 °C. All measurements were carried out in triplicate and the mean calculated. Error bars represent standard deviation. 106
Figure 5.14. Library of naphthalene protected dipeptides 110
Figure 5.15. Stability study of amino acid derivatives of linifanib (5.51-5.56) and acetoxyacetic acid of linifanib (5.36) using 0.5 % (w/v) of compound in 20% (v/v) DMSO/water at pH 4.0 and 37 °C. All measurements were carried out in triplicate and the mean calculated 112
Figure 5.16. Hydrolysis of valopicitabine at pH 4.5 and 7.2. 113
Figure 5.17. Amplitude sweep of 0.5% w/v of serine (5.52) (red) and glycine (5.54) (green) derivatives of linifanib using 5% v/v DMSO/phosphate buffer 7.4 mixture at 37 °C. The measurements were performed at strains of 0.01% to 100% strain at 10 rad s and were carried out in triplicate and the mean calculated. Error bars represent standard deviation. Gels were formed instantly and measurements were taken after 3 hours. 114
Figure 5.18. Vial inversion tests of 0.125-1% w/v serine analogue of linifanib (5.52) in 5% v/v DMSO/phosphate buffer (6-8.1). The red boxes represent the positive gels. 116
Figure 5.19. Amplitude sweep of 0.5% w/v serine analogue of linifanib (5.52) using 5% DMSO/phosphate buffer pH 6.0-7.4 at 37 °C. Only G' was showed. All measurements were carried out in triplicate and the mean calculated. Error

bars represent standard deviation. Gels were formed instantly and measurements were taken after 3 hours 116
Figure 5.20. Correlation between storage modulus (G') of 0.5% w/v serine derivative (5.52) in 5% v/v DMSO/phosphate buffer 6-7.4 and pH at 1% strain and 37 °C.....117
Figure 5.21. Frequency sweep of 0.5% w/v of serine derivative of linifanib (5.52) in 5% v/v DMSO/phosphate buffer 7.4 at 37 °C. All measurements were carried out in triplicate and the mean calculated. Error bars represent standard deviation.....118
Figure 5.22. H NMR of serine derivative of linifanib (5.52) (10% w/v) in 5% v/v DMSO-d_6: D_2O (gel).....119
Figure 5.23. Comparison of H NMR of serine derivative of linifanib (5.52) in 5% v/v DMSO-d_6: D_2O (gel) (blue) and DMSO-d_6 (solution) (red).....119
Figure 5.24. H NMR of serine derivative of linifanib (5.52) (10% w/v) in 5% v/v DMSO-d_6: D_2O (gel) immediately after preparation (blue) and 5 hours after preparation (red).....120
Figure 5.25. FT-IR spectroscopy of the amide region of serine derivative of linifanib (5.52) for the solid (1 mg), 0.5% w/v DMSO solution and 0.5% w/v in 5% DMSO/phosphate buffer 7.4 at room temperature. 121
Figure 5.26. FT-IR spectroscopy of the amide region of glycine derivative of linifanib (5.54) for the solid (1 mg), 0.5% w/v DMSO solution and 0.5% w/v in 5% DMSO/phosphate buffer 7.4 at room temperature. 122
Figure 5.27. Transmission electron micrograph (TEM) of 0.5% (w/v) serine derivative of linifanib (5.52) in 5% (v/v) DMSO/phosphate buffer 7.4; scale bar = 100 nm using JEOL JEM –2000FXII transmission electron microscope and accelerating voltage of 100 kV. Gel formed instantly and the experiment was carried out after 24 hours. 123
Figure 5.28. Transmission electron micrograph (TEM) of 0.5% (w/v) glycine derivative of linifanib (5.52) in 5% (v/v) DMSO/phosphate buffer 7.4; scale bar = 0.2 μm using JEOL JEM –2000FXII transmission electron microscope and accelerating voltage of 100 kV. Gel formed instantly and the experiment was carried out after 24 hours. 123

Figure 5.29. Plasma stability study of linifanib in mouse, rat and human plasma medium, n= 2. (The study was carried out at carried out at Sygnature Discovery) 124
Figure 5.30. Plasma stability study of serine derivative of linifanib (5.52) in mouse, rat and human plasma medium, n = 2. (The study was carried out at carried out at Sygnature Discovery).....125

List of Tables

Table 2.1. Hydrgen bonding, lipophilicity (clog P) and aromaticity of compounds 2.1-2.9. HBD: hydrogen bond donor, HBA: hydrogen bond acceptor 44

Table 2.2. Data table of vial inversion tests of 0.5% (w/v) compounds (2.1-2.9) in 5-50%(v/v) DMSO/water at room temperature. G: gel, P: precipitate, S: solution 50

Table 3.1. Data table of vial inversion tests of 0.5 % w/v linifanib and its analogues (3.17-3.25) in DMSO/water mixtures where gel (G), weak gel (WG), solution *(S)* and precipitate (P). Observations were carried out after 5 minute of cooling to room temperature. 68

Table 3.2. Vial inversion screen of linifanib in binary mixtures of DMSO and water where gel (G), solution *(S)* and precipitate (P). Observations were carried out after 5 minute of cooling to room temperature 70

Table 4.1. Data table of vial inversion tests in DMSO/water mixtures of 0.25 % w/v of carbamate analogues of linifanib with % DMSO from 5 – 50% v/v, where P: precipitate, S: solution. Observations were carried out after 3 hours of cooling to room temperature 84

Table 5.1. Data table of vial inversion tests in DMSO/water mixtures of 0.5 % w/v of amide analogues of linifanib (5.36-5.40) with % v/v DMSO from 5 – 25%, where G: gel, WG, weak gel, P: precipitate, and S: solution. Observations were carried out after 5 minutes of cooling to room temperature 100

Table 5.2. Predicted clog P for amide analogues of linifanib (5.36-5.40) and their vial inversion gelation tests. 101

Table 5.3. Data table of vial inversion tests in DMSO/water mixtures of 0.5 % w/v of dipeptide derivatives of linifanib (5.44-5.50) with % v/v DMSO from 5 – 25%, where G: gel, P: precipitate, and S: solution. Observations were carried out after 3 hours of cooling to room temperature 105

Table 5.4. Data table of vial inversion tests in DMSO/water mixtures of 0.25 and 0.5 % w/v of amino acid analogues of linifanib (5.51-5.56) with % v/v DMSO from 5 – 25%, where G: gel, WG: weak gel, P: precipitate, and S: solution. Observations were carried out after 3 hours of cooling to room temperature 108

Table 5.5. Data table of vial inversion tests in 5% v/v DMSO/phosphate buffer (pH 6.0-8.1) mixtures of 0.125, 0.25, 0.5 and 1% w/v of serine analogue of linifanib (5.52) where G: gel, WG: weak gel, P: precipitate, and S: solution. Observations were carried out after 5 minutes of cooling to room temperature 115
Table 7.1. Amounts of compound, DMSO and water required for gel preparation using 100 % DMSO stock solution 134
Table 7.2: Amounts of compound, solvent and water required for gel preparation using 50 % DMSO/EtOH stock solution.....134
Table 7.3: Amounts of compound, solvent and water required for gel preparation using 25 % DMSO/EtOH stock solution.....135
Table 7.4. Solution A and B aliquots required to prepare the desired pH 136

List of Schemes

Scheme 2.1. Synthesis of semaxanib (2.3).....44
Scheme 2.2. The mechanism of Knoevenagel condensation used to form semaxanib.....45
Scheme 2.3. Synthesis of orantinib (2.4) 46
Scheme 2.4. Mechanism of hydrogenation of compound (2.4a) 46
Scheme 2.5. Mechanism of decarboxylation of intermediate (2.4b) 47
Scheme 2.6. Mechanism of formylation of intermediate (2.4c).....47
Scheme 2.7. Mechanism of ester deprotection of compound (2.4d).....47
Scheme 2.8. Synthesis of quinol derivatives (2.5-2.9).....48
Scheme 2.9. Mechanism of formation of intermediate 2.5c. 48
Scheme 3.1. General synthesis of linifanib and its analogues (3.17-3.24) 63
Scheme 3.2. Mechanism of iodo-indazole formation 63
Scheme 3.3. Mechanism of urea boronate formation.....64
Scheme 3.4. Suzuki reaction mechanism 65
Scheme 3.5. Synthesis of compound 3.25.....66
Scheme 3.6. Carboxylic acid activation by thionyl chloride.....66
Scheme 3.7. Amide formation mechanism 67
Scheme 4.1. Mechanism of ester-mediated hydrolysis of N-acyloxyalkoxycarbonyl derivatives into parent amines. 79
Scheme 4.2. Intramolecular acyl transfer in *N*-acyloxyalkoxycarbonyl prodrugs of primary amines.....80
Scheme 4.3. Synthesis of carbamate derivatives of linifanib (4.16-4.21).....82
Scheme 4.4. Synthesis of compound 4.22.....83
Scheme 4.5. Mechanism of the 2-step synthesis of acyloxyalkylcarbonyl carbamates.....83
Scheme 5.1. Synthesis of amide derivatives of linifanib (5.36-5.39). 99
Scheme 5.2. Mechanism of amide bond formation using HATU as the coupling agent and DIPEA as the base. 100
Scheme 5.3. Synthesis of dipeptide analogues of linifanib (5.44-5.50).....104
Scheme 5.4. Synthesis of amino acid analogues of linifanib (5.51-5.56) in the form of HCl salt.....108
Scheme 5.5. Mechanism of base-catalysed amide hydrolysis 112

Chapter One: Introduction

In this chapter, we will present the current cancer status and cancer treatment in general. Then, there will be a description of low molecular weight gelators (LMWGs) as novel drug delivery systems with more emphasis on their application in anticancer drug therapy. A description of two categories of anticancer treatment covered in this study, i.e. tyrosine kinase inhibitors and cytotoxic benzothiazole anticancer agents will be provided. Finally, the aims and objectives of the study will be outlined.

1.1. Cancer: Current status

Cancer represents a generic term of a large group of diseases that can affect any part of the human body. It is characterised by uncontrolled growth and spread of abnormal cells.[1,2] It is the second leading cause of mortality and morbidity across the world according to the American Cancer Society.[3] There are various risk factors which contribute to cancer such as cigarette smoking, heavy alcohol consumption, infection by bacteria and viruses, genetic mutations and immune abnormalities.[4] The most important risk factor is tobacco smoking. In 2016, more than 188,000 out of around 600,000 estimated cancer deaths in the US were caused by smoking. In addition, in the same year, more than 1,600,000 individuals were expected to be diagnosed for cancer. New published reports suggested that people aged 50 years and more are the age group most at risk of developing cancer.[5] With regard to distribution of cancer in different organs of human body, the most common organ of cancer in males were prostate and lung while in females were breast and colo-rectum.[3] It is expected that the global annual cancer cases will increase from 14 million in 2012 to more than 22 million cases in the next twenty years.[4]

1.1.1. Pathogenesis of cancer

Generally, there are three steps involved in carcinogenesis: transformation, proliferation and metastasis. Transformation means that the cell is changed from regulated normal growth to a cell of uncontrolled growth. This mutation in cell growth could be spontaneous or caused by different causative agents such as chemicals, radiation or viruses. These mutations act by different mechanisms such as activation of growth-promoting genes, inactivation of growth inhibiting

genes, alteration of apoptosis (programmed cell death) regulating genes or inactivation of DNA repair genes. Normally, there is a DNA repair mechanism responsible for repairing the mutant genes. If this mechanism stops, the mutant genes begin to express their defective products allowing dysregulated cell growth and genetic instability.[6]

Most cancer cells start to be genetically identical to their precursor cells, but due to more mutations, there will be an increase in genetic variation leading to heterogeneity among their precursors. The new daughter cancer cells will have higher survival capability leading to uncontrolled cell growth then the cancer will progress to greater heterogeneity. This will be followed by an increase in the division of cancer cells, a process called proliferation.[6]

The division of human cells occurs through the mitotic cycle which involves a number of phases. The most important phases are the S and M phase. DNA synthesis occurs during the S phase while the division of the precursor cell into two offspring cells happens during the M (mitosis) phase. In addition, there is a phase called gap 1 (G1) which occurs between DNA synthesis and cell division, and a phase called gap 2 (G2) which is between DNA synthesis and mitosis. Most cytotoxic anticancer drugs interfere with specific stages of the mitotic cycle of cancer cells (Figure 1.1). Furthermore, there is a family of proteins which control the progress through the phases of cell cycle. These proteins are called cyclin-dependent kinases and any mutations in their genes will lead to tumour progression. Therefore, inhibition of these enzymes represents one of the approaches for cancer therapy.[6]

The proliferation of tumour cells requires a certain local optimum environment. To achieve this purpose, cancer cells secrete different chemical mediators. The most important mediators are the growth factors such as epidermal growth factor (EGF), vascular endothelial growth factor (VEGF) and platelet-derived growth factor (PDGF). Interfering with the signalling of these growth factors is another strategy for combating cancer.[7,8]

Most tumours need the stimulation of growth of new blood vessels to supply the tumour with nutrients, a process called angiogenesis. Angiogenesis inhibitors

are used to halt tumour progression by preventing the nutrition pathway to the tumour mass.[9]

The final and ultimate step in cancer progression is metastasis. This means that cancer cells will be capable of invading other tissues and organs which are distant from the tumour centre. Metastasis occurs mainly in response to mutations allowing the cancer cells to invade into other tissues and organs. Additionally, metastasis is more likely to occur in tumours with rapid growth. With regard to treatment, the primary tumour (i.e. before metastasis) responds to chemotherapy in most cases while the complicated metastatic tumours have poor response to classical treatments. Therefore, treatment is highly recommended before the metastasis stage.[6]

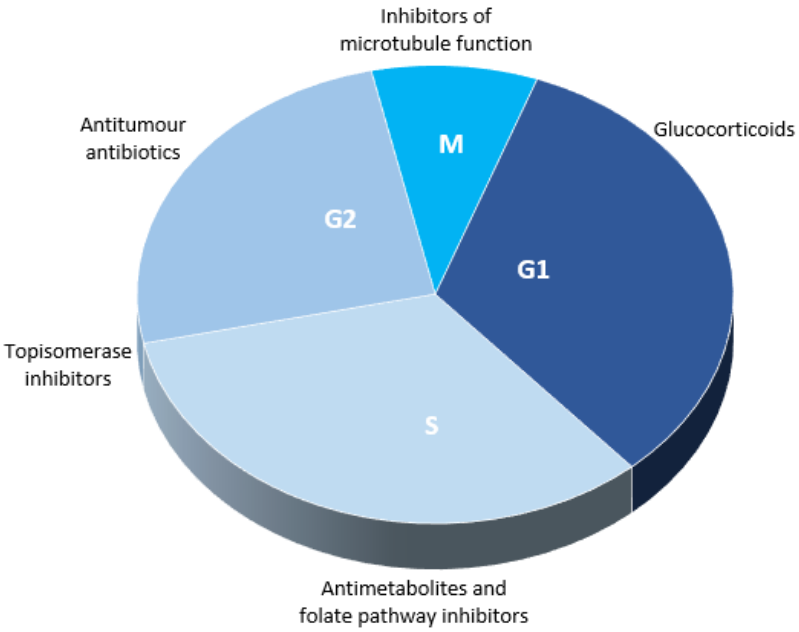


Figure 1.1. The mitotic cycle of cell division and their specificity of some cytotoxic anticancer drug classes. Adapted from ref. [6]

1.1.2. Current treatments of solid tumours

Malignant tumours characterised by solid tumour mass are called solid tumours. The majority of solid tumours are carcinomas which are solid tumours of epithelial tissues while tumours acting on connective or supportive tissues are called sarcomas.[10]

Cancer treatments involve surgery, radiotherapy and anticancer drugs. Surgery is a preferred option for primary tumours. Radiotherapy can be used either as a primary treatment or secondary therapy after surgery to ensure tumour healing.[11]

With regard to anticancer drug treatment, in spite of the development in cancer research and approving many anticancer drugs, there are still many challenges facing cancer therapy. One of these problems is the physicochemical properties of the drug such as low solubility or high lipophilicity which limit its bioavailability.[12]

Adverse effects represent another major challenge to anticancer drugs. This is because the drug should be directed against the cancer cell only depending on certain targets found in that cell exclusively. If this goal is not achieved, these drugs will accumulate in unaffected organs causing serious adverse reactions.[12]

Another limitation of cancer therapy is drug resistance. It is reported that the main reason causing failure of anticancer drugs is the resistance of cancer cells against the drug. The resistance of cancer cell could be natural or acquired after a period of time after treatment with the anticancer drug. There are different mechanisms for developing drug resistance such as inactivation of drug, setting up a drug efflux system, or changing the expression levels or mutation of the drug target.[13]

These challenges have encouraged continuous research regarding developing new strategies for treatment of cancer. One of these approaches is the localised drug therapy which is considered a targeted treatment and is thought to be more efficient than systemic anticancer drug delivery.[12]

The localised therapies of cancer are used after surgical removal of tumour mass to treat the remaining malignant microscopic masses to prevent recurrence of tumour growth. There are many benefits of using localised therapies in anticancer drug delivery such as:

- Direct drug delivery to the cancer site resulting in minimising adverse drug reactions, i.e. more selectivity.
- Prolonged and controlled drug release which will lead to more uptake into the tumour cells during multiple mitotic cycle of cancer cells.
- Capability of loading and release of poorly soluble drugs.
- Minimum frequency of administration. [12]

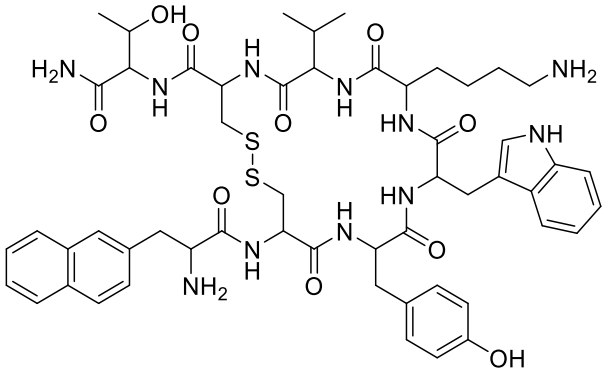
Accordingly, there have been various drug delivery platforms designed to deliver anticancer drugs locally such as polymer-based preparations including wafers, nanoparticles, microspheres and polymer-based gels. [12]

However, there are challenges and drawbacks regarding the localised anticancer therapy. Research is still ongoing to address the challenges required for the development of ideal cancer drug delivery platforms. One of these limitations is the metastatic tumours. Therefore, it is limited to primary solid tumours only. In addition, high drug loading is an important goal in designing new drug delivery systems to ensure the prolonged drug release. Finally, safety, biocompatibility and biodegradation are necessary requirements for future drug delivery platforms to avoid unwanted side effects. [12]

There are several drug delivery systems developed to achieve these criteria.[14-16] Low molecular weight gelators (LMWGs) represent one of these systems.

1.2. Low molecular weight gelators in drug delivery

In recent years, there have been numerous studies in the development of low molecular weight gelators (LMWGs) for medical purposes.[17-19] Research in this area has focused on the evaluation of these LMWGs for drug delivery and tissue engineering applications.[20,21] Recently, the FDA approved the molecular hydrogel of lanreotide (**1.1**).[22] It is an octapeptide analogue of somatostatin used for treatments of neuroendocrine tumours.[23] The hydrogel formulation of this drug is administered subcutaneously once a month.[24]



1.1

One of the approaches to form hydrogels is that LMWGs self-assemble into three-dimensional fibre networks which contain large amounts of associated water. In the presence of low stress, this network will exhibit a solid-like

behaviour even if there is low solid content (less than 2% w/w).[18] Large amounts of associated water and low solid amount make these systems biocompatible, an essential property for drug delivery.[20]

1.2.1. Principle of gelation by LMWGs

The formation of fibre networks is essential for gel formation. This takes place by ordered assembly of the molecule in the network (Figure 1.2). One dimensional fibre formation is favoured over other configurations by the molecular interactions. Thus, the self-assembly into these one-dimensional structures is entropically more favoured than crystallisation.[25] Examples of the molecular interactions are hydrogen bonding and π-π stacking. Although these forces are important in assembly formation, they are weak in water.[18] Therefore, hydrophobic interactions control assembly in aqueous media. Cross linking between the fibres is an essential requirement for the formation of a gel. This results from branching of fibres. In addition, the type of interaction of cross links is non-covalent bonding indicating that these gels are reversible.[25]

There are important factors which control hydrogel mechanical properties. The molecular structure is one of the determinants of gelation. The presence of certain functional groups is essential for gel formation especially those involved in non-covalent interactions such as amide and urea functional groups. Alkyl groups play a role in promoting Van der Waals and hydrophobic forces necessary for the balance in solubility of the gelator in the solvent.[20]

In addition, the solvent plays a key role in determining the gelation process. In a study carried out by the Weiss group, the importance of solvent parameters was highlighted. Hansen solubility parameters (HSP) are used to predict the solubility of the gelator in a solvent. These parameters were considered by this study as an accurate method for determination of solubility of gelators in different solvents which will aid in the selection of the suitable solvent for the gel formation.[26]

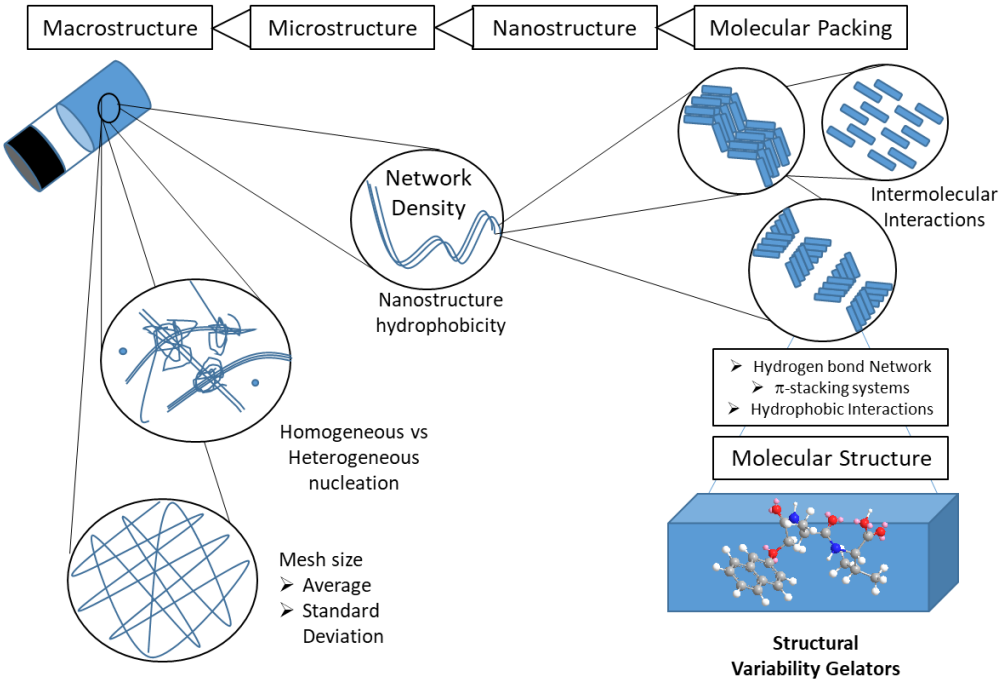


Figure 1.2. Different stages of assembly causing gelation. There are three different molecular packing which lead to formation of the nanostructure and finally the macrostructure. Adapted from ref. [25]

1.2.2. Design of stimuli – responsive LMWGs

Recently, great interest has been focused on the design of LMWGs which are used in drug delivery applications. Generally, LMWGs ae formed in response to various triggers or stimuli. Several triggers are present and can be classified as chemical or physical as shown in (Figure 1.3).[27] In this section, a description will be presented for the most used stimuli such as temperature, pH and enzymes.

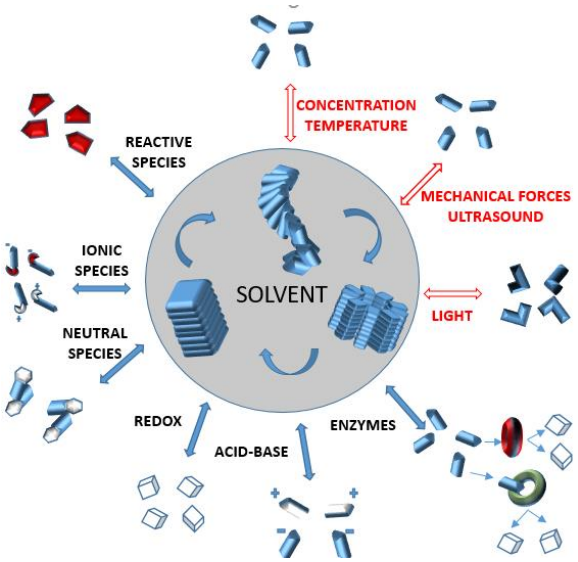
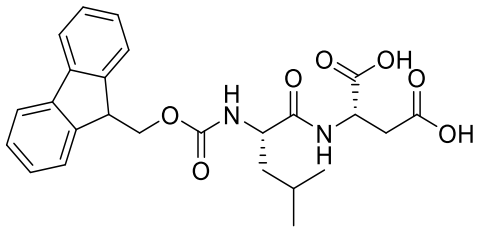


Figure 1.3. Classification of different stimuli which trigger gelation: physical (red) and chemical (black). Adapted from ref. [27]

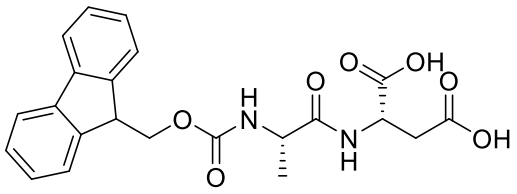
1.2.2.1. Temperature – sensitive gelators

Temperature is a very common trigger for formation of gels. The principle of this method is to use high temperature to ensure complete solubility of the gelator in the desired solvent. This will be followed by slow lowering of the temperature leading to reduced solubility of the gelator and in presence of the uni-directional non-covalent bonding (such as hydrogen bonding and hydrophobic forces) gel structures are formed.[25] This type of gel is referred to as a thermo-responsive gel.

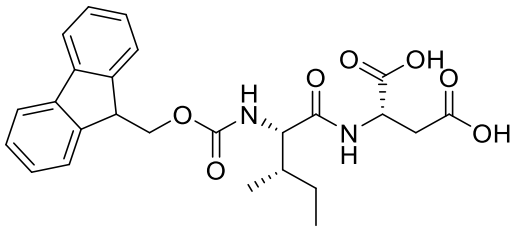
One of the early gels prepared by this method was reported by Vegeners *et al.* A library of seven fluorenylmethyloxycarbonyl (Fmoc)-dipeptides were synthesized and tested for gel formation. Aqueous solutions of these dipeptides were prepared by dissolving the compound in 10 nM phosphate buffer pH 7.4 and the temperature was increased to the boiling point (100 °C). Upon cooling to 60 °C, gels were formed in three of these protected dipeptides which are Fmoc-Leu-Asp (**1.2**), Fmoc-Ala-Asp (**1.3**) and Fmoc-Ile-Asp (**1.4**), whereas turbid solutions were formed in the rest of compounds.[28]



1.2



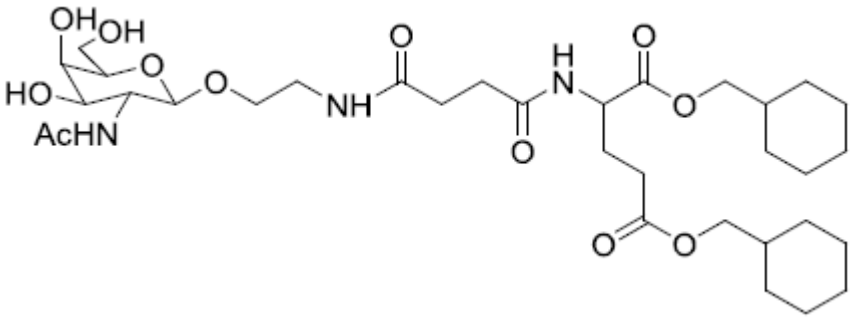
1.3



1.4

Another thermos-responsive gel was reported by Kiyonaka *et al.* who prepared a glycosylated amino acid-based gel (**1.5**).[29] Initially, aqueous solutions of this compound were prepared. It was noticed that there was a phase transition during the change in temperature. At room temperature, water was immobilized in the

gel network while at 65 °C it was partially expelled outside the gel matrix and finally at 72 °C, the mixture was turned to precipitate and most of water was expelled (Figure 1.4).



1.5

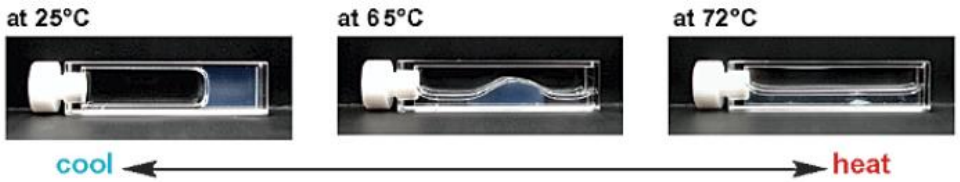


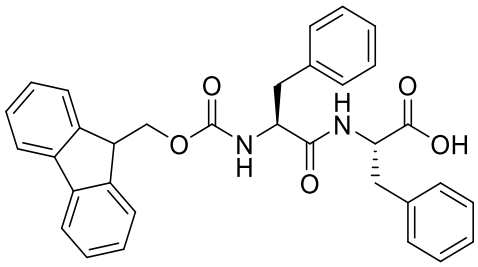
Figure 1.4. Thermally triggered phase transition of the gel of compound 1.5. [29]

1.2.2.2. pH – sensitive gelators

The change in pH of solution is another approach for triggering gel formation.[30-33] This method can be used to create gels for compounds with acidic or basic groups which have poor solubility at neutral pH. Initially, the compound should be completely soluble in the solvent and this is done by increasing or decreasing the pH depending on the nature of compound. This is followed by ionisation leading to increases in the aqueous solubility of the molecule. The pH of solution is then changed using acid such as hydrochloric acid (resulting in protonation of acidic groups and hence decreasing the solubility) or base such as ammonia (leading to deprotonate the basic groups and reduce the solubility as well). The reduction in aqueous solubility causes gel formation due to the self-assembly of the gelation through the non-covalent forces.

Amongst the extensively studied pH responsive gels are Fmoc-protected dipeptide-based LMWGs.[34] These dipeptides formed clear solutions at higher pH and on lowering the pH, the carboxylate part will be protonated leading to gel formation. It was found that the apparent pKa of the carboxylate part is

higher than that predicted for common peptides with the highest reported apparent pKa for Fmoc-Phe-Phe (**1.6**) (9.9).[35] In most cases, gelation is required to happen in specific pH (e.g. the physiologic pH for drug delivery *in vivo*). To achieve this objective, pKa values of many gelators are reported and can be utilized for preparation of pH-responsive gels provided that the degree of ionisation of such gelators decreases at the appropriate pH.[34]



1.6

1.2.2.3. Enzyme – sensitive gelators

The third approach of triggering gelation is the utilisation of enzymes in creating self-assembled gels. Generally, this method involves a precursor of gelator which undergoes either hydrolysis (breaking of bonds) or condensation (formation of new bonds) through specific enzymes to form the desirable gelator which will self-assemble to form fibres which ultimately form the gel network (Figure 1.5).[36]

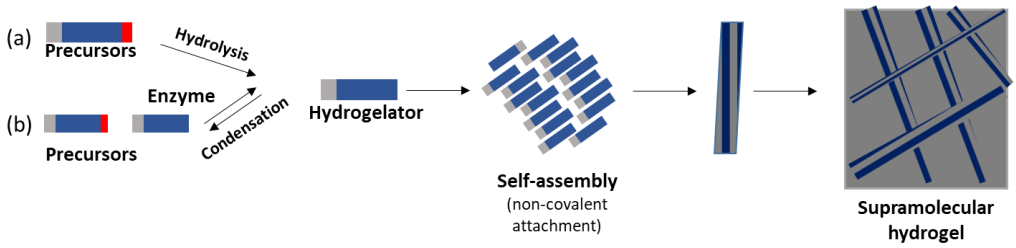
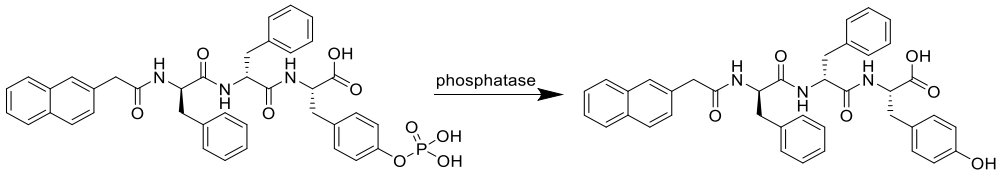


Figure 1.5. General mechanism of formation of enzyme-triggered gelators. (a) Formation of gels through hydrolysis, (b) Formation of gels through condensation. Adapted from ref. [36]

Numerous studies have investigated the application of enzyme-triggered gelation in localised drug delivery. Most of these studies focus on peptide-based gels due to the diversity of amino acids allowing tuning of the properties of these gels. Xu *et al.*[37] and Ulijn *et al.*[38] reported enzyme triggered gelation of di and tripeptide-based hydrogels. These hydrogelators were formed *in situ* from a precursor compound by the action of enzymes. There are two different strategies

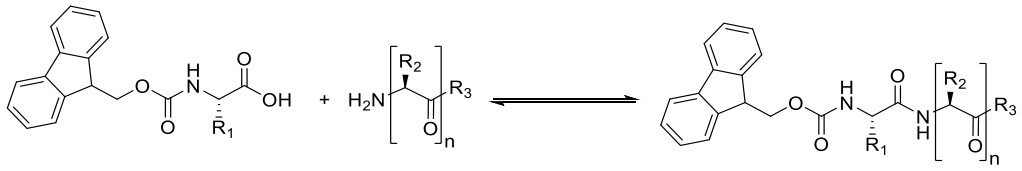
for creation of such gels. The first strategy involves attaching a solubilising enzyme-cleavable group to the dipeptide gelator. By the action of an enzyme, this cleavable group will be removed liberating the hydrogelator. As an example, tyrosine phosphate is attached to the dipeptide to form a tripeptide phosphate (**1.7**). A phosphatase enzyme was used to dephosphorylate the tyrosine (Figure 1.6). This will lead to a decrease in the hydrophilicity of the tripeptide (**1.8**) triggering the self-assembly.[39]



1.7 **1.8**

Figure 1.6. Dephosphoprylation of the tripeptide phosphate (1.7) to tripeptide (1.8) by phosphatase enzyme

The second approach involves the use of enzymes to synthesise the hydrogelator, e.g. the hydrogelator (**1.11**) was synthesised from Fmoc-amino acid (**1.9**) and another C-terminus protected amino acid (**1.10**) using proteases.[40] These enzymes normally are responsible for the peptide bond hydrolysis. Interestingly, the self-assembly of this Fmoc-dipeptide has led the equilibrium towards bond formation instead of hydrolysis resulting in amide formation, a process called reversed hydrolysis (Figure 1.7).[40,41]



1.9 **1.10** **1.11**

Figure 1.7. Reversed hydrolysis of hydrogelator (1.11)

More details regarding the drug delivery applications of enzyme-triggered self-assembly will be discussed in the topic of prodrug-based LMWGs.

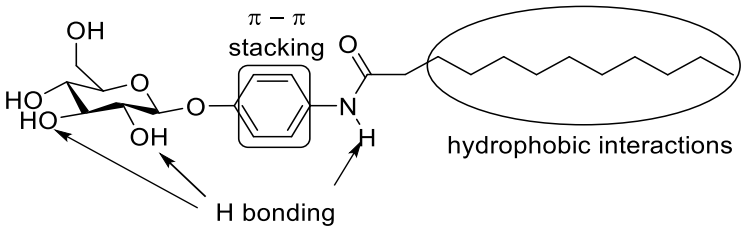
1.2.3. Classification of LMWGs

Low molecular weight gelators are divided mainly into two categories: organogelators (form gels with organic solvents) and hydrogelators (form gels with water or aqueous solvents). The research regarding organogelators

preceded investigating hydrogelators. Terech and Weiss reviewed the organogelator literature[42] and after few years, Hamilton and Estroff offered an extensive review of existing hydrogelator literature.[18] These gelators are composed of a diverse spectrum of chemical structures such as amino acids, saccharides, nucleosides, nucleotides and bile acids. Despite this diversity, most of these compounds share a common property which is the presence of both hydrophilic and hydrophobic portions (amphiphilic nature).[43] However, it can be noted from the above reviews that not all LMWGs possess the amphiphilic nature. This means that most of these gelators were discovered through serendipity rather than rational design.[43] Different classes of LMWGs will be described below to provide a picture of the different chemical scaffolds of these compounds.

1.2.3.1. Hydrogelators

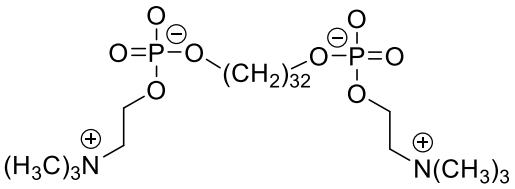
With regard to hydrogelators, one of the saccharide-based gelators is a compound (**1.12**) which is composed of aromatic group with a long alkyl chain in addition to the saccharide moiety (Figure 1.8). This gelator has the ability to create gels with water with a minimum amount of methanol or ethanol at a concentration of 1-30 mg/mL. The driving forces for gelation were suggested to be π – π stacking, hydrogen bonding and hydrophobic interactions.[44]



1.12

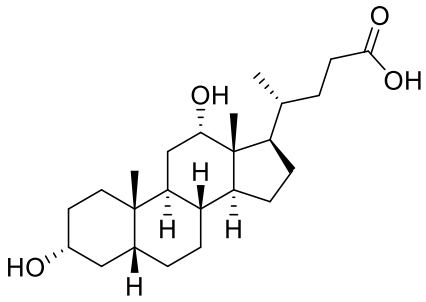
Figure 1.8. Structural features of saccharide-based gelator 1.12

Another class of hydrogelators is represented by the phospholipid-based gel (**1.13**) which gelates water at a concentration of 1-5 mg/mL. This gel has a fibrillar structure. The authors suggested that hydrophobic interactions are the driving force for the gel formation.[45]



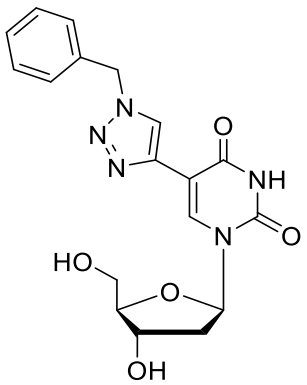
1.13

Bile acid-based gelators are obtained by substitution of the long hydrocarbon chain by a hydrophobic tetracyclic steroid building block. It was found that the gelation ability was highly influenced by the number of hydroxyl groups on the steroid unit. The dihydroxy derivative of bile acid (**1.14**) formed gels with aqueous solutions at pH range of 6.4 to 12. However, the trihydroxy bile acid cholic acid failed in triggering gelation.[46]



1.14

Regarding the nucleoside-based hydrogelators, the 2-deoxyuridine derivative (**1.15**) has the ability to form hydrogels at a concentration of 3 mg/mL. It is composed of a hydrophobic aromatic portion in addition to numerous hydrogen bonding donors and acceptors.[47]

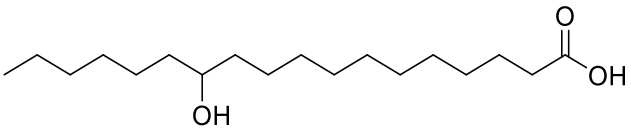


1.15

Amino acid and peptide-based gelators will be described in chapter 5.

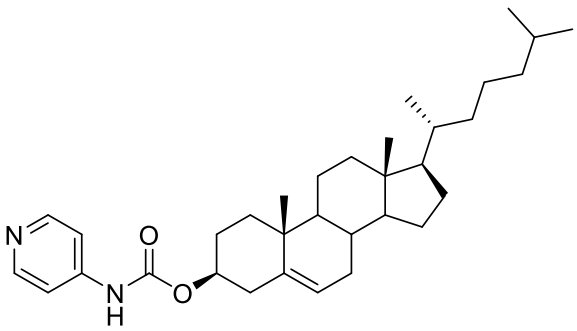
1.2.3.2. Organogelators

On the other hand, there are numerous studies focusing on organogelators. Fatty acid derivatives such as 12-hydroxystearic acid (**1.16**) has the ability to gelate different organic solvents such as toluene, dodecane, paraffin oil, nitrobenzene and silicone oil.[48] A very recent study highlighted the dependence of gelation properties of 12-hydroxystearic acid on chemical modification.[49]



1.16

Another class of organogelators are the cholesterol-based gelators. These gelators consist of an aromatic group (A) connected to steroid unit (S) (cholesterol derivative) through a linker group (L) (ALS compounds). The aromatic unit is thought to provide π – π interaction and the linker could be an ester, amide, urea or azo group which contribute to other non-covalent interactions. The steroid unit represents the hydrophobic segment of the gelator.[50] Compound **(1.17)** is one of the examples of this type of gelators which was able to gelate different organic solvents such as n-hexane, cyclohexane, toluene and DMSO.[51]



1.17

1.2.4. Characterisation of LMWGs

Low molecular weight gels have an extensive 3D interconnected network of fibres, tapes or ribbons giving rise to their viscoelastic nature. Therefore, to fully characterise the gels, their morphology and mechanical strength and as well the interactions involved in self-assembly need to be evaluated.[36]

Also, mechanical stability is an essential requirement for gels intended for localised drug delivery as gel rigidity is important to guarantee that the gel remains localised in the target organ or tissue.[52]

1.2.4.1. Table-top rheology

Table-top rheology is a technique used for preliminary screening of gels. This method does not require complex tools to perform characterisation experiment and results are drawn by visual assessment.[53] There are two variables regarding formation of gels determined by this method:

- Minimum gelation concentration (MGC) which is the minimum gelator concentration necessary for the formation of self-assembled gel at certain temperature.
- Gel – sol transition temperature (T_{gel}) which is the temperature at which the gel becomes a sol.[53]

Assessment of these parameters is made by two main procedures. The first method is tube inversion technique which involves monitoring the gel formation by vial inversion of the gel, i.e. turning the vial upside down after forming the gel. Upon inversion of the vial, stress will be applied to the gel due to forces of gravity. If the sample does not flow and can hold its own weight it can be assumed that the sample is viscoelastic in nature and a gel, whereas a viscous liquid will show appreciable flow. This resistance to flow represents a positive result (Figure 1.9). T_{gel} can be determined by putting the vial containing the gel in a heat-controlled oil bath and measure the temperature at which the gel loses its self-assembly nature and is converted to a sol.[52]

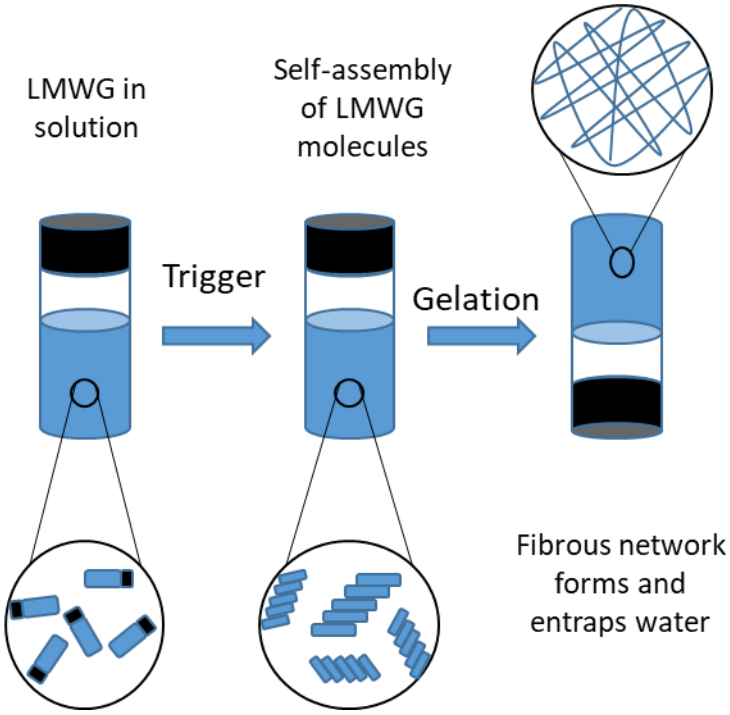


Figure 1.9. Schematic representation of gel formation assessment by tube inversion method. Adapted from ref.[25]

The dropping ball technique is another method used for preliminary gel screening. It involves placing a small metal ball in the gel followed by observation of the dropping of the ball through the gel. The ball stays stationary inside the gel while drops in the sol. The T_{gel} value can be determined by conducting the experiment at different temperatures. The yield stress of the gel depends on the density and radius of the ball.[54]

As mentioned before, these methods are useful for initial gel screening. However, they are not enough to provide a detailed characterisation of the gel such as its mechanical strength, which is needed to differentiate between weak and strong gels.[55]

1.2.4.2. Oscillatory rheology

As gels are soft materials, they can be characterised using rheological measurements which investigate these materials' response to applied stress. To gain more insight into the principle of rheology assessment of mechanical strength of gels, we will describe some terms associated with this technique. Deformation is the relative displacement of points of a given body after applying stress. Flow is the irreversible deformation and occurred when the material does not recover its original status after removal of stress. The properties of flow for

materials can be analysed by defining the viscosity (the resistance to flow). This can be measured by shearing the fluid between two surfaces and determination of its resistance to flow. On the other hand, the reversible type of deformation is called elasticity where the material returns to its original shape when the stress is removed. Materials with both flow and elastic properties are called viscoelastic.[36]

Oscillatory rheology is used to determine the elastic and viscous properties of soft materials such as gels by applying an oscillatory stress then measuring the strain and relaxation. Different parameters are identified during these measurements. The storage modulus (G') represents the elasticity correlated with the energy stored in elastic deformation. On the other hand, the loss modulus (G'') is a measure of the system ability to flow under stress which is associated with energy lost during flow. For the viscoelastic materials, G' should be more than G'' by one order of magnitude for viscoelastic materials meaning that more energy is stored than lost. The material will lose its viscoelastic behaviour when G' is equal G'' and become viscous (regarding gelators, the gel becomes sol). In addition, an important characteristic for viscoelastic gels is the linear viscoelastic region (LVER) which is the region where both storage and loss modulus are independent on the applied stress. Strain sweep and frequency sweep methods are the most commonly used for characterisation of solid-like gels (Figure 1.10).[35,56,57] Furthermore, the measurements are performed using different geometries of plates such as parallel plates, cone and plate and cup and vane.[33]

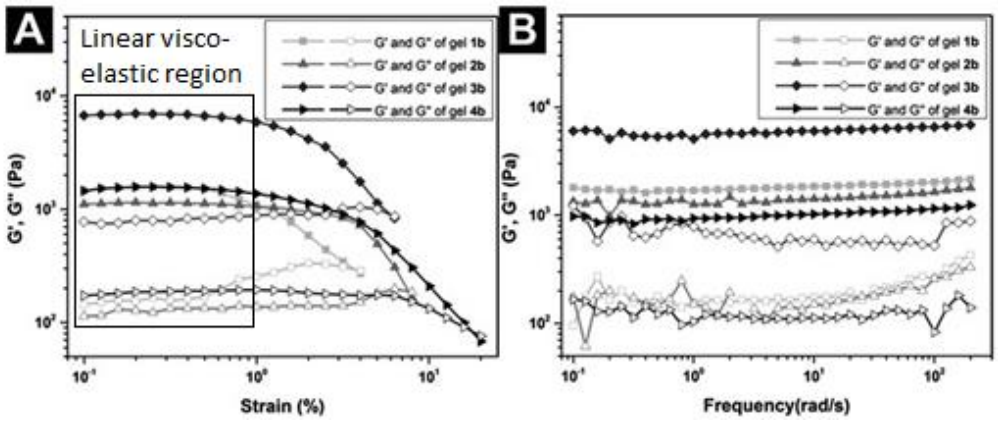


Figure 1.10. Oscillatory rheology analysis of an enzyme-induced gelator. A. Strain sweep, B. frequency sweep.[49]

1.2.4.3. Microscopy

In addition to rheology which investigates the mechanical properties of gels, microscopy methods provide an insight of the morphology of the gel network. This will offer valuable information on the shape of gel aggregate such as fibres, tapes, and ribbons (Figure 1.11). [58] Scanning electron microscope (SEM) is one of microscopy techniques which generates images by scanning over a sample with focusing electron beams. Various signals are produced through the interaction between the beam electrons and electrons of the sample. These signals will provide information about surface composition and topography.[59]

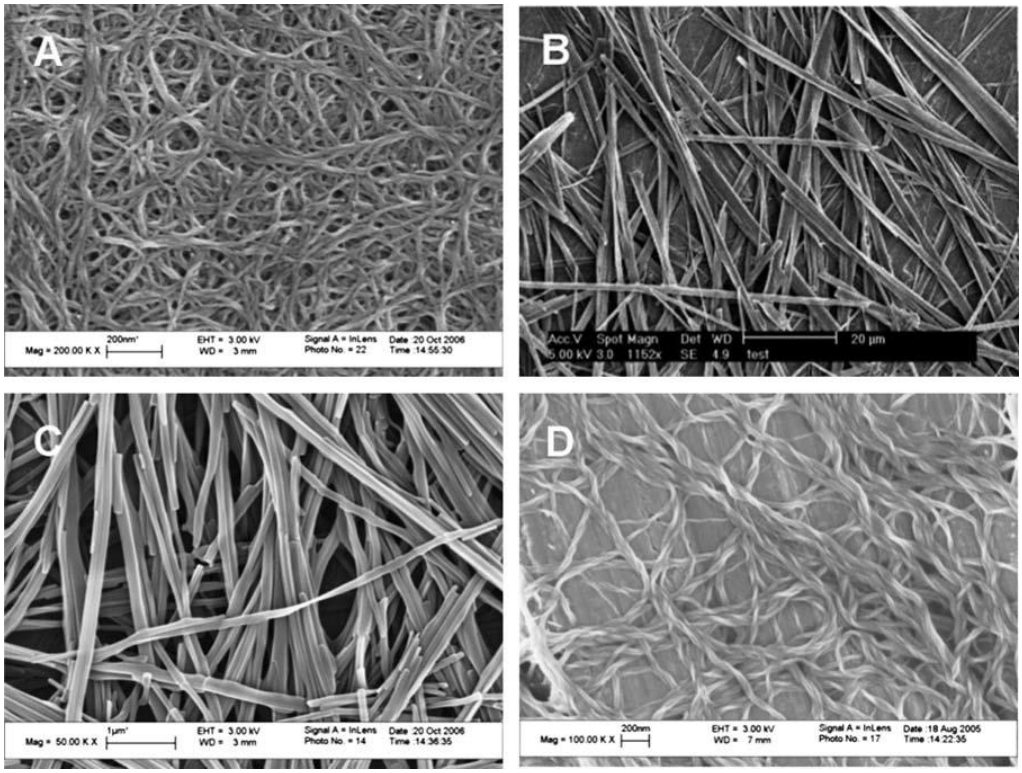


Figure 1.11. Different morphologies detected for some amide, urea and carbamate molecular gels using SEM on the xerogel status.[58]

There are numerous advantages of using SEM in characterisation of LMWGs such as:

- Relatively low cost and wide availability
- Large depth of field due to the very narrow electron beam allowing the focus on large area
- Very high resolution images
- Both low and high magnification power which offer an insight to the whole picture as well as the detailed structure of the tested sample
- High depth of focus which provides 3D images of the sample.[59]

As discussed earlier, LMWGs consist of large number of solvent molecules immobilised by small amount of gelator by triggering the 3D network consisting of fibres with size ranging from few nanometres to tens of micrometres. This size range is suitable for SEM making it ideal for exploring morphology of this drug delivery platform.[36,55,59]

Another microscopy technique is the transmission electron microscopy (TEM) where an electron beam passes the sample and an image is generated as a result of interaction of the electrons with the sample. This will be followed by magnification of the image and focusing on an imaging device such as fluorescent screen. In this type of imaging, the application of a heavy-metal staining is used to enhance the contrast of the produced image. TEM offers morphology analysis of molecules at the sub-nanometre scale. This technique has been used for structural characterisation of many LMWGs to elucidate their gelation process and mechanism (Figure 1.12). [49]

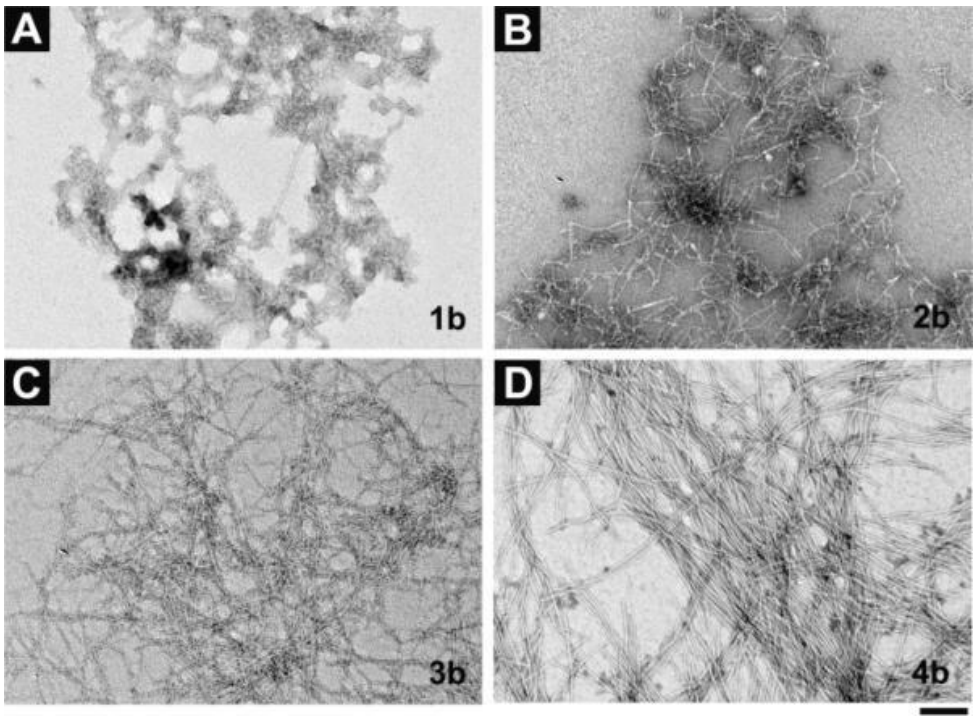


Figure 1.12. Transmission electron microscopy (TEM) of an enzyme-triggered hydrogelator based on nucleobases, amino acids, and saccharide. Scale bar = 100 nm. [49]

For both microscopy techniques, drying of the gel sample is required to form the xerogel. However, in many instances, drying causes disruption of the gel network. Therefore, cryogenic versions (cryo-SEM and cryo-TEM) were developed to characterise such type of gels.[60]

Atomic force microscopy (AFM) is another microscopy technique which provide details about morphology of supramolecular gels on the nanoscale and fibre dimensions. AFM characterisation does not always need drying of the gel.[42]

1.2.4.4. Spectroscopy

Different spectroscopic techniques are used to investigate properties of LMWGs. Nuclear magnetic resonance (NMR) is a characterisation technique for structures of small molecular structures and biomolecules.[59] The importance of this type of spectroscopy comes from its ability to explore the environment associated with each atom nucleus. This will offer deep understanding about the structural features of the formed gel network and the areas responsible for the interactions which contribute to the network stability. The self-assembled gels have relaxation times suitable for analysis by solution-state NMR (and recently, solid-state NMR). This can provide valuable information regarding quantification of immobilised molecules inside the solid gels as well as the solvated molecule within the solvent.[36] This is important especially when investigating multi-component gels to identify the component involved in the self-assembly.[61,62] Therefore, NMR is a very good technique for the analysis of LMWGs on the molecular level.

Infra-red spectroscopy is used for exploring hydrogen bonding between the different regions of the molecule particularly O – H, N – H and C = O stretching are influenced by hydrogen bonding. In addition, van der Waals forces can be detected by probing changes in C – H stretching in many occasions.[63,64]

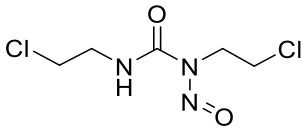
Other characterisation techniques include small angle X-ray scattering (SAXS),[65] circular dichroism (chiral gels),[49] fluorescence spectroscopy[66] and differential scan calorimetry (DSC).[67]

1.3. The role of LMWGs in localised drug delivery

Classical approaches of cancer drug delivery depend on the human body transport systems to deliver the therapeutic to the target tissue or organ. Generally, most drugs are administered to the body using either oral or parenteral routes. With regard to cancer therapy, chemotherapy suffers from several disadvantages such as the toxic drug delivery to healthy cells leading to

dangerous adverse effects such as bone marrow death.[68] On the other hand, localised drug delivery provides many advantages such as improved efficacy, reduced toxic side effects in addition to better patient compliance.[68]

Current localised drug delivery approaches mainly utilise polymers as carriers of the drug such as Gliadel, an FDA approved polymer for the treatment of an aggressive variant of brain cancer, glioblastoma. This therapeutic polymer is in the form of implanted wafers in the tumour resection site. Carmustine (**1.18**) which is an anti-cancer drug will be released from these wafers. The advantage of this type of anti-cancer delivery is to inhibit the metastasis of cancer cells remaining after tumour resection.[12]



1.18

There is a growing interest focused on the potential importance of LMWGs in localised drug delivery systems. The inherent nature of gels allows them to be formed into any shape necessary for application in localised drug delivery.[21] Additionally, as discussed earlier, the formation of gels by LMWGs could be in response to different triggers.[27] This will provide superior advantage to other approaches of drug delivery as they can be designed specifically to be activated in the proposed site of action by enzymes, change in pH and others.[21]

In general, there are three approaches for localised delivery with LMWGs. These will be detailed in the following sections.

1.3.1. LMWGs using inert matrix intended for drug delivery

The first approach is to incorporate the drug within the gel network. The drug is dissolved in the solvent which constitutes the liquid part of the gel followed by the formation of the gel network. The drug delivery is then achieved through passive means such as diffusion or gel network degradation (Figure 1.13).[69]

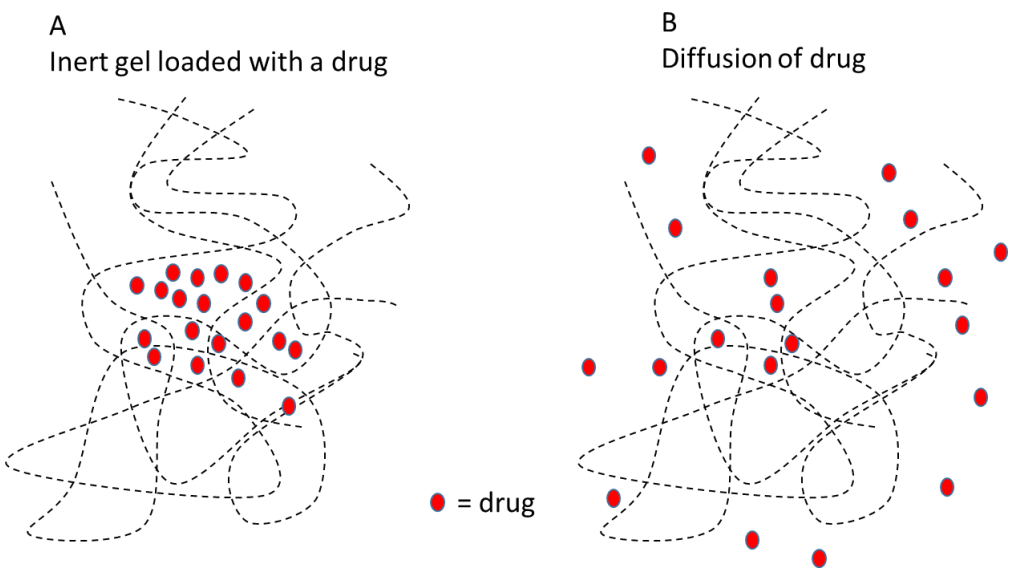
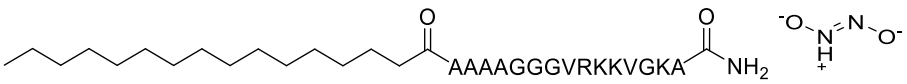


Figure 1.13. Inert matrix drug delivery approach: incorporation of the drug within a gel network followed by diffusion of the drug. Adapted from ref.[69]

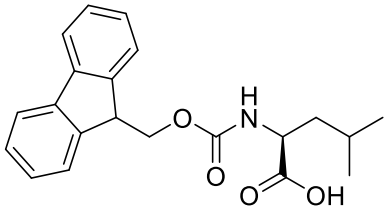
Nitric oxide inhibits the neointimal hyperplasia (the narrowing of arteries after surgery) in animal models. Kapadia *et al.* generated LMWG-based delivery system for nitric oxide intended for perivascular application. The formation of gels was achieved by mixing equivalent portions of the peptide gelator (**1.18**) in pure water, the nitric oxide derivative (diazeniumdiolate) (**1.19**) in phosphate-buffered saline (PBS) and heparin in the same buffer.[70]



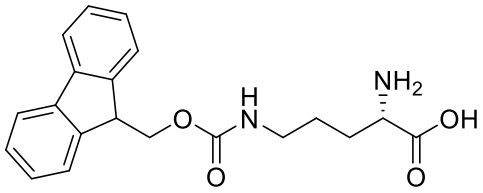
1.18 **1.19**

It was found that the inclusion of the nitric oxide derivative in the gel extended the release of nitric oxide *in vitro* to 4 days. In addition, this peptide-based gel drug delivery system demonstrated promising clinical efficacy in reduction of neointimal hyperplasia by up to 77% compared with the control.[70]

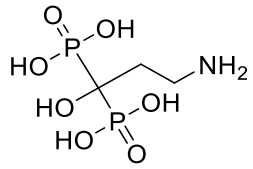
In a study conducted by Xu *et al.*, the topical application of a hydrogel consisting of Fmoc-L-leucine (**1.20**) and ε-Fmoc-lysine (**1.21**) together with pamidronate drug (uranyl nitrate chelating ligand) (**1.22**) was successful in treating mice skin contaminated with uranyl nitrate. In addition, the gel had the ability to trap the uranium oxide from a uranyl nitrate solution. This will further reduce the toxicity caused by poisoning with uranyl nitrate.[71]



1.20

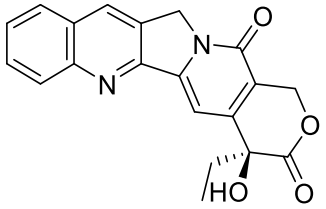


1.21



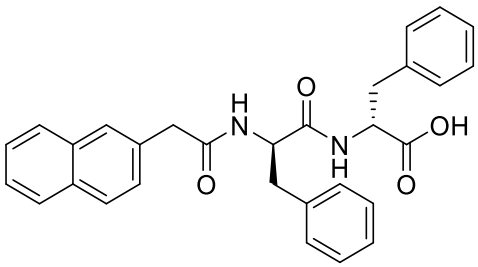
1.22

Another work by Stupp *et al.* reported the incorporation of the hydrophobic anticancer drug, camptothecin (**1.23**) into a self-assembling amphiphile consisting of a palmitic tail connected to the tripeptide Ala-Gly-Glu. This led to increased solubility of the drug by 50-fold, in addition to enhancement of tumour growth inhibition both in *vitro* and in *vivo*.[72]



1.23

The kinetics of drug release is an important part in localised drug delivery. For this reason, Liang *et al*. investigated the release kinetics of a radiolabelled I^{125} from a sodium iodide (NaI) gel made of a number of protected D-dipeptides. They found that 1% (w/w) of the hydrogelator (naphthalene-D-Phe-D-Phe) (**1.24**) was a good platform for controlled release of drug *in vivo*. The reason of the extended release is the biostability of the unnatural amino acids against hydrolysis by proteinase K, a hydrolysis enzyme for a wide range of peptides.



1.24

1.3.2. Self-assembling LMWGs prodrugs

The second strategy of LMWG-based drug delivery is the prodrug approach. A functional group is covalently bound to the parent drug to create an amphiphilic prodrug which will self-assemble to form a low molecular weight gel in aqueous solution (Figure 1.14).[73]

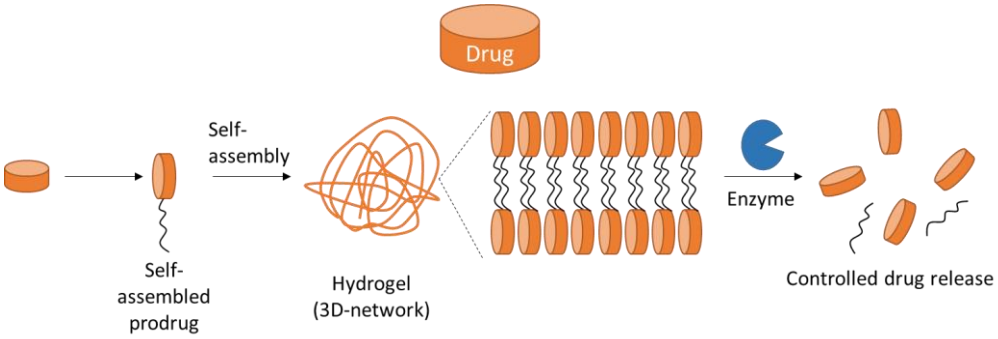


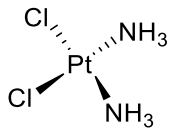
Figure 1.14. Self-assembled prodrugs. Synthesis of amphiphilic prodrugs that could self-assemble to form hydrogels and the enzyme-triggered release of drug. Adapted from ref.[73]

An important advantage of this strategy is the increase in drug loading as every molecule in the gelator includes in part a drug molecule. Therefore, the most important step in the design of self-assembled prodrugs is the selection of the appropriate functional group responsible for the molecular interactions essential for self-assembly. Upon administration of the prodrug, the parent drug will be released by the action of the appropriate enzyme.[73]

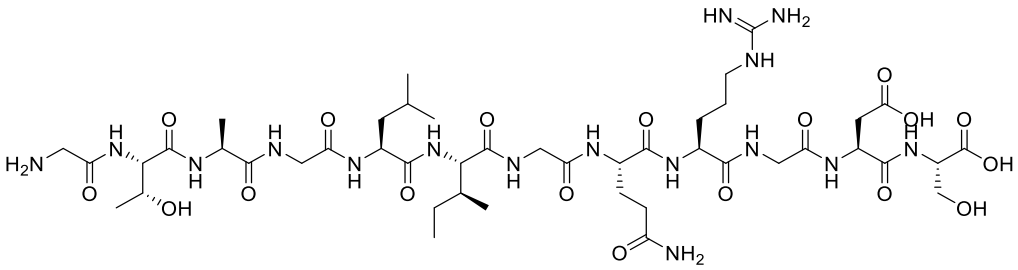
Regarding cancer treatment, the efficacy of current drugs is limited by the serious side effects caused by distribution of the drug to the healthy tissues and organs. Therefore, designing a self-assembled LMWG of a cancer therapeutic is thought to increase of drug concentration inside the tumour as well as reducing toxicity associated with its systemic distribution.[21]

One of the early studies in this field is the work by Kim and co-workers. They design a targeted delivery of the anticancer agent, cisplatin (**1.25**).[74] This drug is used for treatment of different cancers such as glioma and testicular cancer.[75] The clinical use of cisplatin was limited due to its severe adverse effects such as neurotoxicity and nephrotoxicity.[76,77] Therefore, the prodrug approach was investigated to create localised cisplatin delivery to cancer cells to eliminate the associated toxicity with systemic delivery. This drug is complexed with the peptide sequence (**1.26**) from the C-terminus of serine. This peptide sequence is

susceptible to the action of matrix metalloproteinase-2 (MMP-2) which is overexpressed in different solid tumours, playing an important role in different cancer-specific processes such as tumour progression, metastasis and angiogenesis.[78,79] Accordingly, cisplatin was released from the gel network by the action of MMP-2 and the release was dependent on the enzyme concentration. In addition, the gel network was capable of loading about 3-fold more cisplatin greater than its solubility.[74]



1.25



1.26

Several studies have focused on the development of self-assembling prodrugs of the hydrophobic anticancer drug, paclitaxel to improve its water solubility. Gao *et al.* prepared a self-assembled hydrogel of this drug which consisted of a linker, a self-assembling group (naphthalene-Phe-Phe-Lys-Tyr) and an enzyme-sensitive group to generate the prodrug (**1.27**) (Figure 1.15). After the addition of alkaline phosphatase, the prodrug (**1.27**) will be dephosphorylated to yield compound (**1.28**) which formed a hydrogel in water. This strategy was useful in converting the poorly soluble drug paclitaxel into a prodrug hydrogel system without disrupting its biological activity.[80]

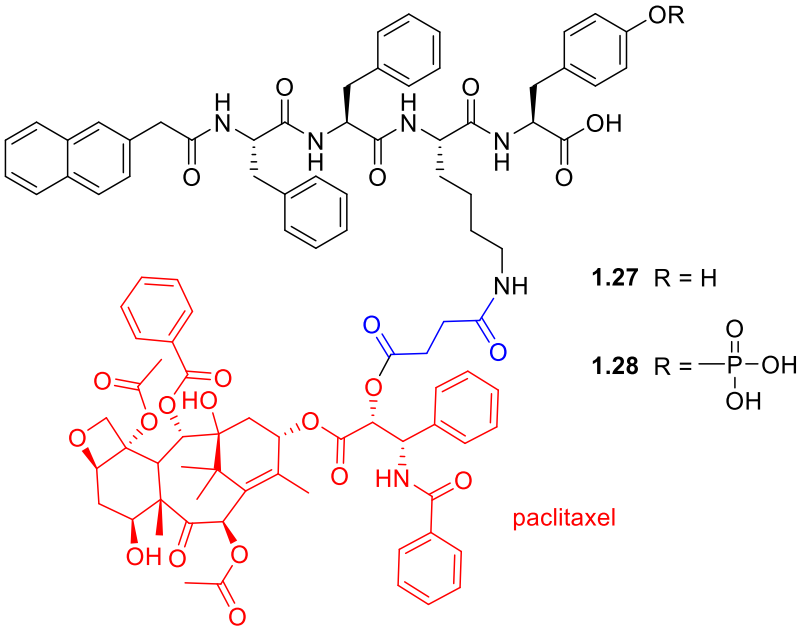
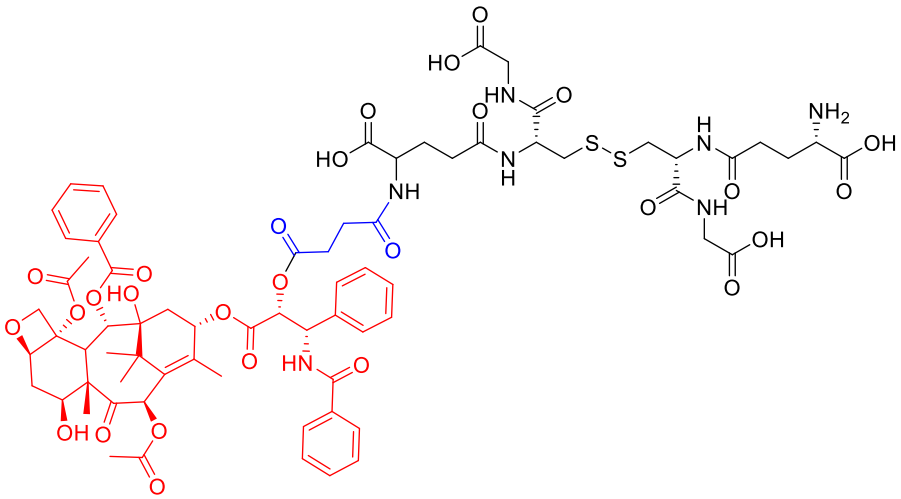


Figure 1.15. Molecular structure of paclitaxel (red), the linker (blue) and the self-assembling protected tetrapeptide (black)

Another prodrug of paclitaxel was reported by the same authors. The prodrug (**1.29**) consisted of the parent drug, linked to the drug by a succinate group in addition to the oxidised glutathione. Hydrogels were formed in PBS following ester bond hydrolysis between the drug and succinic acid. Results drawn from *in vivo* studies indicated this hydrogel was more effective in inhibiting tumour growth and metastasis compared with the intravenous injection of the parent drug, paclitaxel.[81]



1.29

Recently, a study by Tanaka and co-workers reported cancer cell death by self-assembly of an enzyme triggered gelator. A gelator precursor (ER-C16) which is a polypeptide linked to a palmitoyl group from the amine group of the terminal

glycine was synthesised. Upon the action of matrix metalloproteinase-7 (MMP-7) the precursor will be converted to the gelator (G-C16) which was taken up by tumour cells. Inside these cells, the gelator will undergo self-assembly process to create nanofiber which cause cellular dysfunction and ultimately selective cancer cell death (Figure 1.16). Another advantage of this approach, is the distinctive mechanism of cytotoxicity which means that cancer cells will not develop resistance quickly comparing with traditional cytotoxic cancer treatment.[82]

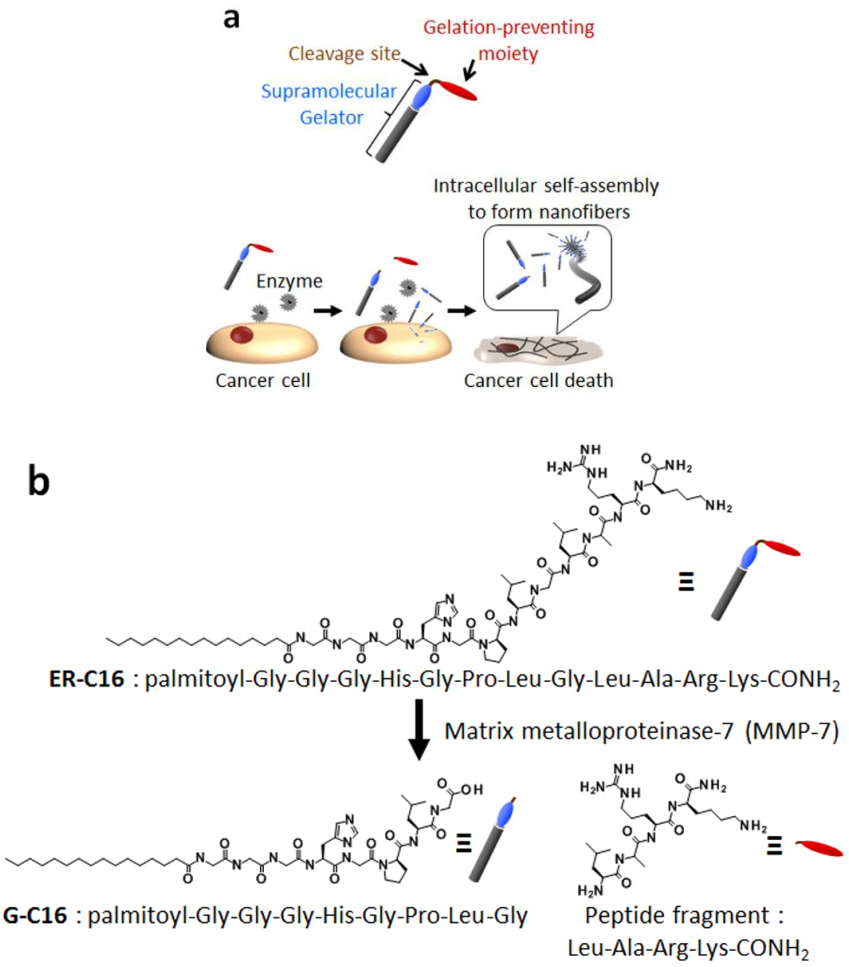
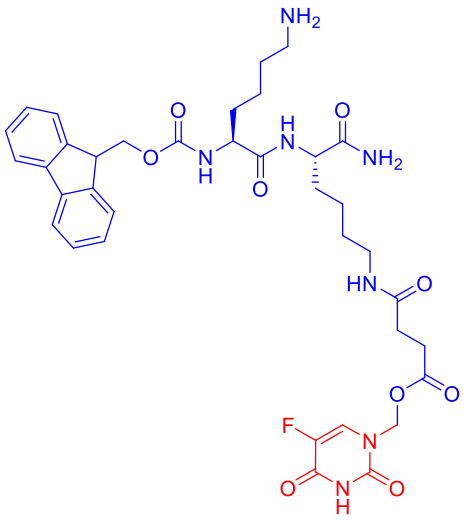


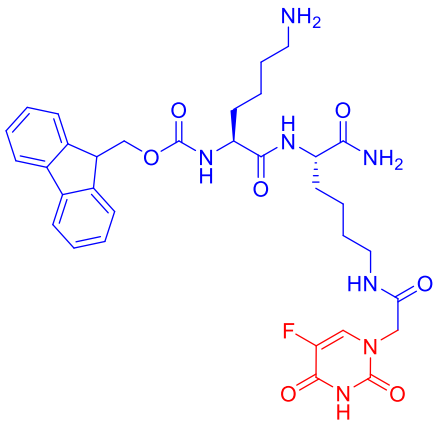
Figure 1.16. a. Mechanism of cancer cell death triggered by enzyme-stimulated gelator. b. Molecular structure of the gelator precursor (ER-C16), the gelator (G-C16) and the peptide fragment. [82]

Another work by Parquette *et al.* investigated the self-assembly of a dipeptide hydrogel prodrug of 5-fluorouracil (5-FU) which is a drug used for treatment of breast, colorectal and skin cancers.[83,84] Two dipeptide prodrugs of 5-FU were prepared and comprised Fmoc-dilysine residue connected to N-1 of the drug at the ε-amine of the C-terminus lysine by two different linkers (Figure 1.17). The

linker of the prodrug (**1.30**) is the hydrolytic, self-cleaving succinate whereas the prodrug (**1.31**) is linked via the stable acetamide linkage. These two compounds formed gels in phosphate buffered saline (PBS) at pH 7.4 and room temperature. Different properties were observed for the two prodrugs. The succinate-linked prodrug (**1.30**) exhibited gelation with nanotube morphology at a concentration of 20 mM while the other prodrug (**1.31**) formed nanofiber gels at 10 mM. In addition, cytotoxicity was confirmed only for the succinate-linked prodrug while the second prodrug was inactive. This strategy offered a slow release of the drug from the gel network making it suitable for sustained localised drug delivery.[85]



1.30



1.31

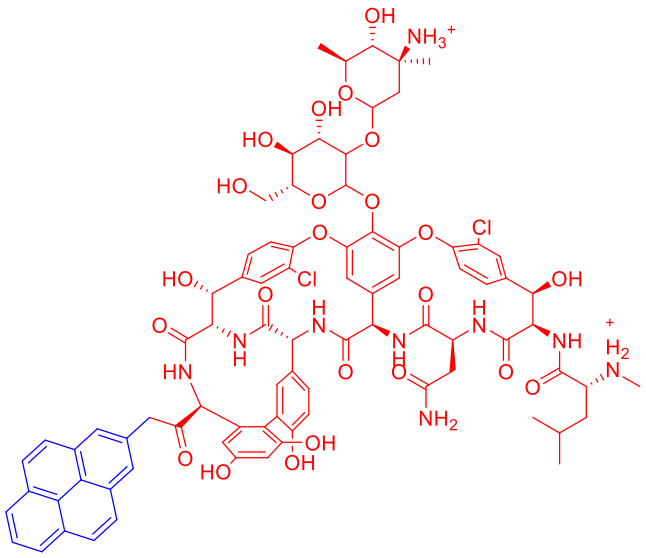
Figure 1.17. Prodrugs of 5-FU.

1.3.3. Therapeutic LMWGs

The third strategy of LMWG-based drug delivery involves the incorporation of a gelator motif to the therapeutic agent which retains the biological activity of the drug. This means the drug derivative itself will be the gel. The main advantage of this strategy is that there is no need for a release mechanism (either passive or triggered) to deliver the drug to the target tissue or organ.[36]

One of the early examples of this approach is the vancomycin derivative gel. Vancomycin antibiotic is used in treatment of infections caused by gram positive bacteria. Xing *et al.* reported the synthesis of vancomycin – pyrene derivative (**1.32**). The pyrene group is introduced at the C-terminus of vancomycin through amide bond formation. The incorporation of pyrene group triggers the formation of vancomycin gel in addition to 11-fold increase in the

antibiotic activity compared with ordinary vancomycin. The driving force of self-assembly is thought to be the π – π stacking of the pyrene group.[86]



1.32

Ozriozola and co-authors developed an interesting approach for the conversion of drugs into hydrogelators without chemical modification. These gels were prepared by reacting the mucolytic drug N-acetyl cysteine (**1.33**) with metal salts such as gold tetrachloride ($HAuCl_4$), silver nitrate ($AgNO_3$) and copper (II) chloride ($CuCl_2$) to yield the corresponding metal (I) thiolates (**1.34**). These thiolates self-assembled by metallophilic interactions leading to the formation of the hydrogel (**1.35**) (Figure 1.18). The silver and gold hydrogels were stable for months whereas the copper hydrogel was unstable and decomposed within hours with blue colour. This was thought to be due to the oxidation of Cu(I) to Cu(II) upon exposure to air. The main limitation of these gels is the dependence on pH. These gels were stable at pH up to 4 which was attributed to the presence of free carboxyl group. As a result, more efforts should be focused on the design of this type of hydrogels stable at the physiologic pH.[87]

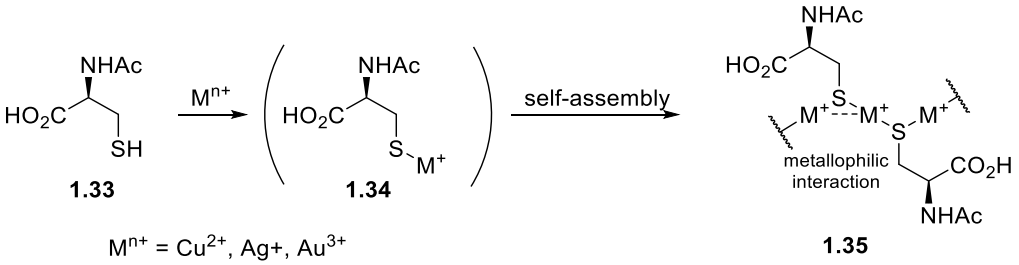
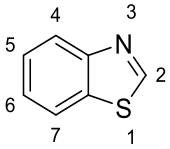


Figure 1.18. Self-assembly of N-acetyl cysteine hydrogels.

1.4. Benzothiazole-quinols: A cytotoxic cancer treatment

Heterocyclic compounds have great importance in medicinal chemistry. Benzothiazoles are an important heterocyclic scaffold and have several biological activities such as anticancer, antiviral, antibacterial and antidiabetic activities.[88]

During the middle of last century, many benzothiazoles were extensively studied for their cytotoxic anticancer activity.[89] The original compound, benzothiazole (**1.36**) was modified to improve the anticancer activity especially by substitutions at C2 and C7.[90]



1.36

Structure-activity relationship studies reveal four essential requirements for antitumor activity (Figure 1.19) which are:

1. The presence of free nitrogen is essential for the anticancer activity.
2. The molecule should be planar to promote interaction with DNA.
3. Steric hindrance of the free nitrogen not suitable for activity.
4. Halogens and alkyl substitutions at the appropriate positions are important to protect the molecule from metabolism.[90]

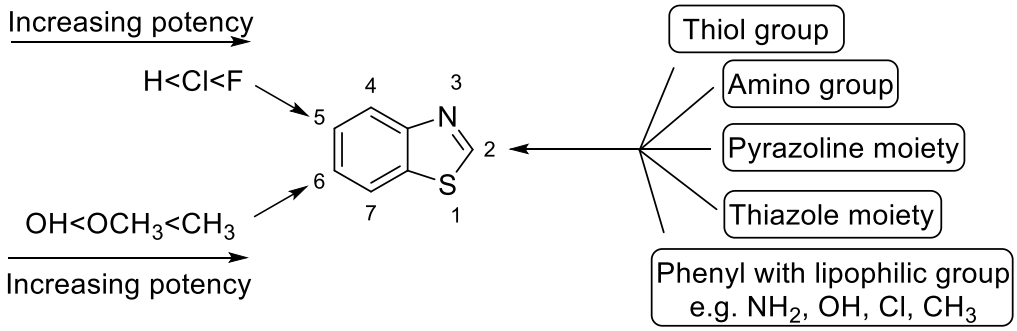
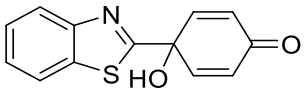


Figure 1.19. Structure-activity relationship of benzothiazole scaffold. Adapted from ref. [90]

One of these compounds is the benzothiazole-substituted 4-hydroxycyclo hexadieneone (AW 464) (**1.37**) which is the first compound of quinol series with potent anticancer activity especially renal and colon cancer. The target of these compounds is the thioredoxin system.[91]



1.37

Thioredoxin system consists of thioredoxin, thioredoxin reductase and NADPH. It is a thiol redox system which plays an important role in different cell signalling pathways contributing to cell survival and proliferation.[92,93]

Thioredoxin reductase catalyses the reduction of the disulphide bond between Cys32 and Cys35 of oxidised thioredoxin. The reduced form of thioredoxin participates in numerous biological activities such as:

- Protection of cellular proteins from oxidative damage.
- Antioxidant which as an electron donor to scavengers of peroxide.
- Redox control of some transcription factors such as hypoxia-inducible factor-1 (HIF-1).
- Electron donor for ribonucleotide reductase which is an essential enzyme in DNA synthesis.[91-94]

In cancer, the biological effects and properties of thioredoxin system promote tumour growth and progression.[95] There is increased support to the fact that thioredoxin system is an ideal target for cancer therapy. Overexpression of thioredoxin reported in numerous cancers is evidence which support this approach for the treatment of cancer.[96-98]

During a drug discovery programme, a search of novel chemical compounds with potential biological activities was launched. This led to the synthesis of a series of heteroaromatic-substituted 4-hydroxyclyclohexa-2,5-dienones (termed as quinols) which proved selective and potent activity against renal, colon and breast cancer cell lines.[99] An *in vitro* study provided evidence that these quinols bind irreversibly to the seleno-cysteine residues in the active site of thioredoxin leading to the inhibition of the signal transduction of thioredoxin system.[100] This binding exhibited a dose-, concentration- and NADPH-dependent mode. This suggested that thioredoxin is the molecular target of quinols.[91,101]

1.5. Tyrosine kinase inhibitors

1.5.1. Tumour targeting

Treatment of tumours by cytotoxic cancer therapy is commonly associated with toxicity because many anticancer drugs act on healthy tissues in addition to cancer cells which will result in serious adverse effects that limit its therapeutic benefit. In contrast, targeted cancer therapy acts on molecular targets which play an important role in the growth or progression of cancer. As these targets exist inside the tumour cells, targeted therapies could be highly specific toward these cells. This will provide a better therapeutic action with less toxic unwanted effects. In addition, targeted therapy is used occasionally together with cytotoxic drugs or radiotherapy in treatment of cancer. Thus, this approach represents a promising move towards safe and effective cancer therapy.[102-106]

One of the important approaches of targeted cancer therapy is inhibition of tyrosine kinases. These enzymes play an important role in the signalling modulation of growth factors. Activation of these enzymes leads to the increase in both growth and proliferation of tumour cells promoting angiogenesis and metastasis. One of the known mechanisms of tumour pathogenesis is the activation of tyrosine kinases by mutation. Due to all of these effects caused by these enzymes, designing tyrosine kinase inhibitors represents an important approach for combating cancer.[106]

1.5.2. Tyrosine kinases

Tyrosine kinases are enzymes which catalyse the γ phosphate group transfer from adenosine triphosphate (ATP) to target proteins. These enzymes are divided into receptor and non-receptor protein kinases. The receptor tyrosine kinases are proteins found in the cell surfaces which play crucial roles in the extracellular signal transductions.[107] Generally, scientists identified 58 receptor tyrosine kinases which are further divided into around 20 subfamilies depending on the receptor and/or ligand.[107] These enzymes consist of immunoglobulin-like sequences in their N-terminus extracellular domains, A C-terminus intracellular domain and a lipophilic transmembrane segment.[104,108]

1.5.3. Mechanism of action

Upon ligand binding, receptor tyrosine kinases undergo dimerization leading to cytoplasmic domain autophosphorylation and activation of the enzyme. There are different signalling pathways such as phosphoinositol-3-kinase/Akt pathway, Ras (rapidly accelerated sarcoma)/Raf (rapidly accelerated fibrosarcoma) mitogen activated protein kinase pathway and protein kinase C pathway.[102-104] This will be followed by signal transduction from membrane receptors into the nucleus by the intracellular mediators leading to DNA synthesis and cell division in addition to other biological activities such as cell growth and differentiation (Figure 1.20).[112,113]

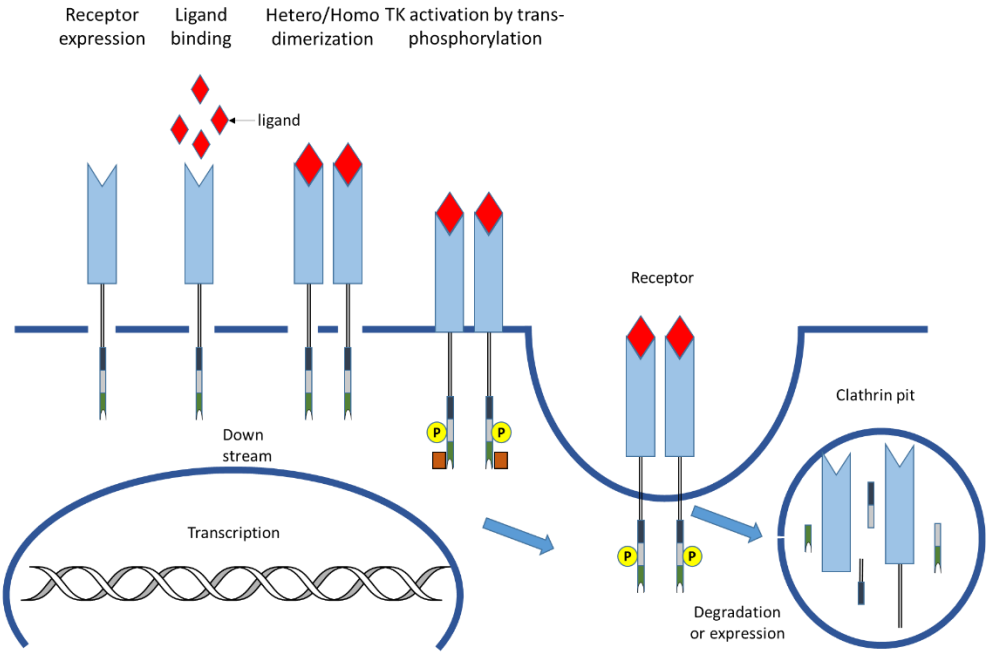


Figure 1.20. Mechanism of action of tyrosine kinases. Adopted from ref. [110]

Under normal physiological conditions, the phosphorylation of tyrosine kinase is controlled by the antagonist effect of both tyrosine kinase and phosphatases. However, due to certain mechanisms such as mutation, the control system will be halted leading to continuous activation causing the activation of other signalling secondary messengers. This will initiate the slowdown of regulatory process of cell division, growth and apoptosis which will ultimately end with tumour formation.[114] The main receptor tyrosine kinases involved in tumorigenesis are vascular endothelial growth factor receptor (VEGFR), platelet-derived growth factor receptor (PDGFR) and epidermal growth factor receptor (EGFR).

1.5.4. Vascular endothelial growth factor receptor (VEGFR)

Vascular endothelial growth factor is a receptor tyrosine kinase which promotes normal and tumour angiogenesis.[115-118] It stimulates the proliferation and formation of endothelial cells.[119] This enzyme is implicated in numerous pathologic conditions such as diabetic retinopathy, rheumatoid arthritis, psoriasis and macular degeneration.[120]

VEGF binds to $VEGFR_1$ and $VEGFR_2$. It is produced by different cells such as neutrophils, platelets and macrophages during physiologic angiogenesis. In the case of tumours, VEGF is overexpressed causing development of the pathological angiogenesis to support the tumour mass survival.[117] Therefore, disrupting VEGF pathways is a powerful approach for treatment of solid tumours. There are different classes of anti-VEGF therapy such as monoclonal antibodies against VEGF and VEGFRs, small-molecule VEGFR inhibitors, soluble VEGF receptors and ribozymes (Figure 1.21).[121,122] This type of therapy is cytostatic rather than cytotoxic. This is because inhibition of these enzymes leads to prevent the formation of new blood vessels instead of destroying the established ones.[117] Therefore, combination of VEGFR inhibitors with chemotherapy or radiation results with greater synergistic anticancer activity.[123]

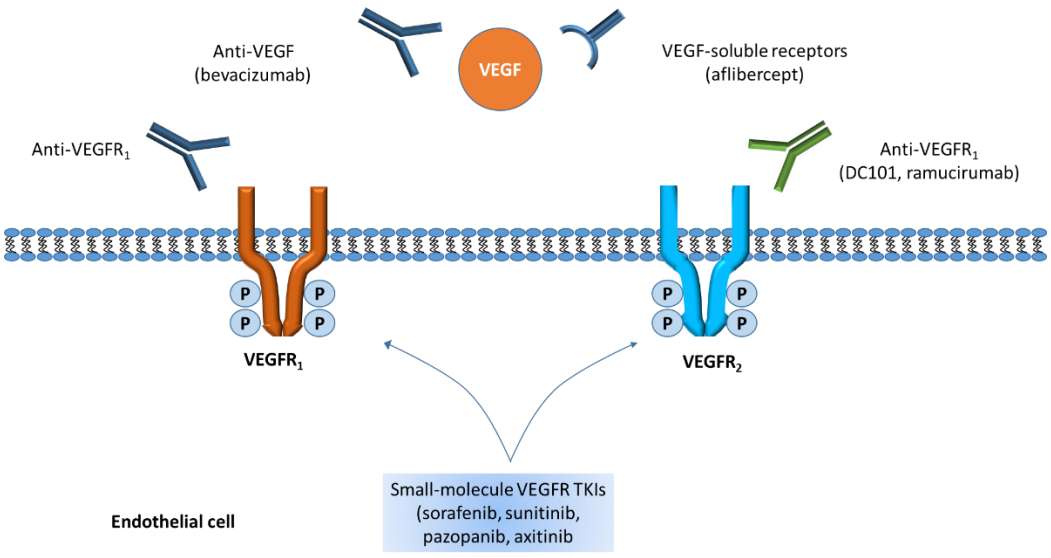


Figure 1.21. Different classes of anti-VEGF therapy with examples of drugs of each class. Adopt from ref. [120]

1.5.5. Platelet-derived growth factor receptor (PDGFR)

Another important receptor tyrosine kinase is the platelet-derived growth factor (PDGF). Similar to VEGF, this growth factor plays an important role in stimulating angiogenesis during tumour growth.[124,125] This is thought to be through recruitment of pericytes (the cells which support the endothelial lining of blood vessels) which will provide more strength to the newly formed blood vessels. Generally, there are five PDGF types: PDGF-AA, -AB, -BB, -CC, and -DD which act through PDGFR α and β.[126] Upon ligand binding to the receptor, dimerization of receptor leads to autophosphorylation which triggers intracellular signalling pathway and ultimately induction of cell proliferation.[118] There are three PDGF-induced processes which contribute to cancer development. The first process is the autocrine stimulation of cancer cell which means that the cell is stimulated to secrete its own survival factors. The second process is the paracrine stimulation of neighbouring stromal fibroblast and perivascular cells. Finally, direct triggering of angiogenesis is the third process (Figure 1.22).[118] As a result, PDGFR inhibition represents another class of targeted cancer therapy.

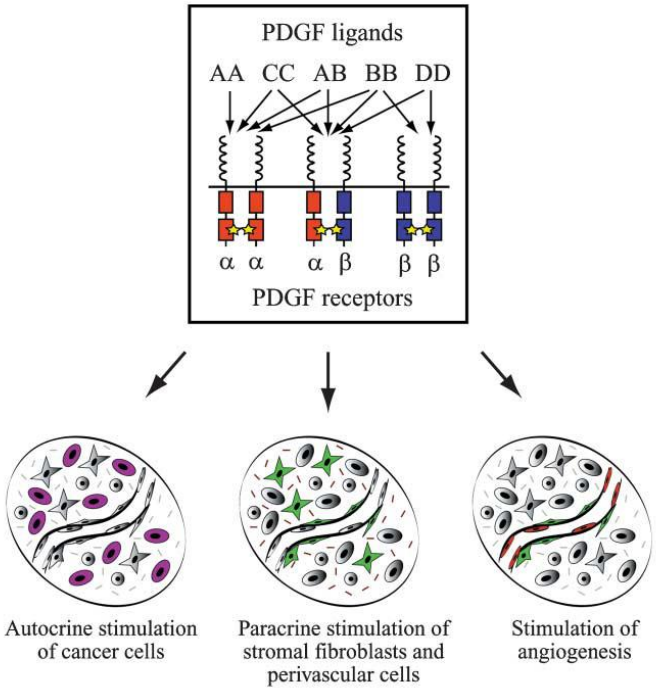


Figure 1.22. Tumour-associated process which are stimulated by PDGF. Purple: tumour cells, red: endothelial cells, green: fibroblasts, smooth muscle cells and pericytes, brown: extracellular matrix. [118]

1.5.6. Epidermal growth factor receptor (EGFR)

Epidermal growth factor is a polypeptide which upon binding to its receptor on the cell surface stimulates the growth, survival and proliferation of these cells (Figure 1.23).[127,128] Normally, this mechanism is used, for example, for the regulation of the new cell growth in the lining of the intestine.[128] The epidermal growth factor receptor (EGFR) is a transmembrane receptor while the intracellular domain is a kinase enzyme.[128] The analysis of different tumours such as lung and colon cancer indicated overexpression of EGF or EGFR.[129] Therefore, inhibition of EGFR signalling pathways is a useful approach for retarding the growth of tumours exhibiting abnormalities in this enzyme.[128]

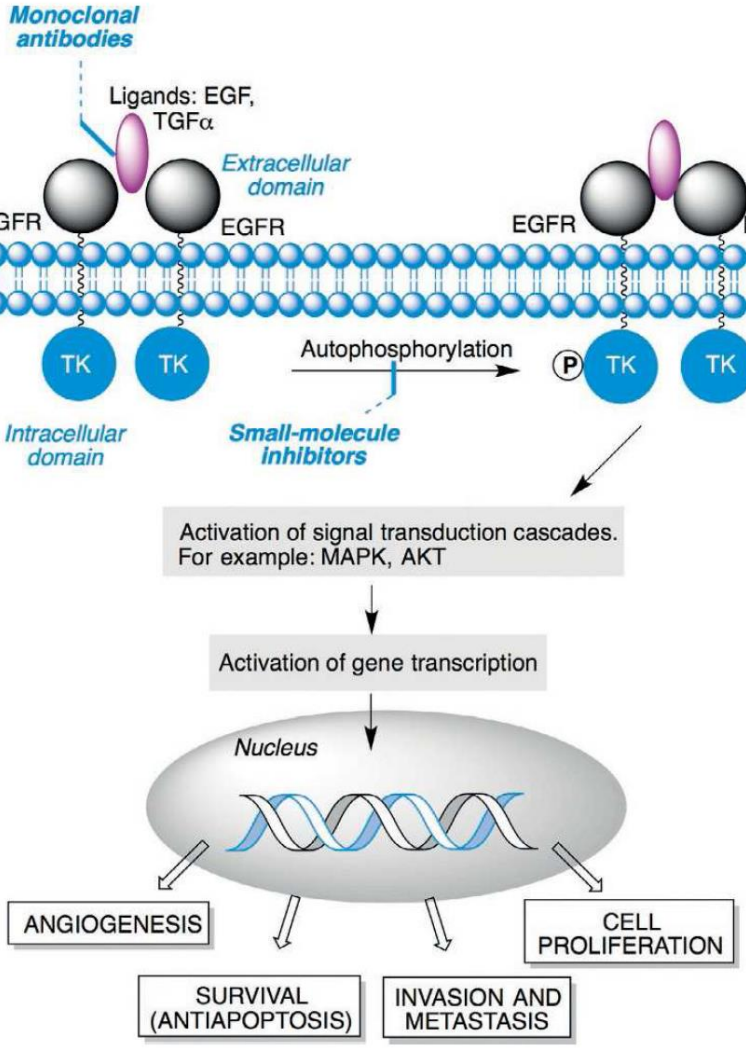


Figure 1.23. Mechanism of activation of EGFR showing possible sites for anti-EGF therapy. [128]

1.6. Aims and Objectives of the PhD

The main aim of this PhD project is the development of self-assembled prodrugs for targeted drug delivery at tumour resection sites. The approach used in this project is the design and synthesis of amphiphilic derivatives by linking gelator motifs such as amino acids using hydrolysable linkers to create prodrugs of the parent drug.

Two classes of anticancer therapy were selected, benzothiazole-based quinols (cytotoxic therapy) and tyrosine kinase inhibitors (molecularly targeted therapy). The drugs and drug candidates were selected with different scaffolds to explore the effect of molecular structure on self-assembly and also to investigate different approaches used to induce gelation.

The reason of selecting these two categories of cancer therapy is that many of these anticancer drugs suffer from toxicity or limited localisation at the tumour resection site. Therefore, creating self-assembled prodrugs of these compounds is thought to help overcoming these problems which restrict their clinical use.

Further objectives in this study is the characterisation of the synthesised derivatives to confirm the gelation behaviour. The techniques used are electron microscopy to investigate gel morphology and rheological experiments to study the mechanical strength of gels. Stability studies will be carried out to monitor the degradation of the prodrug to the parent compound and to determine their potential as controlled-release preparations for targeted cancer delivery.

In **chapter two**, preliminary gelation screening of five benzothiazole-quinols and four tyrosine kinase inhibitors was carried out by table-top rheology, i.e. vial inversion to determine the best promising compound for further gelation studies.

In **chapter three**, the self-assembling properties of the potent tyrosine kinase inhibitor, linifanib was further characterised by oscillatory rheology and microscopy. In addition, a library of eight structurally-related linifanib analogues was synthesised and tested for gelation to investigate the effect of slight structural modification on gelation.

In **chapter four**, the synthesis of acyloxyalkoxy carbamate prodrugs of linifanib will be reported. Gelation screening by vial inversion was carried out on the prodrugs.

In **chapter five**, the gelation behaviour of amide derivatives of linifanib will be described. A series of aliphatic amides, mono- and di-amino acid linifanib derivatives was synthesised and characterised for gelation. Positive gels were further characterised by rheology. Stability study for the amino acid linifanib derivatives was carried out to monitor their degradation to linifanib. The effect of pH on self-assembly behaviour was explored for the most promising linifanib derivatives.

Finally, in **chapter six**, a summary of results described above will be presented in addition to the plans for future work regarding further optimisation.

Chapter Two: Preliminary Gelation Screening of Selected Anticancer Agents

2.1. Introduction

One of the main challenges in cancer therapy is toxicity following systemic administration of the cytotoxic drugs. One of the approaches used to overcome this problem is through a localised drug delivery approach.[12,130-133] This means that the anticancer drug is administered locally at the tumour resection site which will improve the toxicity profile of the often non-selective anticancer drugs. Low molecular weight gelators (LMWGs) represent an important class for localised anticancer drug delivery.[12,134-136]

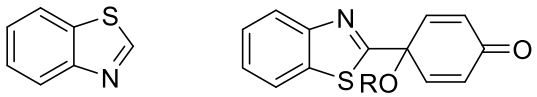
Indeed, low molecular weight gelators (LMWGs) are one of the promising novel drug delivery systems.[20,21,42,137] With regard to cancer therapy, one of the advantages of this drug delivery platform is the ability to design a controllable release of the active drug from the gel network using different mechanisms, such as the change in pH or through enzymatic hydrolysis.[21] These gelators can provide a sustained and controlled drug delivery within tumour resection site while minimizing the adverse effects of systemic drug administration. In addition, the use of LMWGs can overcome the poor solubility observed with many chemotherapeutic agents, minimising the required dose of drug and increasing the amount that reaches the tumour site.[138]

One of the approaches used for the design of new gelators is the understanding of the link between the known gelators and their structures, i.e. trying to find the structural features of these gelators which leads to formation of gels.[36] In this area, scientists have recognised some of these features such as the presence of physical intermolecular interactions which promote the aggregation of molecules such as hydrogen bonding, hydrophobic interactions and $\pi - \pi$ stacking.[139] Also, the existence of certain functional groups such as ureas promotes the unidirectional orientation essential for one-dimensional assembly.[140] Finally, conformational rigidity is an essential requirement for many LMWGs. This is because rigidity is thought to be responsible for decreasing the loss in entropy during aggregation of gelator molecules as in cholesterol which is an organogelator for various organic solvents.[141,142] In addition, rigidity of certain

sugar-based gelators was essential in directing the intermolecular hydrogen-bonding formed by the amide and hydroxyl groups.[18]

There are different approaches for treatment of solid tumours such as surgery, radiotherapy and drug treatment which is subdivided into chemotherapy and molecularly targeted therapy.[143] In this chapter, we will focus on the two classes of drug treatment: anticancer benzothiazoles (chemotherapy) and tyrosine kinase inhibitors (drugs which inhibit certain molecular targets overexpressed in tumour cells).

Benzothiazoles (Figure 2.1A) represent an important scaffold in cytotoxic anticancer drug design as a large number of benzothiazoles have showed cytotoxic activity against many tumours.[90] Benzothiazole-substituted quinols (Figure 2.1B) are an interesting class of these anticancer agents. They are compounds which showed good cell growth inhibition against various cancer cell lines.[91,99]



A B

Figure 2.1. Molecular structures of (A) benzothiazole scaffold and (B) benzothiazole substituted quinols

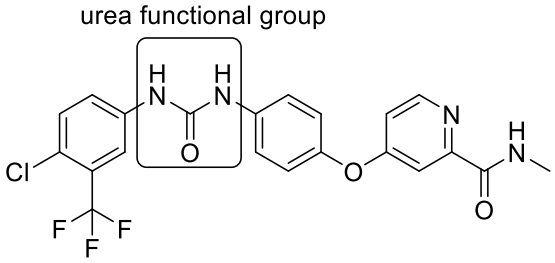
Whilst, tyrosine kinase inhibitors are designed to selectively inhibit specific tyrosine kinases which are overexpressed in tumours causing cancer cell proliferation and angiogenesis.[106]

Although there are a few preclinical studies demonstrating the efficacy of LMWGs in cancer based upon paclitaxel,[21,137,144-147] additional efforts in this field are still warranted to further explore other anticancer drugs.

In this chapter, a brief overview of selected anticancer agents will be discussed and the structural features related to gel formation will be illustrated for each example. An evaluation of the gelation features will be carried out to get an anticancer agent which self-assembles to form a gel. The criteria of selection of these drugs are the presence of structural features reported to be gelator motifs such as hydrogen bond donors and/or acceptors, aromatic rings (for $\pi - \pi$ stacking) and alkyl side chain (for the hydrophobic interactions). Then, preliminary gel screening will be reported. The compound(s) which demonstrates gelation will then be selected for further evaluation.

2.1.1. Sorafenib

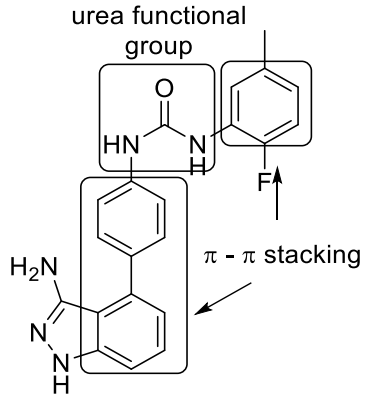
Sorafenib is a multi-targeted kinase inhibitor approved for the treatment of renal cell carcinoma and hepatocellular carcinoma.[143] It acts by inhibiting different tyrosine kinase inhibitors mainly proto-oncogene serine/threonine-protein kinase (Raf1) (IC_{50} 6 nM), vascular endothelial growth factor receptors (VEGFR) (IC_{50} 26 nM for $VEGFR_1$ and 90 nM for $VEGFR_2$) and platelet-derived growth factor receptors (PDGFR) (IC_{50} 57 nM).[148] Chemically, it is 4-[4-[[4-chloro-3- (trifluoromethyl) phenyl] carbamoylamino] phenoxy]- *N*-methyl-pyridine-2-carboxamide (**2.1**). This compound contains the urea functional group in its structure which is a structural feature reported in many LMWGs.[140]



2.1

2.1.2. Linifanib

This tyrosine kinase inhibitor (**2.2**) will be discussed in detail in Section 3.2. As with sorafenib, this anti-VEGF compound contains a urea functionality in addition to aromatic rings which are associated with possible $\pi - \pi$ stacking interactions.

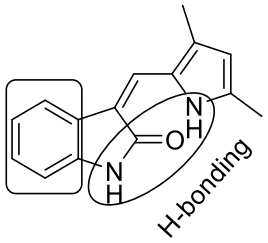


2.2

2.1.3. Semaxanib

Semaxanib is a small lipophilic multi-kinase inhibitor. It mainly inhibits $VEGFR_2$ (IC_{50} 1.23 μM).[149] It was an investigational drug in phase III clinical

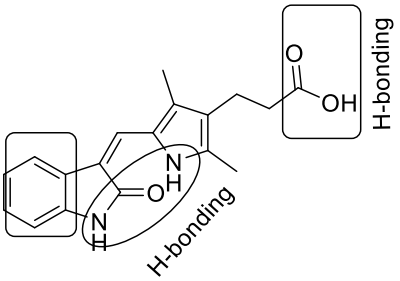
drug development for treatment of colorectal cancer.[149] Chemically, it is (3*Z*)-3-[(3,5-dimethyl-1*H*-pyrrol-2-yl)methylidene] -1,3-dihydro-2*H*-indol-2-one (**2.3**). This compound contains hydrogen bond donors and acceptors in addition to aromatic functional groups for possible $\pi - \pi$ interactions.



2.3

2.1.4. Orantinib

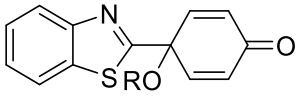
Orantinib is an oral tyrosine kinase inhibitor. It inhibits PDGFR (IC_{50} 8 nM) $VEGFR_2$ (IC_{50} 2.1 μM, and FGFR (IC_{50} 1.2 μM).[150] It is under clinical drug development for treatment of hepatocellular carcinoma.[151] Chemically, it is (Z)-3-(2,4-dimethyl-5-((2-oxoindolin-3-ylidene)methyl)-1H-pyrrol-3-yl)propanoic acid (**2.4**). This compound has the same structural features of semaxanib in addition to the carboxylic functional group.



2.4

2.1.5. Benzothiazole-substituted quinols

These cytotoxic compounds were thought to act on thioredoxins protein family. These proteins are oxidoreductase enzymes. Thioredoxin reductase enzyme is overexpressed in many tumours such as in colorectal cancer. These derivatives of quinols (**2.5-2.9**) show good cell growth inhibition against different tumours *in vitro* as well as *in vivo*.[91] Also, benzothiazoles have been reported as both anticancer hydrogelators[152] and organogelators.[153]



2.5 R = H
2.6 R = Me
2.7 R = Et
2.8 R = *n*-Pr
2.9 R = Ac

2.2. Results and Discussion

Tyrosine kinase inhibitors are extensively studied for treatment of various cancers. These anticancer agents target different enzymes of the tyrosine kinase family such as VEGFRs, PDGEF, EFGF … etc. These receptors are overexpressed in cancer cells making them good targets for therapy. However, many of these therapeutics suffer from serious adverse effects resulting from systemic administration. This is because these receptors are expressed in different organs of the body and not limited to tumours only. In addition, poor water solubility limits their dose.[137] The use of local drug delivery in the formulation of these drugs is thought to significantly minimise these unwanted side effects. Low molecular weight gelators are one of the novel drug delivery systems intended to deliver drugs locally. The intended molecular gel will be formed through the self-assembly of these gelators. The chemotherapeutic will then be released after injection into the tumour or tumour resection site.

In this chapter, we have screened therapeutic agents which contain the previously mentioned structural features for gelation using table-top rheology.

We selected four tyrosine kinase inhibitors in order to investigate their gelation potential. Sorafenib and linifanib have biaryl urea functionality in their structures. Orantinib and semaxanib are pyrrole-containing compounds with hydrogen bond donors and acceptors. Initially we will report the synthesis of semaxanib and orantinib. Sorafenib was purchased from CarboSynth and linifanib will be discussed in detail in chapter three.

With regard to benzothiazole-substituted quinols, a library of six derivatives were synthesised and screened for gelation. Different terminal alkyl groups were selected to evaluate the effect of the nature and length of side chain on the self-assembly of the resulting compounds. The length of the side chain can influence the hydrophobicity of these compounds (c log P) in addition to its impact on the molecular packing which is an essential feature for the one-dimensional order and hence self-assembly of the molecule.

The physicochemical properties of these anticancer agents which are important for gelation are shown in Table 2.1.

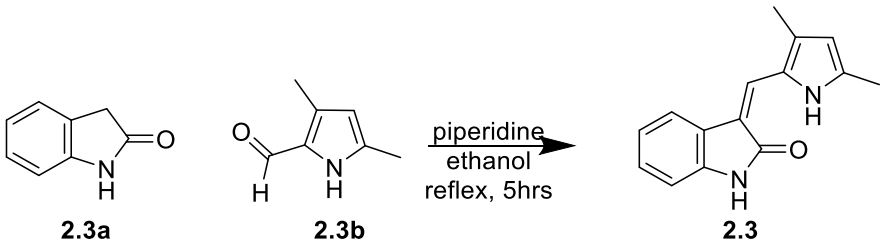
Table 2.1. Hydrgen bonding, lipophilicity (clog P) and aromaticity of compounds 2.1-2.9. HBD: hydrogen bond donor, HBA: hydrogen bond acceptor

Compound	HBD	HBA	clog P	Aromaticity
2.1	3	7	5.45	++
2.2	6	5	4.49	+++
2.3	2	3	2.83	+
2.4	3	4	2.34	+
2.5	0	3	0.60	-
2.6	0	3	1.44	-
2.7	0	3	1.83	-
2.8	0	3	2.36	-
2.9	0	4	1.46	-

2.2.1. Synthesis

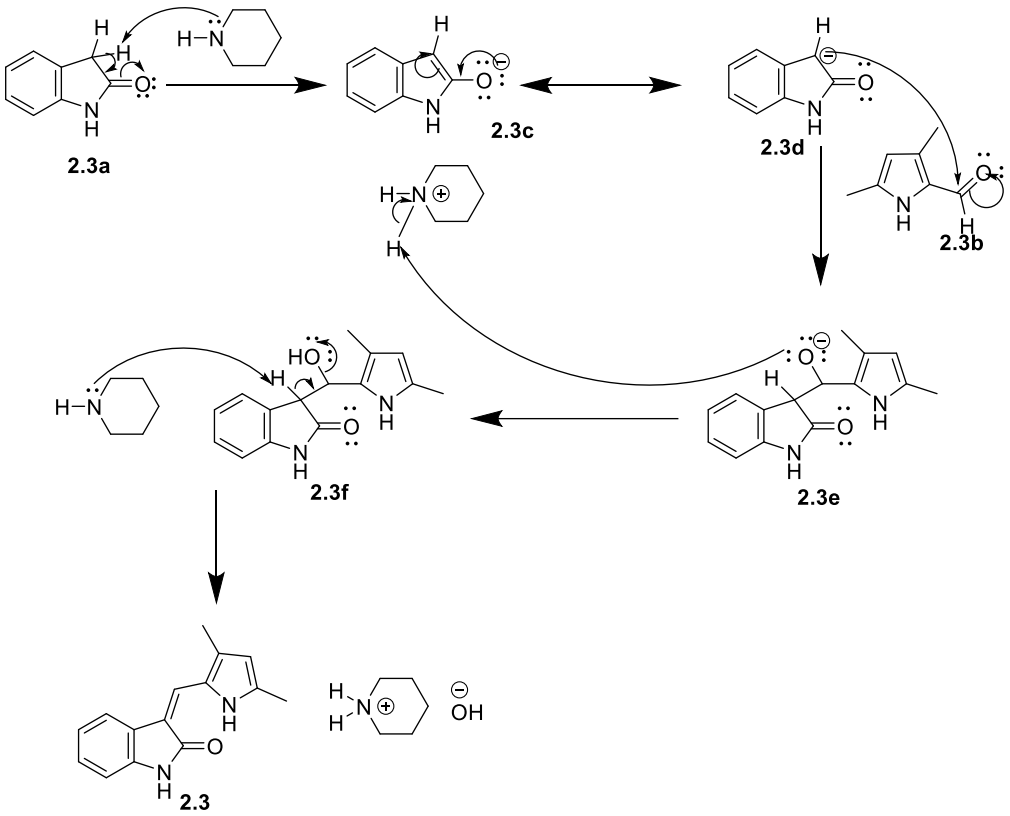
2.2.1.1. Semaxanib

Semaxanib was synthesised through Knoevenagel condensation of compound (**2.3a**) with the aldehyde (**2.3b**) using piperidine as the base and ethanol as the solvent. The crude product was purified by washing with ethyl acetate to get the final product, semaxanib (**2.3**) with 85% yield (Scheme 2.1).



Scheme 2.1. Synthesis of semaxanib (2.3)

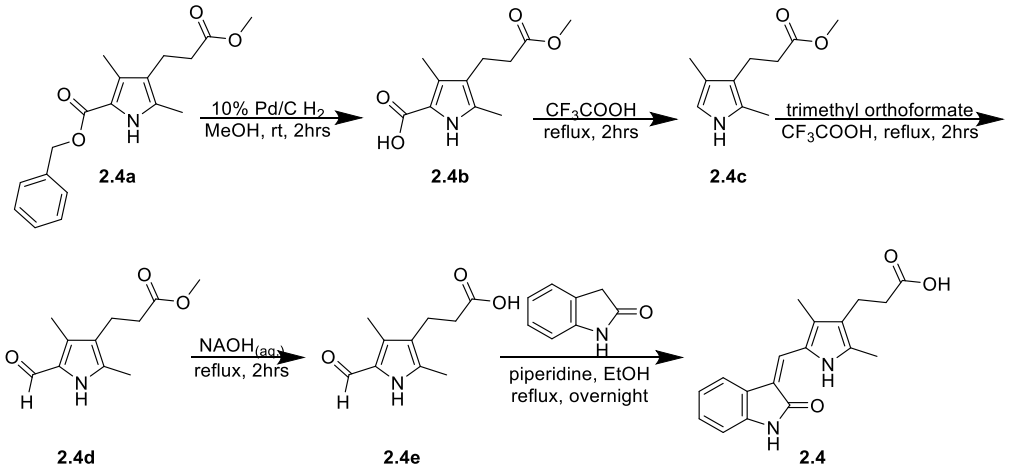
The mechanism of Knoevenagel condensation involves the deprotonation of the oxindole (**2.3a**) by the piperidine to form the enol intermediate (**2.3c**). The enol formed (**2.3d**) then attacks the carbonyl group of the aldehyde (**2.3b**) to form the aldol (**2.3f**). Subsequent base induced elimination results in the formation of final product (**2.3**) (Scheme 2.2).



Scheme 2.2. The mechanism of Knoevenagel condensation used to form semaxanib

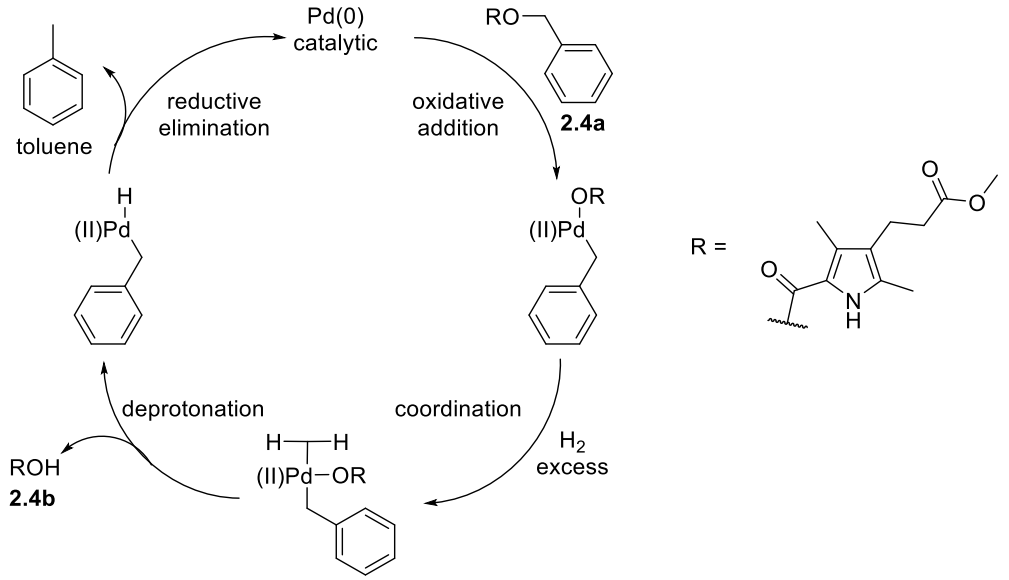
2.2.1.2. Orantinib

Orantinib was synthesised starting from 4-(2-methoxycarbonylethyl)-3,5-dimethyl-*1H*-pyrrole-2-carboxylic acid benzyl ester **(2.4a)** which is hydrogenated using 10% wt palladium in carbon to form the intermediate (**2.4b**). This intermediate was decarboxylated using trifluoroacetic acid resulting in the formation of compound (**2.4c**). Formylation of this intermediate at the 3-position was achieved using trimethyl orthoformate leading to the formation of compound (**2.4d**) which was subsequently hydrolysed using aqueous sodium hydroxide to form the intermediate **(2.4e)**. Condensation of the indolinone with the intermediate (**2.4e**) using piperidine gave the final product, orantinib (**2.4**) (Scheme 2.3).



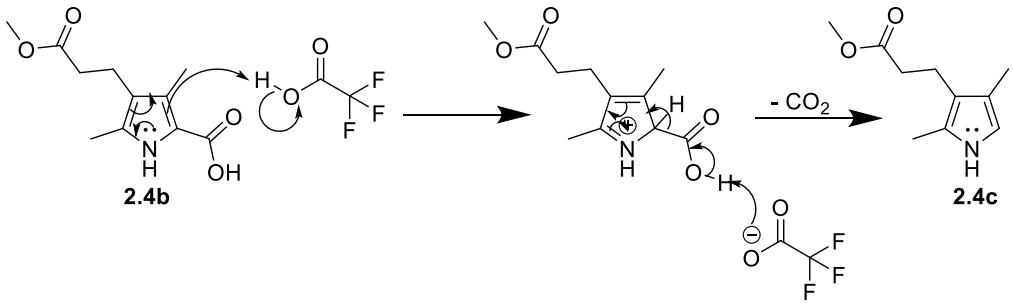
Scheme 2.3. Synthesis of orantinib (2.4)

Hydrogenation step starts with the oxidative addition of palladium catalyst to compound (**2.4a**) followed by coordination and deprotonation to eliminate the deprotected compound (**2.4b**). Reductive elimination results in regeneration of palladium (0) catalyst and elimination of toluene as shown in Scheme 2.4.



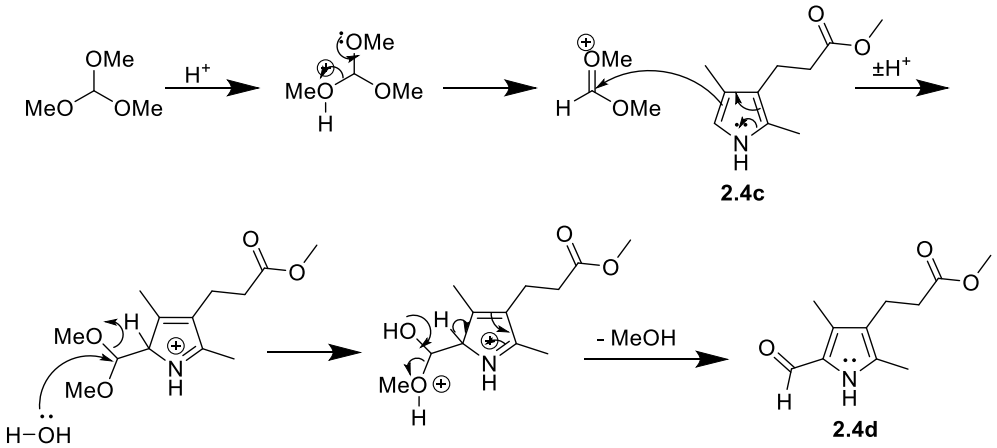
Scheme 2.4. Mechanism of hydrogenation of compound (2.4a)

This intermediate undergoes acid catalysed decarboxylation using trifluoroacetic acid. Rearrangement leads to the formation of the decarboxylated product (**2.4c**) (Scheme 2.5).



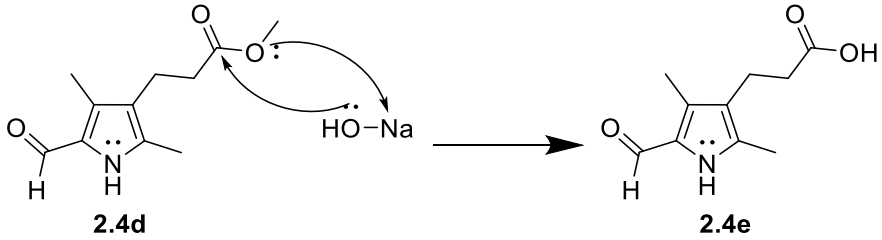
Scheme 2.5. Mechanism of decarboxylation of intermediate (2.4b)

The next step will be the formylation of the intermediate (**2.4c**) which will be achieved by using trimethyl orthoformate and trifluoroacetic acid. Water is then added leading to formation of the formylated intermediate (**2.4d**).



Scheme 2.6. Mechanism of formylation of intermediate (2.4c)

Ester hydrolysis of intermediate (**2.4d**) was achieved with aqueous sodium hydroxide solution leading to the formation of compound (**2.4e**)



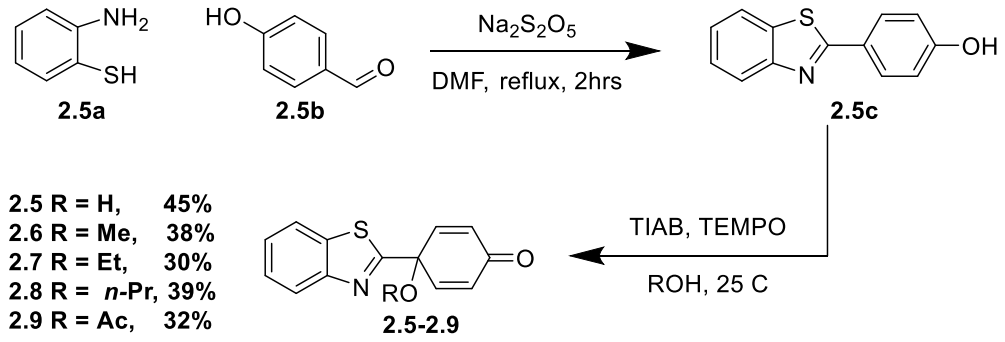
Scheme 2.7. Mechanism of ester deprotection of compound (2.4d)

The final step is the Knoevenagel condensation (Scheme 2.2) of the indolinone and compound (**2.4d**) results in generation of the final product, orantinib (**2.4**).

2.2.1.3. Benzothiazole-derived quinols

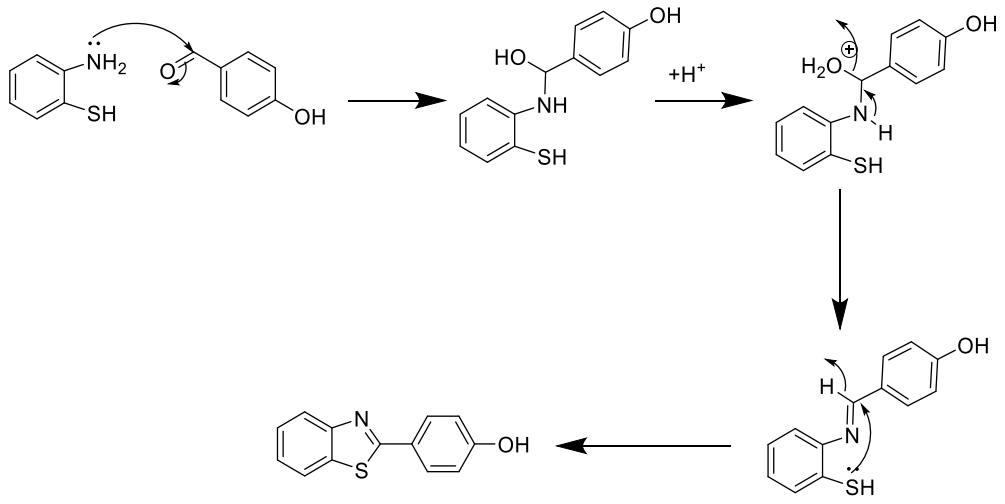
Synthesis of quinol derivatives (**2.5-2.9**) was achieved by reacting 2-aminothiophenol (**2.5a**) with 4-hydroxybenzaldehyde (**2.5b**) using sodium metabisulphite ($Na_2S_2O_5$) as a catalyst leading to the formation of the

intermediate (**2.5c**). This intermediate was oxidised using the hypervalent iodine oxidising agent *bis*(trifluoroacetoxy)iodo]benzene (TIAB) as oxidant and 2,2,6,6-tetramethyl-1-piperidinyloxy (TEMPO) as a radical quenching agent to yield the final product which depended on the solvent used, e.g. acetic acid, methanol, … etc. (Scheme 2.8).



Scheme 2.8. Synthesis of quinol derivatives (2.5-2.9)

The intermediate (**2.5c**) was created through imine formation between the amino group of the aminothiophenol and the substituted benzaldehyde as shown in Scheme 2.9.



Scheme 2.9. Mechanism of formation of intermediate 2.5c.

2.2.2. Preliminary gelation screening

Table-top rheology is used as a preliminary simple test for gelation.[53] It is useful in determining the temperature of gelation. Different methods are used such as dropping ball in which a small ball is put on the top of gel during heating, the temperature of gelation is the temperature at which the ball falls through the

viscous fluid. Another method is the vial inversion in which a gel is formed and after cooling the vial is inverted. If the gel remains stable without flowing, this indicates that the sample has a degree of elasticity.[53] These tests provide a preliminary screen of gelation. However, they are subjective assessments in that viscous solutions may be easily mistaken as a gel.[18]

Initial gelation screening was performed on the selected tyrosine kinase inhibitors as well as benzothiazole-derived quinols using the vial inversion test to investigate gel formation. The method used was a solvent switch method where gels were formed by dissolving the compound in DMSO, followed by adding water at 60 °C. The solvent mixture was chosen as DMSO is a very good solvent for poorly water-soluble compounds. These compounds are insoluble in water alone at the required concentration.

Indeed, it is an essential requirement for gelation that there is solubility in the solvent before starting self-assembly process and the formation of the gel. When water is then added to the DMSO solution there is a change in the solubility of gelator triggering the gelation process.[154]

In addition, DMSO was selected because it has been investigated for its ability to improve drug delivery of some therapeutic agents and it is included in certain formulations of polymeric pharmaceuticals.[155] This solvent should also be used with caution as it has some unwanted adverse effects.[155]

Finally, there are some reports showing that DMSO caused positive effects on some ovarian and pancreatic cancers in reducing the tumour mass.[156,157]

For these advantages, DMSO was the recommended organic solvent in creating self-assembled gels to be used in localised cancer drug delivery.

Vial inversion tests were performed on tyrosine kinase inhibitors (**2.1-2.4**) and benzothiazole-based quinols (**2.5-2.9**). All of these compounds were tested at concentration of 0.5% w/v and 5 to 50% (v/v) DMSO/ water. Observations were made within 1 hour after cooling to room temperature. Outcomes of gelation screening were recorded in Table 2.2.

Table 2.2. Data table of vial inversion tests of 0.5% (w/v) compounds (2.1-2.9) in 5-50%(v/v) DMSO/water at room temperature. G: gel, P: precipitate, S: solution

Compound / %DMSO	2.1	2.2	2.3	2.4	2.5	2.6	2.7	2.8	2.9
5	P	G	P	P	P	P	P	P	P
10	P	G	P	P	P	P	P	P	P
15	P	G	P	P	P	P	P	P	P
20	P	P	P	P	P	P	P	P	P
25	P	P	P	P	P	P	P	P	P
30	P	P	P	S	S	P	P	P	S
40	S	S	S	S	S	S	S	S	S
50	S	S	S	S	S	S	S	S	S

It can be noticed that three of the tyrosine kinase inhibitors (**2.1, 2.3** and **2.4**) failed in gelation tests and demonstrated either precipitation or solutions. Whereas linifanib (**2.2**) formed gels instantly at 5 to 15% (v/v) DMSO ratios followed by precipitation and solution. With regard to benzothiazole-based quinols, all of the five derivatives (**2.5-2.9**) exhibited either precipitation (at low DMSO solvent ratios) or solution (at higher DMSO solvent ratios).

To understand these results, it is useful to describe the established methods for the design of new low molecular weight gelators. In the early development of LMWGs, property-based design was used to design new gelators. This approach focused on the structure-property relationships of some known gelators by making slight changes in the molecular structure to identify the structural features contributing to gelation. Upon development of solid-phase synthesis, the design of new gelators used this technique for creation of libraries of new chemical structures through slight modification of a known gelator molecule. This helps in evaluation of gelation property of large number of compounds in short time period. This approach can be compared to combinatorial synthesis in drug discovery. The third approach is the structure-based approach which involves the construction of design criteria for new gelators. These criteria are originated from the large number of gelators reported in the literature. According to these design rules, a gelator molecule should have certain features

such as presence of different molecular interactions, hydrogen bond donors and/or acceptors, some factors which prevent crystallisation, functional groups which promote the one-dimensional order and balance of hydrophobic and hydrophilic parts. The last approach is using a known gelator as a scaffold for designing new gelators. This means that the gelator molecule is modified without changing the features responsible for gelation. This approach is similar to the property-design method, but is used to improve some of gelator properties instead of formulation of a new gelator.[36]

These results are not unexpected as most gelators described in the literature have been discovered by one of the above-mentioned approaches which depend on the screening of the proposed compounds for gelation and building the design rules based on screening outcomes. In most cases, a slight change in the structure of a gelator molecule can cause the compound to be a non-gelator. In addition, as gelation is a kinetically trapped state, it ends with crystallisation of the metastable gel instead of evolution of the true gel in many cases. Therefore, it is hard to tell if the compound which fulfils the gelator requirements will be a true gelator until it is evaluated experimentally for gelation.[158]

Linifanib is one of the most rigid VEGF inhibitors.[159] Rigidity is thought to be one of the triggers for gel formation through supporting strong aggregation of molecules.[36] In addition, it contains higher number of hydrogen bond donors and acceptors in comparison to the rest of compounds studied.[159] Finally, linifanib molecule is found to be planar[159] and this is thought to contribute to its gelation. However, further investigation is needed to confirm the structural features which promote self-assembly of linifanib molecules.

2.3. Conclusions

In this chapter, we have reported the synthesis and preliminary gelation screening of two classes of anticancer agents, four tyrosine kinase inhibitors (targeted therapy) and five benzothiazole-based quinols (cytotoxic anticancers). These compounds have different scaffolds and were selected to investigate their gelation and to find the best compound with gelation properties.

Preliminary gelation screening was performed using solvent and temperature switch method with DMSO/water mixtures ranging from 5 to 50% v/v. These experiments revealed that linifanib was the only compound which demonstrated stable gels at DMSO/water mixtures range of 5 to 15%. This is thought to be due to the high number of hydrogen bond donors/acceptors and structural rigidity. Therefore, this tyrosine kinase inhibitor was selected to undergo a series of characterisation experiments to explore the relationship between structure and gelation. This work will be described in the next chapter.

Chapter Three: Linifanib as a Multi-targeted Tyrosine Kinase Inhibitor and a Low Molecular Weight Gelator

In chapter two, we reported the preliminary gel screening of a number of anticancer agents. These results revealed that linifanib was a promising gelator. Therefore, in this chapter we will review urea-based low molecular weight gelators as the urea functional group is a key part of the linifanib pharmacophore important for biological activity. Our hypothesis is that both urea and the aromatic ring promote the self-assembly of linifanib molecules. Investigation of this hypothesis was achieved synthesis of a library of structurally – related analogues of linifanib by modification of aromatic ring substituents and urea functional group. Finally, a detailed characterisation of linifanib gels will be carried out to provide an insight to the strength and morphology of this gelator.

3.1. Introduction

One of the main approaches of designing LMWGs is the introduction of functional groups which promote self-assembly through physical forces such as van der Waals interactions, π–π stacking and hydrogen bonding. The urea functional group is one of the important groups considered as a gelator motif.[140] It is both a hydrogen bond donor and acceptor. This property is favoured in creating one dimensional assembly leading to gel formation.[140] The two urea N – H hydrogens can form hydrogen bonds along with the carbonyl oxygen of adjacent urea forming six – membered hydrogen bonding rings. This type of linkage is called an α-urea tape.[160]

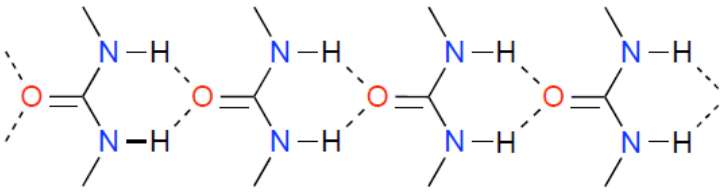


Figure 3.1. Urea hydrogen bond urea α-tape.[160]

The strong unidirectional character of the urea functional group leads to the growth of strong fibres and hence gel formation. To explain this in more detail,

we can suggest a *bis* (urea) gel as the primary structure created from strands linked by hydrogen bonding. Secondary structure of the gel is made up from groups of strands which will ultimately form fibres of relatively similar diameter. Then 3D gel network will be formed by entanglement and crosslinking of these fibres through physical interactions.[160] This process is represented in Figure 3.2

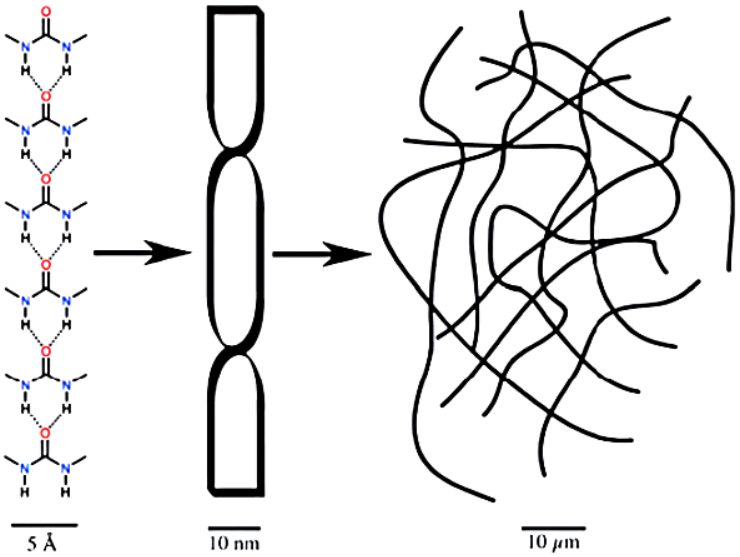
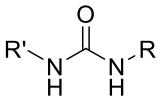


Figure 3.2. Schematic representation of primary, secondary and tertiary structure of self-assembly process of urea-based gelator.[160]

The strong unidirectional character of this structure described above explains why this functional group is widely used in the design of low molecular weight organo- and hydro-gelators. Different examples of mono-, *bis*- and *tris*-urea gelators will be described to provide a general picture of the literature regarding urea-based LMWGs.

Weiss and co-authors prepared a series of urea and thiourea-based organogelators. The urea-based gelators consisted of urea functional group substituted by *n*-alkyl side chain (**3.1**). Gelation experiments were conducted using numerous organic solvents. Most of these compounds formed organogels with silicone oil and toluene. Further characterisation studies (infra-red, SEM, X-ray diffraction … etc.) on stable gels of this series showed that hydrogen bonding was the main driving force of gelation and also responsible for different molecular packing within the gel network. Additionally, it was found that urea-

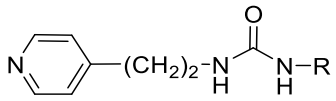
based gelators were more efficient in gel formation than their thiourea analogues.[161]



R = C_nH_{2n+2}, n = 1-18

3.1

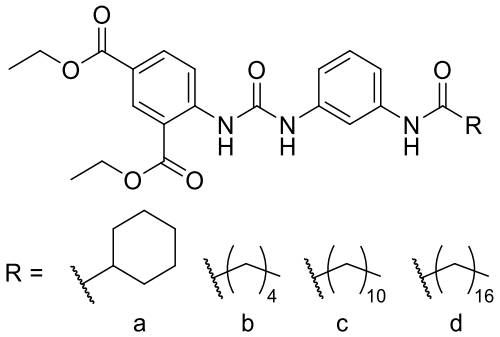
In addition, Takemura *et al.* reported the synthesis of three mono urea derivatives with pyridyl groups (**3.2**). A vial inversion, for gels prepared by heating/cooling, showed no gel formation for all derivatives. However, addition of silver(I) pentafluoropropionate ($AgC_2F_5CO_2$) to these solvents resulted in the formation of gels for the urea-based derivative (**3.2**, n=7) with aromatic solvents such as benzene, *p*-xylene and tetralin. The interaction between silver(I) with pyridyl group was thought to form coordination complexes facilitating the self-assembly. Also, the interaction of these gelators was through intermolecular hydrogen bonding of the urea functional groups.[162]



R = $-(CH_2)_nCH_3$, n = 5, 7, 11

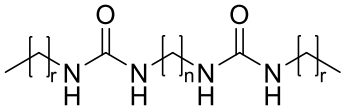
3.2

The Hayes group investigated the gelation properties of four diaryl urea derivatives (**3.3**). These compounds were tested for gelation of different organic solvents. The derivative (**3.3a**) formed gels with chloroform, dichloromethane and ethanol, whereas (**3.3b**) gelled only chloroform. Analogues (**3.3c, d**) share the same gelation behaviour and demonstrated gelation with chloroform, dichloromethane and toluene. Rheological studies showed that the storage modulus (G') increased with increasing the concentration due to the increased density of the hydrogen bonding.[163]



3.3

The presence of two or more urea groups in the gelator structure was investigated in order to enhance the strength and unidirectional character of urea hydrogen bonds. In addition, the nature of other substituents is thought to play an important role in optimisation of self-assembly process.[164] Therefore, a library of *bis*(urea) compounds (**3.4-3.9**) was synthesised (Figure 3.3).



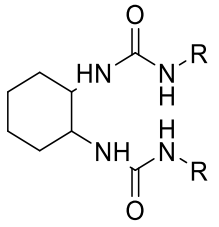
	R	n
3.4	*n*-dodecyl	$-(CH_2)_6-$
3.5	*n*-dodecyl	$-(CH_2)_9-$
3.6	*n*-dodecyl	$-(CH_2)_{12}-$
3.7	*n*-dodecyl	4,4'-biphenyl
3.8	benzyl	$-(CH_2)_9-$
3.9	*(R)*-1-ethylphenyl	$-(CH_2)_9-$

Figure 3.3. Library of *bis*(urea) derivatives 3.1-3.6

These compounds formed fibres after cooling from hot solutions leading to gelation in organic solvents. Compound **3.5** was the most potent one in terms of gelation; it promoted gelation of different organic solvents at very low concentration (<3 mg/mL). These compounds also demonstrated an excellent long-term gel stability.[164]

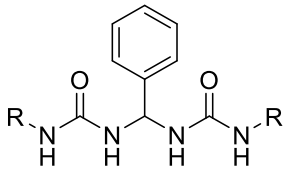
Another *bis*(urea) gelator is compound **3.10** which is based on cyclohexane, a more rigid scaffold. This compound was found to be a very good gelator for both polar and nonpolar solvents. The solvent effects on gelation were investigated for this gelator using various alcohol solvents. Rheological

measurements were performed on this gel to investigate the effect of solvent on the mechanical strength. Results showed that the dynamic modulus (G^{∞}) increased in the order 1-octanol < 1-hexanol < 1-butanol < 1-propanol meaning that there is direct relationship between solvent polarity and dynamic mechanical strength. [165,166]



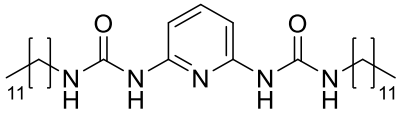
3.10

In addition, geminal *bis*(urea) compounds were also investigated for their gelation properties. Again, these compounds such as **3.11** were found to be capable of forming gels with many organic solvents with similar behaviour to compounds **3.10**. This study confirmed the unidirectional molecular interaction by the use of NMR and molecular modelling. [167]



3.11

Interestingly, the pyridine-based geminal *bis*(urea) gelator **3.12** demonstrated different gelation behaviour. This was thought to be due to the role of pyridine as a hydrogen bond acceptor which will form intra-molecular hydrogen bonding with the urea group.



3.12

The enhanced self-assembly of gelator **3.12** was the result of combined effect of intra- and inter-molecular hydrogen bonding between the gelator molecules as shown in Figure 3.4.[168]

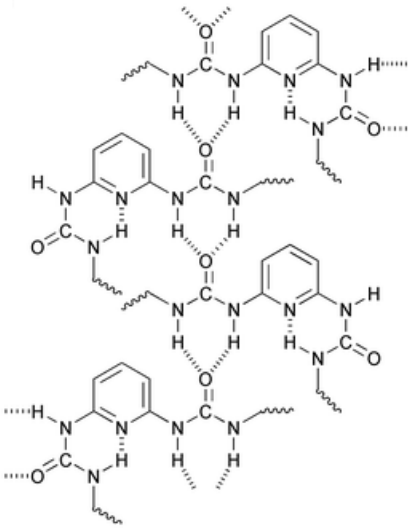
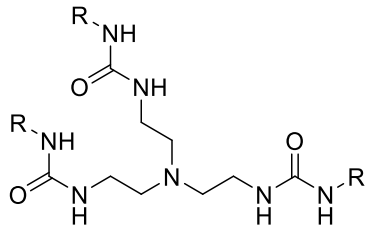


Figure 3.4. Inter- and intra-molecular hydrogen interactions between molecules of gelator 3.12. [168]

Regarding *tris*(urea) gelators, multiple urea groups can modify strength of the gel because they provide additional hydrogen bonding interactions. However, there are few studies focused on *tris*(urea) gelators compared to *bis*(urea) gelators. This may be due to their low solubility in nonpolar solvents.[140] Compounds **3.13** were known gelators due to their ability to complex phosphates and some metal ions. It was found that gelation stability of these compounds was not substantially different as compared to their *bis*(urea) analogues. This could be because of the formation of intra-molecular hydrogen bonding which reduced the inter-molecular bonding required for aggregation of molecules and this was confirmed by X-ray analysis.[169]



R = n-alkyl, aryl or substituted aryl

3.13

Overall, the urea functional group is widely used to create low molecular weight gelators for both aqueous and organic solvents. The urea functional group (as a hydrogen bond donor and acceptor) in addition to the aromatic rings (which cause $\pi - \pi$ stacking) were considered to the promoting factors for self-assembly of the potent tyrosine kinase inhibitor, linifanib.

3.2. Linifanib

Linifanib is an orally active multi – targeted receptor tyrosine kinase inhibitor previously developed and progressed into clinical trials to treat advanced or metastatic non-small cell lung cancer and renal cancer. Chemically, it is (1-[4-(3-amino-1H-indazol-4-yl)phenyl]-3-(2-fluoro-5-methylphenyl) urea) (Figure 3.5). This compound was designed to act as a vascular endothelial growth factor (VEGF) and a platelet-derived growth factor receptor (PDGF) inhibitor.[170] Linifanib is a very potent VEGF inhibitor with an IC_{50} of 3 nM for $VEGFR_1$ and 4 nM for $VEGFR_2$.[171]

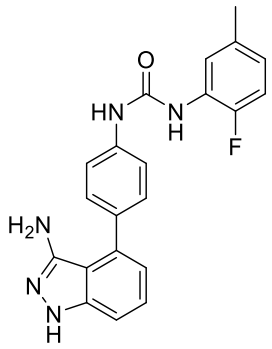


Figure 3.5. Chemical structure of linifanib.

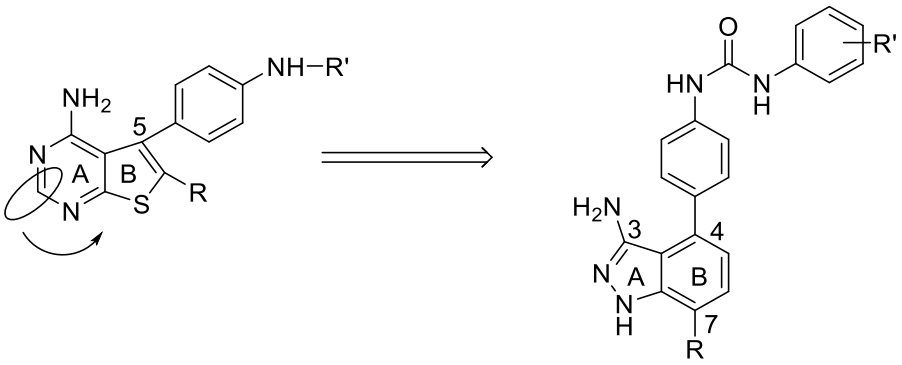
1.1.1. Chemistry and rational drug design

Different mechanisms participate in cancer progression. One of these mechanisms involves the role of receptor tyrosine kinases (RTKs) in tumour growth such as VEGF, PDGF and others which contribute to tumour growth through the process of angiogenesis.[172] It is suggested that the design of multi-targeted inhibitors is better than selective treatment because these inhibitors have the ability to stop multiple mechanisms which contribute to tumour progression.[173,174]

The efforts to find novel and potent tyrosine kinase inhibitors resulted in identification of a group of compounds containing thienopyrimidine urea moiety which proved potent inhibition of VEGF and PDGF receptor families.[175] The thienopyrimidine portion bound to the ATP component of the $VEGFR_2$ hinge region through hydrogen bonding. The *N,N'*-diaryl urea component extended to the hydrophobic region of the VEGF receptor and it was responsible for the affinity of the inhibitor to the enzyme. Diaryl urea is a privileged structure in anticancer agents.[176] Therefore, it was decided that the urea portion should be

retained in the design of new $VEGFR_2$ inhibitors. This template should have two important characteristics: the ability to form hydrogen bonds with the $VEGFR_2$ hinge region and the optimum orientation of the diaryl urea to interact with the hydrophobic pocket of the enzyme. As a result, the structure of thienopyrimidine (**3.14)** and (**3.15)** was converted into 3-aminoindazole derivatives (**3.16)** as shown in Figure 3.6 to achieve these features. The 3-amino group and the ring nitrogen (N2) should mimic the adenine of ATP to form two hydrogen bonds with the hinge region of the enzyme. The endocyclic nitrogen could provide a third position for hydrogen bonding. In addition, the presence of diaryl urea at the C4 position of the indazole provided the optimum orientation to interact with the hydrophobic pocket.[177]

A series of 3-aminoindazole urea compounds was synthesised with different modifications of R and R' groups to explore the effect of these substitutions on the inhibitor affinity to the enzyme. The screening of these compounds indicated that the compound **3.14** with R = H and R' = 2-F-5-methyl was the most potent for both $VEGFR_2$ and PDGFR. This compound was extensively studied for its pharmacokinetic properties then progressed to clinical evaluation of its anticancer activity. Indeed, linifanib was progressed to phase III clinical trial development.[177]



3.14: R = Me, R' = H **3.16**

3.15: R = Me, R' = CONH(*m*-tolyl)

Figure 3.6. Rational design of 3-aminoindazole urea RTK inhibitors.[177]

1.1.2. Mechanism of action and related toxicity

Linifanib inhibits $VEGFR_2$ leading to significant inhibition of angiogenesis which contributes to several pathological conditions such as tumour growth and

diabetic retinopathy. As shown in Figure 3.7, it forms three hydrogen bonding interaction with the receptor catalytic site. The first one is between the external NH of the urea with Glu885 carboxylate group, the second bond is between the amino group of indazole and Glu917 carbonyl group and the last interaction is between the ring nitrogen and Cys919 NH.[177]

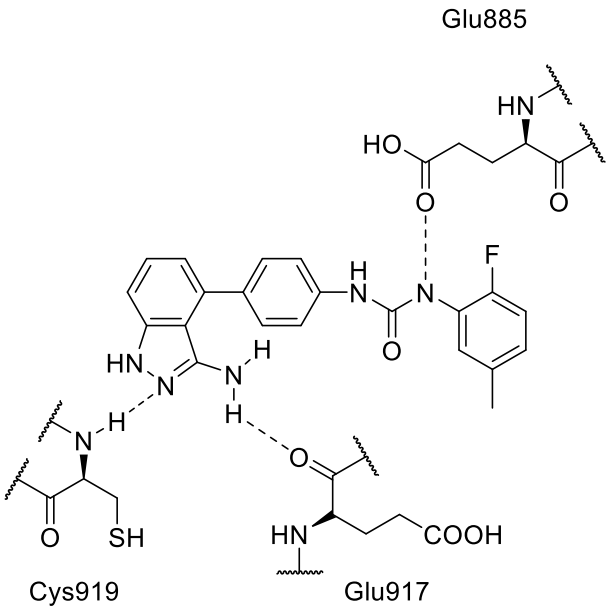


Figure 3.7. Binding of linifanib to catalytic site of VEGF2 receptor. [177]

Linifanib showed a promising activity profile during pre-clinical and early clinical trials.[178,179] This VEGF inhibitor was tested against various solid tumours such as non-small cell lung cancer,[180] renal cancer,[181] colorectal cancer[182] and hepatocellular carcinoma.[183] However, in phase III trials this drug candidate had some challenges related to its efficacy and toxicity profile especially with increasing the dose. In a clinical trial of linifanib in hepatocellular carcinoma, 1035 patients received linifanib with a dose of 17.5 mg daily. The main adverse effects recorded were grades 3 and 4 hypertension (54%) encephalopathy, ascites and hyperbilirubinemia (20%).[184] In their recent expert review of linifanib, Zucchini *et al.*[171] stated that further efforts should be focused on overcoming challenges related to this VEGF inhibitor toxicity profile.

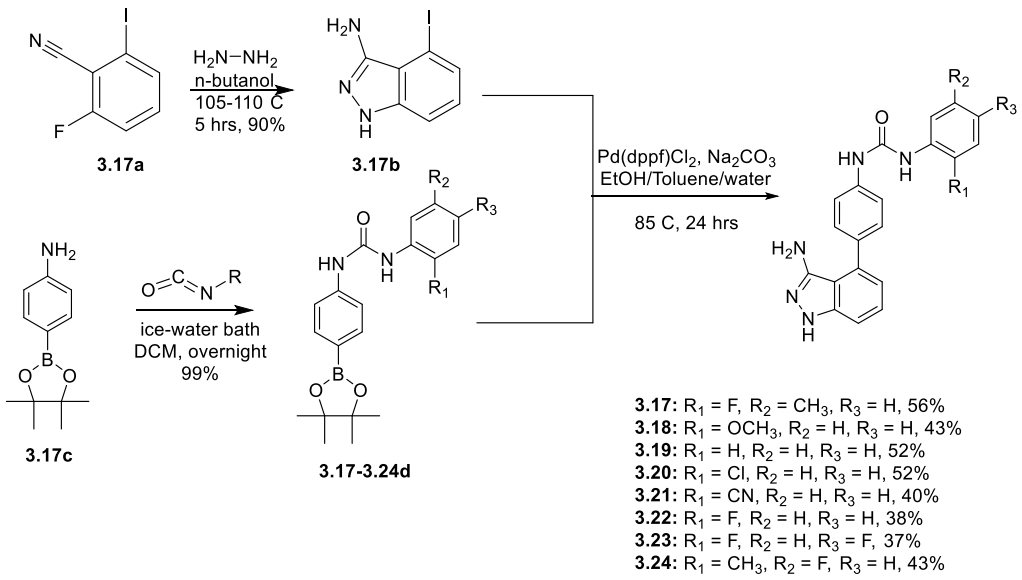
3.3. Results and Discussion

There have been many reports regarding LMWG which indicate that the urea functionality is an important structural common feature in many hydrogelators.[140, 18, 185,186,17] Linifanib, which is a structurally novel anti – VEGF inhibitor, includes urea in its structure and that is why it was selected to explore its ability to act as a hydrogelator. Linifanib also contains aromatic rings flanking the urea functional group, which is reported to promote π–π stacking interactions which in turn have the potential to trigger self-assembly.[187]

Based on our hypothesis of both the urea functional group and the aromatic rings promoting gelation in linifanib, we synthesised seven close analogues by modification of the substituents on the terminal aromatic ring adjacent to the urea (**3.17-3.24**) and an additional analogue containing an amide group instead of the urea group (**3.25**). The amide was chosen since it also can provide complimentary hydrogen bonding interactions required to promote self-assembly.[18] Consequently, the gelation studies of these analogues may lead to the structure gelation relationship i.e. to identify which part of the structure of linifanib is responsible for gelation. Prior to discussion of this data we will review the synthesis of linifanib and its analogues by a 3-step reaction – the most important step being the Suzuki coupling between the urea boronate (**3.17d**) and the iodoindazole (**3.17b**).

3.3.1. General mechanism of synthesis of linifanib and its analogues:

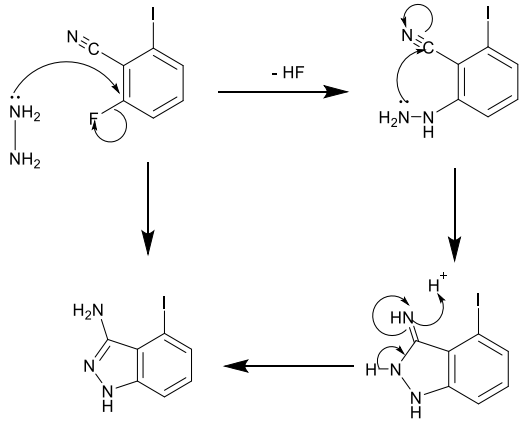
The general outline of synthesis of linifanib and its analogues (**3.17-3.24**) is shown in Scheme 3.1.



Scheme 3.1. General synthesis of linifanib and its analogues (3.17-3.24)

3.3.2. Iodoindazole synthesis

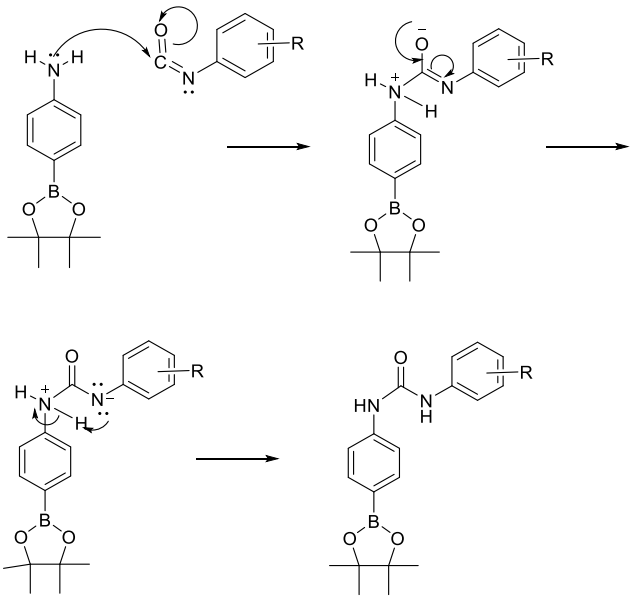
The first step involves the conversion of benzonitrile **(3.17a)** into the indazole **(3.17b)** in presence of hydrazine. Hydrazine is incorporated by substitution of the aryl fluoride followed by cyclisation. The elimination of the hydrazine resulted in the iodo-indazole formation as shown in Scheme 3.2.



Scheme 3.2. Mechanism of iodo-indazole formation

3.3.3. Urea boronate synthesis

The second step is the formation of urea boronate by the reaction between boronic acid and the corresponding isocyanate. The reaction proceeds by nucleophilic attack of the carbonyl carbon by the unshared pair of electron of the aryl amine group as illustrated in Scheme 3.3.



Scheme 3.3. Mechanism of urea boronate formation

3.3.4. Suzuki reaction

The Suzuki reaction was first discovered by the Japanese scientist Akira Suzuki in 1979. It is an organic coupling reaction where the coupling partners are a boronic acid with a halide in the presence of palladium(0) catalyst.[188,189,190]

The best explanation of Suzuki coupling mechanism is from the perspective of palladium catalytic cycle. It involves three main steps: oxidative addition, transmetallation and reductive elimination.

3.3.4.1. Oxidative addition

This step is the rate limiting step in the palladium catalytic cycle. The palladium is oxidised from Pd(0) to Pd(II) and the carbon-halogen bond is broken with the binding of palladium to the halogen and the alkyl group which leads to the formation of organopalladium product **3**. This reacts with base to yield an intermediate that enter the second step, transmetallation.

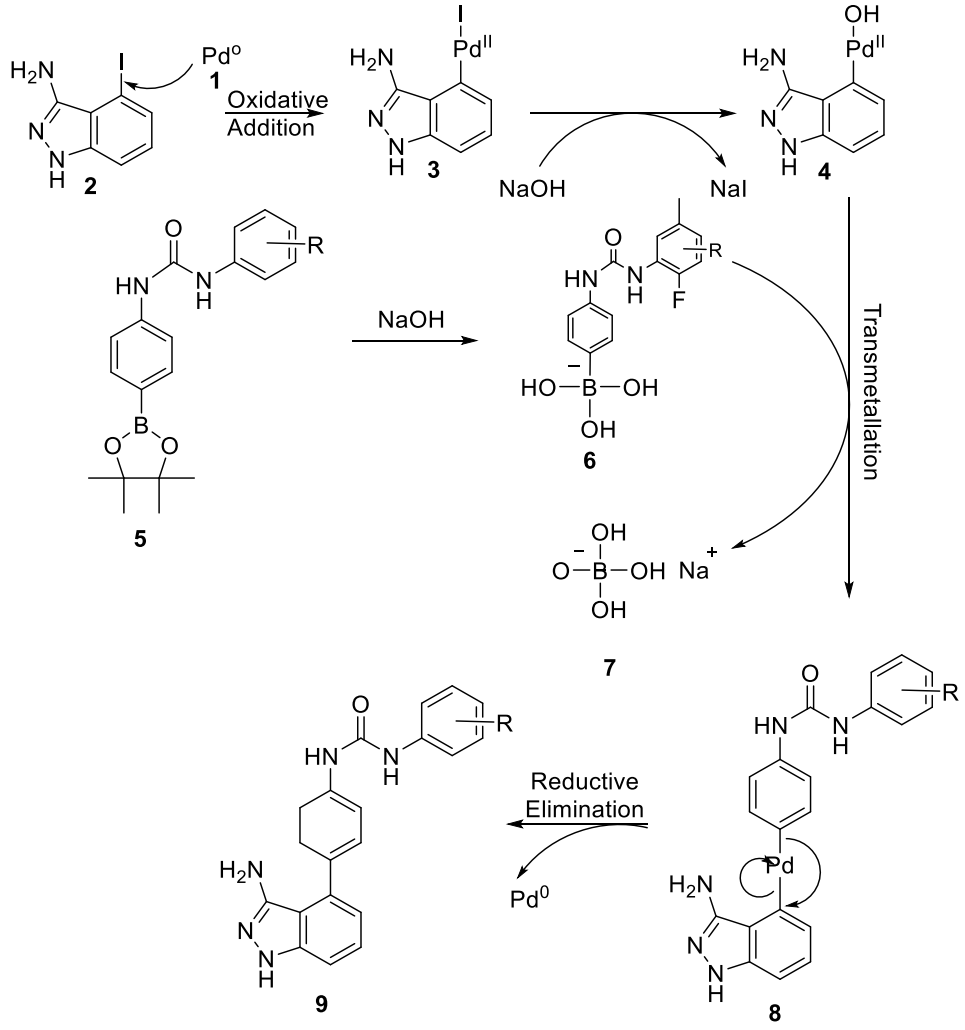
3.3.4.2. Transmetallation

Transmetallation involves the transfer of ligands from one species to another. During Suzuki coupling, there will be a transfer of ligands from the organoboron species **6** to the palladium(II) complex **4**. Prior to transmetallation step the base is added to be exchanged with the R_1 group of the organoboron compound to give palladium(II) complex **8**. This step does not exist in the absence of base;

therefore, it is thought that the base activates the organoboron species and facilitates the formation of compound **4** from compound **3**.

3.3.4.3. Reductive elimination

The third step is the reductive elimination of the final compound **9** to release the palladium to complete its cycle.

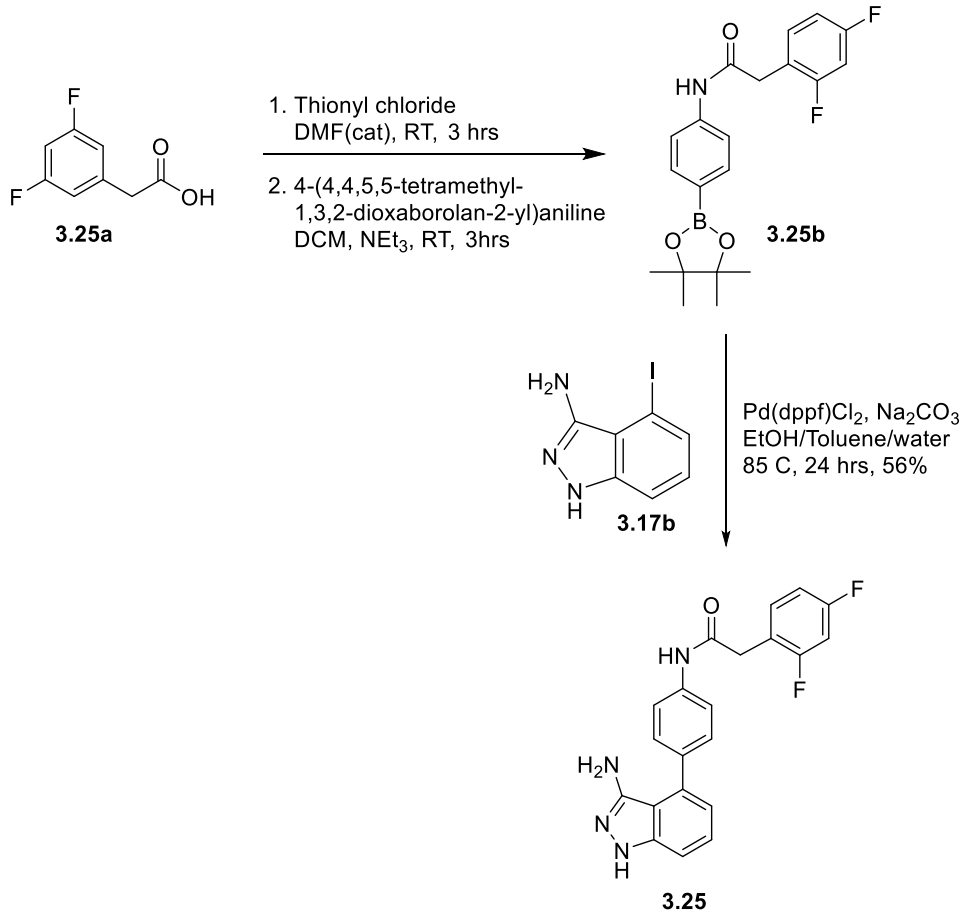


Scheme 3.4. Suzuki reaction mechanism

The reaction takes place in the presence of a base which has a triple role: the formation of palladium species **4**, the formation of trialkyl boronate **6** and finally the acceleration of the reductive elimination by the reaction of alkoxide with the palladium species.[191]

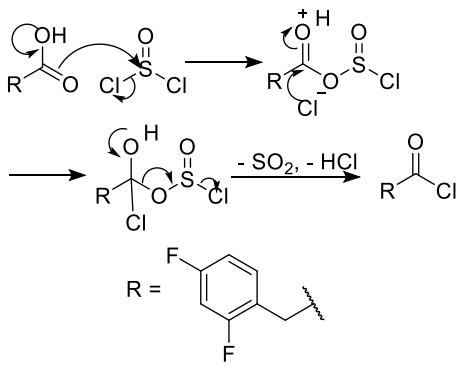
3.3.5. Synthesis of amide analogue (compound 3.25)

This synthesis consists of three steps: conversion of carboxylic acid (**3.25a**) to the acid chloride by thionyl chloride, reaction with boronic acid (**3.17c**) to form the amide boronate (**3.25b**) and finally the Suzuki coupling with iodoindazole (**3.17b**) (Scheme 3.5).



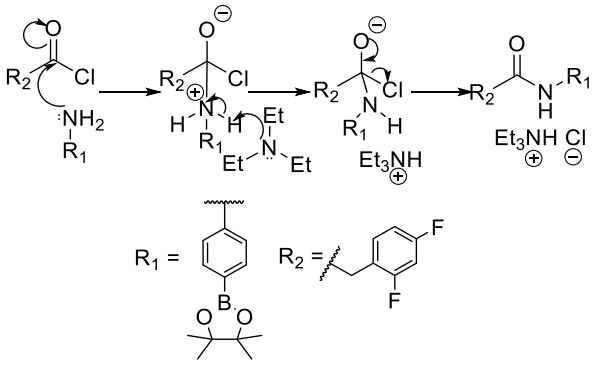
Scheme 3.5. Synthesis of compound 3.25

The mechanism of acyl chloride reaction with carboxylic acid is summarised in Scheme 3.6.



Scheme 3.6. Carboxylic acid activation by thionyl chloride

The second step is the amide formation by the reaction of the primary amine of boronic acid with the acyl chloride as shown in Scheme 3.7. Initially, there is a nucleophilic attack between the amine and carbonyl group to form an ammonium intermediate. This is followed by the addition of the triethylamine to abstract a proton from the intermediate and finally the chloride ion is removed to yield the amide analogue.



Scheme 3.7. Amide formation mechanism

The last step is the Suzuki coupling between the amide boronate and the iodoindazole. The mechanism of reaction is the same for the other linifanib urea analogues (**3.17-3.24**).

3.3.6. Structural Analysis of Gels

Following synthesis of linifanib and its analogues, it is important to test the gelation properties of these compounds and characterise their physical properties. Mechanical strength is one of the important properties of LMWG gelation because it will influence the tissue retention of these gels when under strain *in vivo*.[20]

3.3.6.1. Vial Inversion Test

Linifanib and its analogues were characterised initially by vial inversion tests and the results of this tests are shown in Table 3.2. The solvent mixture used was DMSO/water ranging from 5 % v/v to 25 % v/v. These solvent mixtures were chosen as linifanib is soluble in DMSO but insoluble in water at the required concentration; there is significant literature precedent for using this anti-solvent approach;[192,193] and increased concentrations of DMSO are potentially advantageous in cancer where DMSO has been shown to reduce the tumourigenicity of human pancreatic cell lines.[157]

Table 3.1. Data table of vial inversion tests of 0.5 % w/v linifanib and its analogues (3.17-3.25) in DMSO/water mixtures where gel (G), weak gel (WG), solution *(S)* and precipitate (P). Observations were carried out after 5 minute of cooling to room temperature.

Analogue / % DMSO	**3.17**	**3.18**	**3.19**	**3.20**	**3.21**	**3.22**	**3.23***	**3.24**	**3.25**
Clog P	4.49	4.10	4.00	4.45	4.13	3.99	4.24	4.38	3.97
5	G	P	P	P	P	WG	G	WG	P
10	G	P	P	P	P	WG	G	WG	P
15	G	P	P	P	P	P	G	WG	P
20	P	P	P	P	P	P	G	P	P
25	P	P	P	P	P	P	G	P	P

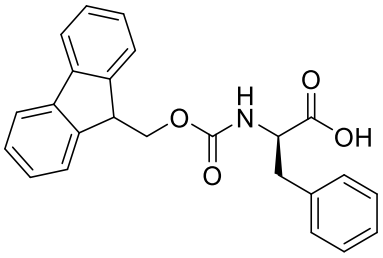
* Analogue **3.23** gave positive inversion test at 0.25 % (w/v).

From these results, it seemed that linifanib and three fluorine – containing analogues (**3.22-3.24)** were positive in the vial inversion test. In addition, the role of the urea functional group to promote gelation was demonstrated by comparison of the gelation behaviour of **3.23** and **3.25**. This structural change from urea (gel) to amide (precipitate) in the vial inversion screen demonstrated the important role that the urea functional group plays in the gelation of linifanib and its structural analogues. However, the 2-methoxy analogue (**3.18**) and the un-substituted terminal aromatic ring analogue (**3.19**), formed precipitates under all the conditions and likewise both the 2-chloro analogue (**3.20**) and the nitrile analogue (**3.21**) failed to gel, even though they both had electron-withdrawing substituents on the terminal aromatic ring. These observations are not surprising given the previously reported data of Nilsson *et al*[187] who showed that minor substitutions on the aromatic ring of fluorenylmethyloxycarbonyl-protected aromatic amino acids influenced gelation. They demonstrated the effect was a result of both steric and electronic changes in π–π stacking interactions. Specifically, they describe how a fluorine atom substituted on a toluene ring (also present in the terminal aromatic ring of linifanib) can create a more electron deficient aromatic ring as compared to substitution with other halogens and also fluorine has a beneficial smaller molecular volume. [187] Also, described in the Nilsson paper is that the halogen identity and position of substitution on the ring influences the gel strength. We also found in our studies that linifanib,

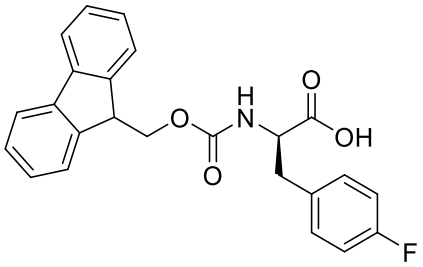
with an *ortho* – substituted fluorine (**3.23)**, gave stronger gels as compared to its fluorine – substituted analogues **3.22** (2, 3 (di-fluoro substituted) and **3.24** (*meta* substituted fluorine)) respectively in the vial inversion screen and confirmed by rheology for analogue **3.23.**

Recently, several investigations explored the role of halogen atom in gelation.[194-197] Wang and co-authors prepared three halogenated (F, Br, Cl) derivatives of Fmoc-Phe (**3.27-3.29**) to study the effect of introduction of halogen atom on gelation properties of this protected amino acid. The halogen atom was introduced in the *para* position of the aromatic ring in the side chain of the amino acid. It was found that all the three halogenated derivatives exhibited more stability than Fmoc-phenylalanine and the Fmoc-4-fluoro-phenylalanine (**3.27**) was the most stable derivative. In addition, the effect of halogen atom on mechanical strength was also investigated. It was found that the storage modulus (G') of the halogenated analogues was larger than the protected amino acid with the highest value for the bromo – substituted gel followed by the fluoro – and finally the chloro – substituted gel.[87]

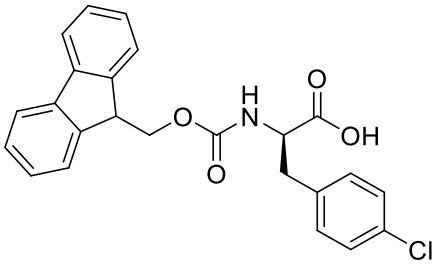
Linifanib was selected for further physical characterisation to determine its mechanical strength as this is an important attribute for drug delivery applications where mechanical strength can influence localization at an injection site.[52,198]



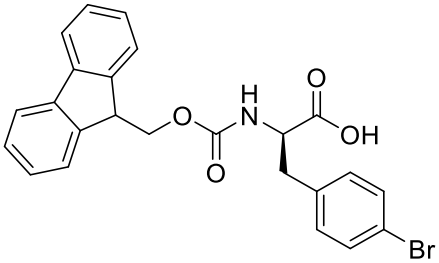
3.26



3.27



3.28



3.29

Firstly, further vial inversion screening for gelation was carried out with a series of binary mixtures of DMSO and water (Table 3.2). These results indicated that DMSO/water ratio had a significant effect on gelation which has also been observed for other LMWGs.[192,199]| The linifanib gels that were most stable to vial inversion were obtained with 5% (v/v) DMSO/ water. Interestingly, there seems to be an optimum ratio of linifanib to DMSO in that too much DMSO causes failure of gelation. This could be explained by the higher solubility of linifanib in DMSO compared to water, due to their lipophilic nature.

Table 3.2. Vial inversion screen of linifanib in binary mixtures of DMSO and water where gel (G), solution *(S)* and precipitate (P). Observations were carried out after 5 minutes of cooling to room temperature

% v/v DMSO	% w/v linifanib		
	0.5	0.25	0.125
5	G	G	G
10	G	G	P
15	G	P	P
20	P	P	S
25	P	S	S
30	S	S	S
40	S	S	S
50	S	S	S

3.3.6.2. Rheology characterisation

While the vial inversion test is a qualitative analysis of gels, rheology provides quantitative assessment of gels in terms of gel strength. It offers information about the type of the structure of gel network. It differentiates between viscous fluids and true gels as well as strong and weak gels.[200]

Rheology measurement involves the application of oscillatory strain on the material and measuring its response. Different variables are provided during this process such as G' (elastic modulus), G" (loss modulus) and G* (complex viscosity). These variables are used to evaluate the mechanical strength of gels. They are plotted against the strain (amplitude sweep) and frequency (frequency sweep).[201]

Linifanib and its difluoro analogue **(3.23)** showed strong gels in the vial inversion test; therefore, it was decided to carry out oscillatory rheology on these gels. With regard to linifanib, rheology experiments were undertaken with concentrations from 0.0625 to 1.25% (w/v) in 5% (v/v) DMSO/water. The measurements were performed at strains of 0.01% to 100% strain at 10 rad s^{-1} and the storage modulus (G') and loss modulus (G") were reported from within the linear viscoelastic region (Figure 3.8).

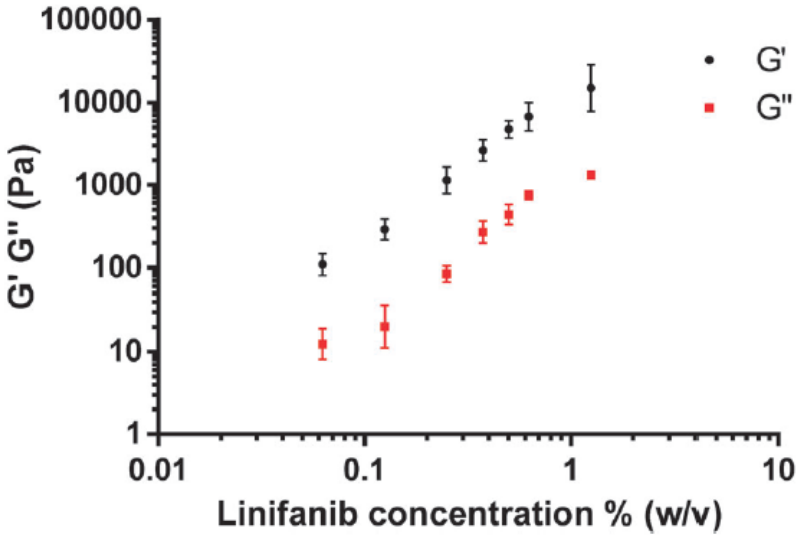
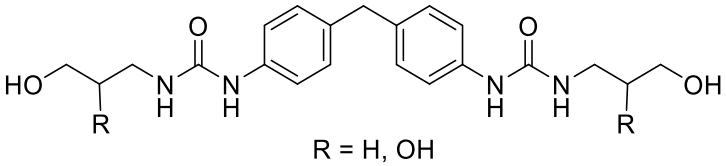


Figure 3.8. Storage modulus (G') (black circle) and loss modulus (G") (red square) versus linifanib concentration (% (w/v)) in 5% (v/v) DMSO/water at 1% strain and angular frequency of 10 rad s^{-1} and 37 °C. All measurements were carried out in triplicate and the mean calculated. Error bars represent standard deviation.

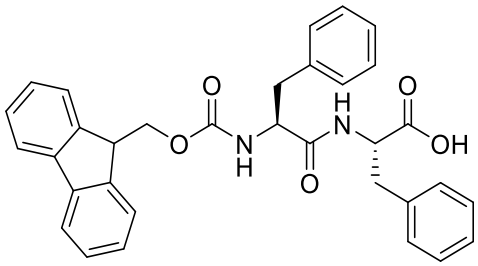
These experiments provided key evidence of gelation of linifanib in DMSO/water as demonstrated by the G' exceeding G" by at least an order of magnitude proving the viscoelastic nature of the gel.[59] Additionally, a sustained linear viscoelastic region was found between 0.01 – 1 % (Figure 3.9). Our G' data (1.5 x 10^4 Pa) is lower than the gels (10^6 Pa) as reported Kleinsmann[202] and Yu[59] but greater than the G' 100 Pa of gels as reported by Ren[203] for a Gemcitabine LMWG.

An increase in the moduli with increasing concentration of linifanib was also observed with other LMWGs, for example the simple chiral *bis*-ureas of Rodriguez-Llansola *et al.*[204] (**3.30**) which demonstrated an increase in G' (storage modulus) and G" (loss modulus) in a concentration range of 2-20 mM.



3.30

Adams *et al*. described a power law relationship between the concentration of Fmoc-Phe-Phe (**3.31**) and its mechanical strength in terms of G' i.e. $G' \propto C^x$. They suggested that x indicates the network type.[154] Colloidal gels were reported to have x value from 3 to 6 while for cross-linked polymers, x should be around 2.5 and finally the entangled networks have x about 1.4. In a similar manner, we found that x for linifanib was 1.86 which indicates the formation of a semi-entangled network (Figure 3.10).



3.31

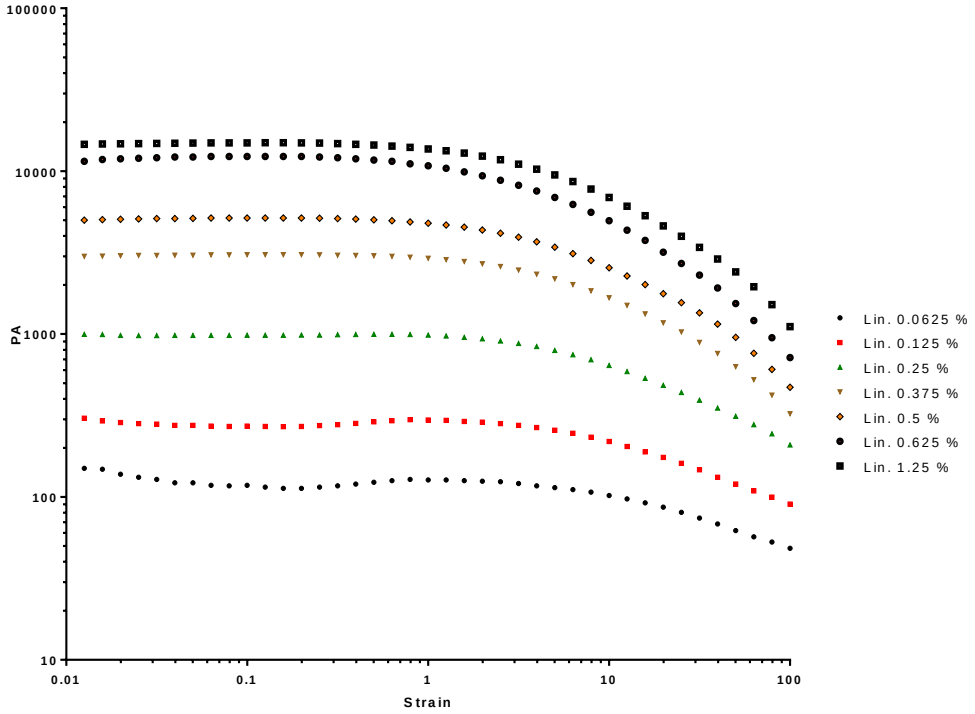


Figure 3.9. Amplitude sweep of linifanib gels at different concentrations (0.0625-1.25 w/v) in 5% w/v DMSO/water at angular frequency of 10 rad/s and 37 °C. Only storage modulus G' shown. Gels were formed instantly and measurements were taken after 3 hours.

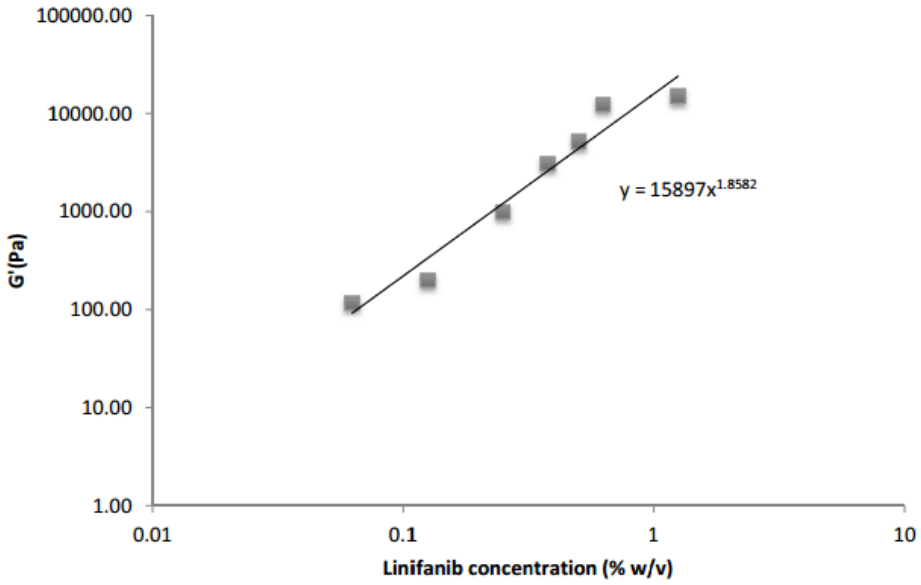


Figure 3.10. Storage modulus (G') versus linifanib concentration (% (w/v) in 0.5% (v/v) DMSO/water at 37 °C. All measurements were carried out at 1% strain and angular frequency of 10 rad s^{-1} in triplicate and the mean calculated. Slope = 1.86 to 2 decimal places. Gels were formed instantly and measurements were taken after 3 hours.

On the other hand, the difluoro analogue (**3.23)** showed positive inversion test in the 0.25 % concentration and this was further characterised by oscillatory rheology (Figure 3.9). Amplitude sweep of this compound indicated that G' was lower than that of its corresponding linifanib concentration.

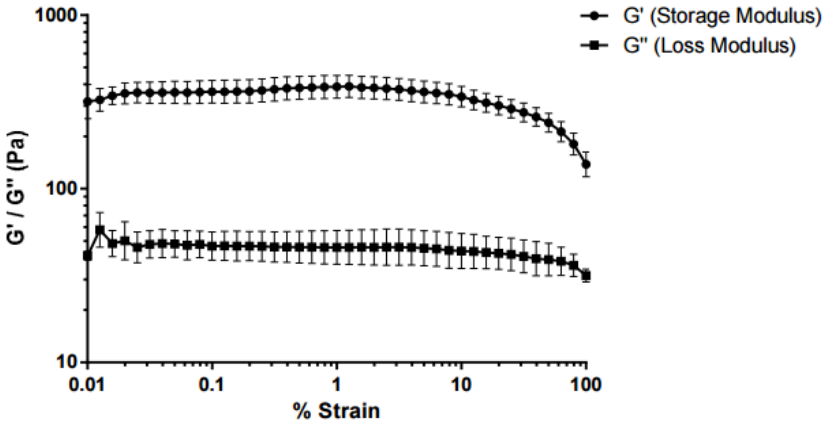


Figure 3.11. Amplitude sweep of difluoro analogue of linifanib (3.23) at 0.25 % (w/w) at 37 °C. All measurements were carried out at 1% strain and angular frequency of 10 rad s^{-1} in triplicate and the mean calculated. Error bars represent standard deviation. Gels were formed instantly and measurements were taken after 3 hours.

3.3.6.3. Transmission electron microscopy (TEM) imaging

The vial inversion and rheology offer information about the mechanical strength of the gels. However, full characterisation requires additional information to confirm the microscopic structure.

Transmission electron microscopy (TEM) is a high-resolution microscope (0.2 nm) which offer valuable information on the shape of gel aggregate such as fibres and tapes. To confirm this structure, a single sample of linifanib was selected with a concentration of 0.5 % by weight having a solvent ratio of 1:19 DMSO/water was dried prior to imaging by the TEM. Linifanib gel demonstrated a branched pattern of fibres 100 to 300 nm in width and 4.5 to 9 microns in length as shown in Figure 3.12.

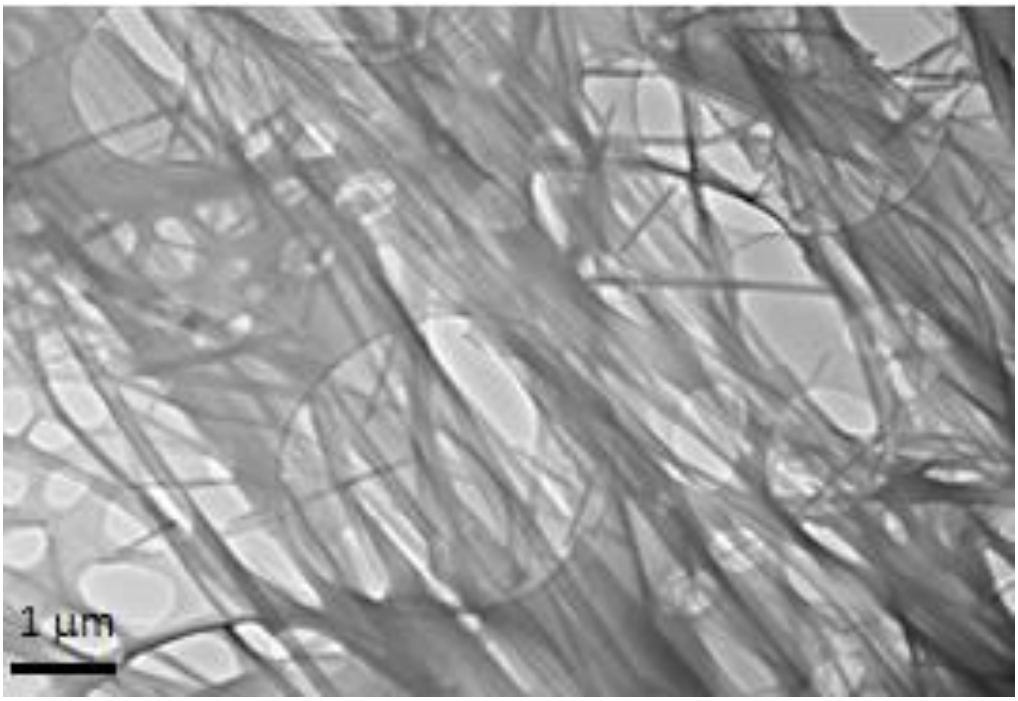


Figure 3.12. Transmission electron micrograph (TEM): 0.5% (w/v) linifanib in 5% (v/v) DMSO–water; scale bar = 1 µm using JEOL JEM –2000FXII transmission electron microscope and accelerating voltage of 100 kV

It should be kept in mind that these images showed the morphology of the dried gel (xerogel) and not the original gel network. Drying of the gel is thought to have a little effect on the network structure. However, a recent study investigated the effect of drying of the gel on its morphology. It was noticed in many instances the imaging showed the aggregation of fibrils instead of showing the full characteristics of the network. Therefore, it was recommended extra care should be spent while studying these images.[205]

3.4. Conclusions

In this chapter, the design and synthesis of linifanib and eight structurally related analogues were reported. Seven analogues were designed by modification of substituents of the aromatic ring next to urea, while the last analogue was designed by replacement of urea by amide.

Gelation experiments demonstrated that the tyrosine kinase inhibitor, linifanib, with a urea containing pharmacophore, is a LMWG and forms a hydrogel in low solvent ratios of DMSO/water. Representative gels were studied using rheology and TEM and their 3D fibre structure confirmed.

Through the synthesis of structurally related analogues we have also shown the importance of both the urea functional group and the position of the essential fluorine substitution on the terminal aromatic ring in promoting gelation. We also showed that linifanib has superior mechanical strength to its structurally-related analogues and hence increased potential for localisation at an injection site for drug delivery applications.[20]

In the following chapters, we will discuss the design and synthesis of self-assembled linifanib-based derivatives. All of these derivatives will be linked to the indazole ring. Firstly, we will report the design, synthesis and gel screening of a library of acyloxy alkoxy carbamate prodrugs of linifanib which could have a mechanism of release of active compound through either enzymatic or chemical hydrolysis. The effect of the introduction of side chain on gelation will be investigated. Then we will report the design and synthesis of amide derivatives of linifanib. These derivatives include aliphatic carboxylic acids, amino acids and dipeptides side chains.

Chapter Four: Carbamate Analogues of Linifanib as Candidates for Self-Assembly

4.1. Introduction

In the preceding chapter, we confirmed the gelation behaviour of linifanib. One of the approaches for creating a controlled drug delivery is the prodrug approach (section 1.3.2). The design of self-assembling prodrugs of linifanib will provide a controlled delivery of this drug candidate. The endocyclic secondary amine of the indazole ring of linifanib was selected to be linked to the pro-moiety. The distance between the indazole ring and the aromatic and urea portions of the molecule is thought to be enough that not disrupting linifanib self-assembly. In this chapter, a carbamate linker was selected to create potential prodrugs of linifanib which might self-assemble into hydrogels (Figure 4.1). The carbamate moiety is reported in the literature in many LMWGs [206-208] and prodrugs due to its chemical stability but susceptibility to esterase enzymes [209,210].

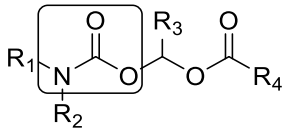
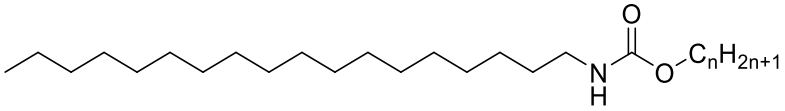


Figure 4.1. Structure of carbamate prodrug of amine-containing drug

4.1.1. Carbamate group as a gelator motif

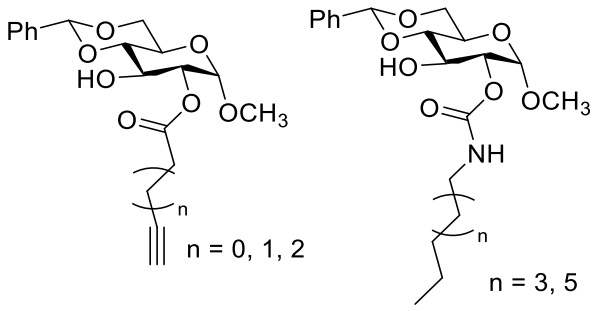
In several studies, the carbamate functional group has been reported to contribute to the self-assembly through its hydrogen bonding ability. Moniruzzaman and Sundararajan indicated that carbamates with alkyl side chains (**4.**1) have the ability to produce gels when the alkane side chain length is 12 carbon atoms. In addition, they reported that crystallisation dominates when the alkane chain is greater than 12 carbons because of the dominance of van der Waals forces between the alkyl chains. In their studies, they used benzonitrile as the solvent and temperature switch as the trigger of organogelation. In addition, they reported that the thickness of fibres was affected by the chain length of alkane.[208]



n = 4, 7, 8, 10, 12, 16, 18

4.1

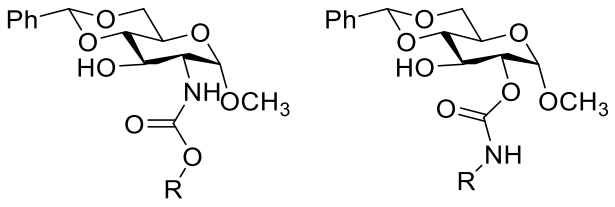
In addition, Wang *et al.* reported the synthesis and characterisation of monosaccharide derived carbamates as LMWGs. This study is based on the synthesis of a series of carbamate **(4.2)** and ester **(4.3)** analogues of 4,6-O-benzylidene methyl-R-D-glucopyranoside where they found that carbamates substituted with five and seven carbon alkyl chains formed gels (Figure 4.2).[211]



4.2 **4.3**

Figure 4.2. Structures of 4,6-O-benzylidene methyl-R-D-glucopyranoside carbamate and ester derivatives

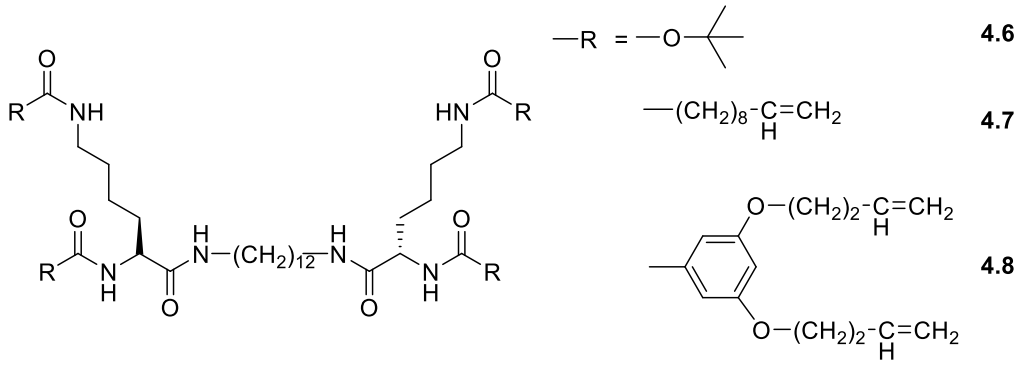
To investigate requirements for gelation of the carbamate analogues, a series of derivatives with different alkyl substitutions were synthesised. These analogues consisted of 2 series of compounds: O-linked **(4.4)** and N-linked **(4.5)** glucopyranose carbamates. They found that carbamate derivatives with saturated alkyl chains had good properties for gelation whereas the corresponding ester derivatives preferred alkyl chains containing a terminal acetylene group. In addition, aryl side chains were common in both ester and carbamate groups in driving gelation. Another finding of this study is that carbamate gels were stronger than their ester counterparts. This demonstrates the effect of the extra hydrogen bond donor (NH) present in the carbamate group which imparts extra strength to the gel. Finally, the N-linked carbamates (the linkage is between sugar and amine group of carbamate) were able to gelate DMSO/water and ethanol solutions.[211]



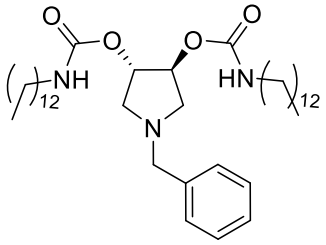
4.4 **4.5**

Figure 4.3. Chemical structure of O- and N-linked glucopyranose carbamates

Moffat and Smith investigate three organogelators, gelator **(4.6)** contains carbamate group while gelators **(4.7)** and **(4.8)** include amide moieties. They found that mixtures of gelators **(4.6** and **4.7)** were stronger than gelators **(4.7** and **4.8)**. They argued that although hydrogen bonding between amide groups are favoured over amide-carbamate groups with regards to driving self-assembly, the difference in the hydrogen bond forming group may be another factor contributing to gel formation process.[207]



Cicchi *et al.* investigated chiral organogels based on carbamate functionality. They created and characterised (3S, 4S)-1-benzylpyrrolidine-3,4-diyl *bis*(dodecylcarbamate) **(4.9)** which formed gels in both aqueous and nonpolar solvents. Several techniques were used to characterise these gels such as AFM, DSC, and microscopy in addition to computational methods. X ray crystallography showed that multiple hydrogen bonds were present between carbamate groups of benzylpyrrolidine nucleus arranged in an antiparallel manner.[206]



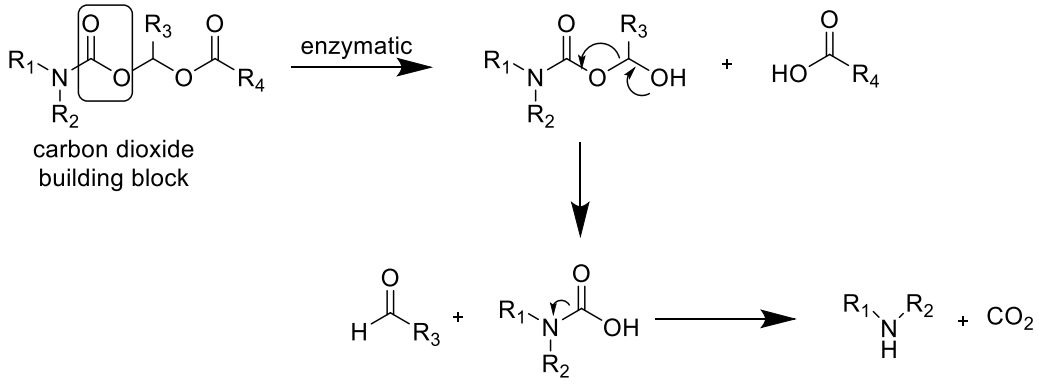
4.9

Overall, these studies support the approach of using the carbamate group substituted with alkyl chains as a possible gelator motif. This is important as the carbamate functionality can be also used to create prodrugs which will now be described.

4.1.2. Carbamate-based Prodrugs

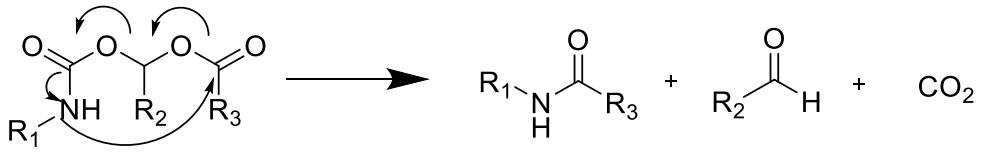
Prodrugs are derivatives of pharmacologically active compounds which must undergo enzymatic and/or chemical modification inside the body to release the parent drug. In this, the self-assembled prodrug gel will act as a reservoir which slowly release the pharmacologically active drug. Furthermore, it should be considered that the degradation products of the prodrug should be nontoxic and easily excreted from the body.[210] Prodrugs are designed by linking the drug to the prodrug moiety by covalent binding. Ester prodrugs are the most commonly used linkers in prodrug approach. However, prodrugs could be created using amides or carbamates especially for amine containing drugs.[212]

A useful approach to create prodrugs of amines is to add a spacer group ending with an alcohol.[210] This can then be esterified to make it susceptible to esterase in plasma. The principle of this approach is that the esterase-sensitive prodrug will be converted to the unstable carbamic acid derivative.[209] This will lead to spontaneous release of the active compound with carbon dioxide (Scheme 4.1).[213] The acyloxymethyl ester generates formaldehyde during the release of parent drugs. Therefore, the use of acyloxy ethyl esters ($R_3 = CH_3$) is preferred to avoid toxicity.



Scheme 4.1. Mechanism of ester-mediated hydrolysis of N-acyloxyalkoxycarbonyl derivatives into parent amines.

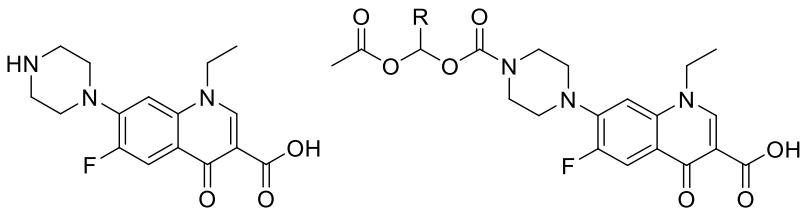
However, this prodrug approach is limited to secondary amines. In primary amines, there will be intramolecular acyl transfer instead of the release of parent drug as shown in Scheme 4.2.[213]



Scheme 4.2. Intramolecular acyl transfer in *N*-acyloxyalkoxycarbonyl prodrugs of primary amines

This approach was successfully applied to a number of amine-containing therapeutic agents. Alexander and his colleagues showed that acyloxyalkyl derivatives of a number of water-soluble beta blockers demonstrated significant increase in permeation of the skin and cornea.[214] Another study by the same group monitored the release of parent drug in human plasma. They found that esterases were responsible for the release of the active amine compound. In addition, acyloxycarbonyl prodrugs of secondary amines demonstrated quantitative release of the parent amine in contrast to their primary amine counterpart. This is due to the above mentioned difference in the mechanism of release and formation of N-acyl adducts in the case of primary amines.[215]

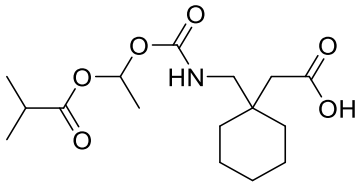
Another example is the taste masking prodrugs (**4.11)** of the antibacterial agent norfloxacin **(4.10)**. The bitter taste of this drug was a problem for its oral administration. Alexander and co-workers used a prodrug strategy to mask the bitter taste of the parent drug. They linked an acyloxycarbonyl group to the piprazino nitrogen. Another advantage of this linkage is that carbamates are not ionised under physiological pH. The prodrug succeeded in masking the bitter taste of norfloxacin. However, these prodrugs had less water solubility than parent compound.[216]



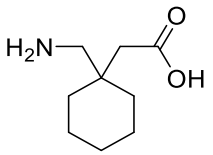
4.10 **4.11**

In another study, Cundy and his group developed a gabapentin prodrug with acyloxyalkoxycarbonyl moiety, XP13512 (**4.12**). The main disadvantage of gabapentin (**4.13**) is its short half-life. The prodrug was designed to overcome this problem. The oral bioavailability of gabapentin was significantly increased

to 84% in monkeys in a dose of 36 mg gabapentin equivalent per kg compared with 25% after gabapentin oral administration.[217,218]

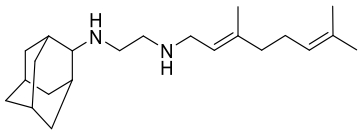


4.12

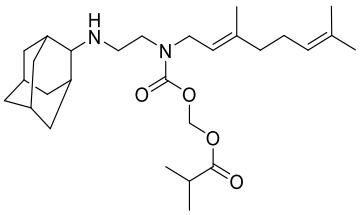


4.13

Finally, this prodrug approach was used to improve oral bioavailability. The investigational anti – tuberculosis agent SQ109 **(4.14)** suffers from extensive first pass metabolism. Meng *et al.* reported the synthesis of carbamate prodrugs of this compound. Metabolism of the prodrug **(4.15)** to SQ109 resulted in higher concentration in plasma when compared to that of parent compound. Prodrug **4.15** was the best carbamate analogue which was selected for further *in vivo* studies.[219]



4.14



4.15

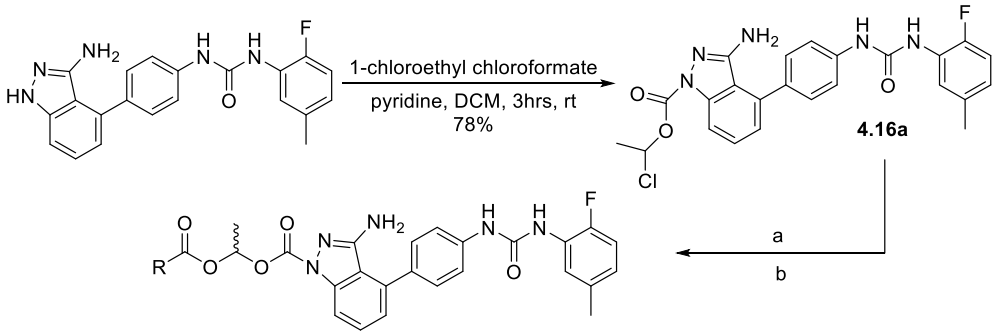
According to the above literature, carbamate group has the properties of being gelator motif and prodrug moiety. This was the rationale of the design of carbamate derivatives of linifanib which are in the following section.

4.2. Results and Discussion

4.2.1. Design and synthesis of linifanib carbamate derivatives

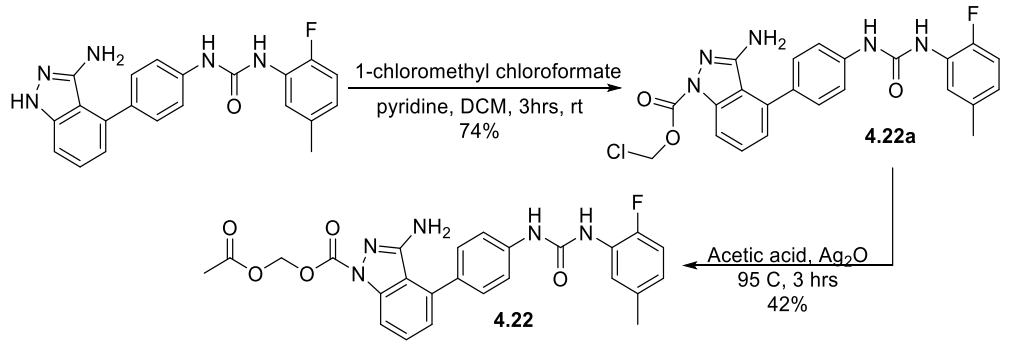
Carbamate derivatives of linifanib were proposed as potential prodrug gelators. It is hypothesised that these self-assembled prodrug gelators will provide sustained release of the drug from the gel network at the site of action, i.e., intra-tumour or at the tumour resection site. As discussed earlier, this type of prodrug depends on both enzymatic and chemical mechanism to release the parent drug. A series of acyloxyalkoxycarbonyl analogues of linifanib was synthesised. Different terminal alkyl groups were used to evaluate the effect of the side chain on the self-assembly property of the resulting prodrugs.

Synthesis of compounds (**4.16-4.21**) was accomplished by a 2-step synthetic route. The first step involves the synthesis of intermediate (**4.16a**) using linifanib, 1-chloroethyl chloroformate and pyridine as the base to yield the carbamate alkyl chloride intermediate. This intermediate reacts with the corresponding acid using silver **(I)** oxide to generate carbamate ester analogues (Scheme 4.3). Compound **4.22** was synthesised in the similar route except replacement of 1-chloroethyl chloroformate by 1-chloromethyl chloroformate (Scheme 4.4). Silver (I) oxide is used to generate salts of carboxylate ions (Scheme 4.5). Purification of crude products was done by flash column chromatography eluting with 20:80 ethyl acetate: petroleum ether to neat ethyl acetate to provide final compounds in yields ranging from 29-47%.

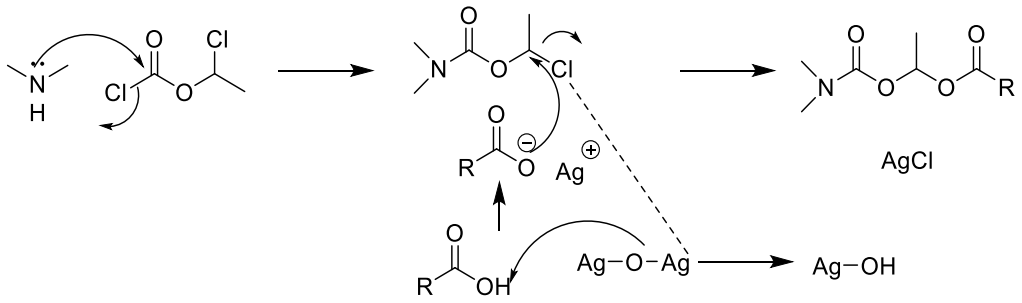


4.16 R = CH_3, a: acetic acid, b: silver oxide(I), 95 C, 3hrs, 47%
4.17 R = C_2H_5, a: propionic acid, b: silver oxide(I), 95 C, 3hrs, 41%
4.18 R = C_3H_7, a: butyric acid, b: silver oxide(I), 95 C, 3hrs, 42%
4.19 R = $CH(CH_3)_3$, a: pivalic acid, b: silver oxide(I), 95 C, 3hrs, 37%
4.20 R = phenyl, a: benzoic acid, b: silver oxide(I), DMF, 95 C, 24 hrs, 30%
4.21 R = *o*-Acetyl phenyl, a: aspirin, b: silver oxide(I), DMF, 95 C, 24 hrs, 29%

Scheme 4.3. Synthesis of carbamate derivatives of linifanib (4.16-4.21)



Scheme 4.4. Synthesis of compound 4.22



Scheme 4.5. Mechanism of the 2-step synthesis of acyloxyalkylcarbonyl carbamates

4.2.2. Gelation tests of carbamate prodrugs of linifanib

Vial inversion tests were performed on compounds (**4.16-4.22)** by the temperature and solvent switch methods. DMSO was used as the organic solvent in mixtures with water. All compounds demonstrated either precipitation or solution formation. A similar pattern was observed with all the carbamate analogues (**4.16-4.22**) which was the formation of a precipitate at low DMSO ratio whilst a solution was formed by increasing DMSO/water ratio (% DMSO > 40%). This reflects the high lipophilicity of these compounds (Table 4.1).

Table 4.1. Data table of vial inversion tests in DMSO/water mixtures of 0.25 % w/v of carbamate analogues of linifanib with % DMSO from 5 – 50% v/v, where P: precipitate, S: solution. Observations were carried out after 3 hours of cooling to room temperature

%v/v DMSO	4.16	4.17	4.18	4.19	4.20	4.21	4.22
clog P	4.19	4.72	5.24	5.77	5.8	5.19	3.88
05	P	P	P	P	P	P	P
10	P	P	P	P	P	P	P
15	P	P	P	P	P	P	P
20	P	P	P	P	P	P	P
25	P	P	P	P	P	P	P
30	P	P	P	P	P	P	P
35	P	P	P	P	P	P	P
40	S	S	P	P	P	P	P
45	S	S	S	S	P	P	S
50	S	S	S	S	S	S	S

These findings showed that linking a carbamate moiety to linifanib resulted in the loss of self-assembly property of parent compound, linifanib. There was no difference in behaviour between alkyl side chains with different length as well as changing terminal alkyl group to an aromatic ring. The failure of these compounds to form gels is thought to be due to several reasons. The high hydrophobicity of these derivatives in comparison to linifanib may cause disruption to the solubility needed to form linifanib hydrogels. Another reason, is the extra hydrogen bond acceptors of the carbamate functional group might result in the disruption of the one-dimensional order essential for the self-assembly. Finally, the length of the carbamate side chain may cause steric disruption of the confirmed planar conformation of the diary urea moiety. As discussed in chapter two, the planarity of this part of linifanib molecule is thought to be the main driving force of self-assembly through $\pi - \pi$ stacking of the aromatic rings and hydrogen bonding of urea functional groups.

As a result of failure of all the compounds to form a gel, further characterisation was not undertaken.

4.3. Conclusions

In this chapter, synthesis of 7 carbamate derivatives of linifanib was reported. In addition, gelation property of these compounds was evaluated using table-top rheology, i.e. vial inversion by solvent switch using DMSO/water mixtures of 5-50% v/v.

Vial inversion tests of linifanib carbamate analogues showed the formation of precipitate or solutions rather than gels demonstrating the lack of these compounds to self-assemble. This means that derivatisation of linifanib with carbamate moiety results in the loss of gelation behaviour confirmed for linifanib. Screening results showed that this was independent of the length or nature of side chain of the carbamate moiety.

In conclusion, carbamate prodrug strategy was not suitable for generation of self-assembled prodrugs of linifanib. As a result, another prodrug strategy was selected which is the design and synthesis of amide derivatives of linifanib. It is believed that these derivatives will overcome the disadvantages of the carbamate analogues such as hydrogen bonding disruption and steric hindrance. The amide side chains such as amino acids are thought to overcome these two main challenges. In addition, the diversity of amide derivatives will provide a wide range of expected water solubility of these compounds and offer more opportunity to have self-assembled prodrugs of linifanib. Finally, the amino acid and dipeptide prodrugs are extensively studied and this will provide valuable information regarding their synthesis and their chemical and/or enzymatic release of the parent drug.

The amide derivatives will include three different libraries of compounds which will be discussed in the following chapter.

Chapter Five: Self-Assembling Amide Derivatives of Linifanib

5.1. Introduction

In chapter four, we reported the synthesis of carbamate derivatives of linifanib. All of these compounds failed in gelation which may be due to hydrogen bonding disruption and/or steric interference. Therefore, another strategy was to prepare a series of aliphatic and mono- and di-amino acid amides of linifanib. These libraries were selected such that they fulfil the aim of this project which was the design of self-assembled prodrugs of linifanib. The derivatives should have two main features: gelation and cleavage to linifanib. The common feature between these three libraries is the amide linkage between the parent compound, linifanib and the moiety. The amide bond has been reported in a large number of gelators as described below. Indeed, the amide bond is both a hydrogen bond donor and acceptor giving rise to hydrogen bonding which is one of the non-covalent interactions known to promote self-assembly.[220] As confirmed from chapter three, the urea functional group and the halogenated toluene ring were essential for gelation of linifanib, it is thought that the amide linkage at the indazole ring will not disrupt these important features. In addition, aliphatic and mono acid amides of linifanib have been included as they have smaller side chains compared to the carbamates and potentially are less likely sterically to disrupt the one-dimensional order required for self-assembly. Furthermore, the increased aqueous solubility of these compounds, especially with the derivatives in the HCl form, can promote gelation.[254]

It should be noted that there are two points to consider regarding the outcomes of gelation screening of these derivatives. The first point is the rationale why some derivatives gel and others not. The second aspect to focus on is the relationship between the chemical structure of the gelator and gel formation. This will help in establishing a model to design further gelators of this drug candidate.

With regard to the prodrug approach, there are numerous reports which describe the design and synthesis of amide prodrugs which are proposed to cleave by enzymes to release the parent compound. Most of these reports have focused on the dipeptide and amino acid prodrugs which cleave by either a chemical

mechanism (basic amide hydrolysis) or enzymes such as proteases or peptidases.[221] The advantage of self-assembled prodrugs is to provide a mechanism by which drug release can be controlled for localised drug delivery.[20,73] The three libraries of the amide derivatives of linifanib are shown in Figure 5.1.

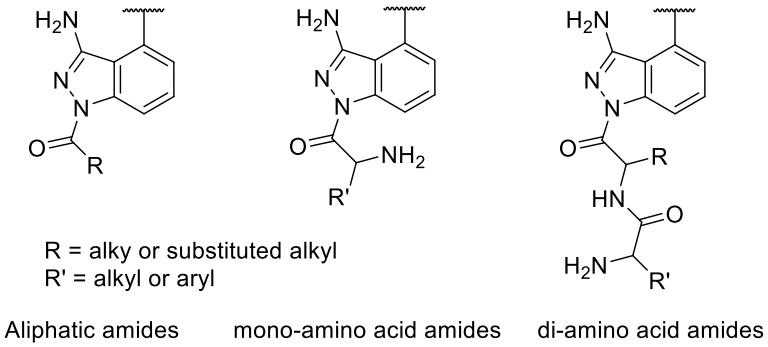
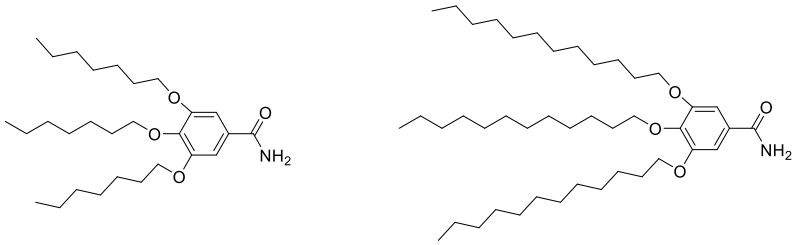


Figure 5.1. General structures of aliphatic and mono- and di-amino acid amides of linifanib

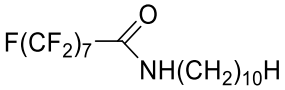
5.1.1. Amide gelators

The hydrogen bonding of amide-containing compounds is one of the important elements in many LMWGs.[220] This type of interaction is favoured in both lipophilic organic and aqueous solutions. As the self-assembly process depends mainly on noncovalent intermolecular interaction which induces unidirectional aggregation, the design of LMWGs based on amide building blocks will be a useful approach for creating successful gelators.[220] The structurally simple amide gelators **5.1** and **5.2** were shown to gelate in both polar solvents (methanol, ethanol and DMF) and lipophilic organic solvents (*n*-octane and toluene) with a minimum concentration of 2.5% w/w.[222]



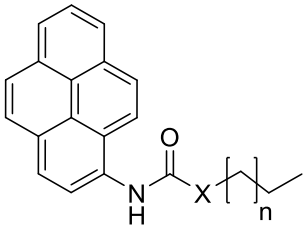
5.1 **5.2**

The Weiss group prepared a series of *N*-alkyl perfluoroalkanamides. The derivative **5.3** was an organogelator with a minimum gelation concentration of 2.5% w/w in different organic solvents such as ethanol, *n*-butanol, *n*-octanol, hexane, benzyl alcohol and toluene. Aggregation of these molecules resulted in gel formation stabilized by intermolecular hydrogen bonding between the amide groups.[223]



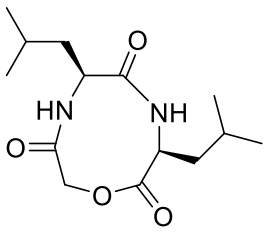
5.3

A group of pyrene-based gelators has been investigated. These compounds included the amide (**5.4)**, and carbamate (**5.5)** functional groups. Gel screening showed gel formation in many organic solvents with a wide range of polarity such as *n*-butanol, *tert*-butanol, *n*-octanol, cyclohexanol cyclohexane, *n*-hexane, *n*-decane, *n*-dodecane, carbon tetrachloride and toluene. FTIR studies and absorption spectra indicated that the self-assembly of molecules was through intermolecular hydrogen bonding and π-stacking.[224,225]



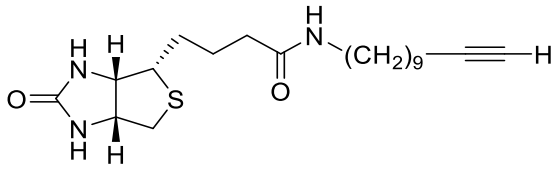
	X	n
5.4	CH_2	15
5.5	O	14

In addition, the cyclic compound **5.6** was able to form gels with acetonitrile and diethyl ether. This compound was insoluble in these solvents; therefore, a drop of methanol was used to solubilize the compound in the two solvents then immediately the gel was formed. This gel was reported to be physically stable for months.[226]



5.6

Finally, the biotin derivative **5.7** was able to gelate chloroform and acetonitrile. NMR spectroscopy confirmed that the hydrogen bonding induced the formation of organogels. Other derivatives based on this compound were synthesised in order to gelate more organic solvents but unfortunately the number of gelated solvents remained limited.[227]

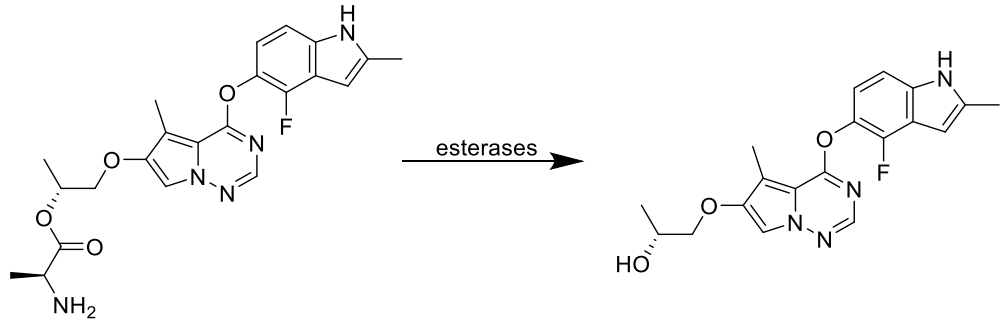


5.7

5.1.2. Amino acids as moieties in prodrug design

A wide range of prodrug moieties have been utilised to overcome problems associated with many drugs such as poor aqueous solubility, limited efficacy and adverse effects. The moieties are selected depending on different criteria such as the type of problem associated with the drug, the suitable functional group in the drug for prodrug design, chemical and enzymatic mechanism for conversion of prodrug to active drug and finally the prodrug safety profile. Amino acids offer many advantages in prodrug design. Structural diversity is one of the main advantages of amino acids as there are 20 natural amino acids in addition to the unnatural amino acids such as β-alanine and γ-aminobutyric acid (GABA). In addition, there is a wide range of functional groups available for linking with the parent drug such as the terminal amino and carboxyl group and the side chain functional groups. Regarding safety, amino acids are the building blocks of proteins which means they are considered a safe prodrug moiety. Other advantages of amino acids are their commercial availability and well-established prodrug synthetic procedures.[221] Accordingly, amino acid prodrug strategies have proven successful in overcoming a variety of problems regarding the delivery of many drugs and below is a review of some successful examples.

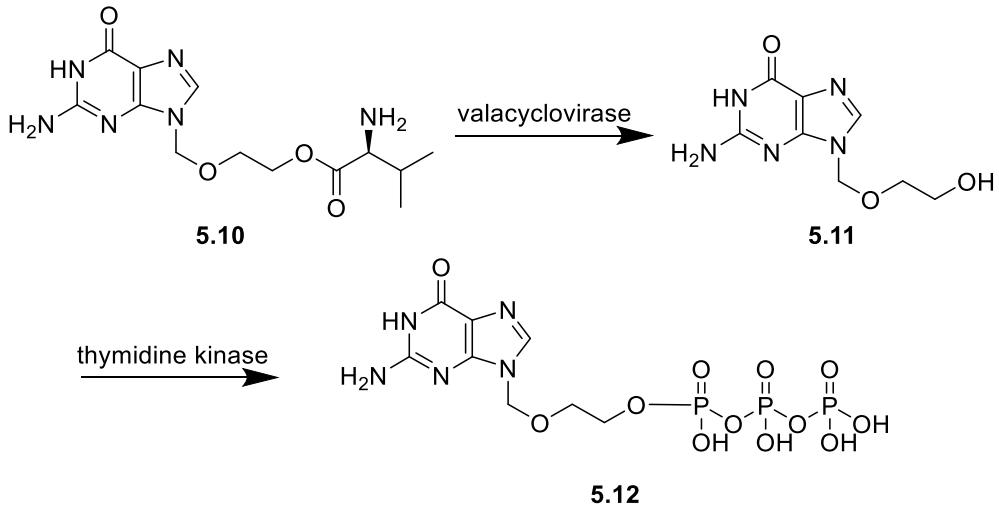
Brivanib **(5.9)** is a $VEGFR_2$ and a fibroblast growth factor receptor 1 ($EGFR_1$) inhibitor under development for treatment of colorectal cancer and hepatocellular carcinoma.[228] This drug candidate has very low water solubility (<1 μg/mL at pH 6.5) which limited its oral bioavailability to 22% in mice. Brivanib alaninate **(5.8)** had very high water solubility (73 mg/mL at pH 5.8) which contributed to an increase in its bioavailability to 52-97% in different animals.[229] This prodrug was rapidly converted to its parent drug, brivanib by esterase enzymes as shown in Figure 5.2.



5.8 **5.9**

Figure 5.2. Enzymatic conversion of brivanib alaninate to brivanib

Amino acid prodrugs have also been used to increase bioavailability using the intestinal transporters as will now be described. Valacyclovir **(5.10)** was the first approved L-valyl ester prodrug of the antiviral drug, acyclovir **(5.11)**.[230] The prodrug had an oral bioavailability (> 60%) which is more than 3-fold the bioavailability of acyclovir (~ 20%).[231,232] Absorption of valacyclovir is achieved by the human peptide transporter 1 (hPepT1) and rapidly hydrolysed to acyclovir mainly by the enzyme valacylovirase.[233] Finally acyclovir will be phosphorylated to acyclovir triphosphate **(5.12)** by the action of cellular kinases (Figure 5.3).[234]



5.10 **5.11** **5.12**

Figure 5.3. Enzymatic conversion of valacyclovir to its parent drug and then to its triphosphate active form

Human peptide transporter 1 (hPepT1) was utilised in anticancer prodrug design as it is overexpressed in cancer cells compared to normal cells.[235,236] Gemcitabine **(5.13)** which is a nucleoside anticancer drug suffers from significant metabolism of the cytidine group by cytidine deaminase and low membrane permeability due to its high polarity.[235] A number of amino acid

prodrugs of gemcitabine were synthesised to improve its permeability. It was found that 5'-L-isoleucyl derivative **(5.14)** showed increased transport in cancer cells expressing hPepT1. In addition, this prodrug demonstrated good resistance to cytidine deaminase leading to a longer half-life (Figure 5.4).[235]

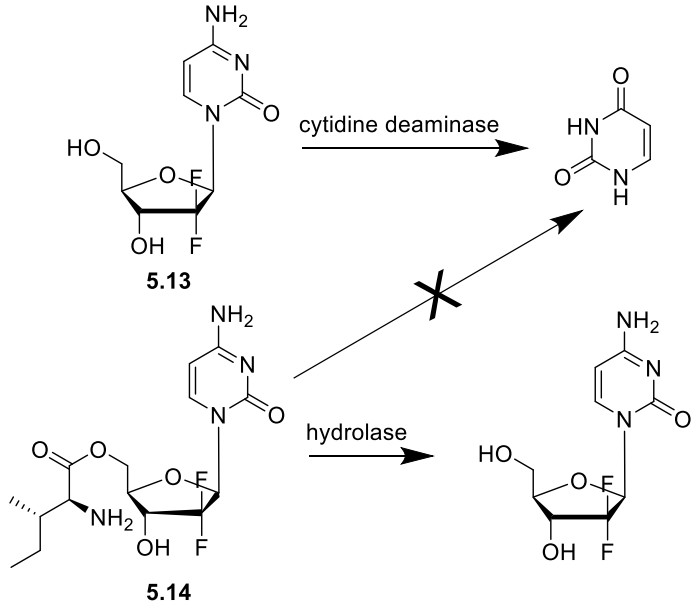
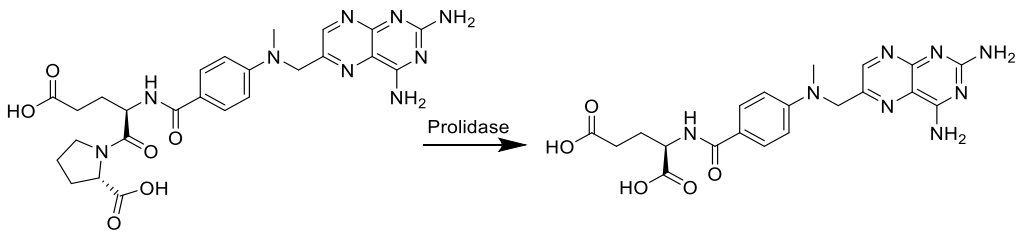


Figure 5.4. 5'-L-isoleucyl gemcitabine mechanism of resistance to deamination by cytidine deaminase.

Methotrexate **(5.16)** which is an alkylating anticancer drug suffers from resistance by breast cancer cells.[237] A proline prodrug of methotrexate **(5.15)** demonstrated increased cytotoxic activity against breast cancer cell lines reflecting the ability of the prodrug to overcome the resistance to the parent drugs. This prodrug underwent hydrolysis to the parent drug by prolidase enzyme (Figure 5.5). Two mechanisms were thought to be behind the increase in activity; the first one is the active transport of the proline containing compound by amino acid transporters and secondly is the high concentration of prolidase enzyme in breast cancer cell lines when compared to normal cells. This advantage also provided more cancer cell selectivity to methotrexate.[237]



5.15 **5.16**

Figure 5.5. Hydrolysis of proline prodrug of methotrexate.

Finally, dipeptides have been utilised in prodrug design. These prodrugs are converted to parent drugs through an enzyme-independent mechanism called diketopiperazine formation. This is achieved by the nucleophilic attack on the C-terminus of the first amino acid by the unshared pair of N-terminus electrons to form the six membered diketopiperazine ring (Figure 5.6).[238]

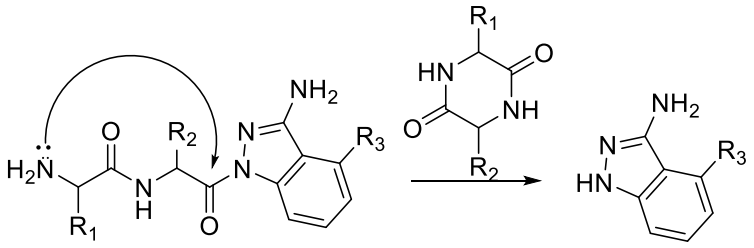
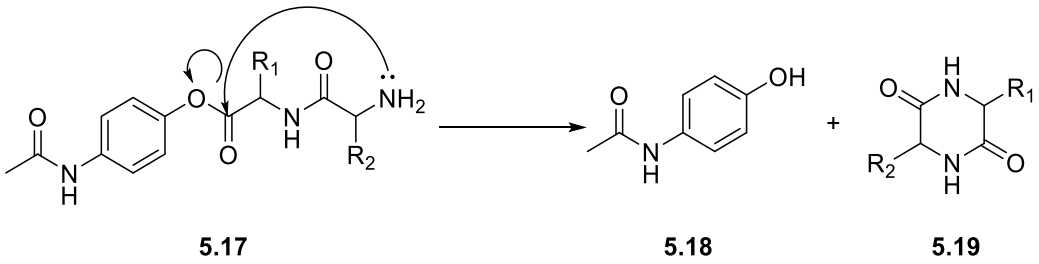


Figure 5.6. Mechanism of diketopiperazine formation

Dipeptide esters of paracetamol **(5.17)** are examples of this type of prodrug.[239] These prodrugs showed a significant decrease of hepatotoxicity in mice. It was found that these prodrugs were hydrolysed to paracetamol **(5.18)** and diketopiperazine derivative **(5.19)** at pH 7.4 (Figure 5.7).



5.17 **5.18** **5.19**

Figure 5.7. Hydrolysis of paracetamol dipeptide esters to paracetamol

5.1.3. LMWGs based on amino acids

Peptides are common platforms for both organo- and hydro-gelators since these scaffolds have many properties which contribute to the self-assembly process.[240-242] These include hydrogen bonding, electrostatic forces and π–π interactions.[241] In addition, there are several advantages of using amino acids in the design of new LMWG-based drug delivery systems. L-amino acids are one of the essential components of the human body and hence they are characterised by biocompatibility, biodegradation and nontoxicity.[243] In addition, amino acids and peptides are commercially available and have well established synthetic procedures for their derivatives.[243]

L-lysine-based gelators are one of the most extensively studied gelators which are based on single amino acid. N^{ε}-Lauroyl-N^{α}-stearylaminocarbonyl-L-lysine

ethyl ester (**5.20)** was the first of the family of L-lysine-based organogelators (Figure 5.8). This compound formed gels with wide spectrum of organic solvents and fluids such as alkanes, alcohols, ketones, esters, cyclic ethers, aromatic solvents, polar solvents and mineral and vegetable oils.[244]

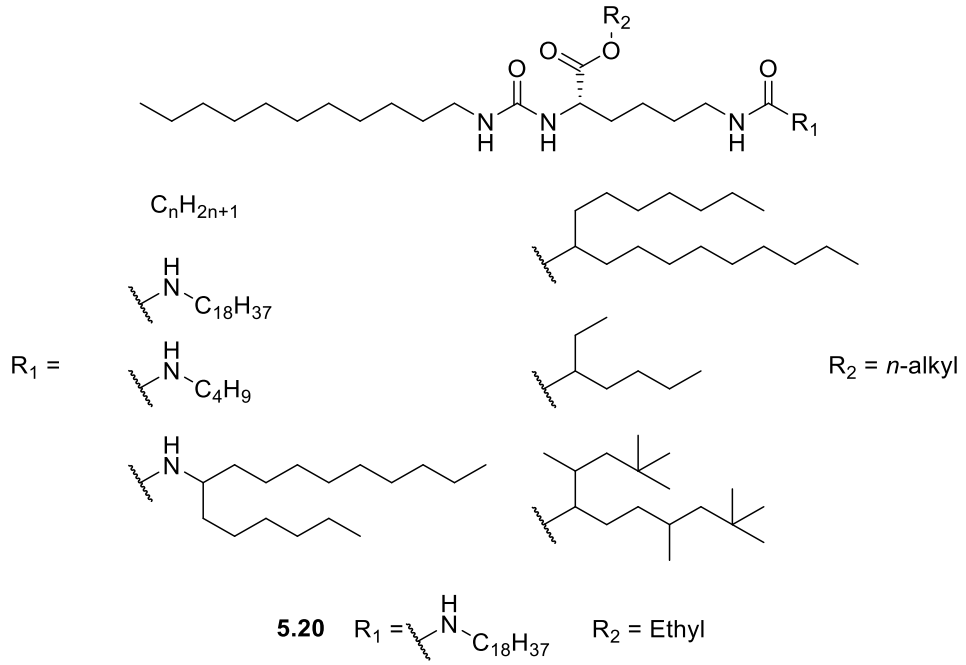
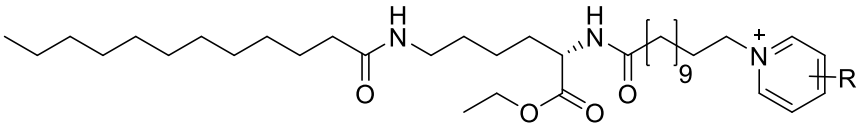


Figure 5.8. Library of lysine-based organogelators

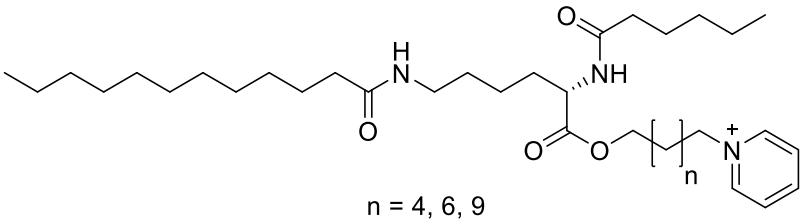
In addition, a library of compounds was prepared by modification of the R_1 and R_2 groups. It was found that urea containing compounds (R_1 = secondary amine) were better organogelators than compounds with amide bond (R_1 = alkyl). This was thought to be due to the stronger hydrogen bonding capability of the urea functional group comparing with that of the amide bond. Also, it was noticed that increasing the length of alkyl chain of the R_1 group and decreasing the length of alkyl chain of the R_2 group resulted in increasing organogelation ability.[244]

Alternatively, lysine-based hydrogelators were also prepared. The pyridinium ion was introduced to the side chain of the organogelator to get a water-soluble lysine gelator. The position of pyridinium cation was either on the terminal R group (**5.21)**[245] or in the branched ester group (**5.22)** (Figure 5.9) [246]. Gelators **5.21** forms gels with water at a concentration of 1% w/w. With regards to gelators **5.22** the ability to form a gel increases with the increase of the length of spacer between the amino acid and pyridinium ion and precipitation was observed when n = 4.



R = alkyl or substituted alkyl

5.21

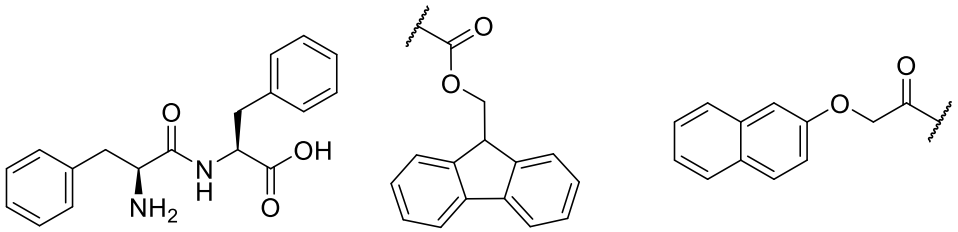


n = 4, 6, 9

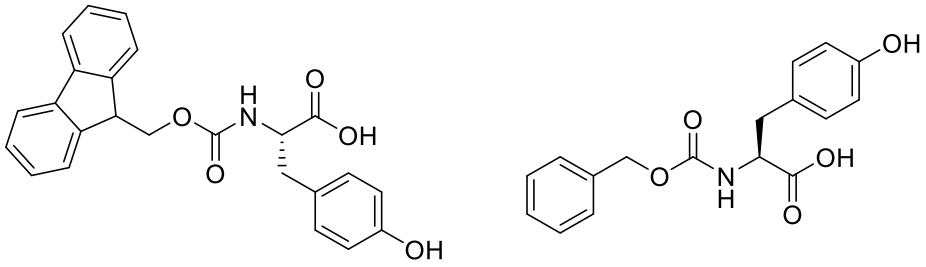
5.22

Figure 5.9. The lysine-based hydrogelators 5.21 and 5.22

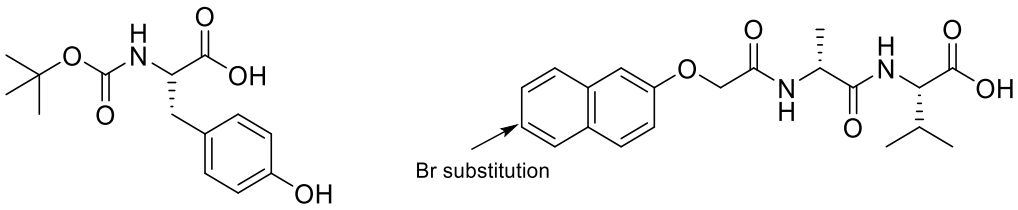
The above examples represent gelators based on a single amino acid. Peptide-based gelators have been also investigated as will be described further. Peptide-based systems are characterised by hydrogen-bonding which depends on the sequence of amino acids. This can lead to the formation of ordered secondary structures including α-helices, β-sheets and anti-parallel β-sheets.[34] Diphenylalanine **(5.23)** was one of the first dipeptides which was shown to self-assemble in solution.[247] Demirel *et al.* proposed that hydrophobic interactions are responsible for self-assembly of Phe-Phe dipeptide.[248] In addition, Yan *et al.* showed that diphenylalanine was able to form gels in chloroform, toluene and xylene but not methanol, acetone and DMF.[249] The addition of an aromatic protecting group such as fluorenyl-9-methoxycarbonyl (Fmoc) (**5.24)** or naphthalene (Nap) **(5.25)** to the amine group of the dipeptide enhanced the strength of hydrogelation.[240] An example of the role of different protecting groups in triggering gelation is where Fmoc-Tyr-OH (**5.26)** was a hydrogelator while carboxybenzyl-Tyr-OH (**5.27)** and *tert*-butyloxycarbonyl -Tyr-OH (**5.28)** were not. [70] The role of π–π stacking by aromatic groups in enhancing self-assembly was investigated. Molecular dynamic analysis of peptide gels using computational mechanics software supported that π–π stacking had an important role in formation of hydrogel (Figure 5.10).[250,251] In contrast, other studies revealed that disrupting π–π stacking of naphthalene-Ala-Val-OH (**5.29)** by attaching a bromine substituent to the naphthalene ring had no negative effect on gel formation.[32]



5.23 **5.24** **5.25**



5.26 **5.27**



5.28 **5.29**

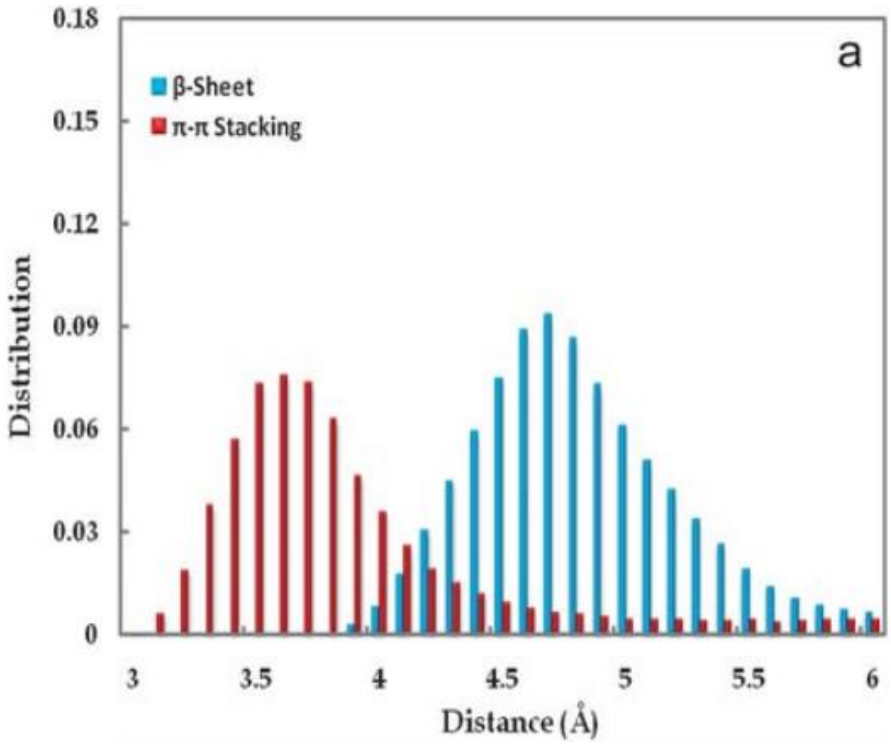
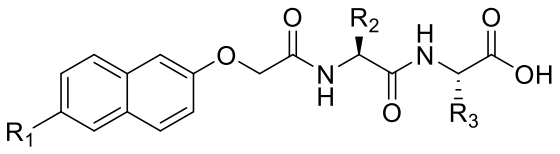


Figure 5.10. Molecular dynamic simulation showing the distribution of β-sheet distances between the Fmoc-protected amino acids molecules and π–π stacking distances between Fmoc residues described in reference [247]

The effect of hydrophobicity on hydrogelation of peptide gelators has also been investigated by Adams and co-workers who studied the gelation of selected set of Fmoc dipeptides. The study demonstrated that there is a correlation between hydrophobicity and gel formation. Compounds with log P less than 2.8 were weak or unstable gelators while when log P was greater than 5.5, the dipeptides were too hydrophobic to gel. The best range for stable gels was when log P was between 3.4 and 5.5.[33]

Interestingly, a number of studies tried to explore the correlation between the pKa of the carboxylic acid of the dipeptide with self-assembly.[33,35,252] It was found that the dipeptides entrapped within organised structures (such as the gel fibre) have a higher pKa value than the free form in solution. This may be attributed to the incorporation of the carboxyl group into the hydrophobic portion of the structure. As mentioned before, Fmoc diphenylalanine is a gelator with a predicted pKa of 3.5 in solution, and forms gels with water at pH 7.0. It is thought that the trigger of gelation process is change of ionisation state of the C-terminus of the dipeptide. A correlation between hydrophobicity (calculated by predicted clog P) and the change in pKa has been investigated by the Adams group. A library of 18 naphthalene-diphenylalanine derivatives with different substituents on naphthalene and various alkyl side chain of the amino acid were prepared (**5.30)**. [32,250]



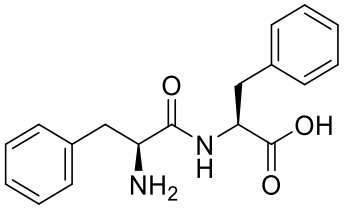
R_1 = H, Br, CN
R_2 = Methyl, Benzyl
R_3 = H, Methyl, Isopropyl

5.30

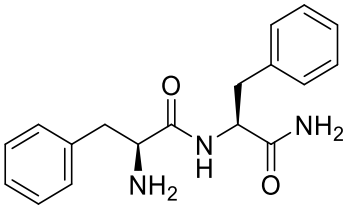
Solutions of all the compounds in this library were prepared at high pH then the pH was lowered resulting in protonation of the free carboxyl group leading to gel formation. Fifteen compounds successfully formed gels whilst the remaining three formed crystals. This was followed by measurement of pKa of the dipeptide contained in the gel network. The pH at which the gel was formed was below the measured pKa for these derivatives. The authors also reported that the

relationship between pKa, lipophilicity and pH for Fmoc dipeptides could be applied in the future design of peptide-based LMWGs.[253]

Ulijn and co-workers reported the formation of metastable gels of diphenylalanine (free acid and amide). Gelation was triggered by both solvent switch and sonication. The dipeptide was initially dissolved in 1,1,1,3,3,3-hexafluoro-2-propanol and the pH was adjusted to pH 8.0. Upon sonication, the solution was changed to an opaque gel which contracted shortly due to the release of moisture present in the gel network, a process called syneresis.[254]

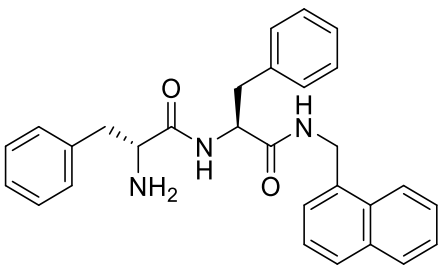


5.31

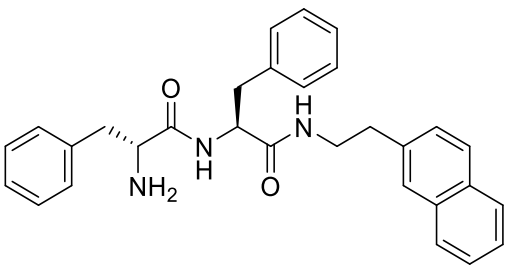


5.32

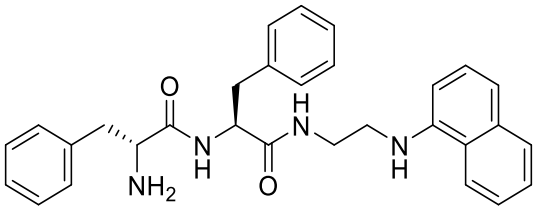
Another study focused on diphenylalanine-based gels was conducted by Xu *et al*. They linked naphthalene to the C-terminus of diphenylalanine using three different spacers. These three compounds formed stable hydrogels in water with concentrations of 0.8% w/w at pH 5-6. They suggested that the aromatic-aromatic interactions ($\pi - \pi$ stacking) and protonation of the terminal amine group were the driving force of gelation. Interestingly, these hydrogelators were found to exhibit selective toxicity against HeLa cancer cell lines.[255]



5.33



5.34



5.35

5.2. Results and discussion

Different amide derivatives of linifanib were synthesised and evaluated for gel formation. Three libraries of compounds were made where the side chains were linked to the endocyclic NH of the indazole ring of linifanib. These side chains were either an aliphatic carboxylic acid, dipeptides or a single amino acid. Initially we synthesised the aliphatic carboxylic acid because it is much shorter than the carbamate side chain and hence thought to less likely to disrupt sterically self-assembly. Amino acids and dipeptides derivatives were synthesised as these side chains are reported extensively as gelator motifs. Also they were synthesised as the HCl salts to enhance aqueous solubility through ionisation. Also, dipeptides represent one of the important pro-moieties of several prodrugs. The derivatives which demonstrated gelation and cleavage to linifanib were further characterised to assess their mechanical strength, morphology, and stability in plasma.

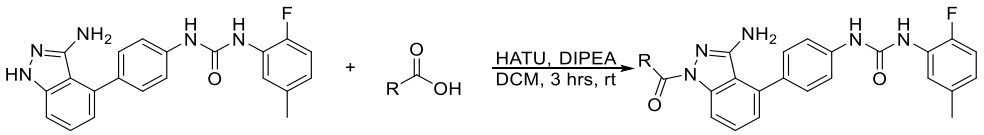
5.2.1. Amide derivatives of linifanib with aliphatic carboxylic acid side chain

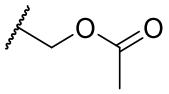
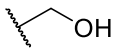
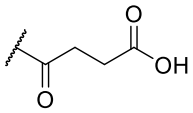
At this stage of the project, we tried to understand the relationship between the chemical structures of the linifanib derivatives with gelation behaviour. Firstly a series of amide analogues of linifanib was synthesised by reacting linifanib with aliphatic carboxylic acids with different alkyl chain lengths, branching and also with different numbers of hydrogen bond donor and acceptors as shown in Scheme 5.1. These different structural features of the side chain were to probe how sterically the side chain and the number of hydrogen bond donors and acceptors influenced gelation.

In addition, predicted clog P was used to estimate the lipophilicity which was reported in many studies to have a strong effect on gel formation as it is essential to have a balance between hydrophilic and hydrophobic parts in the gelator molecule.[26,253,256] Initially, we report the synthesis of these compounds, then vial inversion screening. Stable gels identified as part of the vial inversion screening were then further characterised by rheology.

5.2.1.1. Synthesis

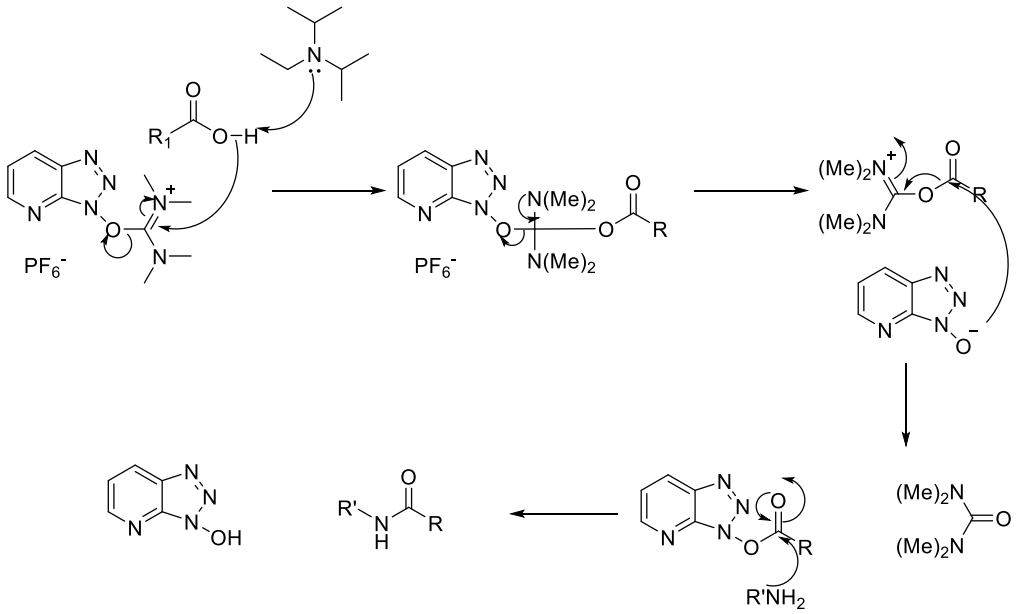
The amide derivatives of linifanib (**5.36-5.40**) were synthesised using (1-[*bis* (dimethylamino) methylene] -1H- 1,2,3- triazolo [4,5-b] pyridinium 3-oxid hexafluorophosphate) (HATU) as the activating agent and *N*,*N*-diisopropylethylamine (DIPEA) as the base under room temperature (Scheme 5.1). DIPEA base was used to deprotonate the carboxylic acid. The resulting carboxylate anion attacks the electron deficient HATU. This is followed by the reaction of the resulting anion with the activated carboxylic acid to form an activated ester which reacts with the amine to form the desired compounds (Scheme 5.2). Purification of the crude product was achieved through silica gel chromatography eluting with 20-80% ethyl acetate/petroleum ether to get the pure compounds in yields of 40-60%.



Compound	Carboxylic acid	R group	Yield	HBD and/ or HBA	clog P
5.36	Acetoxy acetic		47%	2	3.98
5.37	Acetic		44%	0	4.19
5.38	Propionic		50%	0	4.72
5.39	Glycolic		40%	1	3.38
5.40	Succinic*		60%	3	3.88

Scheme 5.1. Synthesis of amide derivatives of linifanib (5.36-5.39). HBD: hydrogen bond donor, HBA: hydrogen bond acceptor

* Succinic anhydride was used instead of succinic acid.



Scheme 5.2. Mechanism of amide bond formation using HATU as the coupling agent and DIPEA as the base.

5.2.1.2. Vial inversion screening

Initial gel screening was performed using the solvent switch and heating/cooling method. This involves dissolving the intended amount of compound in DMSO with heating to 60 °C. This is followed by addition of pre-heated water (70 °C) to make the final concentration of 0.5% w/v. DMSO/water mixtures in ratios of 5-25% v/v were used. The results were recorded after cooling down to room temperature (Table 5.1).

Table 5.1. Data table of vial inversion tests in DMSO/water mixtures of 0.5 % w/v of amide analogues of linifanib (5.36-5.40) with % v/v DMSO from 5 – 25%, where G: gel, WG, weak gel, P: precipitate, and S: solution. Observations were carried out after 5 minutes of cooling to room temperature

% v/v DMSO	5.36	5.37	5.38	5.39	5.40
5	G	WG	G	P	P
10	G	WG	G	P	P
15	G	P	G	P	P
20	G	P	P	P	P
25	G	S	P	P	P

These findings showed that three of the amide analogues gelled. However, compound **(5.37)** which is the acetic acid derivative of linifanib only formed weak gels only at 5-10% v/v DMSO whilst it precipitated between 15 and 25%.

The propionic acid derivative (**5.38)** demonstrated better gelation behaviour at 5-15% v/v DMSO. Interestingly, compound (**5.36**) bearing the acetoxyacetyl moiety was found to gel at all solvent ratios. Finally, the glycolic (**5.39)** and succinic (**5.40)** derivatives precipitated at all solvent ratios. These results can be justified in terms of hydrogen bonding and steric hindrance. Firstly, it was noted that the three derivatives which formed gels (**5.36**-**5.38**) did not have any hydrogen bond donor groups, whereas the glycolic (**5.39**) and succinic (**5.40**) derivatives have a terminal hydroxyl group (H-bond donor). This suggests that hydrogen bonding of the side chain is disrupting the one-dimensional order needed for the gel formation. Secondly, as compared to carbamates in Chapter 4, all the derivatives that gelled had much shorter side chains and hence less potential to sterically disrupt packing. However, these findings cannot be generalised to all derivatives of linifanib as one dimensional order is not the only determinant for gel formation.

In addition, these results showed that there may be a correlation between self-assembly and the predicted octanol/water partition coefficient of these analogues (clog P, predicted using ChemOffice Professional 2016 software) as shown in Table 5.2.

Table 5.2. Predicted clog P for amide analogues of linifanib (5.36-5.40) and their vial inversion gelation tests.

Compound	Gelation	clog P
5.38	+	4.72
5.37	+	4.19
5.36	+	3.98
5.40	-	3.88
5.39	-	3.38

Based on this correlation, gelation occurred for linifanib analogues having clog P > 3.98. Also, linifanib had a predicted clog P of 4.49. Our data is in agreement with that reported by Adams *et al.* where they analysed the hydrogelation of Fmoc-dipeptides as discussed in 5.1.3. In summary, they found that stable gels have a clog P range of 3.4-5.5.[33]

The relationship between hydrophobicity and gelation can be explained below. The aqueous solubility of the gelator is directly related to clog P (hydrophobicity) where the aqueous supersaturated solubility of the gelator (created by "solvent switch" and heating/cooling herein) drives gelation. Indeed, the branching of the fibres to form the 3D fibre network is thought to be a result of supersaturation of the gelator. Additionally, it has been suggested that higher clog P values (increased hydrophobicity) increase the supersaturation of the gelator which in turn leads to increased gel strength.[33]

Although this amount of data cannot give an exclusive conclusion; they provide a preliminary indication about the optimum range for creation of self-assembled linifanib-based amide gels in terms of lipophilicity.

*5.2.1.3. Rheology characterisation of compound **5.36***

An amplitude sweep experiment was performed on the acetoxyacetic derivative of linifanib (**5.36)** to determine its mechanical strength and then compared with the gel strength of linifanib (Figure 5.11).

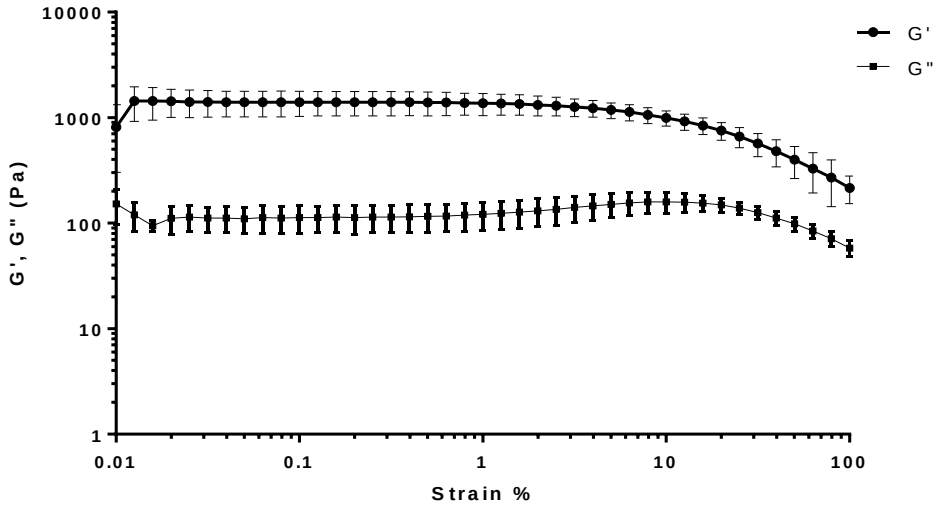
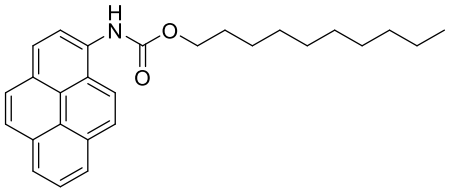


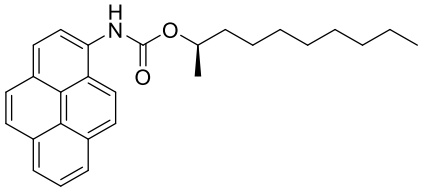
Figure 5.11. Amplitude sweep of 0.5% w/v acetoxyacetate derivative of linifanib (5.36) using 5% v/v DMSO/water mixture at 37 °C. The measurements were performed at strains of 0.01% to 100% strain at 10 rad s^{-1} and were carried out in triplicate and the mean calculated. Error bars represent standard deviation. Gels were formed instantly and measurements were taken after 3 hours.

These data showed that G' of compound (5.34) (1000 Pa) is lower than that of the corresponding concentration of linifanib (15000 Pa) under the same conditions (section 3.3.6.2) demonstrating that linifanib had a superior

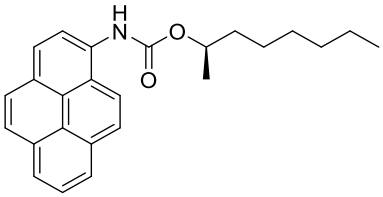
mechanical strength to its derivative. The effect of side chain on mechanical strength of gels was investigated by Maitra, *et al.* They carried out the measurements of mechanical properties of three alkyl-1-pyrenyl urethanes (**5.41**-**5.43**). All three of these compounds formed gels in hydrocarbon solvents such as dodecane and isooctane at 20 °C.



5.41



5.42



5.43

The storage modulus (G') of the achiral gel from (**5.41**) was 4600 Pa whereas the compound (**5.42**) had a G' of 43100 Pa. The highest storage modulus was observed with the gel (**5.43**). In this study, the self-assembly was thought to be driven by the $\pi - \pi$ stacking of the pyrene rings, hydrogen bonding of the urethane units and the packing of the alkyl chains. The difference in the mechanical strength is thought to be due to the difference in packing of the alkyl chains because of steric effects and hydrophobic interactions.[257] This steric effect is supposed to have a significant impact on the difference in mechanical strength in the case of the linifanib derivative (**5.39**) described above.

The stability of acetoxyacetic derivative of linifanib (**5.39**) against degradation to linifanib within the gel was investigated and shown to be resistant to degradation (Figure 5.15). This means that it cannot be considered as potential prodrug of linifanib. As a result, it was decided to design and synthesise another library of linifanib derivatives.

5.2.2. Dipeptide derivatives of linifanib

As described above, linking dipeptides to certain drugs is a useful approach for creating prodrugs. These prodrugs could liberate the parent drug by chemical mechanism through diketopiperazine (DKP) formation or by the action of

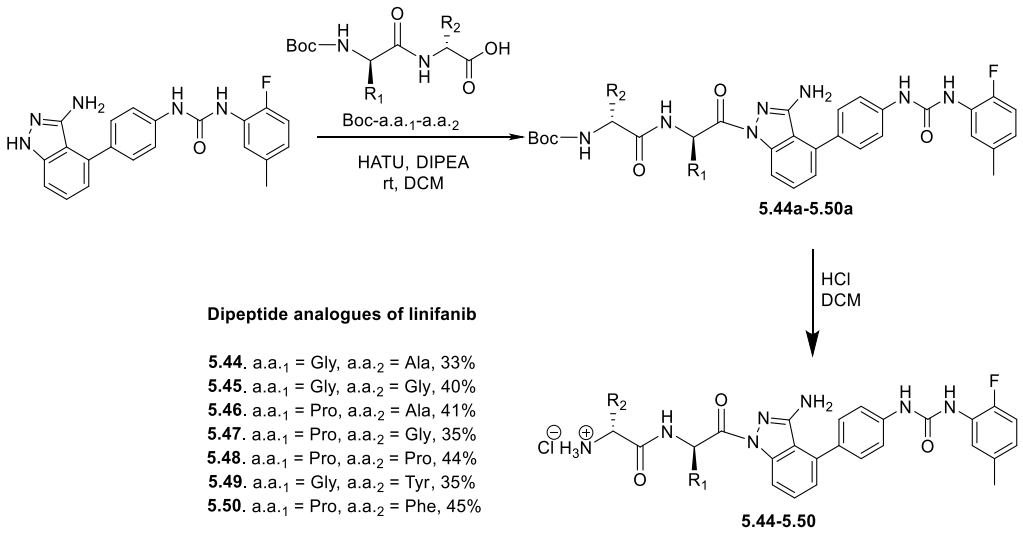
peptidase enzymes. Dipeptides side chains have also been widely used in designing gelators.[32,34,85,258]

Based on these considerations, a series of dipeptide derivatives of linifanib with different amino acids were designed and synthesised. The amino acids used to design these derivatives were selected such that their predicted clog P (lipophilicity) should be in the range of 3-5 as this was optimum for creation of amide gels as described in the previous section.

These compounds were tested for their ability to gel using vial inversion tests. In addition, a chemical stability study was undertaken to investigate the cleavage of derivatives to linifanib and also to study the effect of the amino acid on the cleavage rate.

5.2.2.1. Synthesis

Synthesis of compounds (**5.44-5.50)** was achieved by solution phase peptide synthesis. As used with amide derivatives, Boc-protected dipeptides were linked to the endocyclic NH of indazole ring of linifanib using HATU as the coupling agent and DIPEA as the base. The protected intermediates were purified by flash column chromatography using 20-100% ethyl acetate/petroleum ether as eluent. This was followed by deprotection using HCl to give the desired product in the form of hydrochloride salt. Yields of final products ranged from 30-45%. The mechanism of reaction is illustrated in Scheme 5.2.



Scheme 5.3. Synthesis of dipeptide analogues of linifanib (5.44-5.50).

5.2.2.2. Vial inversion screening

Preliminary gel screening of dipeptide derivatives of linifanib was performed using solvent switch and heating/cooling. This involves dissolving the intended amount of compound in DMSO with heating to 60 °C. This is followed by addition of pre-heated (70 °C) water to make the final concentration of 0.5% w/v. DMSO/water mixtures in ratios of 5-25% v/v were used. The results were recorded after cooling down to room temperature (Table 5.3).

Table 5.3. Data table of vial inversion tests in DMSO/water mixtures of 0.5 % w/v of dipeptide derivatives of linifanib (5.44-5.50) with % v/v DMSO from 5 – 25%, where G: gel, P: precipitate, and S: solution. Observations were carried out after 3 hours of cooling to room temperature

Compound	% v/v DMSO					clog P
	5	10	15	20	25	
5.44	P	P	P	P	S	2.91
5.45	P	P	P	P	S	2.6
5.46	P	P	P	P	P	3.88
5.47	P	P	P	P	P	3.57
5.48*	G	G	G	G	G	4.58
5.49	P	P	P	P	P	3.66
5.50	P	P	P	P	P	5.30

* This derivative demonstrated gelation after 7 days

The proline-proline linifanib analogue (**5.48**) was the only compound which demonstrated gelation at DMSO/water ratios of 10-25% after a period of 7 days (Figure 5.12). The gel was analysed by LC-MS and it was found that 95% of the compound was converted to linifanib which suggests that the gel was the parent compound, linifanib. As a result, it was decided to run a chemical stability study for all the dipeptide analogues to investigate the conversion of these compounds to linifanib and the effect of different amino acids on the rate of cleavage.

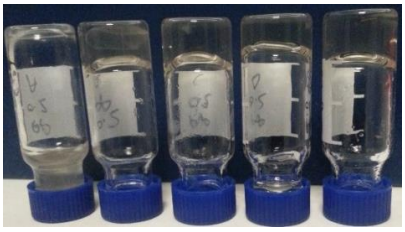


Figure 5.12. Vial inversion test 0.5 % (w/v) Pro-Pro derivative of linifanib (5.48) in 5-25 % (v/v) DMSO/water.

5.2.2.3. Chemical stability study

Samples of the dipeptide derivatives of linifanib were prepared using the same method as used for gel screening. The concentration used was 20% v/v DMSO/water mixture as this was the ratio of most stable gel of the proline-proline derivative of linifanib (Table 5.3). The degradation of the dipeptide derivatives to linifanib was monitored by measuring the amount of linifanib in these samples at different time points using LC-MS for a period of 32 days at 37 °C (Figure 5.13).

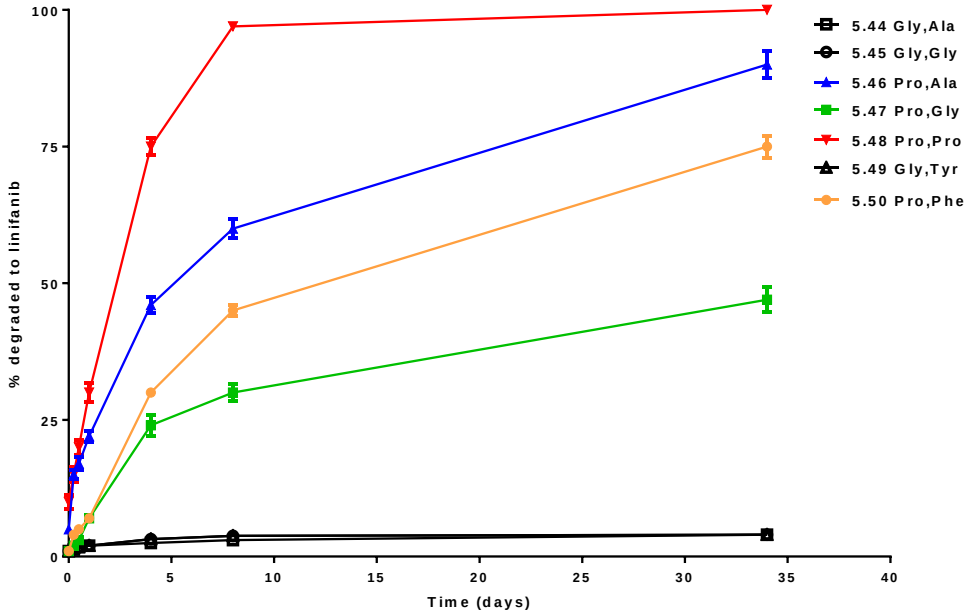


Figure 5.13. Stability study of dipeptide analogues of linifanib (5.44-5.50) using 0.5 % (w/v) of compound in 20% (v/v) DMSO/water at pH 4.0 and 37 °C. All measurements were carried out in triplicate and the mean calculated. Error bars represent standard deviation.

From these results, it seems that proline-containing linifanib derivatives had a higher rate of cleavage compared with other compounds with the highest rate for the proline-proline derivative (**5.48**). It can be noticed that as both amino acids had bulkier side chain, it is likely for the compound to cleave faster. The only exception to this was the dipeptide analogue (**5.50**) which consisted of two bulky amino acids, proline and phenylalanine.

Borchardt and Goolcharan carried out a study to analyse the rate of formation of diketopiperazine from different peptides.[259] Their model peptide was X-Pro-*p*-nitroaniline (where X = Gly, Ala, Val, Phe, Arg, and β-cyclohexylalanine) and the analysis was carried out at pH 7.0. It was found that the rate of DKP formation increased with the increase in the bulkiness of amino acid side chain.

However, the alanine derivative underwent cyclisation faster than the bulkier valine derivative. They claimed that the difference in DKP formation is affected by various factors such as the difference in the pKa of the terminal amino group of these peptides, the steric bulkiness of amino acid side chain, the peptide bond ability to undergo cis/trans isomerisation and the conformational stability of the diketopiperazine product.

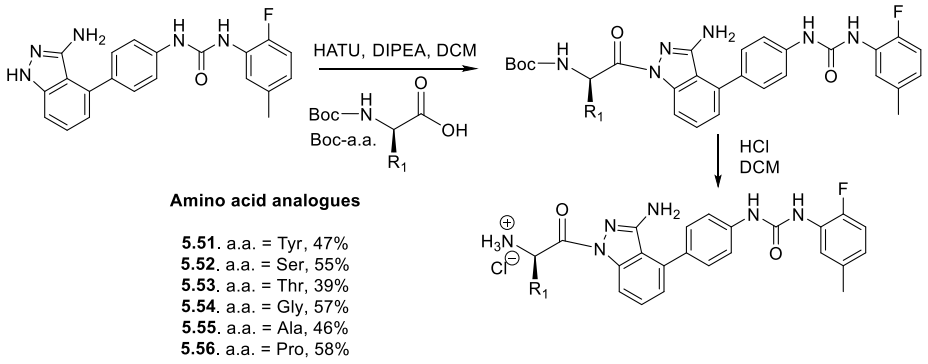
It can be concluded from these results that these derivatives can be considered as potential prodrugs of linifanib as they slowly cleaved to the parent compound. In addition, if we consider the plasma stability study described later for the serine derivative, it is expected that these prodrugs could have quicker cleavage rate due to the presence of peptidases and other proteolytic enzymes. With regard to gelation, only one derivative which is the di-proline derivative formed a gel after 7 days which was due to its degradation to linifanib. Therefore, this approach was not suitable in creation of linifanib-based self-assembled prodrugs.

5.2.3. Amino acid analogues of linifanib

The use of single amino acids derivatives to induce gelation has been extensively described in the literature as discussed in the introduction of this chapter. A library of amino acid analogues was synthesised by linking single amino acids to the endocyclic NH of indazole ring of linifanib. This is thought to be due to less steric hindrance and the lack of a hydrogen bond donors on the side amide side chain. Accordingly, it is proposed that these analogues will have an improved gelation profile than dipeptide derivatives.

5.2.3.1. Synthesis

The synthesis of compounds (**5.51-5.56**) achieved through liquid phase peptide synthesis as in section 5.2.2.1 (Scheme 5.4). Amino acids were selected with different side chains such as alkyl (glycine and alanine), hydroxyl group containing (serine, threonine and tyrosine) and cycloalkyl (proline). The final products are in the form of HCl salts and had a predicted clog P (measure of hydrophobicity) of 2 to 5.



Scheme 5.4. Synthesis of amino acid analogues of linifanib (5.51-5.56) in the form of HCl salt.

5.2.3.2. Vial inversion screening

Initially, gelation was assessed by vial inversion and a solvent switch method and heating/cooling as described above (section 5.2.2.2) used to create the gels. Two concentrations were tested for gel formation, 0.25% w/v and 0.5% w/v for all of the six amino acid analogues. The outcomes of gel screening are presented in Table 5.4.

Table 5.4. Data table of vial inversion tests in DMSO/water mixtures of 0.25 and 0.5 % w/v of amino acid analogues of linifanib (5.51-5.56) with % v/v DMSO from 5 – 25%, where G: gel, WG: weak gel, P: precipitate, and S: solution. Observations were carried out after 3 hours of cooling to room temperature

Cpd	% DMSO										clogP*
	5		10		15		20		25		
	0.5	0.25	0.5	0.25	0.5	0.25	0.5	0.25	0.5	0.25	
5.51	P	P	P	P	P	P	P	S	S	S	4.25
5.52	G	G	G	G	G	G	G	G	G	G	2.27
5.53	P	P	P	P	P	P	P	P	P	P	2.58
5.54	WG	WG	WG	WG	WG	WG	WG	WG	WG	WG	3.17
5.55	P	G	P	G	P	G	P	G	P	G	3.48
5.56	P	P	P	P	P	P	S	S	S	S	4.18

- clog P was predicted using ChemOffice Professional 2016 software.

Preliminary gel screening showed that the most stable gel was the serine derivative (**5.52**) which was a gel after 2 to 3 hours at both concentrations and

all DMSO/water ratios. Weak gels were formed with glycine derivative (**5.54**). In addition, alanine derivative (**5.55**) had different behaviour with the two concentrations. Gels were formed only at 0.25% w/v concentration (during 10 days) whereas precipitation occurred at 0.5% w/v in all solvent ratios. The two bulky amino acid derivatives of linifanib (tyrosine, **5.51** and proline, **5.56**) had similar behaviour in vial inversion tests. These two analogues showed precipitation at DMSO/water solvent ratios of 5-15% whereas clear solutions were formed at 20-25% DMSO/water mixtures. This reflects the effect of DMSO ratio on solubility of these two analogues. Finally, threonine derivative of linifanib (**5.53**) precipitated at both concentrations and all solvent ratios.

It seems that there is similar gelation behaviour of the amino acid derivatives in comparison to the amide derivatives discussed earlier. The glycine (**5.54**) and alanine (**5.55**) derivatives formed gels and the reason behind this is thought to be the short side chain with the absence of any hydrogen bond donor to disrupt the self-assembly. Alternatively, the compounds which precipitated in all solvent ratios have bulky groups which may produce steric hindrance preventing the one-dimensional order such as the aromatic substituent (tyrosine derivative) and cycloalkyl (proline derivative) or a hydrogen bond donor (threonine derivative (**5.53**). However, the gelation of the serine derivative (**5.52**) does not follow this theory. This is thought be due to intramolecular hydrogen bonding of the serine hydroxyl group (H-bond donor) with carbonyl (hydrogen acceptor) of the amide bond.

The effect of varying the amino acid on gelation was investigated for a library of naphthalene protected dipeptides (Figure 5.14). Nap-Gly-Gly, Nap-Gly-Ala and Nap-Gly-Ser were hydrogelators whereas Nap-Gly-Val and Nap-Gly-Leu failed in inducing gelation with water.[254] This reflects the effect of steric hindrance on preventing the self-assembly. Additionally, these findings means that a small change in the molecular structure of a gelator may result in gelation not occurring.[34]

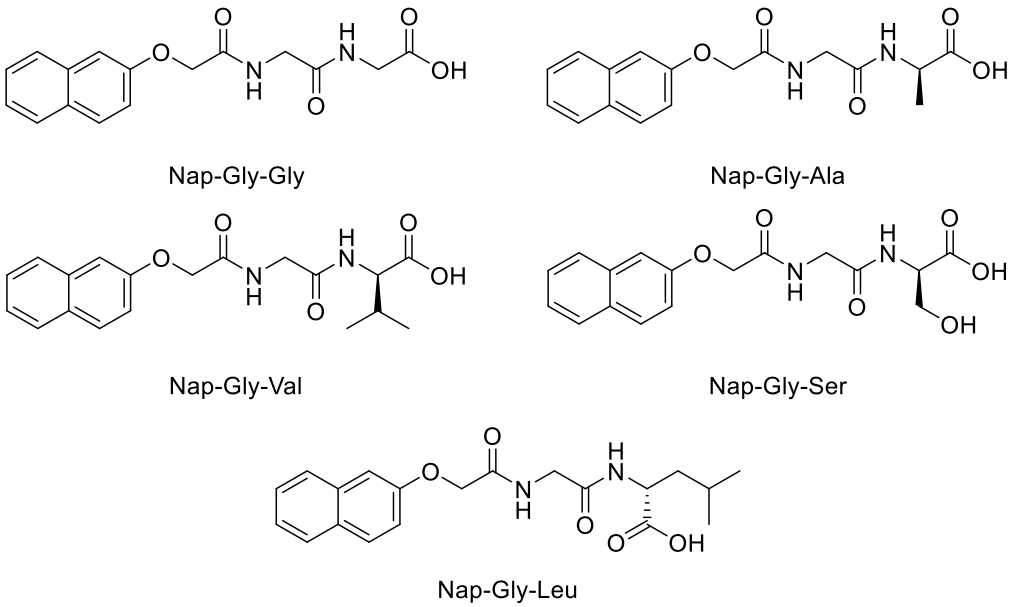
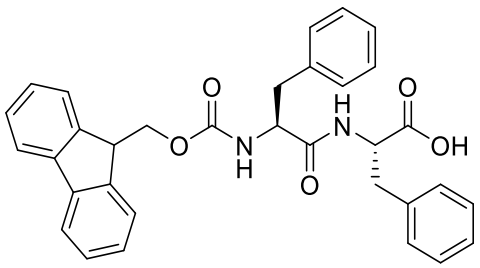


Figure 5.14. Library of naphthalene protected dipeptides

The effect of the DMSO: water solvent ratio gelation was studied by Adams *et al*. Gelation screening of Fmoc-Phe-Phe (**5.57**) showed that different solvent ratios has led to formation of different network morphology. This was explained by the difference in the gelation kinetics when the solvent ratio is changed.[154]



5.57

With regard to hydrophobicity, gels were formed with derivatives having clog P between 2.27 and 3.48. However, threonine derivative (**5.53**) which has a clog P of 2.58 fails in inducing gelation. This means that although hydrophobicity should be considered when analysing gelation outcomes, it is not always the only driving force for self-assembly.

In a recent review by Adams, a discussion about the self-assembly mechanism was presented focusing on two points. Firstly, what is the main reason which make some peptide conjugates form gels and others do not. This is thought to be due to a complicated interaction of the molecular packing and the changes in

physicochemical properties (such as hydrophobicity) on the kinetics of self-assembly. This can be achieved by the detailed understanding on the molecular level to understand the mechanism by which these changes exert significant effect on self-assembly and gelation. The above example of naphthalene protected dipeptides indicated that the steric hindrance was a determinant for gel formation. The second point was the relationship between the chemical structure of the gelator and the gel formation process.[34]

The second point was the correlation between the molecular structure and gelation. It seems that the kinetics and method of self-assembly have the major contribution regarding the gel properties. This means that the direct correlation with the gelator chemical structure is quite difficult. For many protected dipeptides, the main material properties of these compounds were associated with their apparent pKa. There was a good correlation between the apparent pKa and the pH at which gels formed. Whereas, the hydrophobicity did not clearly correlated with gel formation. In addition, there was no correlation between the gels formed at low pH and the molecular structure.[253] Thus, the structure of gel resulting from the fibrillary network will be determined by kinetics of gel formation, molecular structure and final solution conditions. Hence, the molecular structure cannot be used as a direct determinant for gelation.[34]

5.2.3.3. Chemical stability study

Amino acid analogues were investigated for their stability in DMSO/water. The concentration used was 20% v/v DMSO/water (in addition to another sample of the serine derivative (**5.52**) using DMSO/phosphate buffer 7.4 as solvent). These samples were monitored using LC-MS as described above for a period of 35 days at 37 °C to identify the pattern of cleavage and compare it with the dipeptides as the later ones cleaved through diketopiperazine formation. The results of the study were illustrated in Figure 5.15.

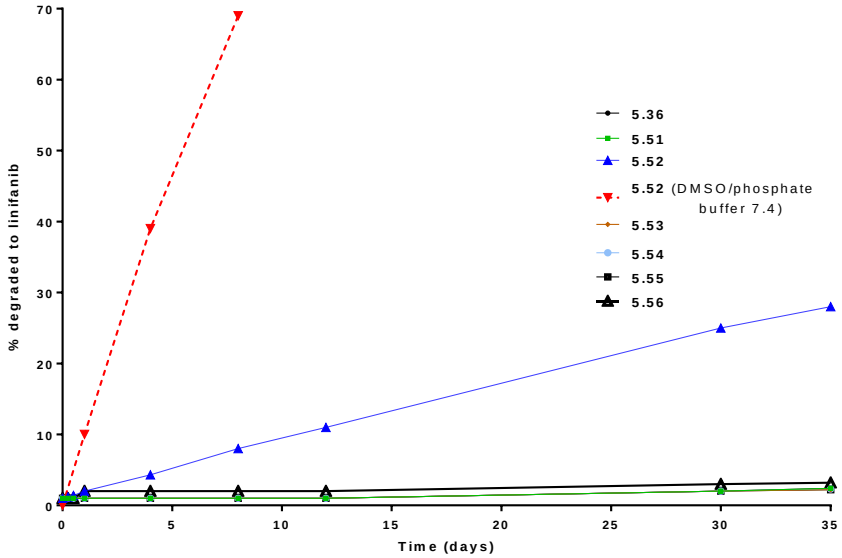
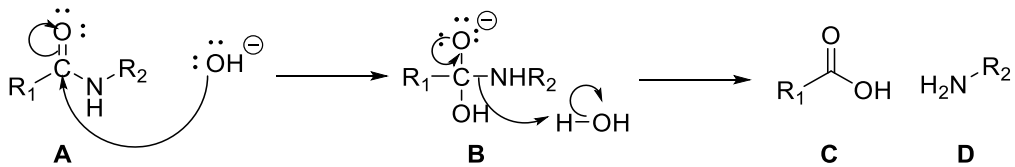


Figure 5.15. Stability study of amino acid derivatives of linifanib (5.51-5.56) and acetoxyacetic acid of linifanib (5.36) using 0.5 % (w/v) of compound in 20% (v/v) DMSO/water at pH 4.0 and 37 °C. All measurements were carried out in triplicate and the mean calculated

The data obtained from this study indicated clearly that only the serine derivative of linifanib (**5.52**) cleaved partially to linifanib while all other analogues had insignificant hydrolysis.

The general mechanism of amide hydrolysis requires a nucleophile such as the hydroxyl group which attacks the carbonyl group of the amide (**A**) to form the intermediate (**B**). This is followed by the cleavage of the amide bond under the presence of water as a source of proton to form the free carboxylic acid (**C**) and the free amine (**D**) (Scheme 5.5).[260] With regard to the amino acid derivatives of linifanib, there are three derivatives which contain hydroxyl group: tyrosine derivative (**5.51**), serine derivative (**5.52**) and threonine derivative (**5.53**). However, only the serine derivative demonstrated slow cleavage to linifanib while the hydrolysis of the other two derivatives was insignificant. It is suggested that steric hindrance in the case of threonine and tyrosine derivatives was responsible for preventing the hydroxyl group from attacking the carbonyl group.



Scheme 5.5. Mechanism of base-catalysed amide hydrolysis

The dotted line in Figure 5.15 represents the cleavage of derivative (**5.48**) using DMSO/phosphate buffer pH 7.4. The half-life of the degradation of this linifanib derivative was 7 days at pH 7.4 whereas it was estimated to be more than 50 days with DMSO/water mixture (pH 4.0). This effect of pH on the cleavage rate was also observed in the hydrolysis of the prodrug of the anti-HIV agent 2'-*C*-methylcytidine, valopicitabine (Figure 5.16). [261]

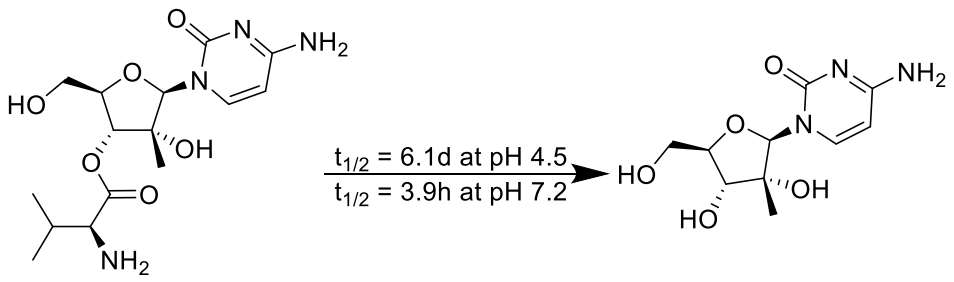


Figure 5.16. Hydrolysis of valopicitabine at pH 4.5 and 7.2.

This difference in cleavage rate is thought to be due to different percent ionisation of the compound in both water and the phosphate buffer. At pH 4.0, the serine derivative is almost completely ionised (99.9%) whilst the percent ionisation is around 39% at pH 7.4 meaning that the major portion of the derivative is in the unionised form.

5.2.3.4. Rheology

From the preliminary vial inversion screening, it was noted that the serine (**5.52**) and glycine (**5.54**) derivatives formed gels in DMSO/water mixtures (pH 4.0). These compounds are in the form of hydrochloride salts with a predicted pKa of 7.2 and 7.7 (using Marvin Sketch software 16.5.16, 2016) respectively. Hence these compounds in solution will be ionised and the percentage ionised will depend on the pH of the solution according to Henderson Hasselbalch equation for bases:[262]

$$pH = pK_a + log\left(\frac{[B]}{[BH^+]}\right)$$

There are numerous studies which investigated the relationship between the pKa and self-assembly process.[258,263-265] Fmoc-Phe-Phe is one of the most extensively studied hydrogelators. At high pH, the gelator molecules become ionised and in solution which means that no gel is formed. The first pKa transition was observed at pH 9.5-10.2 due to the self-assembly of both

protonated and neutral species and the charges related to the terminal carboxylic group will be located on the fibres surface. Finally, at the critical gelation concentration (CGC), these fibres will entangle to form the 3D network and eventually a hydrogel.[35] Similarly, the self-assembly of other Fmoc-protected dipeptides has led to reduction of ionisation resulting in pKa shifts (apparent pKa) in comparison to their calculated pKa. This suggested that the terminal carboxyl group is entrapped in a hydrophobic environment during self-assembly. [258]

It was decided to carry out rheological experiments for both derivatives at the physiological pH (7.4) as a starting point. This will assess the mechanical strength of these compounds and provide an idea regarding the effect of slight difference in chemical structure on the gel strength.

Amplitude sweep was conducted at 37 °C using 0.5% w/v concentration of the two derivatives and results were recorded in Figure 5.17.

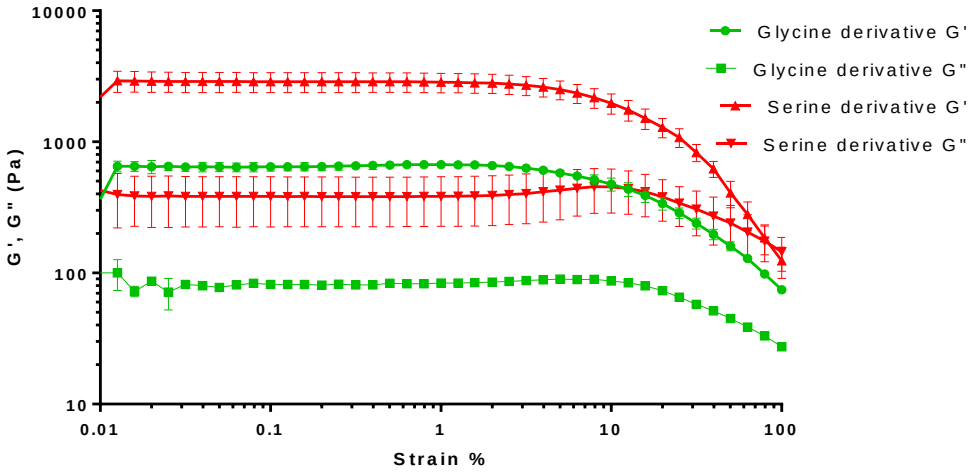


Figure 5.17. Amplitude sweep of 0.5% w/v of serine (5.52) (red) and glycine (5.54) (green) derivatives of linifanib using 5% v/v DMSO/phosphate buffer 7.4 mixture at 37 °C. The measurements were performed at strains of 0.01% to 100% strain at 10 rad s^{-1} and were carried out in triplicate and the mean calculated. Error bars represent standard deviation. Gels were formed instantly and measurements were taken after 3 hours.

It was clear that the serine derivative (**5.52**) had a superior mechanical strength on the glycine derivative (**5.54**). This difference in mechanical strength is thought to be due to the extra hydrogen bonding provided by the hydroxyl group of serine. In addition, Saiani *et al*. suggested that the nature of amino acid side chain had a significant effect on the self-assembly process which may be due to the steric and hydrophobic effects.[266]

As the serine derivative (**5.52**) cleaved slowly to linifanib in addition to its superior mechanical strength, it was decided to perform further characterisation on this compound to provide more insight on its gelation characteristics.

5.2.3.5. Vial inversion test using DMSO/phosphate buffer mixtures

Vial inversion screening of 0.125-1% w/v serine analogue of linifanib (**5.52**) was undertaken using solvent mixtures of 5% (v/v) DMSO/phosphate buffers (pH 6-8.1). This pH range was selected to provide an opportunity to explore the effect of different degrees of ionisation of the serine analogue (10-90%) on gel formation. The gelation tests were shown in Table 5.5 and Figure 5.18.

Table 5.5. Data table of vial inversion tests in 5% v/v DMSO/phosphate buffer (pH 6.0-8.1) mixtures of 0.125, 0.25, 0.5 and 1% w/v of serine analogue of linifanib (5.52) where G: gel, WG: weak gel, P: precipitate, and S: solution. Observations were carried out after 5 minutes of cooling to room temperature

Conc. / pH	0.125	0.25	0.5	1	% ionisation
6.0	S	G	G*	G	94.1
6.6	S	G	G	G	79.9
6.8	S	G	G	G	71.5
7.0	S	P	G	G	61.3
7.4	S	P	G	G	38.7
7.9	S	P	P	G	16.6
8.1	S	P	P	G	11.2

* Gel was formed after 3 hrs.

These results revealed that the 0.125 % concentration formed solutions for the whole pH range. This may be because the concentration was too low to form gels. Gels were formed from pH of 6.0-6.8 for the 0.25 % concentration which means high % ionisation is needed to form gels at this concentration. At 0.5% concentration, gels were noticed in the pH range of 6.0-7.4. Finally, formation of gels of 1% concentration was independent on pH and gels were observed at the whole pH range. From these data, it appears that a certain concentration of the ionised serine analogue is required and to form the gels and the propensity for forming a precipitate increases with pH. This maybe explained that at a lower pH the supersaturated solubility will be higher and this is probably required to

form gels whilst the unionised form of the free base of the serine analogue is precipitating out at higher pH.

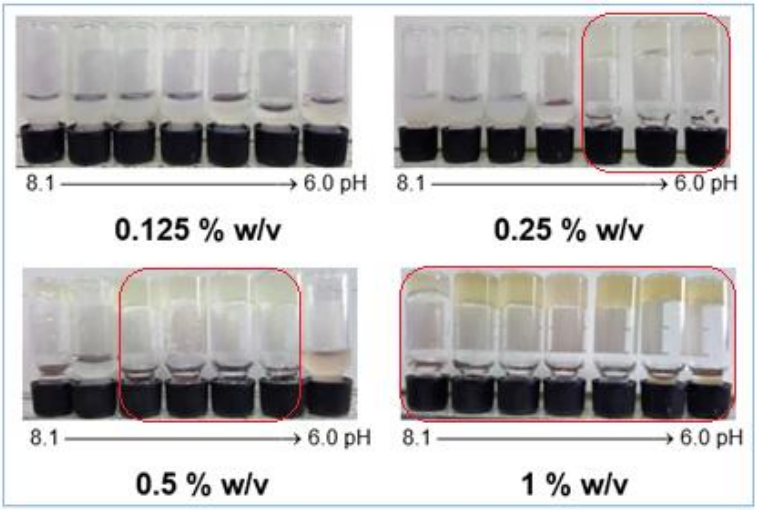


Figure 5.18. Vial inversion tests of 0.125-1% w/v serine analogue of linifanib (5.52) in 5% v/v DMSO/phosphate buffer (6-8.1). The red boxes represent the positive gels.

5.2.3.6. Rheological measurements

Vial inversion tests of the serine analogue (**5.52**) showed that the 0.5 % w/v concentration was the lowest concentration which formed stable gels in most of the pH range. Therefore, it was decided to perform amplitude sweep at a pH range from 6.0 to 7.4. This is important range as it involves both the physiological pH is 7.4 and the pH of tumour microenvironment is 6.8 (Figure 5.19).[267,268].

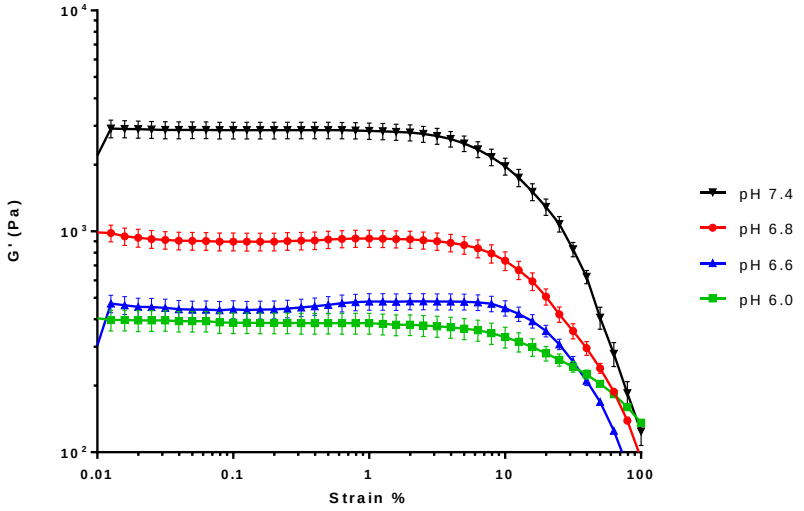


Figure 5.19. Amplitude sweep of 0.5% w/v serine analogue of linifanib (5.52) using 5% DMSO/phosphate buffer pH 6.0-7.4 at 37 °C. Only G' was showed. All measurements were carried out in triplicate and the mean calculated. Error bars represent standard deviation. Gels were formed instantly and measurements were taken after 3 hours

From this data, it can be noticed that the storage modulus G' is directly proportional with the increase in pH within the range examined (Figure 5.20). The previously mentioned work by Adams *et al*. performed amplitude sweeps for the Fmoc-diphenylalanine gels at different pH might give some insight.[192] In comparison, the storage modulus of compound (**5.52**) at pH 7.4 was 3.98 kPa while with Fmoc-diphenylalanine, G' was less than 100 using the same concentration (0.5% w/v) while a G' of 1kPa was observed with pH 6.0. It was suggested that these differences in mechanical strength were because the ionised form of the derivative is in solution whilst the free base form is in the gel network, so at higher pH there is more fraction of the unionised form and hence more amount of the compound is in the gel network leading to increased gel strength.

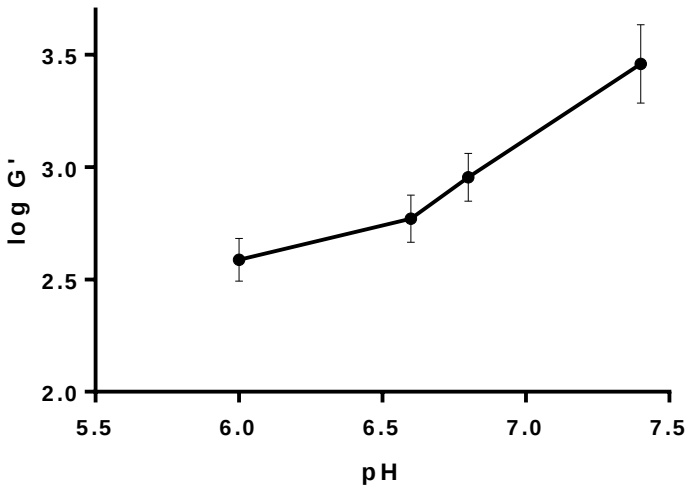


Figure 5.20. Correlation between storage modulus (G') of 0.5% w/v serine derivative (5.52) in 5% v/v DMSO/phosphate buffer 6-7.4 and pH at 1% strain and 37 °C.

Further characterisation was performed on analogue **(5.52**) and the gel with the best mechanical strength was selected (i.e. 0.5% w/v at pH 7.4) to conduct frequency sweep measurement. Results showed that the mechanical strength represented by storage modulus (G') was nearly independent on angular frequency in the range of 0.1- 40 rad/s as shown in Figure 5.21.

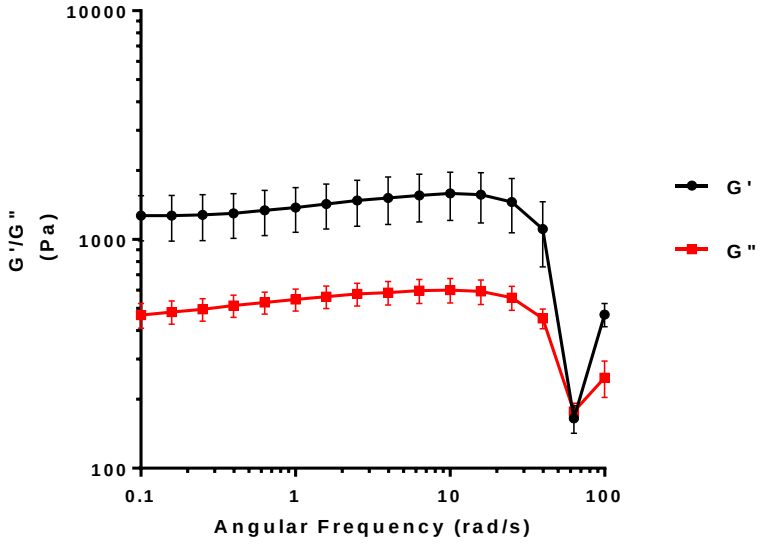


Figure 5.21. Frequency sweep of 0.5% w/v of serine derivative of linifanib (5.52) in 5% v/v DMSO/phosphate buffer 7.4 at 37 °C. All measurements were carried out in triplicate and the mean calculated. Error bars represent standard deviation.

5.2.3.7. Solid State NMR

NMR spectroscopy provides valuable information regarding the molecular interactions within the gel network. At low temperatures in the gel state, the functional groups that are involved in gelation are immobilised within the solid-like gel network because of the strong intermolecular interactions, with broadening or disappearing of the NMR signal. In contrast, groups that did not participate in the self-assembly give sharp peaks, as a consequence of their mobility in solution. An increase in temperature results in gel-sol transition, due to the increased motion of molecules, and subsequent appearance of signals from the groups involved in the self-assembly.[59] Therefore, solid-state NMR was carried out on the serine derivative (**5.52**).

At low concentration of the derivative (1% w/v) in 5% v/v DMSO-d_6: D_2O, ^1H NMR with water suppression, there was no detection of aromatic protons due to the very low concentration. Therefore, it was decided to increase the concentration to 10% w/v. This allows the observation of aromatic protons as shown in Figure 5.22

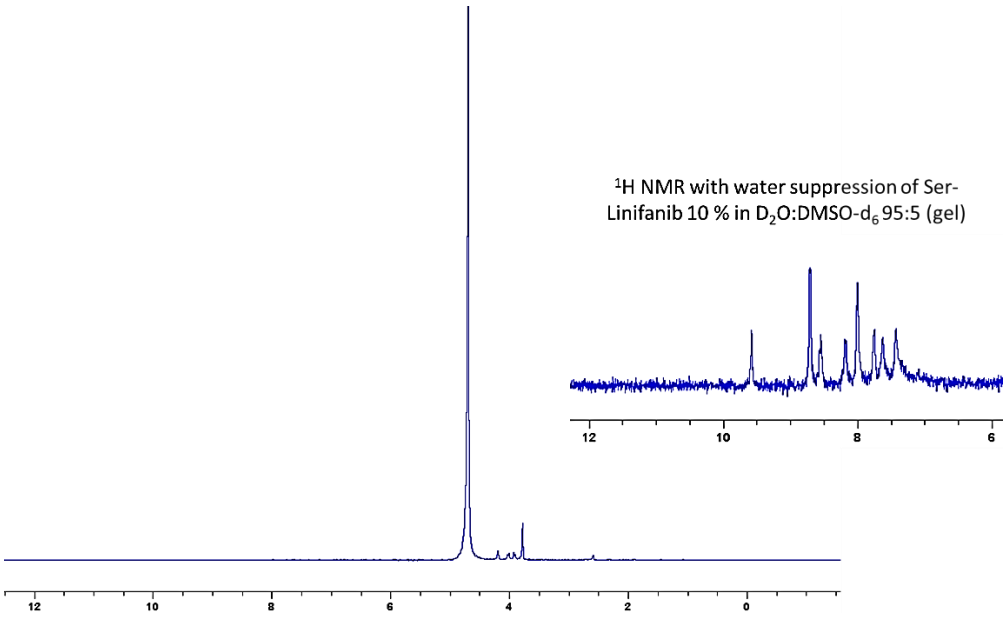


Figure 5.22. ^{1}H NMR of serine derivative of linifanib (5.52) (10% w/v) in 5% v/v DMSO-d_6: D_2O (gel)

A comparison between the spectra of the derivative in both solution and gel state was done to track any changes in chemical shifts (Figure 5.23). This will provide more insight to the molecular interactions as described earlier. Due to different polarities of the solvents used in both cases, the chemical shifts are different. Therefore, nothing can be concluded on the variation of chemical shifts upon gelation.

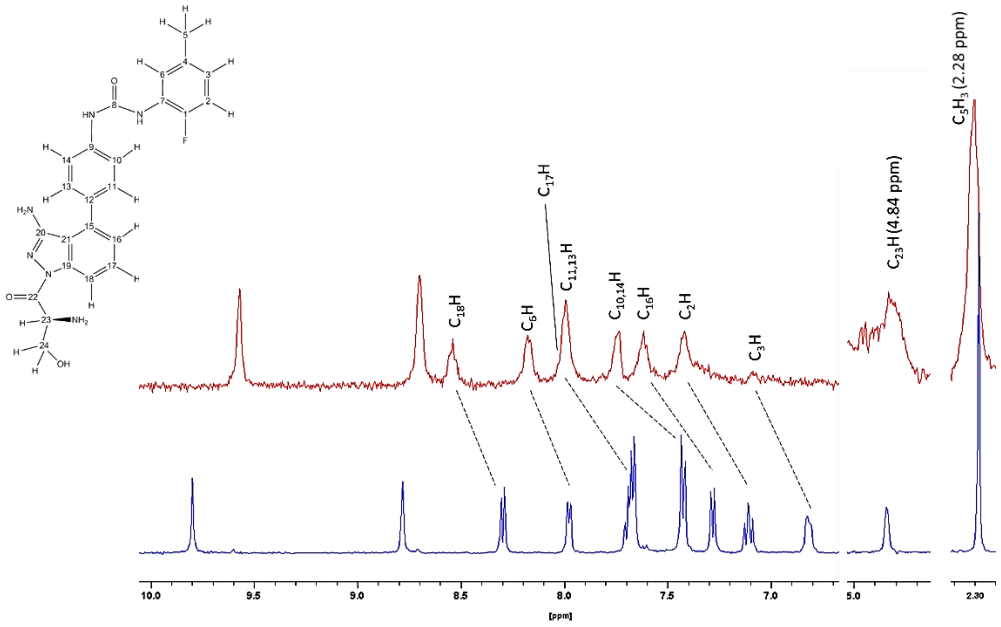


Figure 5.23. Comparison of ^{1}H NMR of serine derivative of linifanib (5.52) in 5% v/v DMSO-d_6: D_2O (gel) (blue) and DMSO-d_6 (solution) (red).

To overcome this issue, we tried to monitor gelation over a period of time. Unfortunately, gelation occured very fast and no significant differences in peak intensity or chemical shift were observed between the spectra acquired immediately after gelation and 5 hours later (Figure 5.24).

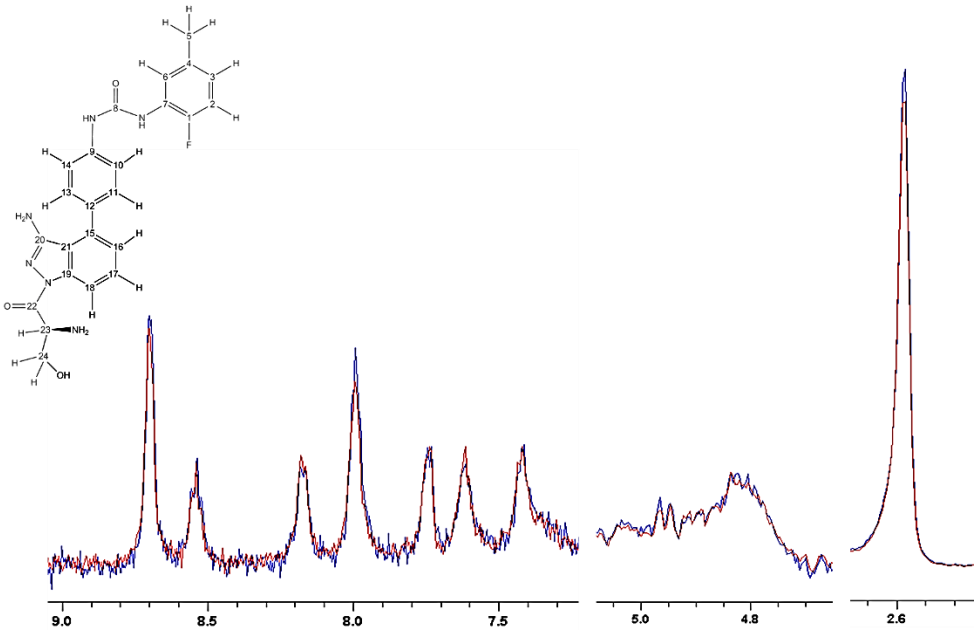


Figure 5.24. ^{1}H NMR of serine derivative of linifanib (5.52) (10% w/v) in 5% v/v DMSO-d_6: D_2O (gel) immediately after preparation (blue) and 5 hours after preparation (red).

The issues encountered with Ser-Linifanib were the fact that it is very insoluble in water, preventing the acquisition of a well-resolved spectra in the solution state; gelation occuring at very low concentrations, creating sensitivity problems; and fast kinetics of gelation that did not allow to take several spectra throughout the process of self-assembly.

5.2.3.8. FT-IR spectroscopy

FT-IR spectroscopy can be used for the characterisation of gel formation process as it provides an understanding of the self-assembly of gelator molecules and allows the determination of the functional groups involved in gelation.[269,270] The detection of peak shifts and broadening of peaks via FT-IR is an indication of hydrogen bonding and have been reported for other gelators.[271,272] This indicates that these free molecules are changed to hydrogen bonded.

FT-IR spectrum of the serine and glycine derivatives (**5.52 and 5.54**) was carried out for the solid, solution and gel forms (Figure 5.25 and Figure 5.26). It was

noticed that the pattern of the spectrum of the solid and liquid form of both derivatives was similar. The peaks of the solid and liquid form were in the approximately in the same position in both derivatives. Regarding the serine derivative, the amide bond peak was shifted from 1699 cm^{-1} in the solution form to 1640 cm^{-1} in the gel with broadening and attenuation of the later peak.

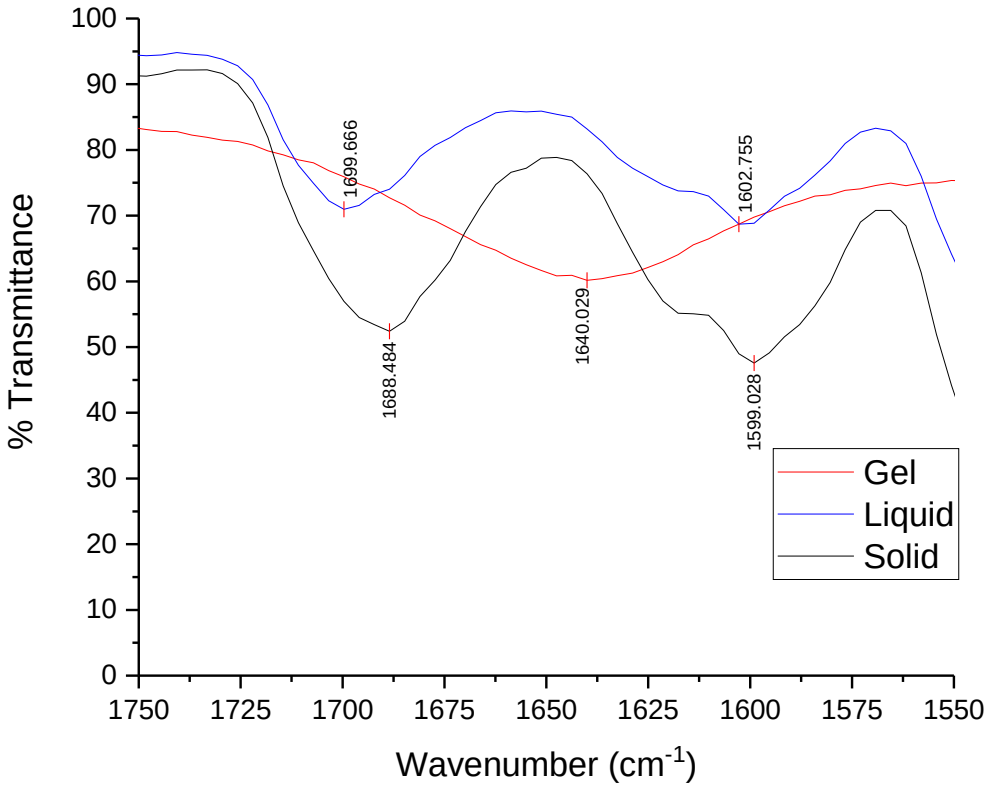


Figure 5.25. FT-IR spectroscopy of the amide region of serine derivative of linifanib (5.52) for the solid (1 mg), 0.5% w/v DMSO solution and 0.5% w/v in 5% DMSO/phosphate buffer 7.4 at room temperature.

On the other hand, the amide peak of the glycine derivative (**5.24**) demonstrated a shift from 1699 cm^{-1} to 1636 cm^{-1}. Again, broadening and weakening was associated with this shift.

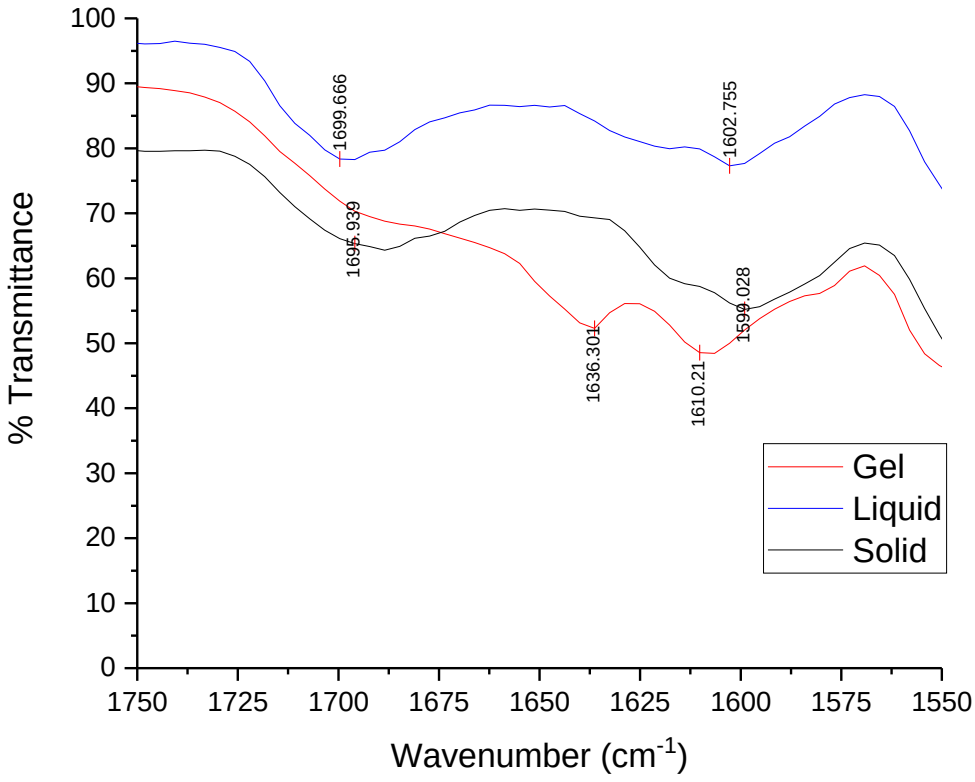


Figure 5.26. FT-IR spectroscopy of the amide region of glycine derivative of linifanib (5.54) for the solid (1 mg), 0.5% w/v DMSO solution and 0.5% w/v in 5% DMSO/phosphate buffer 7.4 at room temperature.

This suggests the role of hydrogen bonding within the gel network. However, because this type of characterisation is not specific as we cannot discount hydrogen bonding with water, this finding can be considered only as a preliminary confirmation of the presence of hydrogen bonding inside the hydrogel.

5.2.3.9. Transmission electron microscopy

Electron microscopy provides an insight to the morphology of LMWGs. Transmission electron microscopy was acquired for both the serine and glycine derivatives of linifanib for imaging of the nanostructure of this gelator. Regarding the serine derivative, Figure 5.27 showed that it consists of cross-linked network of fibres with obvious pores between these fibres. Analysis of these fibres revealed that there are two groups of fibres. The long fibres were with an approximate width of 35-56 nm and a length of approximately 0.6-0.7 μm. whereas the width of the short fibres was approximately 20 nm with lengths of 200 nm.

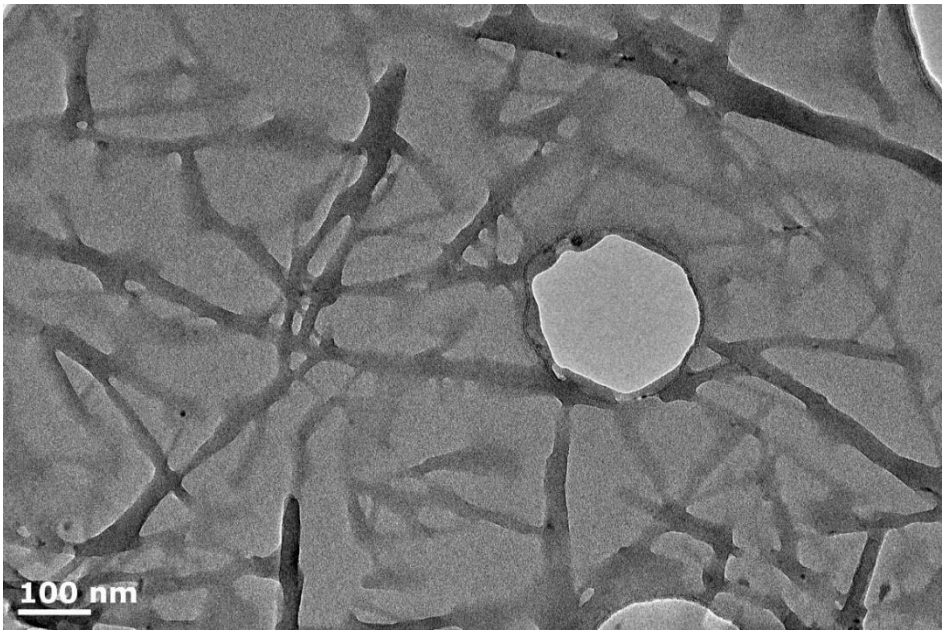


Figure 5.27. Transmission electron micrograph (TEM) of 0.5% (w/v) serine derivative of linifanib (5.52) in 5% (v/v) DMSO/phosphate buffer 7.4; scale bar = 100 nm using JEOL JEM –2000FXII transmission electron microscope and accelerating voltage of 100 kV. Gel formed instantly and the experiment was carried out after 24 hours.

On the other hand, TEM imaging of the glycine derivative showed a similar branching pattern to the serine derivative with two group of fibres. The long fibres have a length of 1.2-1.8 μm and a diameter of 25-45 nm while the short fibres exhibit an approximate length of 0.6-0.9 μm and a diameter of 10-15 nm (Figure 5.28).

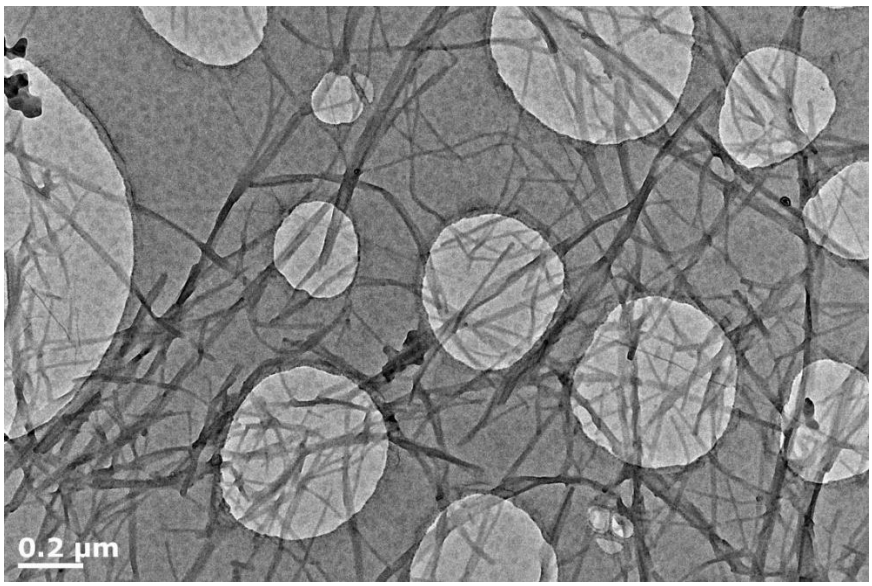


Figure 5.28. Transmission electron micrograph (TEM) of 0.5% (w/v) glycine derivative of linifanib (5.52) in 5% (v/v) DMSO/phosphate buffer 7.4; scale bar = 0.2 μm using JEOL JEM –2000FXII transmission electron microscope and accelerating voltage of 100 kV. Gel formed instantly and the experiment was carried out after 24 hours.

5.2.3.10. Plasma hydrolysis study

From the data obtained from the chemical stability study, the serine derivative of linifanib was slowly degraded to the parent drug, linifanib. This means that this derivative is a potential prodrug of the potent tyrosine kinase inhibitor. One of the key features of prodrugs is that it should involve an activation mechanism to convert it to the active drug. Enzyme-mediated hydrolysis is the commonly reported mechanism of degradation for most prodrugs.[273,274] Amino acid prodrugs are hydrolysed by several enzymes such as proteases and peptidases.[235]

To evaluate the hydrolysis of this derivative, a plasma hydrolysis study was carried out for both linifanib and its serine derivative to determine their stability in plasma. The study involved the determination of the half-life of both compounds in human, mouse and rat plasma. Linifanib was shown to be reasonably stable in all the three plasma samples as shown in Figure 5.29.

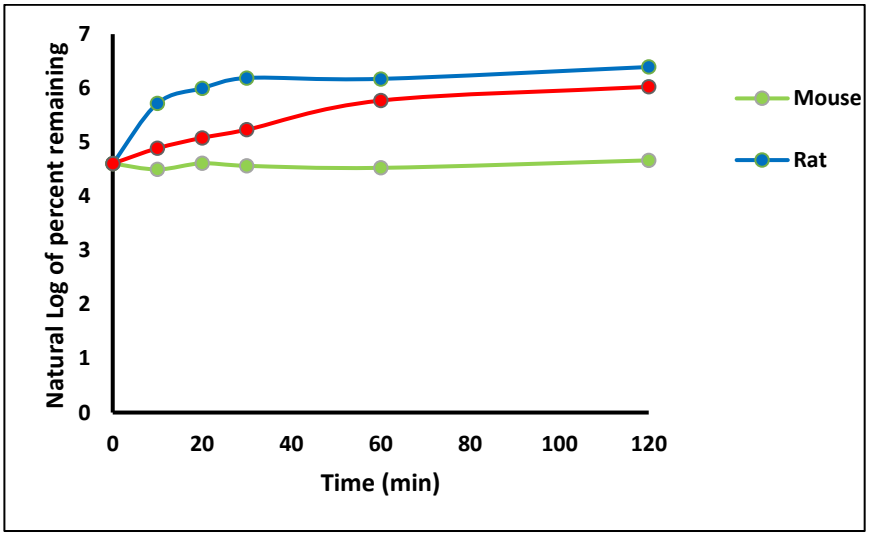


Figure 5.29. Plasma stability study of linifanib in mouse, rat and human plasma medium, n= 2. (The study was carried out at carried out at Sygnature Discovery)

On the other hand, the serine derivative of linifanib (**5.52**) was rapidly converted to linifanib in human plasma exhibiting in vitro half-life of 120 minutes. Figure 5.30). The rapid conversion is thought to be primarily due to the presence of hydrolytic enzymes such as peptidases and proteases. In addition, the half-lives of hydrolysis in mouse and rat were 270 and 30 minutes respectively. These differences are not surprising as the hydrolysis depends on the activity and/or the quantity of enzyme(s) present in these plasma samples.

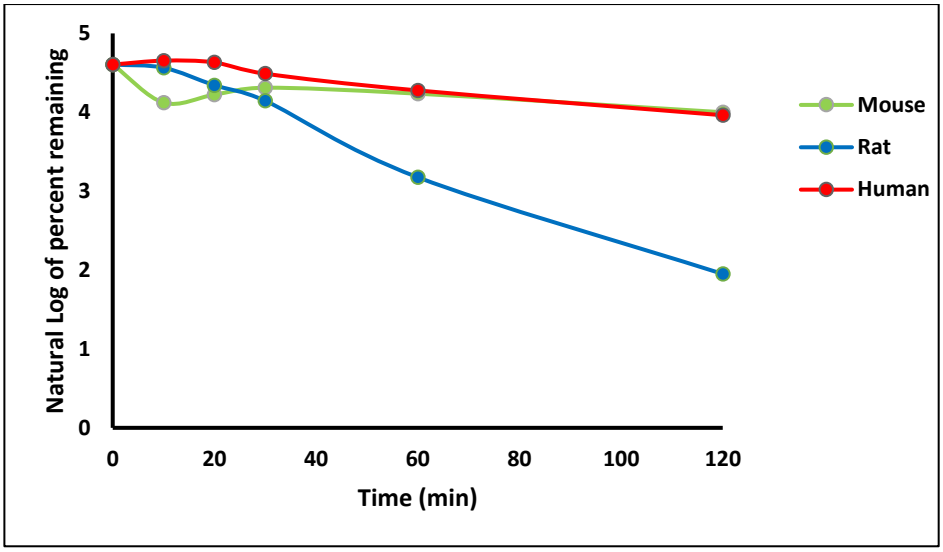
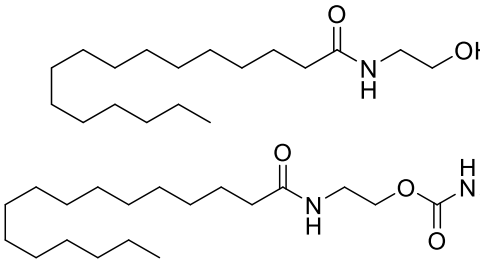


Figure 5.30. Plasma stability study of serine derivative of linifanib (5.52) in mouse, rat and human plasma medium, n = 2. (The study was carried out at carried out at Sygnature Discovery)

In comparison, Rivara *et al.* reported the rat plasma hydrolysis half-lives for a series of amino acid ester derivatives of the anti-inflammatory mediator palmitoylethanolamide (**5.58**) to improve its poor pharmacokinetics.



5.58

5.59. Gly, R = H

5.60. Ala, R = Me

5.61. Val, R = *i*-Pr

It was found that the plasma half-life of the derivatives (**5.59-5.61**) was between 96-98 minutes. This relatively short half-life was attributed to the presence of high amounts of esterases in rat plasma.[275]

Overall, these data revealed that the serine derivative of linifanib creates stable hydrogels with a good mechanical strength (> 1kPa) at the physiological pH suggesting that it is suitable for localised drug delivery since the gel ability to remain localised in a tumour mass is directly related to its stiffness.[20] In addition, the chemical stability and plasma hydrolysis studies revealed that this derivative exhibited cleavage to linifanib which can be controlled by changing pH suggesting that it is a potential prodrug of this potent tyrosine kinase inhibitor.

5.3. Conclusions

In this chapter, synthesis of three amide libraries of linifanib derivatives was reported. All of these derivatives were designed through linkage between the endocyclic indazole NH of linifanib and the carboxyl group of the desired moiety. These moieties were: aliphatic carboxylic acid, dipeptides or single amino acid.

Preliminary gelation screening was performed on all of these derivatives using vial inversion with a solvent switch method being used to form the gels. Derivatives with aliphatic carboxylic acid side chain demonstrated gelation when their clog P was between 3.98 and 4.72.

Vial inversion tests for the second library which was the dipeptide analogues of linifanib were negative for all compounds except the proline-proline derivative which gelled after 7 days. Stability studies of these compounds showed that proline-containing dipeptides converted to linifanib at a quicker cleavage rate than other compounds with the highest cleavage rate for the proline-proline analogue suggesting that the gel observed for this analogue may be due to the gelation of the parent compound, linifanib.

With regard to single amino acid analogues, vial inversion screening showed that only the serine and glycine derivatives of linifanib formed gels at a concentration of 5% v/v DMSO/water.

Further characterisation of these two derivatives using solvent mixtures of DMSO/phosphate buffers (with a pH range of 6-8) showed that the serine derivative has a superior mechanical strength on the glycine derivative and this was attributed to the difference in hydrophobicity and the pKa. The higher mechanical strength was observed with 0.5% w/v serine analogue in 5% v/v DMSO/phosphate buffer pH 7.4 (> 4kPa).

Transmission electron micrographs of the serine and glycine derivatives confirmed the fibre network of both gelators. They were characterised by two populations of thin and thick fibres.

FT-IR spectroscopy of both derivatives provided a preliminary confirmation of the role of hydrogen bonding in gel formation.

Solid state NMR was carried out on the serine derivative. Unfortunately the acquisition of a high resolution spectra was unsuccessful due to the insolubility

in water, fast gelation kinetics and the low concentration at which gelation takes place.

Chemical stability study was performed on all the single amino acid derivatives. The serine derivative was the only compound which degraded slowly to linifanib. This is thought to be due to the presence of the hydroxyl group as a source of nucleophile required for the basic hydrolysis of amides.

Plasma hydrolysis study was carried out on both linifanib and its serine derivative using mouse, rat and human plasma media. Linifanib was stable to degradation in all the three plasma media. Regarding the serine derivative, the *in vitro* half-life of degradation to linifanib in human plasma was about 120 minutes. The rapid conversion is thought to be primarily due to the presence of hydrolytic enzymes such as peptidases and proteases

Overall, the serine analogue of linifanib can be considered as the best gelator prodrug of linifanib because it has met the objectives for the project:

- This analogue exhibited stable gels with a high mechanical strength (> 1kPa) at the physiologic pH which is suitable for localised drug delivery.
- Serine derivative of linifanib demonstrated good cleavage profile (half-life of 7 days in phosphate buffer pH 7.4 and 2 hours in human plasma).

Chapter Six: General Conclusions and Future Work

6.1. Conclusions

Low molecular weight gelators are increasingly investigated for localised targeted delivery of anticancer drugs. Prodrug approach is one of the strategies used to design self-assembling derivatives of drugs. There are several advantages of developing LMWG for cancer therapy such as high drug loading and increasing drug concentration inside the tumour tissues due to the localised delivery. The main gap in this field is the small number of anticancer agents which have been investigated for gelation properties.

In this context, we have conducted gel screening experiments on two categories of anticancer agents, five benzothiazole quinol derivatives (cytotoxic therapy) and four tyrosine kinase inhibitors (molecularly targeted treatment). These drugs are characterised by good activity but suffer from systemic toxicity. The criteria of selection of these compounds depend on the presence of structural features which are reported to promote gel formation. The development of LMWGs prodrugs based on these drugs will make them suitable for localised cancer treatment and significantly reduce the serious side effects.

Linifanib which is a potent vascular endothelial growth factor receptor inhibitor was the only compound tested which formed gels and this was suggested to be due to the high degree of rigidity and hydrogen bond donors and acceptors of linifanib. Therefore, it was decided to focus on this anticancer drug in the main part of this study.

Initially, the synthesis of structurally related analogues has demonstrated the importance of both the urea functional group and position of the essential fluorine substitution on the terminal aromatic ring in promoting gelation in DMSO/water. Additionally, the mechanical strength of linifanib gels was characterised by oscillatory rheology and the results showed that it has superior mechanical strength to its structurally related analogues and hence increased potential for localisation at an injection site for drug delivery applications.

The prodrug approach was applied to linifanib through conjugation with cleavable groups. The advantage of this strategy is the further optimisation of localised cancer delivery of linifanib. The first library of linifanib derivatives was the synthesis of seven acyloxyalkoxy carbamate linifanib prodrugs. Unfortunately, none of these derivatives induced gelation in mixtures of DMSO/water in all ratios. This was suggested to be due to the high hydrophobicity of these compounds in comparison with linifanib which caused disruption in the necessary balance between the hydrophilicity and hydrophobicity.

The final part of this project was the design and synthesis of self-assembling amide derivatives of linifanib. These derivatives are divided into three categories according to the carboxylic acid component. Derivatives with aliphatic carboxylic acid side chain with clog P between 3.98 and 4.72 formed gels with DMSO/water mixtures.

Regarding the dipeptide derivatives of linifanib, all of these compounds failed in inducing gelation except the proline-proline derivative which exhibited gelation after a period of 7 days. Stability studies of these compounds showed that the proline-containing compounds degraded to linifanib quicker than the rest of derivatives with the highest rate to the proline-proline analogue. This highly suggested that the gel formed after 7 days was in fact due to appearance of linifanib.

The third amide library was single amino acid derivatives of linifanib. Preliminary gelation screening showed that only the serine and glycine derivatives of linifanib formed gels at a concentration of 5% v/v DMSO/water. Rheology experiments carried out on these two derivatives using solvent mixtures of DMSO/phosphate buffers (with a pH range of 6-8) showed that the serine derivative has a superior mechanical strength to the glycine derivative and this was attributed to extra hydrogen bonding provided by the hydroxyl group of serine. The higher mechanical strength was observed with 0.5% w/v serine analogue in 5% v/v DMSO/phosphate buffer pH 7.4 (> 4kPa). Transmission electron micrographs of the serine and glycine derivatives confirmed the 3D fibre network of both gelators. They were characterised by

two populations of thin and thick fibres. FT-IR spectroscopy of both derivatives provided a preliminary confirmation of the role of hydrogen bonding in gel formation. Solid state NMR was carried out on the serine derivative. Unfortunately the acquisition of a high resolution spectra was unsuccessful due to the insolubility in water, fast gelation kinetics and the low concentration at which gelation takes place.

Chemical stability study was done on all the single amino acid derivatives. The serine derivative was the only compound which degraded slowly to linifanib. This is thought to be due to the presence of the hydroxyl group as a nucleophile required for the basic hydrolysis of amides. Plasma hydrolysis study was carried out on both linifanib and its serine derivative using mouse, rat and human plasma media. Linifanib was stable to degradation in all the three plasma media. Regarding the serine derivative, the *in vitro* half-life of degradation to linifanib in human plasma was about 120 minutes. The rapid conversion is thought to be primarily due to the presence of hydrolytic enzymes such as peptidases and proteases

The ultimate finding of this study is that the serine derivative of linifanib could be the most promising prodrug gelator of this anticancer drug candidate.

6.2. Future Work

The study carried out on linifanib derivatives as LMWGs prodrugs for cancer therapy offers the basis for further development and optimisation of these compounds. In addition, this approach can be applied to other anticancer drugs to make them suitable for localised delivery.

The preliminary screening for gelation applied in this project to selected anticancer therapeutics can be extended to many anticancer agents which suffer from serious side effects due to systemic administration. Additionally, the screening could be carried out using different triggering methods, wide range of concentrations and different solvents.

Due to the gelation profile of amino acid derivatives of linifanib, further synthesis of a large number of amino acid derivatives (with different physicochemical properties) and investigation of their self-assembly properties is recommended. Also, using other methods for triggering gelation such as pH switch for both existing and planned derivatives could be of great opportunity to discover new linifanib-based self-assembled compounds.

Regarding the best promising gelator reported in this study, the serine derivative of linifanib (**5.52**), there are four main group of experiments needed to evaluate its anticancer activity:

- *In vitro* release studies should be carried out to verify the ability of this gelator to act as a depot for sustained release of the therapeutic agent for localised drug delivery. These studies should be done under physiological conditions (pH 7.4 and 37 °C). Analysis by HPLC will determine the release profile of the prodrug which will provide valuable information regarding the release kinetics. In addition, analysis of the gel content is required to confirm the hydrolysis of the prodrug to the active drug.

- *In vitro* kinase inhibitory activity assays should be prepared using linifanib as a positive control. It is suggested to measure the activity of the prodrug against $VEGFR_1$, $VEGFR_2$, PDGFR and CSF-1R as linifanib demonstrates high selectivity and potency against these receptor tyrosine kinases.

- Cell-growth activity should be evaluated by testing the activity of the prodrug against vascular endothelial cell lines. Cell proliferation assays used for linifanib are used for this purpose for comparison. This will provide a clear picture regarding the anti-angiogenic activity of the compound.

- *In vivo* inhibitory activity experiment should be carried out and compare the IC_{50} of the prodrug with that of linifanib. The suggested cancer models are breast carcinoma, colon adenocarcinoma, acute myeloid leukaemia and small cell lung carcinoma. These are the main cancer models tested for linifanib inhibitory activity. The experiment should clearly determine that the inhibitory activity is due to the prodrug itself or the cleavage to linifanib.

.

Chapter Seven: Experimental

7.1. General Procedures

7.1.1. Materials

Chemicals were supplied from Sigma Aldrich and Acros Organics. They were used without further purification. All solvents used were either analytical reagent or HPLC grade and were purchased from Fisher Scientific. Dry DCM, DMF and DMSO were purchased by Acros Organics. CDCl3 was bought from Cambridge Isotope Laboratories Inc.

7.1.2. General Methods

All reactions were performed at room temperature unless otherwise stated. They were monitored using thin layer chromatography i.e. tracked by pre-coated aluminium-backed plates (Merck Kieselgel 60 F254). The plates were visualised by the use of UV light (254 nm) or $KMnO_4$ staining. Evaporation of organic solvent was performed under vacuum at temperature between 30 and 50 °C (water bath).

Purification of crude reaction products was performed using silica gel flash column chromatography. The silica gel was supplied by Sigma Aldrich (technical grade, 40-63 μm particle size).

7.1.3. Instrumentation

^{1}H NMR spectra were recorded by using a Bruker 400 Ultrashield at 400 MHz at 25 ^{o}C. ^{13}C NMR spectra were recorded on a Bruker 400 Ultrashield at 100 MHz at 25 °C. Solvents used for NMR analysis were DMSO-d_6 ($(CHD_2)_2SO$ at δH 2.50 ppm and, $(CD_3)_2SO$ at 39.52 ppm). Chemical shifts (δ) were interpreted in parts per million (ppm). Coupling constants (*J*) are recorded in Hz (rounded to one decimal place). Multiplicities are described as singlet (s), doublet (d), triplet (t) and multiplet (m).

Liquid chromatography-mass spectrometry (LC-MS) was performed on a Shimadzu UFLCXR system coupled to an Applied Biosystems API2000, and visualised at 220 nm (channel 2) and 254 nm (channel 1). Mass spectra (MS) – time of flight electrospray (TOF ES +/-) were obtained using a Waters 2795 separation module.

7.2. Preparation of gels

Gels were prepared for both linifanib (**3.17**) and its analogues (**compounds 3.18-3.25**) as shown in tables 7.1-7.3

Table 7.1. Amounts of compound, DMSO and water required for gel preparation using 100 % DMSO stock solution

Gel No.	Final conc. wt. %	Compound (mg)	DMSO µL	Water µL	Final volume µL	% DMSO
1	0.5	2.5	25	475	500	5
2	0.5	2.5	50	450	500	10
3	0.5	2.5	75	425	500	15
4	0.5	2.5	100	400	500	20
5	0.5	2.5	125	375	500	25
6	0.5	2.5	150	350	500	30
7	0.5	2.5	180	300	500	40
8	0.5	2.5	230	250	500	50

Table 7.2: Amounts of compound, solvent and water required for gel preparation using 50 % DMSO/EtOH stock solution

Gel No.	Final conc. wt. %	Compound (mg)	DMSO µL	EtOH µL	Water µL	Final volume µL	%DMSO/ EtOH
1	0.5	2.5	10	15	475	5008	2/5
2	0.5	2.5	10	40	450	500	2/8
3	0.5	2.5	10	65	425	500	2/13
4	0.5	2.5	10	90	400	500	2/18
5	0.5	2.5	10	115	375	500	2/23
6	0.5	2.5	10	140	350	500	2/28
7	0.5	2.5	10	170	300	500	2/38
8	0.5	2.5	10	220	250	500	2/48

Table 7.3: Amounts of compound, solvent and water required for gel preparation using 25 % DMSO/EtOH stock solution

Gel No.	Final conc. wt. %	Compound (mg)	DMSO µL	EtOH µL	Water µL	Final volume µL	%DMSO/ EtOH
1	0.5	2.5	5	20	475	500	1/4
2	0.5	2.5	5	45	450	500	1/7
3	0.5	2.5	5	70	425	500	1/14
4	0.5	2.5	5	95	400	500	1/19
5	0.5	2.5	5	120	375	500	1/24
6	0.5	2.5	5	145	350	500	1/29
7	0.5	2.5	5	175	300	500	1/39
8	0.5	2.5	5	225	250	500	1/49

Note: The 0.25 % and 0.125 % were prepared by using 1.25 mg and 0.625 mg as the weight of compound respectively.

Gelation screening was performed by solvent switch method. The compounds were weighed into 1.5 sample vials (Fisherbrand screw top wide opening 9mm short thread 2 mL, 12 mm x 32 mm). DMSO was then added and the vials were heated up to 60 °C in a bespoke heating mantle for a period of time to ensure solubilisation. Pre-heated (70 °C) purified water was added before removal of the vials from the heating block and then allowed to cool down to room temperature. Vial inversion tests were carried out for screening of gelation.

Rheological measurements were performed using an Anton Paar modular compact rheometer MCR302 equipped with a temperature controlled peltier. Cup and vane accessories were used to complete all amplitude sweeps. All gels were prepared at 60 °C in 2-ml sterilin vials and then left to cool down to room temperature 3 hours before the measurement. The strain measurements were performed in the range of 0.01 % – 100 % strain at 10 rad/s frequency. Measurements were performed on three replicate samples.

Transmission electron microscope (TEM) imaging was made using a JEOL JEM – 2000FXII transmission electron microscope. 4 µL of sample was placed on a carbon coated copper grid (300 mesh, Agar Scientific) for 30 seconds. The

sample was blotted with Whatman 50 filter paper, the grid was then inserted in the microscope through a sample holder and high vacuum was applied to the sample. Images were subsequently taken at an accelerating voltage of 100kV.

7.3. Preparation of phosphate buffers

Phosphate buffers were made by preparation of 10 ml of 0.2 M of monobasic hydrogen phosphate (NaH_2PO_4) (solution A) and 10 ml of 0.2 M dibasic hydrogen phosphate (Na_2HPO_4) (solution B).

Solution A was prepared by dissolving 240 mg of compound in 10 ml DW.

Solution B was prepared by dissolving 284 mg of compound in 10 ml DW.

The desired pH will be obtained by mixing solution A and B using aliquots below

Table 7.4. Solution A and B aliquots required to prepare the desired pH

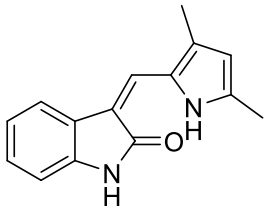
pH	Solution A (ml)	Solution B (ml)
6.0	8.77	1.23
6.6	6.85	3.15
6.8	5.65	4.35
7.0	3.90	6.10
7.4	1.90	8.10
7.9	0.85	9.15
8.1	0.52	9.47

Then these buffers will be diluted with distilled water to 0.01 M phosphate buffer to be used for the preparation of serine analogue of linifanib (**5.52**).

7.4. Experimental Data

Chapter Two

Semaxanib (*Z*)-3-((3,5-dimethyl-1H-pyrrol-2-yl)methylene)indolin-2-one



2.3

A mixture of indolin-2-one (319 mg, 2.4 mmol) and 3,5-dimethylpyrrol-2-carbaldehyde (246 mg, 2 mmol) were refluxed in ethanol (5 ml) with 5 drops of piperidine for 5 h. The crude product was concentrated, washed with ethyl acetate to yield the product (405 mg, 85%).

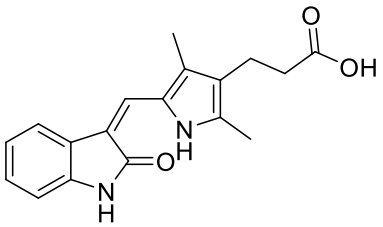
MS: LC-MS [M+H] for $C_{15}H_{15}N_2O^+$ calculated 239.11, found 239.20.

^{1}H NMR (400 MHz, $CDCl_3$): δ 2.36 (s, 3H, CH_3), 2.40 (s, 3H, CH_3), 6.01 (s, 1H, NH), 7.12 (s, 2H, CH_2), 7.44 (s, 1H, CH), 7.52 (m, 1H, Ar-H), 8.25 (m, 1H, Ar-H), 9.44 (m, 1H, Ar-H), 12.92 (s, 1H, NH) ppm.

^{13}C NMR (125 MHz, DMSO-d_6): δ 13.92, 14.53, 112.63, 117.12, 118.04, 121.37, 122.03, 123.18, 125.25, 130.15, 130.79, 131.45, 134.27, 153.78, 164.18 ppm.

Melting point: 192-194 °C.

Orantinib (3-[2,4-dimethyl-5-(2-oxo-1,2-dihydroindol-3-ylidenemethyl)-1H-pyrrol-3-yl] propionic acid



2.4

4-(2-Methoxycarbonylethyl)-3,5-dimethyl-1H-pyrrole-2-carboxylic acid benzyl ester (**2.4a**) (2.0 g, 6.3 mmol) was hydrogenated over 0.2 g of 10% palladium

on carbon in 50 mL of methanol for 2 h at room temperature. The palladium catalyst was removed by filtration and washed with 50 mL of methanol. The filtrate was evaporated to dryness 1.5 g (95% yield) of 4-(2-methoxy carbonylethyl)-3,5-dimethyl-*1H*-pyrrole-2-carboxylic acid (**2.4b**).

Compound (**2.4b**) was then dissolved in 50 mL trifluoracetic acid and heated to reflux for 2 hrs. The product was then cooled and evaporated to give methyl 3-(2,4-dimethyl-1H-pyrrol-3-yl) propanoate (**2.4c**). Trimethyl orthoformate was then added (763 mg, 7.2 mmol) and the mixture was heated to reflux and stirred for 2 hrs. The mixture was then cooled and concentrated to small volume. Water was then added and the product was precipitated and collected by filtration to give methyl 3-(5-formyl-2,4-dimethyl-*1H*-pyrrol-3-yl) propanoate (**2.4d**) as crude product.

Compound (**2.4d**) (0.23 g, 1.1 mmol) in 2 N sodium hydroxide (20 mL) was heated at 100 °C for 2 h. The reaction mixture was cooled to room temperature, acidified with 2 N hydrochloric acid, and extracted with ethyl acetate (10 mL) three times. The combined organic layers were washed with water (10 mL) and of brine (5 mL), dried over anhydrous sodium sulfate, and evaporated to dryness to give 230 mg (100%) of crude 3-(5-formyl-2,4-dimethyl-1H-pyrrol-3-yl) propionic acid (**2.4f**) as a brown oil.

Compound (**2.4f**) (0.22 g, 1.1 mmol), indolin-2-one (150 mg, 1.1 mmol) and piperidine (50 mg, 0.6 mmol) were refluxed in ethanol (10 mL) overnight. The mixture was concentrated, dried purified on a silica gel column chromatography eluting with ethyl acetate-hexane-acetic acid to give 80 mg (23% yield) of orantinib (**2.4**) as a dark yellow solid.

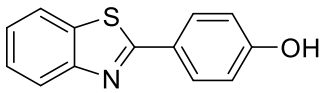
MS: LC-MS [M+H] for $C_{18}H_{19}N_2O_3^+$ calculated 311.13, found 311.3.

^{1}H NMR (400 MHz, DMSO-d$_6$): δ 2.19 (t, J = 6.97 Hz, 2H, CH_2), 2.26 (s, 3H, CH_3), 2.30 (s, 3H, CH_3), 2.61 (t, J = 5.92 Hz, 2H, CH_2), 6.87 (d, J = 7.49 Hz, 1H, Ar-H), 6.96 (t, J = 7.74 Hz, 1H, Ar-H), 7.08 (t, J = 7.69 Hz, 1H, Ar-H), 7.54 (s, 1H, CH), 7.70 (d, J = 7.49 Hz, 1H, Ar-H), 10.76 (s, 1H, NH), 13.39 (s, 1H, OH) ppm.

^{13}C NMR (125 MHz, DMSO-d$_6$): δ 13.92, 12.52, 13.75, 21.22, 27.84, 111.58, 121.58, 122.24, 124.66, 125.94, 127.21, 127.98, 128.71, 129.32, 130.28, 131.57, 142.32, 171.34, 175.22 ppm.

Melting point: 243-245 °C.

4-(Benzo[*d*]thiazol-2-yl)phenol



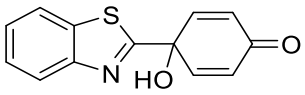
2.5c

2-aminothiophenol (3 mmol, 375 mg) and 4-hydroxybenzaldehyde were dissolved in DMF (10 mL). Sodium metabisulphite ($Na_2S_2O_5$, 600 mg) was then added to the mixture with stirring. The solution was then heated to reflux for 2 hours then it was allowed to cool to room temperature. Water (40 mL) was then added to precipitate the product which was collected by filtration. The final product was yellow solid with yield of 90 % (613 mg).

MS: LC-MS [M+H] for $C_{13}H_{10}NOS^+$ calculated 227.04, found 228.23.

^{1}H NMR (400 MHz, DMSO-d$_6$): δ 6.95 (d, J = 8.68 Hz, 2H, Ar-H), 7.41 (t, J = 7.58 Hz, 1H, Ar-H), 7.51 (t, J = 7.70 Hz, 1H, Ar-H), 7.95 (d, J = 8.56 Hz, 2H, Ar-H), 7.99 (d, J = 8.13 Hz, 1H, Ar-H), 8.09 (d, J = 7.83 Hz, 1H, Ar-H), 10.23 (s, 1H, OH) ppm.

4-(Benzo[*d*]thiazol-2-yl)-4-hydroxycyclohexa-2,5-dien-1-one



2.5

4-(benzo[*d*]thiazol-2-yl)phenol (250 mg, 1.1 mmol) was dissolved in 9:1 acetonitrile/water (10 mL). TEMPO (34 mg, 0.22 mmol) and DIAB (710 mg, 2.2 mmol) were then added to the solution and allowed to stir at room temperature for 2 hrs. The acetonitrile was evaporated under pressure. More water (20 mL) was added and the product was extracted with diethyl ether (20 mL) three times. The combined organic extracts were dried using $MgSO_4$,

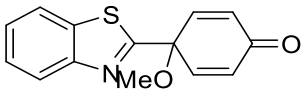
filtered and concentrated. Then the crude product was purified by flash column chromatography using 2:8 ethyl acetate/hexane as eluent to yield the pure product as a yellow solid (105 mg, 45%).

The same procedure was used in preparation of compounds (**2.6-2.9**) using the corresponding alcohols as the solvent.

MS: LC-MS [M+H] for $C_{13}H_{10}NO_2S^+$ calculated 244.04, found 244.1.

^{1}H NMR (400 MHz, DMSO-d$_6$): δ 6.29 (d, J = 9.87 Hz, 2H, 2CH), 7.11 (d, J = 9.64 Hz, 2H, 2CH), 7.48 (m, 2H, Ar-H), 7.52 (s, 1H, OH), 7.97 (d, J = 8.01 Hz, 1H, Ar-H), 8.15 (d, J = 8.06 Hz, 1H, Ar-H) ppm.

4-(Benzo[*d*]thiazol-2-yl)-4-methoxycyclohexa-2,5-dien-1-one



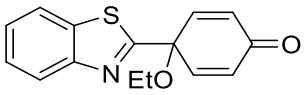
2.6

The product was pale yellow solid (98 mg, 38%).

MS: LC-MS [M+H] for $C_{14}H_{12}NO_2S^+$ calculated 258.05, found 258.14.

^{1}H NMR (400 MHz, DMSO-d$_6$): δ 3.65 (s, 3H, CH_3), 6.27 (d, J = 8.58 Hz, 2H, 2CH), 7.14 (d, J = 9.57 Hz, 2H, 2CH), 7.51 (m, 2H, Ar-H), 8.05 (d, J = 7.95 Hz, 1H, Ar-H), 8.17 (d, J = 7.98 Hz, 1H, Ar-H) ppm.

4-(Benzo[*d*]thiazol-2-yl)-4-ethoxycyclohexa-2,5-dien-1-one



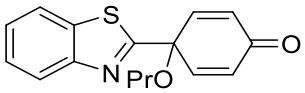
2.7

The product was pale brown solid (82 mg, 30%).

MS: LC-MS [M+H] for $C_{15}H_{14}NO_2S^+$ calculated 272.07, found 272.25.

^{1}H NMR (400 MHz, DMSO-d$_6$): δ 1.35 (t, J = 7.25 Hz, 3H, CH_3), 3.69 (q, J = 7.01 Hz, 2H, CH_2), 6.53 (d, J = 9.82 Hz, 2H, 2CH), 7.05 (d, J = 9.92 Hz, 2H, 2CH), 7.55 (m, 2H, Ar-H), 8.17 (d, J = 8.12 Hz, 1H, Ar-H), 8.29 (d, J = 7.92 Hz, 1H, Ar-H) ppm.

4-(Benzo[*d*]thiazol-2-yl)-4-propoxycyclohexa-2,5-dien-1-one



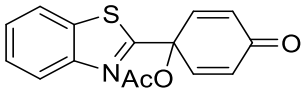
2.8

The product was yellow solid (111 mg, 39%)

MS: LC-MS [M+H] for $C_{16}H_{16}NO_2S^+$ calculated 286.08, found 286.12.

^{1}H NMR (400 MHz, DMSO-d$_6$): δ 1.3 2(t, J = 7. 54Hz, 3H, CH_3), 1.55 (m, 2H, CH_2) 3.65 (q, J = 7.23 Hz, 2H, CH_2), 6.52 (d, J = 9.73 Hz, 2H, 2CH), 7.12 (d, J = 9.73 Hz, 2H, 2CH), 7.58 (m, 2H, Ar-H), 8.22 (d, J = 8.42 Hz, 1H, Ar-H), 8.31 (d, J = 8.05 Hz, 1H, Ar-H) ppm.

1-(Benzo[*d*]thiazol-2-yl)-4-oxocyclohexa-2,5-dien-1-yl acetate



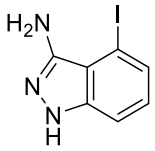
2.9

The product was off-white solid (92 mg, 32%)

MS: LC-MS [M+H] for $C_{15}H_{12}NO_3S^+$ calculated 286.05, found 286.24.

^{1}H NMR (400 MHz, DMSO-d$_6$): δ 2.33 (s, 3H, CH_3), 7.36 (d, J = 8.63 Hz, 2H, 2CH), 7.52 (d, J = 7.84 Hz, 2H, 2CH), 8.08 (d, J = 8.29 Hz, 1H, Ar-H), 8.16 (m, 3H, Ar-H) ppm.

4-Iodo-1H-indazol-3-amine



3.17b

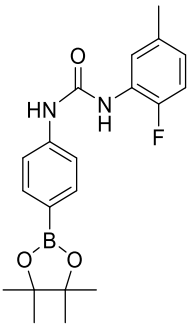
A mixture of 2-fluoro-6-iodobenzonitrile (2.0 g, 8.1 mmol) and hydrazine monohydrate (4 mL) in n-butanol (40 mL) was stirred at 105-110 °C for 5 h and then cooled to room temperature, poured into water, and extracted twice with ethyl acetate. The combined extracts were washed with water and brine, dried ($MgSO_4$), filtered, and concentrated to provide the title compound as a yellow solid (1.88 g, 90%).

MS: m/z (HRMS) calculated for $C_7H_6IN_3$+ 259.9606 [M+H], MS found: 259.7661 [M+H].

^{1}H NMR (400 MHz, $CDCl_3$): δ 4.62 (s, 2H, NH_2), 6.93 (t, J = 7.85 Hz, 1H, Ar-H), 7.28 (s, 1H, Ar-H), 7.45 (d, J = 7.71 Hz, 1H, Ar-H), 9.00 (s, 1H, NH) ppm.

^{13}C NMR (125 MHz, DMSO-d_6): δ 85.28, 109.96, 115.87, 128.36, 129.91, 142.18, 149.20 ppm.

1-(2-Fluoro-5-methylphenyl)-3-(4-(4,4,5,5-tetramethyl-1,3,2-dioxaborolan-2-yl)phenyl)urea



3.17d

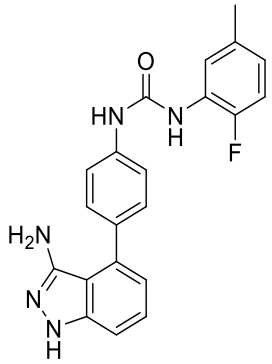
To a stirred solution of 4-(4,4,5,5-tetramethyl-1,3,2-dioxaborolan-2-yl)aniline (238 mg, 2 mmol) in DCM (10 mL) at 0 °C (water ice bath) 2-fluoro-4-methylbenzene isocyanate (302 mg, 2 mmol) was added. The whole solution was allowed to stir overnight. Then, the solution was evaporated under vacuum and purified by flush column chromatography (20-80 % ethyl acetate/hexane) to get the title compound as a white solid (680 mg, 92 %).

MS: m/z (HRMS) calculated for $C_{20}H_{24}BFN_2O_3$ 370.1864 [M+H], MS found: 370.1757 [M+H].

^{1}H NMR (400 MHz, $CDCl_3$): δ 1.35 (s, 12H, $2OC(CH_3)_2$), 2.32 (s, 3H, CH_3), 6.95 (m, 3H, Ar-H), 7.28 (s, 1H, Ar-H), 7.40 (d, J = 8.38 Hz, 1H, Ar-H), 7.79 (d, J = 7.80 Hz, 2H, Ar-H), 7.90 (s, 1H, NH), 7.92 (s, 1H, NH) ppm.

The same procedure was used in preparation of urea boronates of the linifanib analogues by the addition of the corresponding isocyanate to the aniline.

Linifanib (1-(4-(3-amino-1H-indazol-4-yl)phenyl)-3-(2-fluoro-5-methyl phenyl)urea)



3.17

The 4-iodo-1H-indazol-3-amine **3.17b** (259 mg, 1 mmol), urea boronate **3.17d** (444 mg, 1.2 mmol) and Na_2CO_3 (260 mg, 2.4 mmol) were suspended in dimethoxyethane/water (36:12) mixture. Bis(diphenylphosphino) ferrocene] dichloropalladium(II), complex with dichloromethane (50 mg) was then added and the reaction was allowed to stir at 85 °C overnight. TLC indicated complete conversion of the starting material. The solution was cooled, evaporated, extracted twice with ethyl acetate/water twice and dried over $MgSO_4$. The ethyl acetate extract was concentrated down and purified by flash column chromatography (20-80 % MeOH/DCM) to get the product as light brown solid (210 mg, 56 %).

MS: m/z (HRMS) calculated for $C_{21}H_{18}FN_5O$ 376.1495 [M+H], MS found: 376.1150 [M+H].

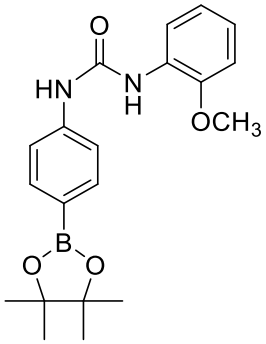
^{1}H NMR (400 MHz, DMSO-d_6): δ 2.29 (s, 3H, CH_3), 4.34 (s, 2H, NH_2), 6.81 (m, 2H, Ar-H), 7.12 (q, 1H, Ar-H), 7.27 (m, 2H, Ar-H), 7.41 (d, J = 8.64 Hz, 2H, Ar-H), 7.60 (d, J = 8.62 Hz, 2H, Ar-H), 8.02 (d, J = 7.93 Hz, 1H, Ar-H), 8.54 (s, 1H, NH), 9.21 (s, 1H, NH), 11.72 (s, 1H, NH) ppm.

^{13}C NMR (125 MHz, DMSO-d$_6$): δ 21.28, 108.46, 114.49, 115.06, 117.33, 117.82, 118.93, 120.81, 121.48, 122.11, 123.27, 127.51, 128.72, 129.83, 130.46, 133.35, 139.05, 152.15, 152.75 ppm.

Melting point: 210-212 °C.

The same method was used in preparation of linifanib analogues by the reaction between the 4-iodo-1H-indazol-3-amine with its corresponding urea boronate.

1-(2-Methoxyphenyl)-3-(4-(4,4,5,5-tetramethyl-1,3,2-dioxaborolan-2-yl)phenyl)urea



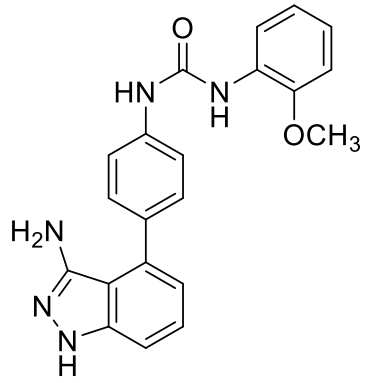
3.18d

By the method outlined for compound **3.17d**, 4-(4,4,5,5-tetramethyl-1,3,2-dioxaborolan-2-yl) aniline (238 mg, 2 mmol) and 2-methoxyphenyl isocyanate (298 mg, 2 mmol) were reacted together in DCM to give the product as a white solid (600 mg, 80 %).

MS: m/z (HRMS) calculated for $C_{20}H_{25}BN_2O_4$ 369.1907 [M+H], MS found: 369.0161 [M+H].

^{1}H NMR (400 MHz, CDCl$_3$): δ 1.30 (s, 12H, 2OC(CH$_3$)$_2$), 3.85 (s, 3H, OCH$_3$), 7.20 (m, 1H, Ar-H), 7.26 (s, 1H, Ar-H), 7.40 (d, J = 8.40 Hz, 2H, Ar-H), 7.77 (d, J = 8.29 Hz, 2H, Ar-H), 8.07 (s, 1H, NH), 8.09 (s, 1H, NH) ppm.

1-(4-(3-A mino-1H-indazol-4-yl)phenyl)-3-(2-methoxyphenyl)urea



3.18

By the method outlined for compound **3.17,** the 4-iodo-1H-indazol-3-amine **3.17b** (259 mg, 1 mmol), urea boronate **3.18d** (441 mg, 1.2 mmol) were reacted to give the product as light grey solid (150 mg, 40 %).

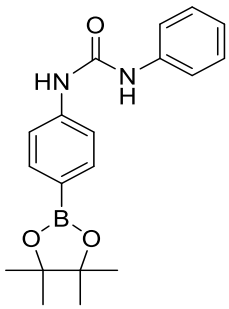
MS: m/z (HRMS) calculated for $C_{21}H_{19}N_5O_2$ 374.1538 [M+H], MS found: 374.1601 [M+H].

^{1}H NMR (400 MHz, DMSO-d$_6$): δ 3.9 (s, 3H, OCH_3), 4.34 (s, 2H, NH_2), 6.79 (dd, J = 1.95 Hz, J = 5.91 Hz, 1H, Ar-H), 6.95 (m, 2H, Ar-H), 7.04 (d, J = 7.95 Hz, 2H, Ar-H), 7.26 (s, 1H, Ar-H), 7.4 (d, J = 8.56 Hz, 2H, Ar-H), 7.61 (d, J = 8.60 Hz, 2H, Ar-H), 8.18 (d, 1H, Ar-H), 8.32 (s, 1H, NH), 9.50 (s, 1H, NH), 11.71 (s, 1H, NH) ppm.

^{13}C NMR (125 MHz, DMSO-d$_6$): δ 31.24, 33.56, 35.40, 56.25, 79.10, 79.45, 79.76, 111.20, 118.18, 118.76, 119.52, 120.50, 121.02, 122.30, 126.75, 128.88, 129.10, 129.79, 132.99, 139.88, 148.12, 152.85 ppm.

Melting point: 215-217 °C.

1-Phenyl-3-(4-(4,4,5,5-tetramethyl-1,3,2-dioxaborolan-2-yl)phenyl)urea



3.19d

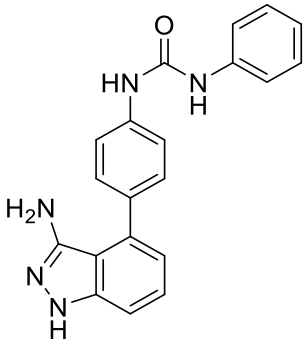
By the method outlined for compound **3.17d**, 4-(4,4,5,5-tetramethyl-1,3,2-dioxaborolan-2-yl) aniline (238 mg, 2 mmol) and 2-phenyl isocyanate (238 mg, 2 mmol) were reacted together in DCM to give the product as white solid (642 mg, 95 %).

MS: m/z (HRMS) calculated for $C_{19}H_{23}BN_2O_3$ 339.1801 [M+H], MS found: 339.0856 [M+H].

^{1}H NMR (400 MHz CDCl$_3$): δ 1.37 (s, 12H, $2OC(CH_3)_2$), 6.70 (s, 1H, Ar-H), 6.75 (s, 1H, Ar-H), 7.15 (m, 1H, Ar-H), 7.35 (s, 2H, Ar-H), 7.36 (s, 2H, Ar-H), 7.38 (s, 2H, Ar-H), 7.77 (s, 1H, NH), 7.79 (s, 1H, NH) ppm.

Melting point 245-247 °C.

1-(4-(3-Amino-1H-indazol-4-yl)phenyl)-3-phenylurea



3.19

By the method outlined for compound **3.17,** the 4-iodo-1H-indazol-3-amine **3.17b** (259 mg, 1 mmol), urea boronate **3.19d** (406 mg, 1.2 mmol) were reacted to give the product as an off-white solid (129 mg, 38 %).

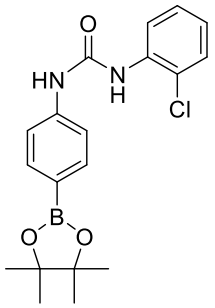
MS: m/z (HRMS) calculated for $C_{20}H_{17}N_5O$ 344.1433 [M+H], MS found: 344.1140 [M+H].

^{1}H NMR (400 MHz, DMSO-d$_6$): δ 4.34 (s, 2H, NH_2), 6.70 (d, J = 8.85 Hz, 1H, Ar-H), 6.80 (dd, J = 2.02 Hz, J = 5.82 Hz, 1H, Ar-H), 7.00 (m, 1H, Ar-H), 7.28 (s, 1H, Ar-H), 7.30 (s, 1H, Ar-H), 7.39 (s, 1H, Ar-H), 7.41 (s, 1H, Ar-H), 7.47 (s, 1H, Ar-H), 7.50 (s, 1H, Ar-H), 7.59 (s, 1H, Ar-H), 7.61 (s, 1H, Ar-H), 8.75 (s, 1H, NH), 8.84 (s, 1H, NH), 9.05 (s, 1H, NH), 11.71 (s, 1H, NH) ppm.

^{13}C NMR (125 MHz, DMSO-d$_6$): δ 109.03, 111.06, 115.73, 118.47, 118.70, 119.51, 122.33, 126.69, 129.26, 129.73, 133.11, 135.97, 139.78, 140.17, 142.54, 148.62, 153.04 ppm.

Melting point: 195-197 °C.

1-(2-Chlorophenyl)-3-(4-(4,4,5,5-tetramethyl-1,3,2-dioxaborolan-2-yl)phenyl)urea



3.20d

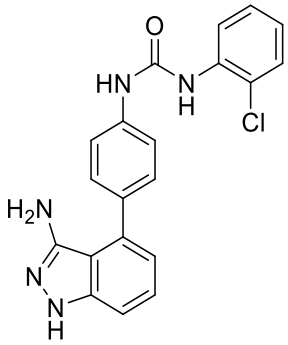
By the method outlined for compound **3.17d**, 4-(4,4,5,5-tetramethyl-1,3,2-dioxaborolan-2-yl)aniline (238 mg, 2 mmol) and 2-chlorophenyl isocyanate

(307 mg, 2 mmol) were reacted together in DCM to give the product as pale yellow solid (692 mg, 93 %).

MS: m/z (HRMS) calculated for $C_{19}H_{22}BClN_2O_3$ 373.1412 [M+H], MS found: 372.9811 [M+H].

^{1}H NMR (400 MHz, $CDCl_3$): δ 1.37 (s, 12H, $2OC(CH_3)_2$), 6.93 (s, 1H, Ar-H), 7.02 (t, J = 7.72 Hz, 1H, Ar-H), 7.22 (s, 1H, Ar-H), 7.28 (s, 1H, Ar-H), 7.36 (dd, J = 1.48 Hz, J = 7.95 Hz, 1H, Ar-H), 7.41 (s, 1H, Ar-H), 7.23 (s, 1H, Ar-H), 7.80 (s, 1H, Ar-H), 7.82 (s, 1H, Ar-H), 8.17 (s, 1H, NH), 8.20 (s, 1H, NH) ppm.

1-(4-(3-Amino-1H-indazol-4-yl)phenyl)-3-(2-chlorophenyl)urea



3.20

By the method outlined for compound **3.17,** the 4-iodo-1H-indazol-3-amine **3.17b** (259 mg, 1 mmol), urea boronate **3.20d** (453 mg, 1.2 mmol) were reacted to give the product as an off-white solid (139 mg, 37 %).

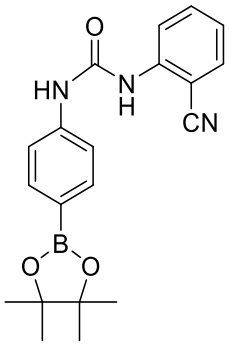
MS: m/z (HRMS) calculated for $C_{20}H_{16}ClN_5O$ 378.1043 [M+H], MS found: 378.1006 [M+H].

^{1}H NMR (400 MHz, DMSO-d_6): δ 4.34 (s, 2H, NH_2), 6.80 (dd, J = 2.28 Hz, J = 5.52, 1H, Ar-H), 7.05 (t, J = 7.74 Hz, 1H, Ar-H), 7.26 (m, 2H, Ar-H), 7.32 (t, 1H, Ar-H), 7.42 (d, J = 8.53 Hz, 2H, Ar-H), 7.48 (d, J = 1.51 Hz, J = 8.00 Hz, 1H, Ar-H), 7.62 (d, J = 8.65 Hz, 2H, Ar-H), 8.20 (dd, 1H, Ar-H), 8.40 (s, 1H, NH), 9.59 (s, 1H, NH), 11.73 (s, 1H, NH) ppm.

^{13}C NMR (125 MHz, DMSO-d_6): δ 60.20, 109.10, 118.50, 119.60, 121.84, 122.49, 123.83, 126.72, 128.10, 129.70, 129.85, 133.40, 135.91, 136.41, 139.48, 152.29 ppm.

Melting point: 223-227 °C.

1-(2-Cyanophenyl)-3-(4-(4,4,5,5-tetramethyl-1,3,2-dioxaborolan-2-yl)phenyl)urea



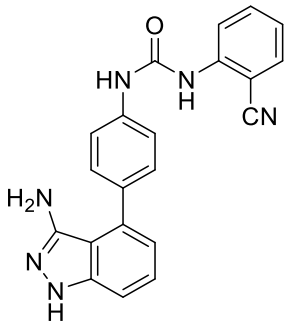
3.21d

By the method outlined for compound **3.17d**, 4-(4,4,5,5-tetramethyl-1,3,2-dioxaborolan-2-yl)aniline (238 mg, 2 mmol) and 2-cyanophenyl isocyanate (288 mg, 2 mmol) were reacted together in DCM to give the product as yellow solid (654 mg, 90 %).

MS: m/z (HRMS) calculated for $C_{20}H_{22}BN_3O_3$ 364.1754 [M+H], MS found: 363.9423 [M+H].

^{1}H NMR (400 MHz, $CDCl_3$): δ 1.37 (s, 12H, $2OC(CH_3)_2$), 7.13 (t, J = 7.65 Hz, 1H, Ar-H), 7.49 (d, J = 8.48 Hz, 2H, Ar-H), 7.59 (d, J = 7.60 Hz, 2H, Ar-H), 7.80 (d, J = 8.42 Hz, 2H, Ar-H), 7.81 (s, 1H, Ar-H), 8.39 (s, 1H, NH), 8.42 (s, 1H, NH) ppm.

1-(4-(3-Amino-1H-indazol-4-yl) phenyl)-3-(2-cyanophenyl)urea



3.21

By the method outlined for compound **3.17,** the 4-iodo-1H-indazol-3-amine **3.17b** (259 mg, 1 mmol), urea boronate **3.21d** (442 mg, 1.2 mmol) were reacted to give the product as dark yellow solid (158 mg, 43 %).

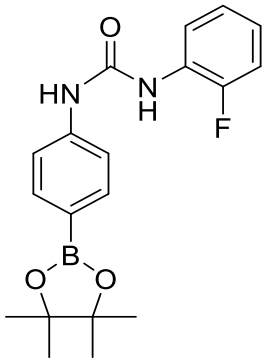
MS: m/z (HRMS) calculated for $C_{21}H_{16}N_6O$ 369.1385 [M+H], MS found: 369.1461 [M+H].

^{1}H NMR (400 MHz, DMSO-d_6): δ 4.34 (s, 2H, NH_2), 6.79 (dd, J = 1.98 Hz, J = 5.69 Hz, 1H, Ar-H), 7.05 (t, J = 7.62 Hz, 1H, Ar-H), 7.27 (m, 2H, Ar-H), 7.32 (m, 1H, Ar-H), 7.42 (d, J = 8.66 Hz, 2H, Ar-H), 7.48 (dd, J = 1.51 Hz, J = 8.08 Hz, 1H, Ar-H), 7.62 (d, J = 8.64 Hz, 2H, Ar-H), 8.20 (dd, J = 1.39 Hz, J = 8.27 Hz, 1H, Ar-H), 8.38 (s, 1H, NH), 9.58 (s, 1H, NH), δ 11.72 (s, 1H, NH) ppm.

^{13}C NMR (125 MHz, DMSO-d_6): δ 60.22, 114.76, 115.76, 119.85, 122.88, 123.01, 126.92, 128.04, 129.62, 129.90, 130.33, 135.62, 139.44, 140.33, 150.70, 162.70 ppm.

Melting point: 194-196 °C.

1-(2-Fluorophenyl)-3-(4-(4,4,5,5-tetramethyl-1,3,2-dioxaborolan-2-yl) phenyl) urea



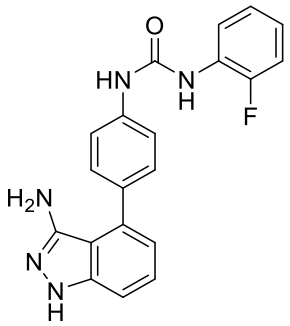
3.22d

By the method outlined for compound **3.17d**, 4-(4,4,5,5-tetramethyl-1,3,2-dioxaborolan-2-yl) aniline (238 mg, 2 mmol) and 2-fluorophenyl isocyanate (274 mg, 2 mmol) were reacted together in DCM to give the product as white solid (690 mg, 97 %).

MS: m/z (HRMS) calculated for $C_{19}H_{22}BFN_2O_3$ 357.1707 [M+H], MS found: 357.1425 [M+H].

^{1}H NMR (400 MHz, $CDCl_3$): δ 1.35 (s, 12H, $2OC(CH_3)_2$), 6.95 (m, 1H, Ar-H), 7.08 (m, 2H, Ar-H), 7.49 (d, J = 8.60, 2H, Ar-H), 7.75 (d, J = 8.55 Hz, 2H, Ar-H), 8.07 (s, 1H, NH), 8.29 (t, J = 8.30 Hz, 1H, Ar-H), 8.47 (s, 1H, NH) ppm.

1-(4-(3-Amino-1H-indazol-4-yl)phenyl)-3-(2-fluorophenyl)urea



3.22

By the method outlined for compound **3.17,** the 4-iodo-1H-indazol-3-amine **3.17b** (259 mg, 1 mmol), urea boronate **3.22d** (427 mg, 1.2 mmol) were reacted to give the product as an off-white solid (160 mg, 43 %).

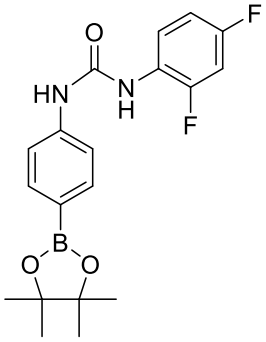
MS: m/z (HRMS) calculated for $C_{20}H_{16}FN_5O$ 362.1338 [M+H], MS found: 361.9376 [M+H].

^{1}H NMR (400 MHz, DMSO-d$_6$): δ 4.34 (s, 2H, NH_2), 6.79 (dd, J = 2.16 Hz, J = 5.70, 1H, Ar-H), 7.02 (m, 1H, Ar-H), 7.16 (t, J = 7.91 Hz, 1H, Ar-H), (s, 1H, Ar-H), 7.27 (m, 3H, Ar-H), 7.41 (d, J = 8.65 Hz, 2H, Ar-H), 7.60 (d, J = 8.65 Hz, 2H, Ar-H), 8.19 (m, 1H, Ar-H), 8.62 (s, 1H, NH), 9.21 (s, 1H, NH), 11.73 (s, 1H, Ar-H) ppm.

^{13}C NMR (125 MHz, DMSO-d$_6$): δ 109.04, 111.00, 115.36, 115.55, 118.39, 119.53, 121.04, 125.01, 126.70, 129.84, 133.36, 135.89, 139.46, 142.55, 148.59, 151.30, 152.66, 153.71 ppm.

Melting point: 205-207 °C.

1-(2,4-Difluorophenyl)-3-(4-(4,4,5,5-tetramethyl-1,3,2-dioxaborolan-2-yl)phenyl) urea



3.23d

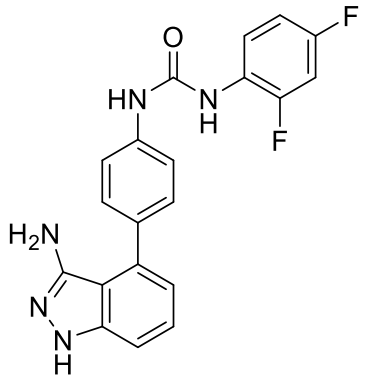
By the method outlined for compound **3.17d**, 4-(4,4,5,5-tetramethyl-1,3,2-dioxaborolan-2-yl) aniline (238 mg, 2 mmol) and 2,4-difluorophenyl isocyanate

(310 mg, 2 mmol) were reacted together in DCM to give the product as white solid (710 mg, 95 %).

MS: m/z (HRMS) calculated for $C_{19}H_{21}BF_2N_2O_3$ 375.1613 [M+H], MS found: 375.1327 [M+H].

^{1}H NMR (400 MHz, $CDCl_3$): δ 1.35 (s, 12H, $2OC(CH_3)_2$), δ 7.06 (m, 3H, Ar-H), δ 7.19 (s, 2H, Ar-H), δ 7.37 (d, J = 8.50 Hz, 2H, Ar-H), δ 7.77 (s, 1H, NH), δ 8.07 (s, 1H, NH) ppm.

1-(4-(3-Amino-1H-indazol-4-yl)phenyl)-3-(2,4-difluorophenyl)urea



3.23

By the method outlined for compound **3.17,** the 4-iodo-1H-indazol-3-amine **3.17b** (259 mg, 1 mmol), urea boronate **3.23d** (449 mg, 1.2 mmol) were reacted to give the product as white solid (197 mg, 52 %).

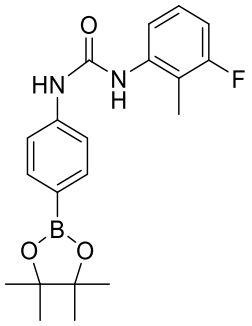
MS: m/z (HRMS) calculated for $C_{20}H_{15}F_2N_5O$ 380.1244 [M+H], MS found: 380.1337 [M+H].

^{1}H NMR (400 MHz, DMSO-d_6): 4.33 (s, 2H, NH_2), 6.79 (dd, J = 2.07 Hz, J = 5.87 Hz, 1H, Ar-H), 7.08 (t, J = 7.93 Hz, 1H, Ar-H), 7.27 (m, 2H, Ar-H), 7.33 (m, 1H, Ar-H), 7.41 (d, J = 8.52 Hz, 2H, Ar-H), 7.59 (d, J = 8.65 Hz, 2H, Ar-H), 8.12 (m, 1H, Ar-H), 8.57 (s, 1H, NH), 9.18 (s, 1H, NH), 11.72 (s, 1H, NH) ppm.

^{13}C NMR (125 MHz, DMSO-d_6): δ 104.01, 104.26, 104.51, 109.12, 111.05, 111.42, 111.63, 118.43, 119.57, 126.74, 129.88, 133.40, 135.90, 139.48, 142.54, 148.62, 152.84 ppm.

Melting point: 195-197 °C.

1-(3-Fluoro-2-methylphenyl)-3-(4-(4,4,5,5-tetramethyl-1,3,2-dioxaborolan-2-yl) phenyl) urea



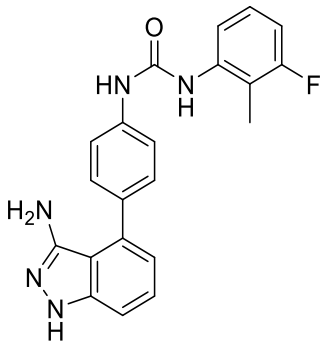
3.24d

By the method outlined for compound **3.17d**, 4-(4,4,5,5-tetramethyl-1,3,2-dioxaborolan-2-yl) aniline (238 mg, 2 mmol) and 2-methyl-3-fluorophenyl isocyanate (302 mg, 2 mmol) were reacted together in DCM to give the product as white solid (710 mg, 95 %).

MS: m/z (HRMS) calculated for $C_{20}H_{24}BFN_2O_3$ 371.1864 [M+H], MS found: 371.1778 [M+H].

^{1}H NMR (400 MHz, $CDCl_3$): δ 1.36 (s, 12H, $2OC(CH_3)_2$), 2.17 (s, 3H, CH_3), 6.52 (s, 1H, Ar-H), 6.80 (s, 1H, Ar-H), 6.93 (t, J = 8.38 Hz, 1H, Ar-H), 7.19 (m, 1H, Ar-H), 7.36 (d, J = 8.62 Hz, 3H, Ar-H), 7.75 (s, 1H, NH), 7.77 (s, 1H, NH) ppm.

1-(4-(3-Amino-1H-indazol-4-yl) phenyl)-3-(3-fluoro-2-methylphenyl)urea



3.24

By the method outlined for compound **3.17,** the 4-iodo-1H-indazol-3-amine **3.17b** (259 mg, 1 mmol), urea boronate **3.24d** (444 mg, 1.2 mmol) were reacted to give the product as an off-white solid (197 mg, 52 %).

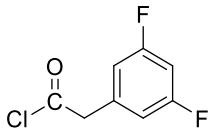
MS: m/z (HRMS) calculated for $C_{21}H_{18}FN_5O$ 376.1495 [M+H], MS found: 375.8643 [M+H].

^{1}H NMR (400 MHz, DMSO-d_6): 2.18 (s, 3H, CH_3), 4.34 (s, 2H, NH_2), 6.79 (dd, J = 2.03 Hz, J = 5.83 Hz, 1H, Ar-H), 6.87 (t, J = 8.83 Hz, 1H, Ar-H), 7.19 (m, 1H, Ar-H), 7.27 (m, 2H, Ar-H), 7.41 (d, J = 8.56 Hz, 2H, Ar-H), 7.61 (d, J = 8.56 Hz, 2H, Ar-H), 7.72 (d, J = 8.28 Hz, 1H, Ar-H), 8.16 (s, 1H, NH), 9.21 (s, 1H, NH), 11.72 (s, 1H, NH) ppm.

^{13}C NMR (125 MHz, DMSO-d_6): 19.9, 109.02, 109.81, 111.01, 115.31, 117.52, 118.39, 119.51, 126.70, 127.23, 129.81, 133.19, 135.92, 139.70, 142.55, 148.59, 152.99, 159.84, 162.23 ppm.

Melting point: 202-204 °C.

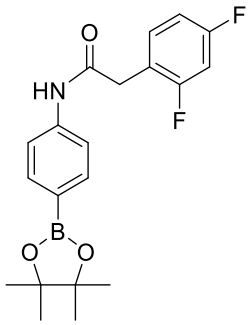
2-(3,5-Difluorophenyl)acetyl chloride



3.25a

To a solution of 2-(3,5-difluorophenyl)acetic acid (344 mg, 2 mmol) in dichloromethane (2 mL) was added thionyl chloride (218 μL, 3 mmol) and dimethylformamide (16 μL, 0.2 mmol) and the mixture stirred at room temperature for 3 hours. The solvent was removed under vacuum to give 2-(3,5-difluorophenyl) acetyl chloride as a yellow oil, which was used without further purification.

2-(3,5-Difluorophenyl)-N-(4-(4,4,5,5-tetramethyl-1,3,2-dioxaborolan-2-yl)phenyl)acetamide



3.25b

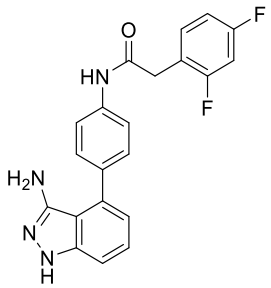
To a solution of 4-(4,4,5,5-tetramethyl-1,3,2-dioxaborolan-2-yl) aniline (438 mg, 2 mmol) in dichloromethane (20 mL) cooled with an ice-water bath was

added triethylamine (418 μL, 3mmol) and 2-(3,5-difluorophenyl) acetyl chloride (217 μL, 2 mmol). The mixture was stirred overnight, washed with water, dried (MgSO4), filtered, and concentrated to give the product as a white solid (708 mg, 95%).

MS: m/z (HRMS) calculated for $C_{20}H_{22}BF_2NO_3$ 374.1660 [M+H], MS found: 374.1731 [M+H].

^{1}H NMR (400 MHz, $CDCl_3$): δ 1.35 (s, 12H, $2OC(CH_3)_2$), 3.75 (s, 2H, CH_2), 6.90 (m, 2H, Ar-H), 7.37 (m, 1H, Ar-H), 7.54 (d, J = 8.28 Hz, 2H, Ar-H), 7.62 (m, 1H, Ar-H), 7.75 (s, 1H, NH), 7.77 (s, 1H, NH) ppm.

N-(4-(3-Amino-1H-indazol-4-yl)phenyl)-2-(2,4-difluorophenyl)acetamide



3.25

The 4-iodo-1H-indazol-3-amine **3.17b** (259 mg, 1 mmol), acetamide **3.25b** (373 mg, 1 mmol) and Na_2CO_3 (78 mg, 0.7 mmol) were suspended in dimethoxyethane/water (36:12) mixture. The Palladium was then added and the reaction was allowed to stir at 85 °C overnight. TLC indicated complete conversion of the starting material. The solution was cooled, evaporated, extracted twice with ethyl acetate/water twice and dried over $MgSO_4$. The EtOAc extract was concentrated down and purified by flash column chromatography (20-80 % MeOH/DCM) to get the product as light brown solid (210 mg, 56 %).

MS: m/z (HRMS) calculated for $C_{21}H_{16}F_2N_4O$ 379.1292 [M+H], MS found: 379.1398 [M+H].

^{1}H NMR (400 MHz, DMSO-d_6): δ 3.77 (s, 2H, CH_2), 4.30 (s, 2H, NH_2), 6.69 (m, 1H, Ar-H), 6.78 (q, 1H, Ar-H), 7.13 (m, 3H, Ar-H), 7.42 (d, J = 8.60 Hz,

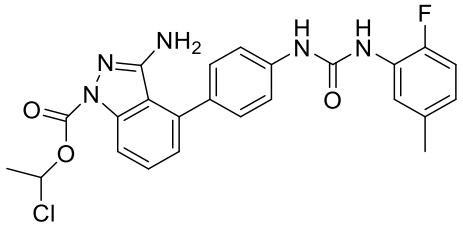
2H, Ar-H), 7.47 (d, J = 6.86 Hz, 1H, Ar-H), 7.73 (d, J = 8.60 Hz, 2H, Ar-H), 10.37 (s, 1H, NH), 11.72 (s, 1H, NH) ppm.

^{13}C NMR (125 MHz, DMSO-d$_6$): 36.23, 104.05, 109.16, 111.00, 111.57, 111.77, 114.14, 119.39, 119.58, 126.69, 129.77, 129.90, 133.43, 134.56, 135.82, 139.09, 142.55, 148.57, 168.48 ppm.

Melting point: 194-196 °C.

Chapter Four

1-Chloroethyl-3-amino-4-(4-(3-(2-fluoro-5-methylphenyl)ureido) phenyl)-1H-indazole-1-carboxylate

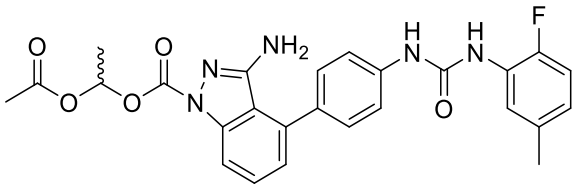


4.16a

Linifanib (375 mg, 1 mmol) was suspended in DCM (10 mL), then 1-chloroethyl chloroformate (130 µl, 1.2 mmol), and pyridine (80 µl) were added at 0 °C. The reaction mixture was warmed to room temperature and allowed to stir for 3 h. The crude product (yellow solid, 378 mg, 78 %) was used for the following reaction without further purification.

^{1}H NMR (400 MHz, DMSO-d$_6$): δ 1.93 (d, J = 5.72 Hz, 3H), 2.29 (S, 3H), 5.40 (s, 2H), 6.82 (s, 1H), 6.94 (s, 1H), 7.13 (m, 2H), 7.23 (d, J = 6.92 Hz, 2H), 7.42 (d, J = 8.74 Hz, 2H), 7.64 (m, 2H), 8.10 (m, 1H), 9.42 (s, 1H), 9.59 (s, 1H) ppm.

1-Acetoxyethyl-3-amino-4-(4-(3-(2-fluoro-5-methylphenyl)ureido) phenyl)-1H-indazole-1-carboxylate



4.16

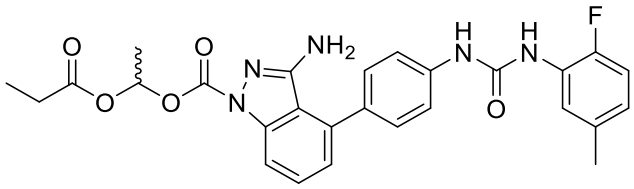
Compound **4.16a** (482 mg, 1 mmol) was suspended in acetic acid (10 mL) and heated to 75 °C, then silver (I) oxide (278 mg, 1.2 mmol) was added and the reaction mixture was heated up to 95°C for 3hrs. The crude product was then cooled, filtered through glass fibre to get rid of silver (I) oxide. The filtrate was then triturated with toluene to get rid from the acid, concentrated and purified by column chromatography using 20-100% ethyl acetate/ petroleum ether to yield the product as an off-white solid (237 mg, 47 %).

^{1}H NMR (400 MHz, DMSO-d$_6$): δ 1.60 (d, J = 5.54 Hz, 3H), 2.10 (s, 3H), 2.29 (s, 3H), 5.28 (s, 2H), 6.82 (m, 1H), 6.99 (m, 1H), 7.12 (m, 2H), 7.20 (d, J = 7.25 Hz, 1H), 7.42 (d, J = 8.74 Hz, 2H), 7.63 (m, 3H), 8.03 (q, J = 5.36 Hz, 1H), 8.57 (s, 1H), 9.27 (s, 1H) ppm.

^{13}C NMR (125 MHz, DMSO-d$_6$): δ 20.00, 21.10, 21.25, 90.69, 113.43, 114.92, 115.13, 116.54, 118.54, 121.46, 123.27, 125.39, 127.44, 129.99, 130.20, 131.42, 134.04, 136.90, 140.23, 148.79, 151.98, 152.61, 152.97, 169.23 ppm.

Melting point: 190-192 °C.

1-(Propionyloxy)ethyl-3-amino-4-(4-(3-(2-fluoro-5-methylphenyl) ureido)phenyl)-1H-indazole-1-carboxylate



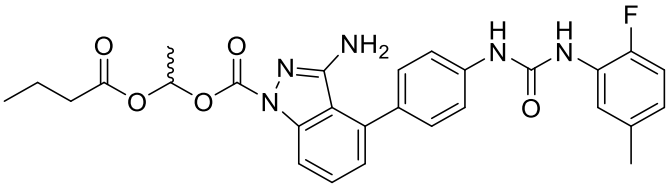
4.17

By the method outlined for synthesis of compound **4.16** and using propionic acid (10 mL), the product was yellow solid (212 mg, 41 %).

^{1}H NMR (400 MHz, DMSO-d$_6$): δ 1.04 (t, J = 7.34 Hz, 3H), 1.60 (d, J = 6.36 Hz, 3H), 2.29 (s, 3H), 2.40 (q, J = 7.83 Hz, 2H), 5.28 (s, 2H), 6.82 (s, 1H), 7.01 (d, J = 5.38 Hz, 1H), 7.13 (m, 2H), 7.20 (d, J = 6.83 Hz, 1H), 7.42 (d, J = 8.32 Hz, 2H), 7.63 (m, 3H), 8.03 (q, J = 6.58 Hz, 1H), 8.56 (s, 1H), 9.27 (s, 1H) ppm.

^{13}C NMR (125 MHz, DMSO-d$_6$): δ 9.11, 20.09, 21.26, 27.16, 90.68, 113.46, 113.04, 115.04, 116.52, 118.57, 121.44, 123.31, 125.42, 127.55, 130.03, 131.48, 134.04, 136.91, 140.22, 141.31, 148.89, 149.67, 152.65, 153.00, 172.59 ppm.

1-(Butyryloxy)ethyl-3-amino-4-(4-(3-(2-fluoro-5-methylphenyl) ureido)phenyl)-1H-indazole-1-carboxylate



4.18

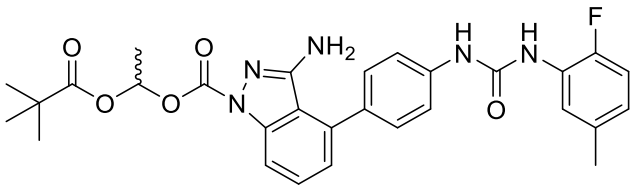
Using butyric acid (10 mL) as the solvent and by the method outlined for synthesis of compound **4.16**, the product was yellow solid (218 mg, 42%).

^{1}H NMR (400 MHz, DMSO-d$_6$): δ 0.90 (t, J = 7.39, 3H), 1.56 (t, J = 7.24 Hz, 2H), 1.61 (d, J = 5.43 Hz, 3H), 2.29 (s, 3H), 2.36 (d, J = 7.09 Hz, 2H), 5.28 (s, 2H), 6.83 (s, 1H), 7.02 (d, J = 5.88 Hz, 1H), 7.13 (m, 2H), 7.20 (d, J = 7.39 Hz, 1H), 7.42 (d, J = 8.60 Hz, 2H), 7.63 (m, 3H), 8.02 (q, J = 6.88 Hz, 1H), 8.57 (s, 1H), 9.27 (s, 1H) ppm.

^{13}C NMR (125 MHz, DMSO-d$_6$): δ 13.98, 18.03, 20.22, 21.57, 35.55, 90.83, 113.49, 114.96, 115.22, 116.63, 118.48, 121.49, 123.29, 125.47, 127.45, 129.95, 130.33, 131.36, 134.05, 137.06, 140.26, 148.91, 149.55, 152.69, 153.07, 171.64 ppm.

Melting point: 184-186 °C.

1-(Pivaloyloxy)ethyl-3-amino-4-(4-(3-(2-fluoro-5-methylphenyl) ureido)phenyl)-1H-indazole-1-carboxylate



4.19

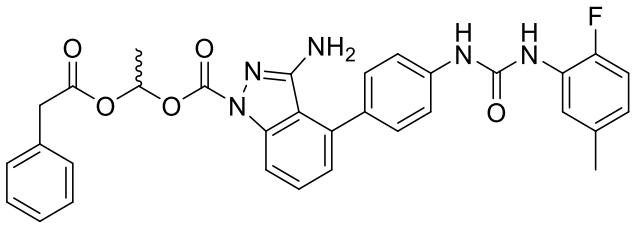
Using pivalic acid (4 g) as the solvent and by the method outlined for synthesis of compound **4.16**, the product was white solid (202 mg, 37%).

^{1}H NMR (400 MHz, DMSO-d$_6$): δ 1.18 (s, 1H), 1.61 (d, J = 5.43 Hz, 3H), 2.29 (s, 3H), 5.27 (s, 2H), 6.83 (s, 1H), 6.99 (d, J = 5.88 Hz, 1H), 7.13 (m, 2H), 7.21 (d, J = 7.24 Hz, 1H), 7.42 (d, J = 8.44 Hz, 2H), 7.63 (m, 3H), 8.01 (q, J = 7.12 Hz, 1H), 8.59 (s, 1H), 9.31 (s, 1H) ppm.

^{13}C NMR (125 MHz, DMSO-d$_6$): δ 19.93, 21.26, 27.01, 27.51, 38.68, 90.99, 113.48, 114.89, 115.13, 116.55, 118.54, 121.52, 123.32, 125.51, 127.38, 127.50, 130.04, 130.18, 131.41, 133.99, 137.01, 140.28, 152.60, 153.04, 176.19 ppm.

Melting point: 202-204 °C.

1-(Benzoyloxy)ethyl-3-amino-4-(4-(3-(2-fluoro-5-methylphenyl) ureido)phenyl)-1H-indazole-1-carboxylate



4.20

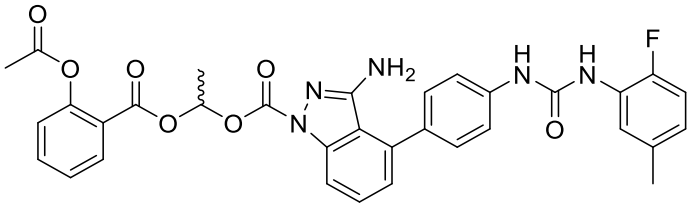
A mixture of compound **4.16a** (240 mg, 0.5 mmol) and benzoic acid (77 mg, 0.6 mmol) were dissolved in DMF and heated to 75 °C. Silver (I) oxide (140 mg, 0.6 mmol) is then added and the mixture was allowed to stir overnight on reflex. The crude mixture was then cooled, filtered through glass fibre paper, concentrated and purified by column chromatography using 20-100 ethyl acetate/petroleum ether as eluent to get the product as white solid (85 mg, 30%).

^{1}H NMR (400 MHz, DMSO-d$_6$): δ 1.77 (d, J = 5.60 Hz, 3H), 2.29 (s, 3H), 5.28 (s, 2H), 6.83 (s, 1H), 7.13 (m, 1H), 7.24 (m, 2H), 7.42 (d, J = 9.14 Hz, 2H), 7.61 (m, 6H), 7.73 (m, 1H), 7.95 (m, 1H), 8.02 (m, 4H), 8.58 (s, 1H), 9.29 (s, 1H) ppm.

^{13}C NMR (125 MHz, DMSO-d$_6$): δ 20.15, 21.30, 91.60, 113.51, 114.94, 115.16, 116.69, 117.57, 118.62, 121.58, 123.28, 125.48, 127.57, 129.05, 129.49, 129.98, 131.41, 134.10, 134.60, 135.31, 137.01, 140.20, 148.88, 149.75, 152.72, 153.16, 169.53 ppm.

Melting point: 210-212 °C.

1-((2-Acetoxybenzoyl)oxy)ethyl-3-amino-4-(4-(3-(2-fluoro-5-methyl phenyl)ureido)phenyl)-1H-indazole-1-carboxylate



4.21

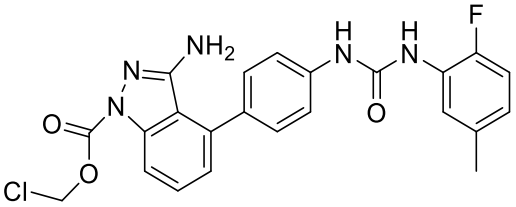
Using aspirin (108 mg, 0.6 mmol) and by the method used for synthesis of compound **4.20,** the product was white solid (180 mg, 29%).

^{1}H NMR (400 MHz, DMSO-d$_6$): δ 1.68 (d, J = 5.60 Hz, 3H), 2.29 (s, 3H), 2.38 (s, 3H), 5.28 (s, 2H), 6.83 (s, 1H), 7.13 (m, 1H), 7.24 (m, 2H), 7.42 (d, J = 8.57 Hz, 2H), 7.62 (m, 4H), 7.73 (m, 1H), 7.95 (m, 1H), 8.02 (m, 3H), 8.58 (s, 1H), 9.29 (s, 1H) ppm.

^{13}C NMR (125 MHz, DMSO-d$_6$): δ 21.62, 22.38, 22.41, 93.28, 108.02, 114, 116.04, 118.66, 119.38, 120.12, 120.25, 122.95, 124.91, 127.43, 127.29, 128.06, 132.48, 132.94, 134.6, 135.13, 137.68, 140.33, 141.73, 147.33, 151.65, 152.23, 154.08, 154.33, 160.85, 164.16, 170.83 ppm.

Melting point: 198-200 °C.

Chloromethyl-3-amino-4-(4-(3-(2-fluoro-5-methylphenyl)ureido) phenyl)-1H-indazole-1-carboxylate

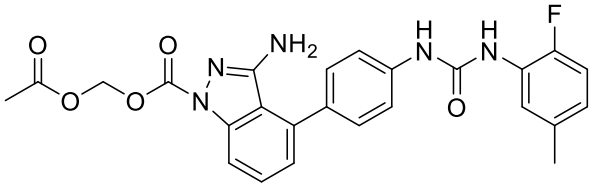


4.22a

Linifanib (188 mg, 0.5 mmol) was suspended in DCM (10 mL), then 1-chloromethyl chloroformate (77 mg, 0.6 mmol), and pyridine (40 μl) were added at 0 °C. The reaction mixture was warmed to room temperature and allowed to stir for 3 hours. The crude mixture was extracted with water to get the product as yellow solid (172 mg, 74 %).

^{1}H NMR (400 MHz, DMSO-d$_6$): δ 2.29 (S, 3H), 5.28 (s, 2H), 5.99 (s, 2H), 6.82 (s, 1H), 6.93 (m, 1H), 7.16 (m, 2H), 7.23 (d, J = 6.92 Hz, 1H), 7.42 (d, J = 7.92 Hz, 2H), 7.63 (m, 3H), 8.56 (s, 1H), 9.23 (s, 1H) ppm.

Acetoxymethyl-3-amino-4-(4-(3-(2-fluoro-5-methylphenyl)ureido) phenyl)-1H-indazole-1-carboxylate



4.22

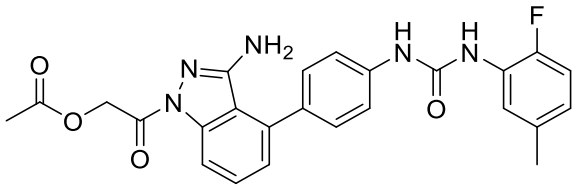
Using compound **4.22a** and by the method outlined for synthesis of compound **4.22**, the product was light yellow solid (76 mg, 42%).

^{1}H NMR (400 MHz, DMSO-d_6): δ 2.15 (s, 3H), 2.29 (s, 3H), 5.29 (s, 2H), 6.00 (s, 2H), 6.83 (s, 1H), 7.18 (m, 3H), 7.43 (d, J = 7.53 Hz, 2H), 7.64 (m, 3H), 8.04 (m, 1H), 8.57 (s, 1H), 9.28 (s, 1H) ppm.

^{13}C NMR (125 MHz, DMSO-d_6): δ 22.24, 21.35, 91.24, 115.53, 115.72, 116.28, 117.68, 118.89, 120.34, 122.84, 126.54, 127.63, 131.30, 131.84, 132.13, 134.32, 138.20, 142.54, 148.23, 152.48, 152.87, 152.47, 170.21.

Melting point: 193-195 °C.

2-(3-Amino-4-(4-(3-(2-fluoro-5-methylphenyl)ureido)phenyl)-1H-indazol-1-yl)-2-oxoethyl acetate



5.36

Acetoxyacetic acid (71 mg, 0.6 mmol), linifanib (188 mg, 0.5 mmol) and HATU (455 mg, 0.6 mmol) were suspended in in DCM (20 mL). DIPEA (0.17 mL, 0.6 mmol) is then added and the mixture was allowed to stir overnight under room temperature. The solution was then evaporated, extracted twice with ethyl acetate/water twice and dried over $MgSO_4$. The ethyl acetate extract was concentrated down was then purified by column chromatography using 20-100% ethyl acetate/petroleum ether to provide the product as a white solid (112 mg, 47 %).

The same procedure was used for synthesis of compounds **5.37-5.40.**

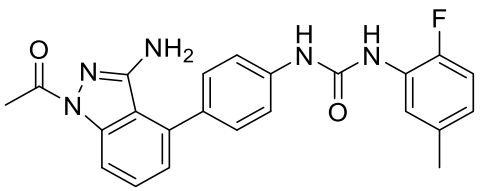
MS: m/z (HRMS) calculated for $C_{25}H_{22}FN_5O_4$ 475.1655 [M+H], MS found: 379.1632 [M+H].

^{1}H NMR (400 MHz, DMSO-d$_6$): δ 2.19 (s, 3H, CH_3), 2.29 (s, 3H, CH_3), 5.33 (s, 2H, NH_2), 5.38 (s, 2H, CH_2), 6.83 (s, 1H, ArH), 7.13 (m, 1H, ArH), 7.24 (d, J = 7.74 Hz, 1H, ArH), 7.40 (d, J = 8.40, 2H, ArH), 8.24 (d, J = 8.23, 2H, ArH), 8.57 (s, 1H, NH), 9.28 (s, 1H, NH) ppm.

^{13}C NMR (125 MHz, DMSO-d$_6$): δ 21.99, 22.48, 70.4, 109.14, 113.77, 116.11, 118.73, 120.5, 120.22, 124.98, 127.56, 128.33, 130.79, 137.7, 137.95, 140.6, 141.7, 151.19, 151.85, 154.55, 154.1, 164.6, 172.24 ppm.

Melting point: 185-187 °C.

1-(4-(1-Acetyl-3-amino-1H-indazol-4-yl)phenyl)-3-(2-fluoro-5-methyl phenyl)urea



5.37

The product was an off-white solid (92 mg, 44%).

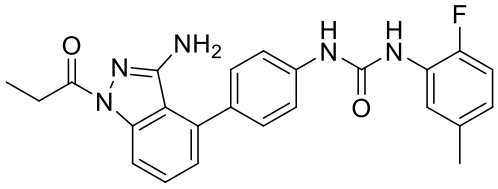
MS: m/z (HRMS) calculated for $C_{23}H_{20}FN_5O_2$ 417.1601 [M+H], MS found: 417.1632 [M+H].

^{1}H NMR (400 MHz, DMSO-d$_6$): δ 2.29 (s, 3H, CH_3), 2.57 (s, 3H, CH_3), 5.21 (s, 2H, NH_2), 6.83 (m, 1H, ArH), 7.13 (m, 1H, ArH), 7.20 (d, J = 7.35 Hz, 1H, ArH), 7.43 (d, J = 8.40 Hz, 2H, ArH), 7.62 (m, 3H, ArH), 8.02 (m, 1H, ArH), 8.30 (m, 1H, ArH), 8.57 (s, 1H, NH), 9.27 (s, 1H, NH) ppm.

^{13}C NMR (125 MHz, DMSO-d$_6$): δ 22.38, 23.87, 110.65, 114.27, 116.01, 118.53, 120.22, 120.72, 124.88, 127.36, 128.13, 130.45, 134.19, 137.75, 140.4, 142.2, 151.04, 151.68, 154.35, 154.6, 171.4 ppm.

Melting point: 191-193 °C.

1-(4-(3-Amino-1-propionyl-1H-indazol-4-yl)phenyl)-3-(2-fluoro-5-methyl phenyl)urea



5.38

The product was yellow solid (108 mg, 50%).

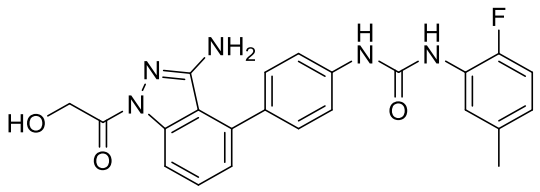
MS: m/z (HRMS) calculated for $C_{24}H_{22}FN_5O_2$ 431.1757 [M+H], MS found: 431.1793 [M+H].

^{1}H NMR (400 MHz, DMSO-d$_6$): δ 1.20 (t, d = 7.83 Hz, 2H, CH_2), 2.30 (s, 3H, CH_3), 3.01 (q, 3H, CH_3), 5.20 (s, 2H, NH_2), 6.83 (m, 1H, ArH), 7.13 (m, 1H, ArH), 7.19 (d, J = 6.63 Hz, 1H, ArH), 7.43 (d, J = 9.04 Hz, 2H, ArH), 7.62 (m, 3H, ArH), 8.02 (m, 1H, ArH), 8.32 (m, 1H, ArH), 8.57 (s, 1H, NH), 9.27 (s, 1H, NH) ppm.

^{13}C NMR (125 MHz, DMSO-d$_6$): δ 10.27, 22.48, 36.05, 109.23, 113.77, 116.11, 118.73, 120.44, 120.22, 124.98, 127.56, 128.33, 130, 134.94, 137.95, 140.6, 141.7, 150.6-1, 151.79, 154.55, 154.1, 167.83 ppm.

Melting point: 181-184 °C.

1-(4-(3-Amino-1-(2-hydroxyacetyl)-1H-indazol-4-yl)phenyl)-3-(2-fluoro-5-methylphenyl)urea



5.39

The product was an off-white solid (217 mg, 40%).

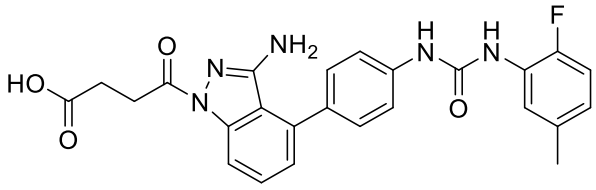
MS: m/z (HRMS) calculated for $C_{23}H_{20}FN_5O_3$ 433.1550 [M+H], MS found: 433.1495 [M+H].

^{1}H NMR (400 MHz, DMSO-d$_6$): δ 2.30 (s, 3H, CH_3), 4.71 (s, 2H, CH_2), 5.22 (s, 2H, NH_2), 6.83 (m, 1H, ArH), 7.13 (m, 1H, ArH), 7.21 (d, J = 6.70 Hz, 1H, ArH), 7.43 (d, J = 8.95 Hz, 2H, ArH), 7.64 (m, 3H, ArH), 8.02 (m, 1H, ArH), 8.30 (m, 1H, ArH), 8.57 (s, 1H, NH), 9.28 (s, 1H, NH) ppm.

^{13}C NMR (125 MHz, DMSO-d$_6$): δ 22.38, 61.67, 108.59, 113.77, 116.01, 118.43, 119.8, 120.22, 124.88, 127.26, 127.83, 130.1, 134.12, 137.65, 140.1, 141.7, 149.69, 151.5, 154.05, 154.1, 164.74 ppm.

Melting point: 195-197 °C.

4-(3-Amino-4-(4-(3-(2-fluoro-5-methylphenyl)ureido)phenyl)-1H-indazol-1-yl)-4-oxobutanoic acid



5.40

The product was off-white solid (143 mg, 60%).

MS: m/z (HRMS) calculated for $C_{25}H_{22}FN_5O_4$ 475.1655 [M+H], MS found: 475.1634 [M+H].

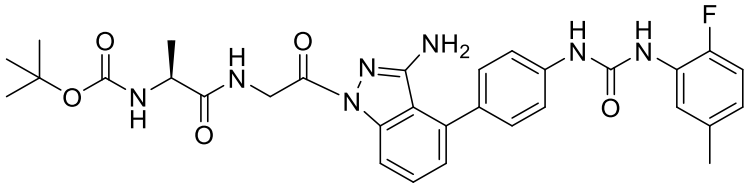
^{1}H NMR (400 MHz, DMSO-d$_6$): δ 2.29 (s, 3H, CH_3), 2.64 (t, J = 6.54 Hz, 2H, CH_2), 2.75 (t, J = 6.43 Hz, 2H, CH_2),), 5.24 (s, 2H, NH_2), 6.83 (m, 1H, ArH),

7.17 (m, 2H, ArH), 7.43 (d, J = 9.26 Hz, 2H, ArH), 7.64 (m, 3H, ArH), 8.02 (m, 1H, ArH), 8.30 (m, 1H, ArH), 8.57 (s, 1H, NH), 9.34 (s, 1H, NH) ppm.

^{13}C NMR (125 MHz, DMSO-d$_6$): δ 22.38, 30.77, 40.02, 108.83, 113.77, 116.01, 118.43, 120.22, 120.23, 124.88, 127.26, 127.83, 130.29, 133.4, 137.65, 140.1, 141.7, 151.17, 151.48, 154.05, 154.1, 166.73, 178.93 ppm.

Melting point: 191-193 °C.

***tert*-Butyl *(S)*-(1-((2-(3-amino-4-(4-(3-(2-fluoro-5-methylphenyl) ureido) phenyl)-1H-indazol-1-yl)-2-oxoethyl)amino)-1-oxopropan-2-yl)carbamate**

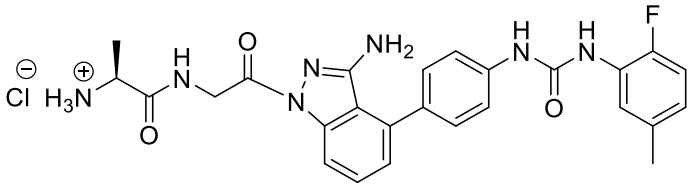


5.44a

Boc-Ala-Gly-OH (148 mg, 0.6 mmol), linifanib (188 mg, 0.5 mmol) and HATU (455 mg, 0.6 mmol) were suspended in in DCM (20 mL). DIPEA (0.17 mL, 0.6 mmol) is then added and the mixture was allowed to stir overnight under room temperature. The solution was then evaporated, extracted twice with ethyl acetate/water twice and dried over $MgSO_4$. The ethyl acetate extract was concentrated down was then purified by column chromatography using 20-100% ethyl acetate/petroleum ether to provide the product as an off-white solid (165 mg, 55%).

^{1}H NMR (400 MHz, DMSO-d$_6$): δ 1.41 (s, 9H, $C(CH_3)_3$), 1.47 (d, J = 7.69 Hz, 3H, CH_3) 2.29 (s, 3H, CH_3), 4.49 (m, 1H, CH), 4.61 (s, 2H, CH_2), 5.32 (s, 2H, NH_2), 6.83 (s, 1H, ArH), 7.00 (d, J = 8.41 Hz, 1H, ArH), 7.13 (m, 1H, ArH), 7.22 (d, J = 7.57 Hz, 1H, ArH), 7.44 (d, J = 8.68 Hz, 2H, ArH), 7.64 (m, 3H, ArH), 8.01 (s, 1H, NH), 8.14 (m, 1H, ArH), 8.26 (s, 1H, NH), 8.56 (s, 1H, NH), 9.27 (s, 1H, NH) ppm.

***(S)*-1-((2-(3-amino-4-(4-(3-(2-fluoro-5-methylphenyl)ureido)phenyl)-1H-indazol-1-yl)-2-oxoethyl)amino)-1-oxopropan-2-aminium chloride**



5.44

Compound **5.44a** (145 mg, 0.24 mmol) was dissolved in DCM (20 mL), and then 4M HCl in dioxane (5 mL) was added. The solution was allowed to stir for 3 hours under room temperature. The product was then evaporated to get the product as light brown solid (120 mg, 63%).

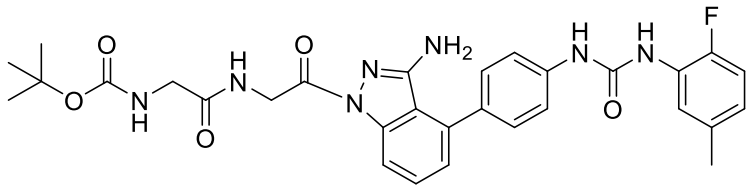
MS: m/z (HRMS) calculated for $C_{26}H_{27}FN_7O_3^+$ 504.2153 [M+H], MS found: 504.2238 [M+H].

^{1}H NMR (400 MHz, DMSO-d$_6$): δ 1.47 (d, J = 7.32 Hz, 3H, CH_3), 2.29 (s, 3H, CH_3), 4.01 (m, 1H, CH), 4.65 (s, 2H, CH_2), 5.33 (s, 2H, NH_2), 6.83 (s, 1H, ArH), 7.12 (m, 1H, ArH), 7.24 (d, J = 7.47 Hz, 1H, ArH), 7.43 (d, J = 8.43 Hz, 2H, ArH), 7.64 (m, 3H, ArH), 8.01 (d, J = 8.61 Hz, 1H, ArH), 8.20 (s, 2H, NH_2), 8.27 (d, J = 8.46 Hz, 1H, ArH), 8.68 (s, 1H, NH), 8.89 (s, 1H, NH), 9.55 (s, 1H, NH) ppm.

^{13}C NMR (125 MHz, DMSO-d$_6$): δ 22.26, 25.1, 52.68, 54.07, 111.5, 119.1, 120.13, 121.15, 125.55, 124.37, 127.6, 132.59, 131.95, 132.76, 138.73, 141.77, 142.82, 147.03, 153.06, 154.26, 159.38, 158.22, 168.02, 179.62 ppm.

Melting point: 191-193 °C.

***tert*-Butyl (2-((2-(3-amino-4-(4-(3-(2-fluoro-5-methylphenyl)ureido) phenyl)-1H-indazol-1-yl)-2-oxoethyl)amino)-2-oxoethyl)carbamate**

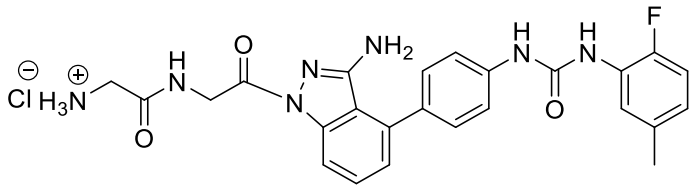


5.45a

By the method outlined for synthesis of compound **5.44a**, the product was brown solid (176 mg, 60%).

^{1}H NMR (400 MHz, DMSO-d$_6$): δ 1.41 (s, 9H, $C(CH_3)_3$), 2.29 (s, 3H, CH_3), 2.70 (s, 2H, CH_2), 4.57 (s, 2H, CH_2), 5.31 (s, 2H, NH_2), 6.82 (s, 1H, ArH), 7.11 (m, 2H, ArH), 7.22 (d, J = 6.62 Hz, 1H, ArH), 7.43 (d, J = 8.56 Hz, 2H, ArH), 7.63 (m, 3H, ArH), 8.01 (d, J = 8.32 Hz, 1H, ArH), 8.19 (s, 1H, NH), 8.27 (s, 1H, NH), 8.57 (s, 1H, NH), 9.27 (s, 1H, NH) ppm.

2-((2-(3-Amino-4-(4-(3-(2-fluoro-5-methylphenyl)ureido)phenyl)-1H-indazol-1-yl)-2-oxoethyl)amino)-2-oxoethan-1-aminium chloride



5.45

By the method outlined for synthesis of compound **5.44**, the product was yellow solid (130 mg, 90%).

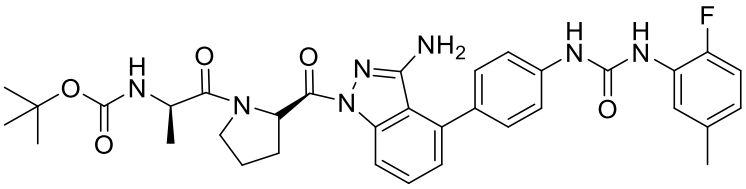
MS: m/z (HRMS) calculated for $C_{25}H_{25}FN_6O_3^+$ 490.1997 [M+H], MS found: 490.2031 [M+H].

^{1}H NMR (400 MHz, DMSO-d$_6$): δ 2.28 (s, 3H, CH_3), 2.70 (s, 2H, CH_2), 3.71 (s, 2H, CH_2), 5.34 (s, 2H, NH_2), 6.82 (s, 1H, ArH), 7.12 (m, 1H, ArH), 7.24 (d, J = 6.75 Hz, 1H, ArH), 7.42 (d, J = 8.56 Hz, 2H, ArH), 7.65 (m, 2H, ArH), 7.99 (d, J = 8.54 Hz, 1H, ArH), 8.13 (m, 2H, ArH), 8.26 (s, 1H, NH), 8.88 (s, 1H, NH), 8.99 (s, 2H, NH_2), 9.60 (s, 1H, NH) ppm.

^{13}C NMR (125 MHz, DMSO-d$_6$): δ 26.15, 39.46, 55.04, 112.82, 116.49, 121.34, 122.55, 122.94, 125.56, 129.21, 129.98, 133.16, 134.41, 135.55, 142.98, 144.22, 144.42, 155.02, 155.71, 156.77, 159.43, 169.37, 174.21 ppm.

Melting point: 187-189 °C.

***tert*-Butyl ((*R*)-1-((*S*)-2-(3-amino-4-(4-(3-(2-fluoro-5-methylphenyl)ureido) phenyl)-1H-indazole-1-carbonyl)pyrrolidin-1-yl)-1-oxopropan-2-yl) carbamate**



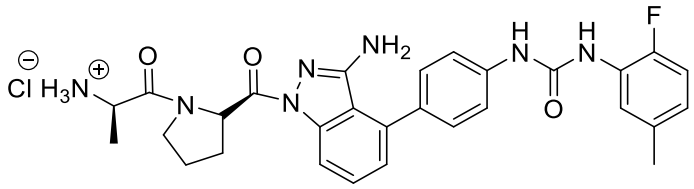
5.46a

By the method outlined for synthesis of compound **5.44a**, the product was brown solid (183 mg, 57%).

^{1}H NMR (400 MHz, DMSO-d$_6$): δ 1.23 (d, 7.26 Hz, 3H, CH_3), 1.37 (s, 9H, $C(CH_3)_3$), 1.47 (d, J = 7.69 Hz, 3H, CH_3), 2.01 (m, 2H, CH_2), 2.29 (s, 3H, 3CH), 3.72 (m, 2H, CH_2), 4.34 (m, 1H, CH), 5.29 (s, 2H, NH_2), 6.82 (s, 1H, ArH), 6.96

(d, J = 7.59 Hz, 1H, ArH), 7.13 (m, 1H, ArH), 7.21 (d, J = 6.96 Hz, 1H, ArH), 7.43 (d, J = 8.23 Hz, 2H, ArH), 7.64 (m, 3H, ArH), 8.00 (d, J = 6.95 Hz, 1H, ArH), 8.25 (s, 1H, NH), 8.60 (s, 1H, NH), 9.30 (s, 1H, NH) ppm.

***(R)*-1-(*(S)*-2-(3-amino-4-(4-(3-(2-fluoro-5-methylphenyl)ureido)phenyl)-1H-indazole-1-carbonyl)pyrrolidin-1-yl)-1-oxopropan-2-aminium chloride**



5.46

By the method outlined for synthesis of compound **5.44**, the product was yellow solid (131 mg, 85%).

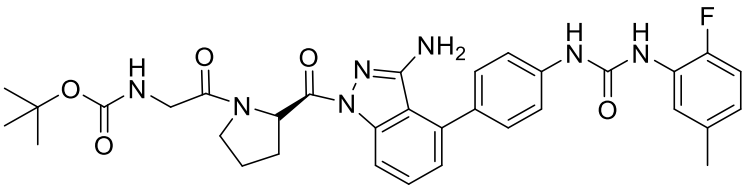
MS: m/z (HRMS) calculated for $C_{29}H_{31}FN_7O_3^+$ 544.2466 [M+H], MS found: 544.2572 [M+H].

^{1}H NMR (400 MHz, DMSO-d$_6$): δ 1.44 (d, J = 6.66 Hz, 3H, CH_3), 2.01 (m, 3H, 3CH), 2.30 (s, 3H, CH_3), 3.64 (m, 2H, CH_2), 3.85 (m, 2H, CH_2), 4.53 (m, 1H, CH), 5.46 (s, 2H, NH_2), 6.82 (s, 1H, ArH), 7.11 (m, 1H, ArH), 7.24 (d, J = 7.88 Hz, 1H, ArH), 7.44 (d, J = 7.82 Hz, 2H, ArH), 7.66 (m, 3H, ArH), 7.98 (d, J = 7.85 Hz, 1H, ArH), 8.23 (s, 2H, NH_2), 8.53 (m, 1H, ArH), 8.78 (s, 1H, NH), 9.81 (s, 1H, NH) ppm.

^{13}C NMR (125 MHz, DMSO-d$_6$): δ 22.28, 25.21, 31.71, 34.02, 48.82, 53.63, 68.96, 113.05, 119.12, 120.13, 121.15, 125.55, 125.66, 127.16, 132.59, 131.95, 132.3, 139.18, 141.77, 142.82, 147.03, 155.4, 155.48, 159.38, 158.22, 170.65, 175.11 ppm.

Melting point: 200-202 °C.

***tert*-Butyl *(S)*-(2-(2-(3-amino-4-(4-(3-(2-fluoro-5-methylphenyl)ureido)phenyl)-1H-indazole-1-carbonyl)pyrrolidin-1-yl)-2-oxoethyl)carbamate**

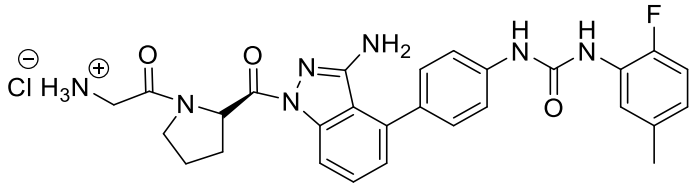


5.47a

By the method outlined for synthesis of compound **5.44a**, the product was brown solid (173 mg, 55%).

^{1}H NMR (400 MHz, DMSO-d$_6$): δ 1.40 (s, 9H, C(CH_3)$_3$), 2.29 (s, 3H, CH_3), 3.14 (m, 3H, 3CH), 3.64 (m, 2H, 2CH), 3.86 (s, 2H, CH_2), 4.79 (m, H, CH), 5.68 (m, 1H, CH), 6.33 (s, 2H, NH_2), 6.55 (d, J = 6.10 Hz, 1H, ArH), 6.83 (m, 2H, ArH), 7.11 (m, 2H, ArH), 7.26 (m, 2H, ArH), 7.63 (d, J = 7.95 Hz, 2H, ArH), 8.05 (d, J = 7.41 Hz, 1H, ArH), 8.15 (s, 1H, NH), 8.55 (s, 1H, NH), 9.25 (s, 1H, NH) ppm.

***(S)*-2-(2-(3-amino-4-(4-(3-(2-fluoro-5-methylphenyl)ureido)phenyl)-1H-indazole-1-carbonyl)pyrrolidin-1-yl)-2-oxoethan-1-aminium chloride**



5.47

By the method outlined for synthesis of compound **5.44**, the product was yellow solid (123 mg, 85%).

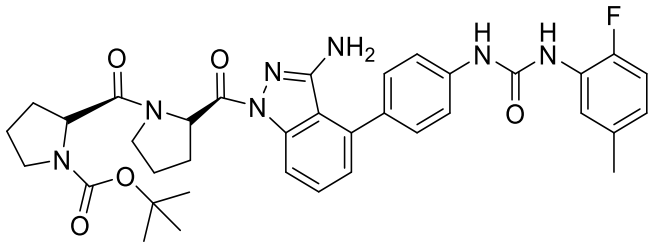
MS: m/z (HRMS) calculated for $C_{28}H_{29}FN_7O_3^+$ 530.2310 [M+H], MS found: 530.2430 [M+H].

^{1}H NMR (400 MHz, DMSO-d$_6$): δ 1.92 (m, 2H, 2CH), 2.03 (m, 2H, 2CH), 2.17 (m, 2H, 2CH), 2.29 (s, 3H, CH_3), 3.12 (m, 2H, CH_2), 3.60 (m, 1H, CH), 5.33 (s, 2H, NH_2), 6.82 (s, 1H, ArH), 7.12 (t, J = 7.89 Hz, 1H, ArH), 7.27 (m, 1H, ArH), 7.43 (t, J = 8.16 Hz, 2H, ArH), 7.64 (m, 3H, ArH), 7.99 (m, 2H, ArH), 8.19 (s, 2H, NH_2), 8.65 (s, 1H, NH), 9.21 (s, 1H, NH) ppm.

^{13}C NMR (125 MHz, DMSO-d$_6$): δ 26.52, 29.4, 35.13, 43.23, 51.32, 69.83, 114.38, 116.79, 121.24, 122.57, 123.24, 126.75, 129.02, 130.28, 133.06, 133.96, 136.3, 142.88, 144.24, 144.72, 156.57, 157.65, 157.07, 159.33, 171.75, 173.45, 174.91 ppm.

Melting point: 194-196 °C.

***tert*-Butyl *(R)*-2-(*(S)*-2-(3-amino-4-(4-(3-(2-fluoro-5-methylphenyl)ureido) phenyl)-1H-indazole-1-carbonyl)pyrrolidine-1-carbonyl)pyrrolidine-1-carboxylate**

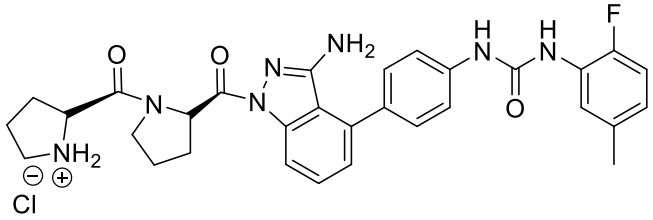


5.48a

By the method outlined for synthesis of compound **5.44a**, the product was brown solid (180 mg, 54%).

^{1}H NMR (400 MHz, DMSO-d$_6$): δ 1.38 (s, 9H, C(CH$_3$)$_3$), 1.84 (m, 3H, 3CH), 2.04 (m, 3H, 3CH), 2.15 (m, 2H, 2CH), 2.30 (s, 3H, CH$_3$), 2.35 (m, 2H, CH), 4.21 (m, 2H, 2CH), 4.33 (m, 2H, 2CH), 5.31 (s, 2H, NH$_2$), 6.82 (s, 1H, ArH), 7.13 (m, 1H, ArH), 7.21 (d, J = 6.52 Hz, 1H, ArH), 7.42 (d, J = 7.94 Hz, 2H, ArH), 7.62 (m, 3H, ArH), 8.02 (d, J = 6.95 Hz, 1H, ArH), 8.26 (m, 1H, ArH), 8.56 (s, 1H, NH), 9.24 (s, 1H, NH) ppm.

***(R)*-2-(*(S)*-2-(3-amino-4-(4-(3-(2-fluoro-5-methylphenyl)ureido)phenyl)-1H -indazole-1-carbonyl)pyrrolidine-1-carbonyl)pyrrolidin-1-ium chloride**



5.48

By the method outlined for synthesis of compound **5.44**, the product was white solid (160 mg, 56%).

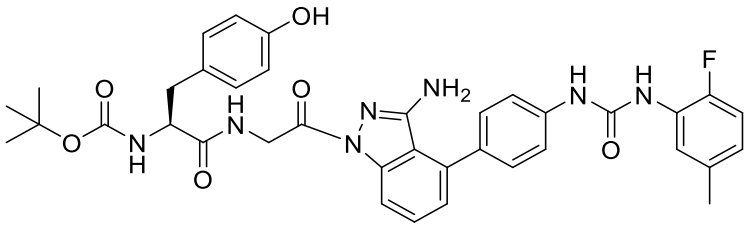
MS: m/z (HRMS) calculated for $C_{31}H_{33}FN_7O_3^+$ 570.2623 [M+H], MS found: 570.2712 [M+H].

^{1}H NMR (400 MHz, DMSO-d$_6$): δ 1.09 (m, 1H, CH), 1.25 (m, 2H, 2CH), 1.80 (m, 2H, 2CH), 2.12 (m, 2H, 2CH), 2.28 (s, 3H, CH$_3$), 2.80 (m, 2H, 2CH), 3.05 (d, J = 7.82 Hz, 2H, 2CH), 4.35 (m, 2H, 2CH), 5.50 (s, 2H, NH$_2$), 6.83 (s, 1H, ArH), 7.11 (m, 1H, ArH), 7.22 (d, J = 6.32 Hz, 1H, ArH), 7.44 (d, J = 7.68 Hz, 2H, ArH), 7.65 (m, 3H, ArH), 7.99 (d, J = 7.04 Hz, 1H, ArH), 8.29 (s, 2H, NH$_2$), 8.58 (m, 1H, ArH), 8.75 (s, 1H, NH), 9.58 (s, 1H, NH) ppm.

^{13}C NMR (125 MHz, DMSO-d$_6$): δ 26.54, 29.43, 34.6, 34.06, 35.02, 50.73, 52.46, 59.34, 68.82, 113.95, 116.82, 121.28, 122.59, 123.27, 126.95, 129.04, 130.31, 133.1, 133.37, 137.78, 142.92, 144.26, 144.75, 156.64, 158.21, 157.15, 161.19, 174.05, 173.28 ppm.

Melting point: 184-186 °C.

***tert*-Butyl *(S)*-(1-((2-(3-amino-4-(4-(3-(2-fluoro-5-methylphenyl)ureido) phenyl)-1H-indazol-1-yl)-2-oxoethyl)amino)-3-(4-hydroxyphenyl)-1-oxopropan-2-yl)carbamate**

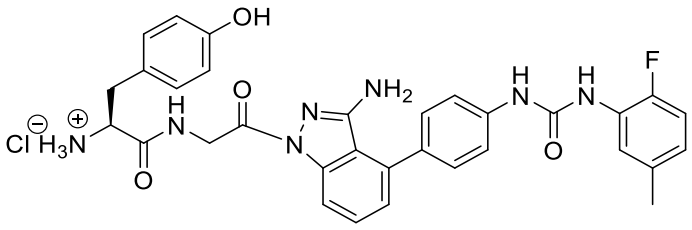


5.49a

By the method outlined for synthesis of compound **5.44a**, the product was yellow solid (166 mg, 48%).

^{1}H NMR (400 MHz, DMSO-d$_6$): δ 1.33 (s, 9H, C(CH$_3$)$_3$), 2.29 (s, 3H, CH$_3$), 3.05 (d, J = 7.36 Hz, 2H, CH$_2$), 3.63 (s, 2H, CH$_2$), 4.58 (t, J = 6.21 Hz, 1H, CH), 5.32 (s, 2H, NH$_2$), 6.66 (m, 3H, ArH), 7.09 (m, 3H, ArH), 7.22 (d, J = 7.84 Hz, 1H, ArH), 7.44 (d, J = 7.82 Hz, 2H, ArH), 7.65 (m, 2H, ArH), 7.99 (m, 2H, ArH), 8.29 (m, 2H, ArH), 8.58 (s, 1H, NH), 9.28 (s, 1H, NH), 9.15 (s, 1H, NH) ppm.

***(S)*-1-((2-(3-amino-4-(4-(3-(2-fluoro-5-methylphenyl)ureido)phenyl)-1H-indazol-1-yl)-2-oxoethyl)amino)-3-(4-hydroxyphenyl)-1-oxopropan-2-aminium chloride**



5.49

By the method outlined for synthesis of compound **5.44**, the product was white solid (121 mg, 85%).

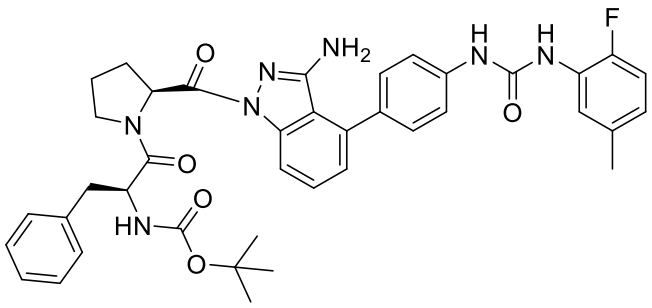
MS: m/z (HRMS) calculated for $C_{32}H_{31}FN_7O_4^+$ 696.2416 [M+H], MS found: 696.2524 [M+H].

^{1}H NMR (400 MHz, DMSO-d$_6$): δ 3.01 (d, J = 6.92 Hz, 2H, CH_2), 3.65 (s, 2H, CH_2), 4.66 (t, J = 6.21 Hz, 1H, CH), 5.34 (s, 2H, NH_2), 6.72 (m, 3H, ArH), 7.13 (m, 3H, ArH), 7.24 (d, J = 7.64 Hz, 1H, ArH), 7.43 (d, J = 7.77 Hz, 2H, ArH), 7.66 (m, 2H, ArH), 8.05 (m, 2H, ArH), 8.18 (s, 2H, NH_2), 8.29 (m, 2H, ArH), 9.23 (s, 1H, NH), 9.35 (s, 1H, NH) ppm.

^{13}C NMR (125 MHz, DMSO-d$_6$): δ 26.5, 41.11, 55.24, 59.37, 112.32, 118.98, 120.13, 119.44, 123.64, 122.74, 123.3, 130.09, 131.38, 130.45, 133.04, 134.63, 134.67, 139.16, 141.77, 143.18, 146.91, 152.01, 154.56, 159.26, 158.22, 160.41, 167.98, 176.6, 157.18, 175.33, 176.41 ppm.

Melting point: 181-184 °C.

***tert*-Butyl ((*S*)-1-((*S*)-2-(3-amino-4-(4-(3-(2-fluoro-5-methylphenyl)ureido) phenyl)-1H-indazole-1-carbonyl)pyrrolidin-1-yl)-1-oxo-3-phenylpropan-2-yl)carbamate**

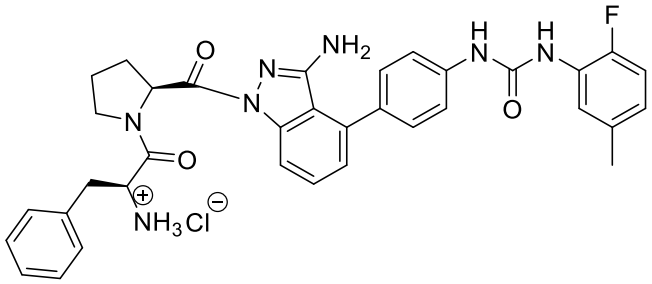


5.50a

By the method outlined for synthesis of compound **5.44a**, the product was yellow solid (161 mg, 45%).

^{1}H NMR (400 MHz, DMSO-d$_6$): δ 1.35 (s, 9H, $C(CH_3)_3$), 2.03 (m, 3H, 3CH), 2.13 (m, 1H, CH), 2.29 (s, 3H, CH_3), 2.85 (m, 3H, 3CH), 3.76 (m, 2H, CH_2), 4.41 (m, 1H, CH), 5.32 (s, 2H, NH_2), 6.83 (s, 1H, ArH), 7.12 (m, 2H, ArH), 7.24 (m, 2H, ArH), 7.32 (m, 2H, ArH), 7.37 (d, J = 7.70 Hz, 1H, ArH), 7.44 (m, 3H, ArH), 7.65 (m, 3H, ArH), 8.02 (d, J = 6.75 Hz, 1H, ArH), 8.30 (s, 1H, NH), 8.57 (s, 1H, NH), 9.29 (s, 1H, NH) ppm.

***(S)*-1-((*S*)-2-(3-amino-4-(4-(3-(2-fluoro-5-methylphenyl)ureido)phenyl)-1H-indazole-1-carbonyl)pyrrolidin-1-yl)-1-oxo-3-phenylpropan-2-aminium chloride**



5.50

By the method outlined for synthesis of compound **5.44**, the product was white solid (121 mg, 87%).

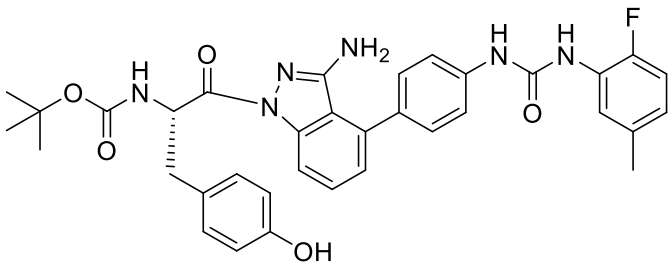
MS: m/z (HRMS) calculated for $C_{35}H_{35}FN_7O_3^+$ 620.2779 [M+H], MS found: 620.2892 [M+H].

^{1}H NMR (400 MHz, DMSO-d$_6$): δ 1.80 (m, 3H, 3CH), 2.18 (m, 1H, CH), 2.29 (s, 3H, CH_3), 2.91 (m, d, J = 7.23 Hz, 1H, CH), 3.05 (d, J = 7.48 Hz, 2H, CH_2), 3.39 (m, 1H, CH), 4.35 (m, 2H, 2CH), 5.50 (s, 2H, NH_2), 6.82 (s, 1H, ArH), 7.11 (m, 1H, ArH), 7.31 (m, 3H, ArH), 7.35 (m, 4H, ArH), 7.45 (m, 2H, ArH), 7.67 (m, 2H, ArH), 8.28 (m, 2H, ArH), 8.59 (s, 2H, NH_2), 8.78 (s, 1H, NH), 9.32 (s, 1H, NH) ppm.

^{13}C NMR (125 MHz, DMSO-d$_6$): δ 26.5, 29.46, 33.04, 34.02, 51.38, 55.58, 67.78, 113.51, 118.98, 120.13, 121.51, 125.43, 125.36, 127.96, 132.47, 131.92, 130.91, 133.54, 133.79, 132.98, 135.32, 138.28, 140.73, 145.31, 145.82, 154.04, 156.46, 158.17, 157.18, 175.33, 176.41 ppm.

Melting point: 210-212 °C.

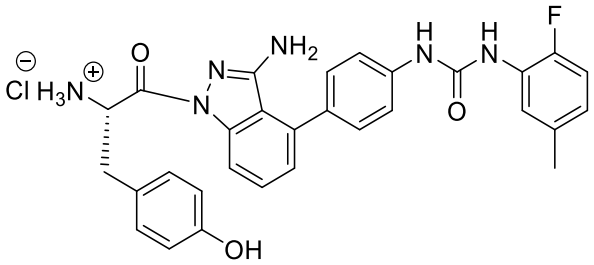
***tert*-Butyl *(S)*-(1-(3-amino-4-(4-(3-(2-fluoro-5-methylphenyl)ureido) phenyl)-1H-indazol-1-yl)-3-(4-hydroxyphenyl)-1-oxopropan-2-yl)carbamate**



5.51a

By the method outlined for synthesis of compound **5.44a**, the product was off-white solid (127 mg, 40%). ^{1}H NMR (400 MHz, DMSO-d_6): δ 1.33 (s, 9H, $C(CH_3)_3$), 2.29 (s, 3H, CH_3), 3.08 (t, J = 6.75, 2H, CH_2), 5.26 (t, J = 6.77 Hz, 1H, CH), 5.35 (s, 2H, NH_2), 6.02 (s, 1H, NH), 6.68 (m, 1H, ArH), 6.83 (s, 1H, ArH), 6.92 (s, 1H, ArH), 7.12 (m, 2H, ArH), 7.23 (m, 2H, ArH), 7.46 (d, J = 8.81, 2H, ArH), 7.65 (m, 2H, ArH), 8.02 (d, J = 6.92, 1H, ArH), 8.31 (d, J = 8.13, 1H, ArH), 8.58 (s, 1H, ArH), 9.20 (s, 1H, NH), 9.30 (s, 1H, NH) ppm.

***(S)*-1-(3-amino-4-(4-(3-(2-fluoro-5-methylphenyl)ureido)phenyl)-1H-indazol-1-yl)-3-(4-hydroxyphenyl)-1-oxopropan-2-aminium chloride**



5.51

By the method outlined for synthesis of compound **5.44**, the product was light brown solid (103 mg, 85%).

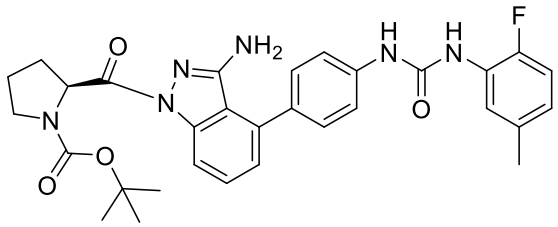
MS: m/z (HRMS) calculated for $C_{30}H_{28}FN_6O_3^+$ 539.2201 [M+H], MS found: 539.2325 [M+H].

^{1}H NMR (400 MHz, DMSO-d_6): δ 2.28 (s, 3H, CH_3), 3.05 (t, J = 6.83, 2H, CH_2), 4.92 (s, 2H, NH_2), 5.28 (t, J = 6.80 Hz, 1H, CH), 5.29 (s, 2H, NH_2), 6.71 (m, 1H, ArH), 6.85 (s, 1H, ArH), 6.97 (s, 1H, ArH), 7.23 (m, 2H, ArH), 7.45 (m, 2H, ArH), 7.78 (d, J = 8.43, 2H, ArH), 7.85 (m, 2H, ArH), 8.21 (d, J = 7.04, 1H, ArH), 8.36 (d, J = 7.95, 1H, ArH), 8.53 (s, 1H, ArH), 9.22 (s, 1H, NH), 9.34 (s, 1H, NH) ppm.

^{13}C NMR (125 MHz, DMSO-d_6): δ 22.43, 29.86, 57.25, 109.65, 115.03, 118.45, 117.95, 119.66, 122.14, 120.27, 126.11, 129.7, 127.88, 129.56, 132.95, 132.35, 137.26, 140.09, 140.15, 142.93, 153.6, 151.75, 155.28, 156.54, 159.55, 167.2 ppm.

Melting point: 190-192 °C.

***tert*-Butyl *(S)*-2-(3-amino-4-(4-(3-(2-fluoro-5-methylphenyl)ureido) phenyl) -1H-indazole-1-carbonyl)pyrrolidine-1-carboxylate**

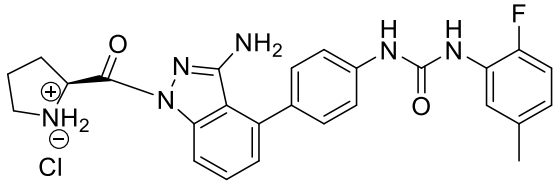


5.52a

By the method outlined for synthesis of compound **5.44a**, the product was yellow solid (354 mg, 62%).

^{1}H NMR (400 MHz, DMSO-d$_6$): δ 1.41 (s, 9H, C(CH$_3$)$_3$), 1.89 (m, 4H, (CH$_2$)$_2$), 2.27 (s, 3H, CH$_3$), 2.33 (t, J = 5.66 Hz, 2H, CH$_2$), 5.25 (s, 2H, NH$_2$), 5.31 (q, J = 4.32 Hz, 1H, CH), 6.82 (s, 1H, ArH), 7.11 (m, 1H, ArH), 7.21 (d, J = 7.38 Hz, 1H, ArH), 7.42 (m, 3H, ArH), 7.62 (d, J = 7.92 Hz, 3H, ArH), 7.97 (d, J = 7.92 Hz, 1H, ArH), 8.55 (s, 1H, NH), 9.26 (s, 1H, NH) ppm.

***(S)*-2-(3-amino-4-(4-(3-(2-fluoro-5-methylphenyl)ureido)phenyl)-1H-indazole-1-carbonyl)pyrrolidin-1-ium chloride**



5.52

By the method outlined for synthesis of compound **5.44**, the product was light yellow solid (268 mg, 92%).

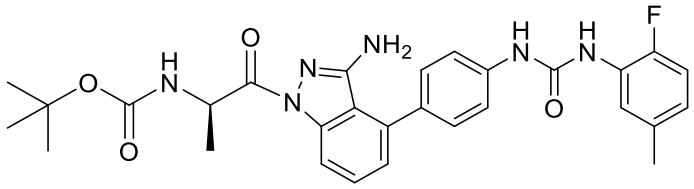
MS: m/z (HRMS) calculated for $C_{26}H_{26}FN_6O_2^+$ 508.1798 [M+H], MS found: 508.1853 [M+H].

^{1}H NMR (400 MHz, DMSO-d$_6$): δ 1.27 (m, 3H, 3CH), 1.92 (m, 1H, CH), 2.28 (s, 3H, CH$_3$), 3.37 (m, 2H, CH$_2$), 4.24 (t, J = 5.34 Hz, 1H, CH), 5.26 (s, 2H, NH$_2$), 5.47 (s, 1H, NH), 6.82 (s, 1H, ArH), 7.12 (t, J = 8.15, 1H, ArH), 7.36 (m, 3H, ArH), 7.59 (d, J = 8.75, 1H, ArH), 7.70 (m, 1H, ArH), 7.81 (t, J = 5.92 Hz, 1H, ArH), 7.99 (d, J = 7.65 Hz, 1H, ArH), 8.38 (d, J = 6.92 Hz, 1H, ArH), 9.13 (s, 1H, NH), 9.33 (s, 1H, NH) ppm.

^{13}C NMR (125 MHz, DMSO-d$_6$): δ 26.48, 30.9, 37.1, 52.9, 65.64, 114.18, 117.87, 119.21, 122.73, 124.32, 123.54, 129.18, 131.36, 131.03, 133.83, 137.18, 140.85, 144.4, 145.8, 154.46, 155.65, 158.15, 157.3, 175.53 ppm.

Melting point: 183-185 °C.

***tert*-Butyl *(R)*-(1-(3-amino-4-(4-(3-(2-fluoro-5-methylphenyl)ureido) phenyl)-1H-indazol-1-yl)-1-oxopropan-2-yl)carbamate**

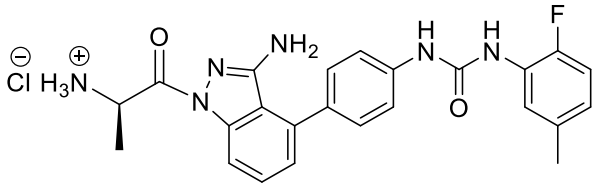


5.53a

By the method outlined for synthesis of compound **5.44a**, the product was off-white solid (240 mg, 44%).

^{1}H NMR (400 MHz, DMSO-d$_6$): δ 1.20 (d, J = 8.52 Hz, 3H, CH_3), 1.40 (s, 9H, $C(CH_3)_3$), 2.29 (s, 3H, CH_3), 5.13 (q, J = 7.19 Hz, 1H, CH), 5.30 (s, 2H, NH_2), 6.82 (s, 1H, ArH), 7.12 (m, 1H, ArH), 7.21 (d, J = 7.12 Hz, 1H, ArH), 7.34 (d, J = 7.31 Hz, 1H, ArH), 7.43 (d, J = 8.72 Hz, 2H, ArH), 7.63 (m, 3H, ArH), 8.01 (d, J = 7.69, 1H, ArH), 8.29 (s,1H, NH), 8.56 (s, 1H, NH), 9.27 (s, 1H, NH) ppm.

***(R)*-1-(3-amino-4-(4-(3-(2-fluoro-5-methylphenyl)ureido)phenyl)-1H-indazol-1-yl)-1-oxopropan-2-aminium chloride**



5.53

By the method outlined for synthesis of compound **5.44**, the product was white solid (176 mg, 88%).

MS: m/z (HRMS) calculated for $C_{24}H_{24}FN_6O_2^+$ 447.1939[M+H], MS found: 447.2021 [M+H].

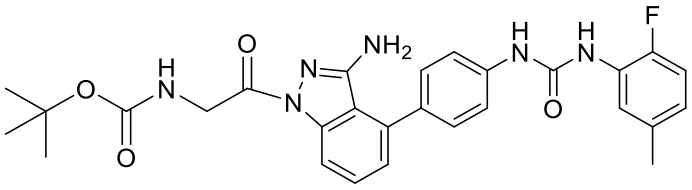
^{1}H NMR (400 MHz, DMSO-d$_6$): δ 1.36 (d, J = 7.45 Hz, 3H, CH_3), 2.28 (s, 3H, CH_3), 4.82 (q, J = 5.43 Hz, 1H, CH), 5.48 (s, 2H, NH_2), 6.80 (s, 1H, ArH), 7.12 (m, 1H, ArH), 7.28 (m, 1H, ArH), 7.39 (t, J = 8.62 Hz, 2H, ArH), 7.65 (m, 3H,

ArH), 7.98 (t, J = 7.54 Hz, 2H, ArH), 8.30 (s, 2H, NH_2), 8.80 (s, 1H, NH), 9.66 (s, 1H, NH) ppm.

^{13}C NMR (125 MHz, DMSO-d$_6$): δ 22.14, 25.38, 54.44, 113.59, 116.77, 120.41, 122.43, 123.21, 124.62, 128.88, 130.26, 132.23, 133.9, 139.42, 142.05, 144.1, 144.7, 155.91, 156.54, 157.05, 158.5, 175.24 ppm.

Melting point: 192-194 °C.

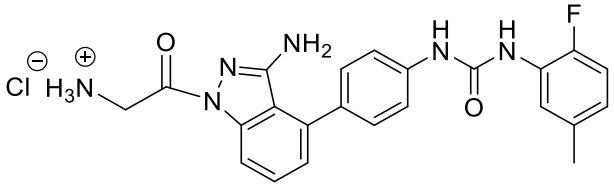
***tert*-Butyl (2-(3-amino-4-(4-(3-(2-fluoro-5-methylphenyl) ureido) phenyl)-1H-indazol-1-yl)-2-oxoethyl)carbamate**



5.54a

By the method outlined for synthesis of compound **5.44a**, the product was off-white solid (255 mg, 48%). ^{1}H NMR (400 MHz, DMSO-d$_6$): δ 1.42 (s, 9H, $C(CH_3)_3$), 2.29 (s, 3H, CH_3), 3.34 (s, 2H, CH_2), 5.30 (s, 2H, NH_2), 6.82 (s, 1H, ArH), 7.13 (m, 1H, ArH), 7.22 (d, J = 6.67 Hz, 2H, ArH), 7.44 (d, J = 8.32 Hz, 2H, ArH), 7.64 (m, 3H, ArH), 8.01 (d, 7.92 Hz, 1H, ArH), 8.27 (s, 1H, NH), 8.57 (s, 1H, NH), 9.28 (s, 1H, NH) ppm.

2-(3-Amino-4-(4-(3-(2-fluoro-5-methylphenyl) ureido) phenyl)-1H-indazol-1-yl)-2-oxoethan-1-aminium chloride



5.54

By the method outlined for synthesis of compound **5.44**, the product was off-white solid (185 mg, 92%).

MS: m/z (HRMS) calculated for $C_{23}H_{22}FN_6O_2^+$ 433.1782 [M+H], MS found: 433.1693 [M+H].

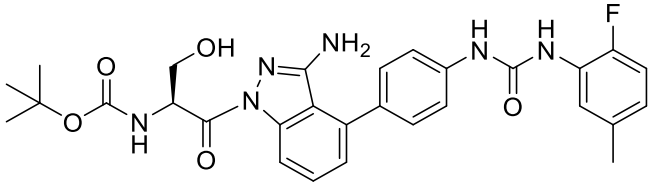
^{1}H NMR (400 MHz, DMSO-d$_6$): δ 2.28 (s, 3H, CH_3), 3.98 (s, 2H, CH_2), 5.38 (s, 2H, NH_2), 6.82 (s, 1H, ArH), 7.10 (m, 2H, ArH), 7.27 (m, 2H, ArH), 7.42

(m, 3H, ArH), 7.61 (d, J = 8.61 Hz, 1H, ArH), 7.66 (s, 2H, NH_2), 7.99 (d, J = 7.56 Hz, 1H, ArH), 8.80 (s, 1H, NH), 9.20 (s, 1H, NH) ppm.

^{13}C NMR (125 MHz, DMSO-d$_6$): δ 26.38, 43.88, 113.2, 117.77, 119.01, 122.83, 124.18, 123.22, 129.28, 131.26, 130.83, 134.54, 139.76, 140.65, 144.5, 145.7, 154.56, 156.25, 158.05, 157.1, 167.59 ppm.

Melting point: 201-204 °C.

***tert*-Butyl *(S)*-(1-(3-amino-4-(4-(3-(2-fluoro-5-methylphenyl)ureido) phenyl) -1H-indazol-1-yl)-3-hydroxy-1-oxopropan-2-yl)carbamate**

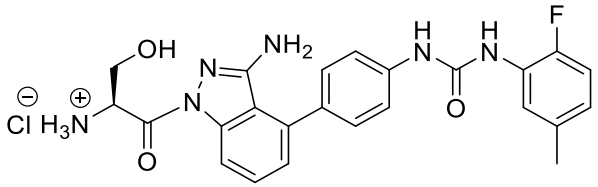


5.55a

By the method outlined for synthesis of compound **5.44a**, the product was white solid (292 mg, 52%).

^{1}H NMR (400 MHz, DMSO-d$_6$): δ 1.41 (s, 9H, $C(CH_3)_3$), 2.29 (s, 3H, CH_3), 3.86 (d, J = 7.95 Hz, 2H, CH_2), 4.92 (t, J = 6.54 Hz, 1H, CH), 5.29 (s, 2H, NH_2), 6.83 (s, 1H, ArH), 7.13 (t, J = 8.30 Hz, 1H, ArH), 7.22 (d, J = 8.14 Hz, 1H, ArH), 7.44 (d, J = 6.98 Hz, 2H, ArH), 7.63 (m, 3H, ArH), 8.02 (d, J = 6.93 Hz, 1H, ArH), 8.29 (s, 1H, NH), 8.57 (s, 1H, NH), 9.28 (s, 1H, NH) ppm.

***(S)*-1-(3-amino-4-(4-(3-(2-fluoro-5-methylphenyl)ureido)phenyl)-1H-indazol-1-yl)-3-hydroxy-1-oxopropan-2-aminium chloride**



5.55

By the method outlined for synthesis of compound **5.44**, the product was white solid (217 mg, 91%).

MS: m/z (HRMS) calculated for $C_{24}H_{24}FN_6O_3^+$ 463.1888 [M+H], MS found: 463.1954 [M+H].

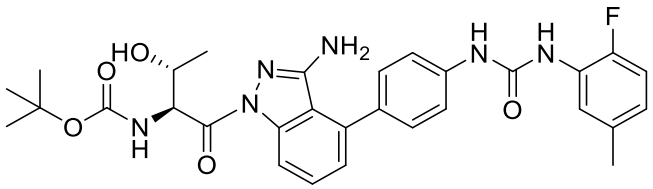
^{1}H NMR (400 MHz, DMSO-d$_6$): δ 2.28 (s, 3H, CH_3), 3.73 (d, J = 6.85 Hz, 2H, CH_2), 4.36 (t, J = 7.21 Hz, 1H, CH), 5.44 (s, 2H, NH_2), 6.81 (s, 1H, ArH), 7.10

(m, 1H, ArH), 7.27 (d, J = 7.25 Hz, 1H, ArH), 7.42 (d, J = 8.38 Hz, 2H, ArH), 7.68 (m, 3H, ArH), 7.99 (d, J = 8.23 Hz, 2H, ArH), 8.27 (s, 2H, NH_2), 8.86 (s, 1H, NH), 9.37 (s, 1H, NH) ppm.

^{13}C NMR (125 MHz, DMSO-d$_6$): δ 21.18, 54.85, 61.87, 107.98, 112.57, 114.81, 117.23, 118.89, 119.02, 123.68, 126.06, 126.63, 128.85, 135.59, 136.45, 138.9, 140.5, 149.99, 152.31, 152.85, 152.9, 164.41 ppm.

Melting point: 191-193 °C.

***tert*-Butyl ((*2S,3R*)-1-(3-amino-4-(4-(3-(2-fluoro-5-methylphenyl)ureido) phenyl)-1H-indazol-1-yl)-3-hydroxy-1-oxobutan-2-yl)carbamate**

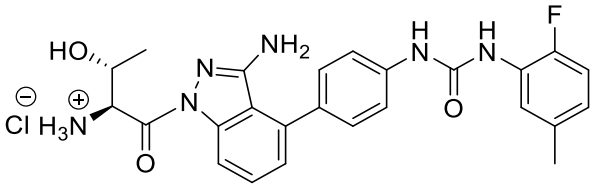


5.56a

By the method outlined for synthesis of compound **5.44a**, the product was brown solid (224 mg, 38%).

^{1}H NMR (400 MHz, DMSO-d$_6$): δ 1.17 (d, J = 6.96, 3H, CH_3), 1.42 (s, 9H, $C(CH_3)_3$), 2.28 (s, 3H, CH_3), 4.16 (m, 1H, CH), 4.37 (s, 1H, CH), 5.30 (s, 2H, NH_2), 6.83 (s, 1H, ArH), 7.13 (t, J = 8.76 Hz, 1H, ArH), 7.22 (d, J = 7.32 Hz, 2H, ArH), 7.44 (d, J = 8.13 Hz, 2H, ArH), 7.63 (m, 3H, ArH), 8.02 (s 1H, NH), 8.29 (d, J = 8.13 Hz, 1H, ArH), 8.57 (s, 1H, NH), 9.28 (s, 1H, NH) ppm.

(*2S,3R*)-1-(3-amino-4-(4-(3-(2-fluoro-5-methylphenyl)ureido)phenyl)-1H-indazol-1-yl)-3-hydroxy-1-oxobutan-2-aminium chloride



5.56

By the method outlined for synthesis of compound **5.44**, the product was brown solid (145 mg, 82%).

MS: m/z (HRMS) calculated for $C_{25}H_{26}FN_6O_3^+$ 477.2044 [M+H], MS found: 477.2132 [M+H].

^{1}H NMR (400 MHz, DMSO-d$_6$): δ 1.27 (d, J = 6.69 Hz, 3H, CH_3), 2.28 (s, 3H, CH_3), 4.03 (m, 1H, CH), 4.42 (m, 1H, CH), 5.28 (s, 2H, NH_2), 6.82 (s, 1H, ArH),

7.12 (t, J = 8.51 Hz, 1H, ArH), 7.28 (d, J = 7.05 Hz, 2H, ArH), 7.44 (d, J = 8.13 Hz, 2H, ArH), 7.67 (m, 3H, ArH), 7.99 (s 2H, NH_2), 8.31 (d, J = 8.75 Hz, 1H, ArH), 8.80 (s, 1H, NH), 9.53 (s, 1H, NH) ppm.

^{13}C NMR (125 MHz, DMSO-d_6): δ 25.74, 25.12, 61.73, 64.94, 111.35, 119.21, 120.13, 121.15, 125.44, 124.34, 127.6, 132.59, 131.95, 132.53, 142.89, 141.77, 142.82, 147.03, 155.67, 154.44, 159.38, 158.22, 172.88 ppm.

Melting point: 179-182 °C.

References

1. Rang, H. P.; Dale, M. M.; Ritter, J. M.; Flower, R. J.; Henderson, G. *Rang and Dale's Pharmacology*; Elsevier Health Sciences, **2015**.
2. Weinberg, R. *The biology of cancer*; Garland science, **2013**.
3. Siegel, R. L.; Miller, K. D.; Jemal, A. Cancer statistics, 2016. *CA: a cancer journal for clinicians,* **2016,** *66* (1), 7.
4. Organization, W. H. *Cancer Fact sheet N 297. February 2014*, **2014**.
5. Ahmad, A.; Ormiston-Smith, N.; Sasieni, P. Trends in the lifetime risk of developing cancer in Great Britain: comparison of risk for those born from 1930 to 1960. *British journal of cancer,* **2015,** *112* (5), 943.
6. Golan, D. E.; Tashjian, A. H.; Armstrong, E. J. *Principles of pharmacology: the pathophysiologic basis of drug therapy*; Lippincott Williams & Wilkins, **2011**.
7. Zhang, J.; Hochwald, S. N. Targeting receptor tyrosine kinases in solid tumors. *Surgical oncology clinics of North America,* **2013,** *22* (4), 685.
8. Zureikat, A. H.; McKee, M. D. Targeted therapy for solid tumors: current status. *Surgical oncology clinics of North America,* **2008,** *17* (2), 279.
9. Minhas, N.; Jackson, C. J.; Xue, M. Angiogenesis Inhibitors. *Compendium of Inflammatory Diseases,* **2016**, 55.
10. Gavhane, Y.; Shete, A.; Bhagat, A.; Shinde, V.; Bhong, K.; Khairnar, G.; Yadav, A. Solid tumors: facts, challenges and solutions. *International Journal of Pharma Sciences and Research,* **2011,** *2* (1), 1.
11. Hesketh, R. *Introduction to cancer biology*; Cambridge University Press, **2013**.
12. Wolinsky, J. B.; Colson, Y. L.; Grinstaff, M. W. Local drug delivery strategies for cancer treatment: gels, nanoparticles, polymeric films, rods, and wafers. *Journal of controlled release*, **2012,** *159* (1), 14.
13. Longley, D.; Johnston, P. Molecular mechanisms of drug resistance. *The Journal of pathology,* **2005,** *205* (2), 275.
14. Feng, Q.; Tong, R. Anticancer Nanoparticulate Polymer-Drug Conjugate. *Bioengineering & Translational Medicine,* **2016**.

15. Li, X.; Wu, M.; Pan, L.; Shi, J. Tumor vascular-targeted co-delivery of anti-angiogenesis and chemotherapeutic agents by mesoporous silica nanoparticle-based drug delivery system for synergetic therapy of tumor. *International journal of nanomedicine,* **2016,** *11*, 93.
16. Bastiancich, C.; Danhier, P.; Préat, V.; Danhier, F. Anticancer drug-loaded hydrogels as drug delivery systems for the local treatment of glioblastoma. *Journal of Controlled Release,* **2016**.
17. Steed, J. W. Supramolecular gel chemistry: developments over the last decade. *Chemical Communications,* **2011,** *47* (5), 1379.
18. Estroff, L. A.; Hamilton, A. D. Water gelation by small organic molecules. *Chemical Reviews,* **2004,** *104* (3), 1201.
19. Weiss, R. G. The past, present, and future of molecular gels. What is the status of the field, and where is it going? *Journal of the American Chemical Society,* **2014,** *136* (21), 7519.
20. Skilling, K. J.; Citossi, F.; Bradshaw, T. D.; Ashford, M.; Kellam, B.; Marlow, M. Insights into low molecular mass organic gelators: a focus on drug delivery and tissue engineering applications. *Soft Matter,* **2014,** *10* (2), 237.
21. Tian, R.; Chen, J.; Niu, R. The development of low-molecular weight hydrogels for applications in cancer therapy. *Nanoscale,* **2014,** *6* (7), 3474.
22. Prommer, E. E. Established and potential therapeutic applications of octreotide in palliative care. *Supportive Care in Cancer,* **2008,** *16* (10), 1117.
23. Pokuri, V. K.; Fong, M. K.; Iyer, R. Octreotide and lanreotide in gastroenteropancreatic neuroendocrine tumors. *Current oncology reports,* **2016,** *18* (1), 7.
24. Buil-Bruna, N.; Garrido, M. J.; Dehez, M.; Manon, A.; Nguyen, T. X. Q.; Gomez-Panzani, E. L.; Trocóniz, I. F. Population Pharmacokinetic Analysis of Lanreotide Autogel®/Depot in the Treatment of Neuroendocrine Tumors: Pooled Analysis of Four Clinical Trials. *Clinical pharmacokinetics,* **2016,** *55* (4), 461.

25. Raeburn, J.; Cardoso, A. Z.; Adams, D. J. The importance of the self-assembly process to control mechanical properties of low molecular weight hydrogels. *Chemical Society Reviews,* **2013,** *42* (12), 5143.
26. Lan, Y.; Corradini, M.; Weiss, R.; Raghavan, S.; Rogers, M. To gel or not to gel: correlating molecular gelation with solvent parameters. *Chemical Society Reviews,* **2015,** *44* (17), 6035.
27. Segarra-Maset, M. D.; Nebot, V. J.; Miravet, J. F.; Escuder, B. Control of molecular gelation by chemical stimuli. *Chemical Society Reviews,* **2013,** *42* (17), 7086.
28. Vegners, R.; Shestakova, I.; Kalvinsh, I.; Ezzell, R. M.; Janmey, P. A. Use of a gel-forming dipeptide derivative as a carrier for antigen presentation. *Journal of Peptide Science,* **1995,** *1* (6), 371.
29. Kiyonaka, S.; Sugiyasu, K.; Shinkai, S.; Hamachi, I. First thermally responsive supramolecular polymer based on glycosylated amino acid. *Journal of the American Chemical Society,* **2002,** *124* (37), 10954.
30. Jayawarna, V.; Ali, M.; Jowitt, T. A.; Miller, A. F.; Saiani, A.; Gough, J. E.; Ulijn, R. V. Nanostructured Hydrogels for Three-Dimensional Cell Culture Through Self-Assembly of Fluorenylmethoxycarbonyl–Dipeptides. *Advanced Materials,* **2006,** *18* (5), 611.
31. Yang, Z.; Liang, G.; Ma, M.; Gao, Y.; Xu, B. Conjugates of naphthalene and dipeptides produce molecular hydrogelators with high efficiency of hydrogelation and superhelical nanofibers. *Journal of Materials Chemistry,* **2007,** *17* (9), 850.
32. Chen, L.; Morris, K.; Laybourn, A.; Elias, D.; Hicks, M. R.; Rodger, A.; Serpell, L.; Adams, D. J. Self-assembly mechanism for a naphthalene−dipeptide leading to hydrogelation. *Langmuir,* **2009,** *26* (7), 5232.
33. Adams, D. J.; Mullen, L. M.; Berta, M.; Chen, L.; Frith, W. J. Relationship between molecular structure, gelation behaviour and gel properties of Fmoc-dipeptides. *Soft Matter,* **2010,** *6* (9), 1971.
34. Adams, D. J. Dipeptide and Tripeptide Conjugates as Low-Molecular-Weight Hydrogelators. *Macromolecular bioscience,* **2011,** *11* (2), 160.
35. Tang, C.; Smith, A. M.; Collins, R. F.; Ulijn, R. V.; Saiani, A. Fmoc-diphenylalanine self-assembly mechanism induces apparent p K a shifts. *Langmuir,* **2009,** *25* (16), 9447.

36. Escuder, B.; Miravet, J. F. *Functional molecular gels*; Royal Society of Chemistry, **2013**.
37. Yang, Z.; Liang, G.; Xu, B. Enzymatic hydrogelation of small molecules. *Accounts of chemical research*, **2008,** *41* (2), 315.
38. Toledano, S.; Williams, R. J.; Jayawarna, V.; Ulijn, R. V. Enzyme-triggered self-assembly of peptide hydrogels via reversed hydrolysis. *Journal of the American Chemical Society*, **2006,** *128* (4), 1070.
39. Yang, Z.; Liang, G.; Ma, M.; Gao, Y.; Xu, B. In Vitro and In Vivo Enzymatic Formation of Supramolecular Hydrogels Based on Self-Assembled Nanofibers of a β-Amino Acid Derivative. *Small*, **2007,** *3* (4), 558.
40. Williams, R. J.; Smith, A. M.; Collins, R.; Hodson, N.; Das, A. K.; Ulijn, R. V. Enzyme-assisted self-assembly under thermodynamic control. *Nature nanotechnology*, **2009,** *4* (1), 19.
41. Das, A. K.; Collins, R.; Ulijn, R. V. Exploiting Enzymatic (Reversed) Hydrolysis in Directed Self-Assembly of Peptide Nanostructures. *Small*, **2008,** *4* (2), 279.
42. Terech, P.; Weiss, R. G. Low molecular mass gelators of organic liquids and the properties of their gels. *Chemical Reviews*, **1997,** *97* (8), 3133.
43. de Loos, M.; Feringa, B. L.; van Esch, J. H. Design and application of self-assembled low molecular weight hydrogels. *European Journal of Organic Chemistry*, **2005,** *2005* (17), 3615.
44. Jung, J. H.; John, G.; Masuda, M.; Yoshida, K.; Shinkai, S.; Shimizu, T. Self-assembly of a sugar-based gelator in water: Its remarkable diversity in gelation ability and aggregate structure. *Langmuir*, **2001,** *17* (23), 7229.
45. Köhler, K.; Förster, G.; Hauser, A.; Dobner, B.; Heiser, U. F.; Ziethe, F.; Richter, W.; Steiniger, F.; Drechsler, M.; Stettin, H. Self-Assembly in a Bipolar Phosphocholine–Water System: The Formation of Nanofibers and Hydrogels. *Angewandte Chemie International Edition*, **2004,** *43* (2), 245.
46. Sangeetha, N. M.; Bhat, S.; Choudhury, A. R.; Maitra, U.; Terech, P. Properties of hydrogels derived from cationic analogues of bile acid:

remarkably distinct flowing characteristics. *The Journal of Physical Chemistry B,* **2004,** *108* (41), 16056.

47. Park, S. M.; Lee, Y. S.; Kim, B. H. Novel low-molecular-weight hydrogelators based on 2′-deoxyuridine. *Chemical communications,* **2003,** (23), 2912.
48. Burkhardt, M.; Kinzel, S.; Gradzielski, M. Macroscopic properties and microstructure of HSA based organogels: sensitivity to polar additives. *Journal of colloid and interface science,* **2009,** *331* (2), 514.
49. Burkhardt, M.; Noirez, L.; Gradzielski, M. Organogels based on 12-hydroxy stearic acid as a leitmotif: Dependence of gelation properties on chemical modifications. *Journal of colloid and interface science,* **2016,** *466*, 369.
50. Mukkamala, R.; Weiss, R. G. Physical gelation of organic fluids by anthraquinone-steroid-based molecules. Structural features influencing the properties of gels. *Langmuir,* **1996,** *12* (6), 1474.
51. Kawano, S.-i.; Fujita, N.; Bommel, K. J. v.; Shinkai, S. Pyridine-containing Cholesterols as Versatile Gelators of Organic Solvents and the Subtle Influence of Ag (I) on the Gel Stability. *Chemistry Letters,* **2003,** *32* (1), 12.
52. Kempe, S.; Mäder, K. In situ forming implants—an attractive formulation principle for parenteral depot formulations. *Journal of controlled release,* **2012,** *161* (2), 668.
53. Raghavan, S. R.; Cipriano, B. H. In *Molecular Gels*; Springer, 2006.
54. Takahashi, A.; Sakai, M.; Kato, T. Melting temperature of thermally reversible gel. VI. Effect of branching on the sol–gel transition of polyethylene gels. *Polymer Journal,* **1980,** *12* (5), 335.
55. Weiss, R. G.; Terech, P. Molecular gels. *Materials with Self-Assembled Fibrillar Networks,* **2006**.
56. Orbach, R.; Mironi-Harpaz, I.; Adler-Abramovich, L.; Mossou, E.; Mitchell, E. P.; Forsyth, V. T.; Gazit, E.; Seliktar, D. The rheological and structural properties of Fmoc-peptide-based hydrogels: the effect of aromatic molecular architecture on self-assembly and physical characteristics. *Langmuir,* **2012,** *28* (4), 2015.

57. Yuan, D.; Zhou, R.; Shi, J.; Du, X.; Li, X.; Xu, B. Enzyme-instructed self-assembly of hydrogelators consisting of nucleobases, amino acids, and saccharide. *RSC advances*, **2014,** *4* (50), 26487.
58. Hardy, J. G.; Hirst, A. R.; Ashworth, I.; Brennan, C.; Smith, D. K. Exploring molecular recognition pathways within a family of gelators with different hydrogen bonding motifs. *Tetrahedron*, **2007,** *63* (31), 7397.
59. Yu, G.; Yan, X.; Han, C.; Huang, F. Characterization of supramolecular gels. *Chemical Society Reviews*, **2013,** *42* (16), 6697.
60. Heeres, A.; van der Pol, C.; Stuart, M.; Friggeri, A.; Feringa, B. L.; van Esch, J. Orthogonal self-assembly of low molecular weight hydrogelators and surfactants. *Journal of the American Chemical Society*, **2003,** *125* (47), 14252.
61. Hirst, A. R.; Miravet, J. F.; Escuder, B.; Noirez, L.; Castelletto, V.; Hamley, I. W.; Smith, D. K. Self-Assembly of Two-Component Gels: Stoichiometric Control and Component Selection. *Chemistry–A European Journal*, **2009,** *15* (2), 372.
62. Edwards, W.; Smith, D. K. Dynamic Evolving Two-Component Supramolecular Gels: Hierarchical Control over Component Selection in Complex Mixtures. *Journal of the American Chemical Society*, **2013,** *135* (15), 5911.
63. Suzuki, M.; Yumoto, M.; Shirai, H.; Hanabusa, K. Supramolecular Gels Formed by Amphiphilic Low-Molecular-Weight Gelators of Nα, Nε-Diacyl-L-Lysine Derivatives. *Chemistry–A European Journal*, **2008,** *14* (7), 2133.
64. Yang, M.; Zhang, Z.; Yuan, F.; Wang, W.; Hess, S.; Lienkamp, K.; Lieberwirth, I.; Wegner, G. Self-Assembled Structures in Organogels of Amphiphilic Diblock Codendrimers. *Chemistry–A European Journal*, **2008,** *14* (11), 3330.
65. Doniach, S. Changes in biomolecular conformation seen by small angle X-ray scattering. *Chemical Reviews*, **2001,** *101* (6), 1763.
66. Kumar, N.; Varghese, S.; Narayan, G.; Das, S. Hierarchical Self-Assembly of Donor–Acceptor-Substituted Butadiene Amphiphiles into

Photoresponsive Vesicles and Gels. *Angewandte Chemie International Edition,* **2006,** *45* (38), 6317.

67. Samanta, S. K.; Pal, A.; Bhattacharya, S. Choice of the End Functional Groups in Tri (p-phenylenevinylene) Derivatives Controls Its Physical Gelation Abilities†. *Langmuir,* **2009,** *25* (15), 8567.
68. Uhrich, K. E.; Cannizzaro, S. M.; Langer, R. S.; Shakesheff, K. M. Polymeric systems for controlled drug release. *Chemical reviews,* **1999,** *99* (11), 3181.
69. Yang, Z.; Gu, H.; Zhang, Y.; Wang, L.; Xu, B. Small molecule hydrogels based on a class of antiinflammatory agents. *Chemical Communications,* **2004,** (2), 208.
70. Kapadia, M. R.; Chow, L. W.; Tsihlis, N. D.; Ahanchi, S. S.; Eng, J. W.; Murar, J.; Martinez, J.; Popowich, D. A.; Jiang, Q.; Hrabie, J. A. Nitric oxide and nanotechnology: a novel approach to inhibit neointimal hyperplasia. *Journal of vascular surgery,* **2008,** *47* (1), 173.
71. Yang, Z.; Xu, K.; Wang, L.; Gu, H.; Wei, H.; Zhang, M.; Xu, B. Self-assembly of small molecules affords multifunctional supramolecular hydrogels for topically treating simulated uranium wounds. *Chemical Communications,* **2005,** (35), 4414.
72. Soukasene, S.; Toft, D. J.; Moyer, T. J.; Lu, H.; Lee, H.-K.; Standley, S. M.; Cryns, V. L.; Stupp, S. I. Antitumor activity of peptide amphiphile nanofiber-encapsulated camptothecin. *ACS nano,* **2011,** *5* (11), 9113.
73. Vemula, P. K.; Wiradharma, N.; Ankrum, J. A.; Miranda, O. R.; John, G.; Karp, J. M. Prodrugs as self-assembled hydrogels: a new paradigm for biomaterials. *Current opinion in biotechnology,* **2013,** *24* (6), 1174.
74. Kim, J.-K.; Anderson, J.; Jun, H.-W.; Repka, M. A.; Jo, S. Self-assembling peptide amphiphile-based nanofiber gel for bioresponsive cisplatin delivery. *Molecular pharmaceutics,* **2009,** *6* (3), 978.
75. Ho, J. W. Potential and cytotoxicity of cis-platinum complex with anti-tumor activity in combination therapy. *Recent patents on anti-cancer drug discovery,* **2006,** *1* (1), 129.
76. Pinzani, V.; Bressolle, F.; Haug, I. J.; Galtier, M.; Blayac, J. P.; Balmès, P. Cisplatin-induced renal toxicity and toxicity-modulating strategies: a review. *Cancer chemotherapy and pharmacology,* **1994,** *35* (1), 1.

77. Screnci, D.; McKeage, M. J. Platinum neurotoxicity: clinical profiles, experimental models and neuroprotective approaches. *Journal of inorganic biochemistry*, **1999,** *77* (1), 105.
78. Mott, J. D.; Werb, Z. Regulation of matrix biology by matrix metalloproteinases. *Current opinion in cell biology*, **2004,** *16* (5), 558.
79. Klein, G.; Vellenga, E.; Fraaije, M.; Kamps, W.; De Bont, E. The possible role of matrix metalloproteinase (MMP)-2 and MMP-9 in cancer, eg acute leukemia. *Critical reviews in oncology/hematology*, **2004,** *50* (2), 87.
80. Gao, Y.; Kuang, Y.; Guo, Z.-F.; Guo, Z.; Krauss, I. J.; Xu, B. Enzyme-instructed molecular self-assembly confers nanofibers and a supramolecular hydrogel of taxol derivative. *Journal of the American Chemical Society*, **2009,** *131* (38), 13576.
81. Wang, H.; Wei, J.; Yang, C.; Zhao, H.; Li, D.; Yin, Z.; Yang, Z. The inhibition of tumor growth and metastasis by self-assembled nanofibers of taxol. *Biomaterials*, **2012,** *33* (24), 5848.
82. Tanaka, A.; Fukuoka, Y.; Morimoto, Y.; Honjo, T.; Koda, D.; Goto, M.; Maruyama, T. Cancer cell death induced by the intracellular self-assembly of an enzyme-responsive supramolecular gelator. *Journal of the American Chemical Society*, **2015,** *137* (2), 770.
83. Carethers, J. M.; Smith, E. J.; Behling, C. A.; Nguyen, L.; Tajima, A.; Doctolero, R. T.; Cabrera, B. L.; Goel, A.; Arnold, C. A.; Miyai, K. Use of 5-fluorouracil and survival in patients with microsatellite-unstable colorectal cancer. *Gastroenterology*, **2004,** *126* (2), 394.
84. Krawtchenko, N.; Roewert-Huber, J.; Ulrich, M.; Mann, I.; Sterry, W.; Stockfleth, E. A randomised study of topical 5% imiquimod vs. topical 5-fluorouracil vs. cryosurgery in immunocompetent patients with actinic keratoses: a comparison of clinical and histological outcomes including 1-year follow-up. *British Journal of Dermatology*, **2007,** *157* (s2), 34.
85. Sun, Y.; Kaplan, J. A.; Shieh, A.; Sun, H.-L.; Croce, C. M.; Grinstaff, M. W.; Parquette, J. R. Self-assembly of a 5-fluorouracil-dipeptide hydrogel. *Chemical Communications*, **2016,** *52* (30), 5254.
86. Xing, B.; Yu, C.-W.; Chow, K.-H.; Ho, P.-L.; Fu, D.; Xu, B. Hydrophobic interaction and hydrogen bonding cooperatively confer a

vancomycin hydrogel: a potential candidate for biomaterials. *Journal of the American Chemical Society*, **2002,** *124* (50), 14846.

87. Casuso, P.; Carrasco, P.; Loinaz, I.; Grande, H. J.; Odriozola, I. Converting drugs into gelators: Supramolecular hydrogels from N-acetyl-L-cysteine and coinage-metal salts. *Organic & biomolecular chemistry*, **2010,** *8* (23), 5455.
88. Sharma, P. C.; Sinhmar, A.; Sharma, A.; Rajak, H.; Pathak, D. P. Medicinal significance of benzothiazole scaffold: an insight view. *Journal of enzyme inhibition and medicinal chemistry*, **2013,** *28* (2), 240.
89. Noolvi, M. N.; Patel, H. M.; Kaur, M. Benzothiazoles: search for anticancer agents. *European journal of medicinal chemistry*, **2012,** *54*, 447.
90. Singh, M.; Singh, S. K. Benzothiazoles: how relevant in cancer drug design strategy? *Anti-Cancer Agents in Medicinal Chemistry (Formerly Current Medicinal Chemistry-Anti-Cancer Agents)*, **2014,** *14* (1), 127.
91. Bradshaw, T. D.; Matthews, C. S.; Cookson, J.; Chew, E.-H.; Shah, M.; Bailey, K.; Monks, A.; Harris, E.; Westwell, A. D.; Wells, G. Elucidation of thioredoxin as a molecular target for antitumor quinols. *Cancer research*, **2005,** *65* (9), 3911.
92. Arnér, E. S.; Holmgren, A. Physiological functions of thioredoxin and thioredoxin reductase. *European Journal of Biochemistry*, **2000,** *267* (20), 6102.
93. Gromer, S.; Urig, S.; Becker, K. The thioredoxin system—from science to clinic. *Medicinal research reviews*, **2004,** *24* (1), 40.
94. Lillig, C. H.; Holmgren, A. Thioredoxin and related molecules-from biology to health and disease. *Antioxidants & redox signaling*, **2007,** *9* (1), 25.
95. Arner, E. S.; Holmgren, A. Seminars in cancer biology, 2006; p 420.
96. Berggren, M.; Gallegos, A.; Gasdaska, J. R.; Gasdaska, P. Y.; Warneke, J.; Powis, G. Thioredoxin and thioredoxin reductase gene expression in human tumors and cell lines, and the effects of serum stimulation and hypoxia. *Anticancer research*, **1995,** *16* (6B), 3459.
97. Soini, Y.; Kahlos, K.; Näpänkangas, U.; Kaarteenaho-Wiik, R.; Säily, M.; Koistinen, P.; Pääakkö, P.; Holmgren, A.; Kinnula, V. L.

Widespread expression of thioredoxin and thioredoxin reductase in non-small cell lung carcinoma. *Clinical cancer research,* **2001,** *7* (6), 1750.

98. Kahlos, K.; Soini, Y.; Säily, M.; Koistinen, P.; Kakko, S.; Pääkkö, P.; Holmgren, A.; Kinnula, V. L. Up-regulation of thioredoxin and thioredoxin reductase in human malignant pleural mesothelioma. *International journal of cancer,* **2001,** *95* (3), 198.
99. Wells, G.; Berry, J. M.; Bradshaw, T. D.; Burger, A. M.; Seaton, A.; Wang, B.; Westwell, A. D.; Stevens, M. F. 4-Substituted 4-hydroxycyclohexa-2, 5-dien-1-ones with selective activities against colon and renal cancer cell lines. *Journal of medicinal chemistry,* **2003,** *46* (4), 532.
100. Papp, L. V.; Lu, J.; Holmgren, A.; Khanna, K. K. From selenium to selenoproteins: synthesis, identity, and their role in human health. *Antioxidants & redox signaling,* **2007,** *9* (7), 775.
101. Chew, E.-H.; Lu, J.; Bradshaw, T. D.; Holmgren, A. Thioredoxin reductase inhibition by antitumor quinols: a quinol pharmacophore effect correlating to antiproliferative activity. *The FASEB Journal,* **2008,** *22* (6), 2072.
102. L Arias, J. Drug targeting strategies in cancer treatment: an overview. *Mini reviews in medicinal chemistry,* **2011,** *11* (1), 1.
103. Lammers, T.; Kiessling, F.; Hennink, W. E.; Storm, G. Drug targeting to tumors: principles, pitfalls and (pre-) clinical progress. *Journal of controlled release,* **2012,** *161* (2), 175.
104. Huang, P. S.; Oliff, A. Drug-targeting strategies in cancer therapy. *Current opinion in genetics & development,* **2001,** *11* (1), 104.
105. Baselga, J. Targeting tyrosine kinases in cancer: the second wave. *Science,* **2006,** *312* (5777), 1175.
106. Arora, A.; Scholar, E. M. Role of tyrosine kinase inhibitors in cancer therapy. *Journal of Pharmacology and Experimental Therapeutics,* **2005,** *315* (3), 971.
107. Pawson, T. Regulation and targets of receptor tyrosine kinases. *European journal of cancer,* **2002,** *38,* S3.

108. Arteaga, C. L. The epidermal growth factor receptor: from mutant oncogene in nonhuman cancers to therapeutic target in human neoplasia. *Journal of Clinical Oncology*, **2001,** *19* (suppl 1), 32s.
109. Bogdan, S.; Klämbt, C. Epidermal growth factor receptor signaling. *Current biology*, **2001,** *11* (8), R292.
110. Paul, M. K.; Mukhopadhyay, A. K. Tyrosine kinase-role and significance in cancer. *Int J Med Sci*, **2004,** *1* (2), 101.
111. Lemmon, M. A.; Schlessinger, J. Cell signaling by receptor tyrosine kinases. *Cell*, **2010,** *141* (7), 1117.
112. Carpenter, G.; Cohen, S. Epidermal growth factor. *J Biol Chem,* **1990,** *265* (14), 7709.
113. Amis, E. S.; Lamer, V. K. The Gelatin of Brom Phenol Blue. *Science,* **1939,** *90* (2326), 90.
114. Bertram, J. S. The molecular biology of cancer. *Molecular aspects of medicine,* **2000,** *21* (6), 167.
115. Kech, P.; Hauser, S.; Krivi, G.; Sanzo, K.; Warren, T.; Feder, J.; Connolly, D. Vascular permeability factor, an endothelial cell mitogen related to platelet derived growth factor. *Science,* **1989,** *246*, 1309.
116. Marlin, S. S.; Stratowa, C.; Dustin, M. Vascular endothelial growth factor is a secreted angiogenic mitogen. **1989**.
117. Ferrara, N. Vascular endothelial growth factor: basic science and clinical progress. *Endocrine reviews,* **2004,** *25* (4), 581.
118. Parikh, A. A.; Ellis, L. M. The vascular endothelial growth factor family and its receptors. *Hematology/oncology clinics of North America,* **2004,** *18* (5), 951.
119. Pepper, M.; Ferrara, N.; Orci, L.; Montesano, R. Potent synergism between vascular endothelial growth factor and basic fibroblast growth factor in the induction of angiogenesis in vitro. *Biochemical and biophysical research communications,* **1992,** *189* (2), 824.
120. Ferrara, N. Seminars in oncology, 2002; p 10.
121. Glade-Bender, J.; Kandel, J. J.; Yamashiro, D. J. VEGF blocking therapy in the treatment of cancer. *Expert opinion on biological therapy,* **2003,** *3* (2), 263.

122. Manley, P. W.; Martiny-Baron, G.; Schlaeppi, J.-M.; Wood, J. M. Therapies directed at vascular endothelial growth factor. *Expert opinion on investigational drugs*, **2002,** *11* (12), 1715.
123. Ziche, M.; Donnini, S.; Morbidelli, L. Development of new drugs in angiogenesis. *Current drug targets*, **2004,** *5* (5), 485.
124. Pietras, K.; Sjöblom, T.; Rubin, K.; Heldin, C.-H.; Östman, A. PDGF receptors as cancer drug targets. *Cancer cell*, **2003,** *3* (5), 439.
125. Östman, A.; Heldin, C. H. PDGF receptors as targets in tumor treatment. *Advances in cancer research*, **2007,** *97*, 247.
126. Heldin, C.-H.; Eriksson, U.; Östman, A. New members of the platelet-derived growth factor family of mitogens. *Archives of biochemistry and biophysics*, **2002,** *398* (2), 284.
127. Avendaño, C.; Menendez, J. C. *Medicinal chemistry of anticancer drugs*; Elsevier, **2015**.
128. Silverman, R. B.; Holladay, M. W. *The organic chemistry of drug design and drug action*; Academic press, **2014**.
129. Normanno, N.; De Luca, A.; Bianco, C.; Strizzi, L.; Mancino, M.; Maiello, M. R.; Carotenuto, A.; De Feo, G.; Caponigro, F.; Salomon, D. S. Epidermal growth factor receptor (EGFR) signaling in cancer. *Gene*, **2006,** *366* (1), 2.
130. Dhanikula, A. B.; Panchagnula, R. Localized paclitaxel delivery. *International Journal of pharmaceutics*, **1999,** *183* (2), 85.
131. Harper, E.; Dang, W.; Lapidus, R. G.; Garver, R. I. Enhanced efficacy of a novel controlled release paclitaxel formulation (PACLIMER delivery system) for local-regional therapy of lung cancer tumor nodules in mice. *Clinical cancer research*, **1999,** *5* (12), 4242.
132. Griset, A. P.; Walpole, J.; Liu, R.; Gaffey, A.; Colson, Y. L.; Grinstaff, M. W. Expansile nanoparticles: synthesis, characterization, and in vivo efficacy of an acid-responsive polymeric drug delivery system. *Journal of the American Chemical Society*, **2009,** *131* (7), 2469.
133. Schulz, M. D.; Zubris, K. A. V.; Wade, J. E.; Padera, R. F.; Xu, X.; Grinstaff, M. W.; Colson, Y. L. Paclitaxel-loaded expansile nanoparticles in a multimodal treatment model of malignant mesothelioma. *The Annals of thoracic surgery*, **2011,** *92* (6), 2007.

134. Gao, J.; Wang, H.; Wang, L.; Wang, J.; Kong, D.; Yang, Z. Enzyme promotes the hydrogelation from a hydrophobic small molecule. *Journal of the American Chemical Society,* **2009,** *131* (32), 11286.
135. Zhao, F.; Gao, Y.; Shi, J.; Browdy, H. M.; Xu, B. Novel anisotropic supramolecular hydrogel with high stability over a wide pH range†. *Langmuir,* **2010,** *27* (4), 1510.
136. Wang, H.; Yang, C.; Wang, L.; Kong, D.; Zhang, Y.; Yang, Z. Self-assembled nanospheres as a novel delivery system for taxol: a molecular hydrogel with nanosphere morphology. *Chemical Communications,* **2011,** *47* (15), 4439.
137. Wang, H.; Yang, Z. Molecular hydrogels of hydrophobic compounds: a novel self-delivery system for anti-cancer drugs. *Soft Matter,* **2012,** *8* (8), 2344.
138. Norouzi, M.; Nazari, B.; Miller, D. W. Injectable hydrogel-based drug delivery systems for local cancer therapy. *Drug Discovery Today,* **2016,** *21* (11), 1835.
139. Hanabusa, K.; Yamada, M.; Kimura, M.; Shirai, H. Prominent Gelation and Chiral Aggregation of Alkylamides Derived from trans-1, 2-Diaminocyclohexane. *Angewandte Chemie International Edition in English,* **1996,** *35* (17), 1949.
140. Yamanaka, M. Urea derivatives as low-molecular-weight gelators. *Journal of Inclusion Phenomena and Macrocyclic Chemistry,* **2013,** *77* (1-4), 33.
141. Willemen, H. M.; Vermonden, T.; Marcelis, A.; Sudhölter, E. J. N-Cholyl Amino Acid Alkyl Esters− A Novel Class of Organogelators. *European Journal of Organic Chemistry,* **2001,** *2001* (12), 2329.
142. Watase, M.; Nakatani, Y.; Itagaki, H. On the origin of the formation and stability of physical gels of di-O-benzylidene-D-sorbitol. *The Journal of Physical Chemistry B,* **1999,** *103* (13), 2366.
143. Neidle, S. *Cancer Drug Design and Discovery*; Academic Press, **2008**.
144. Lin, Z.; Gao, W.; Hu, H.; Ma, K.; He, B.; Dai, W.; Wang, X.; Wang, J.; Zhang, X.; Zhang, Q. Novel thermo-sensitive hydrogel system with paclitaxel nanocrystals: High drug-loading, sustained drug release and

extended local retention guaranteeing better efficacy and lower toxicity. *Journal of Controlled Release,* **2014,** *174*, 161.

145. Xu, S.; Wang, W.; Li, X.; Liu, J.; Dong, A.; Deng, L. Sustained release of PTX-incorporated nanoparticles synergized by burst release of DOX·HCl from thermosensitive modified PEG/PCL hydrogel to improve anti-tumor efficiency. *European Journal of Pharmaceutical Sciences,* **2014,** *62*, 267.
146. Wu, Z.; Zou, X.; Yang, L.; Lin, S.; Fan, J.; Yang, B.; Sun, X.; Wan, Q.; Chen, Y.; Fu, S. Thermosensitive hydrogel used in dual drug delivery system with paclitaxel-loaded micelles for in situ treatment of lung cancer. *Colloids and Surfaces B: Biointerfaces,* **2014,** *122*, 90.
147. Mao, Y.; Li, X.; Chen, G.; Wang, S. Thermosensitive Hydrogel System With Paclitaxel Liposomes Used in Localized Drug Delivery System for In Situ Treatment of Tumor: Better Antitumor Efficacy and Lower Toxicity. *Journal of pharmaceutical sciences,* **2016,** *105* (1), 194.
148. Wilhelm, S.; Carter, C.; Lynch, M.; Lowinger, T.; Dumas, J.; Smith, R. A.; Schwartz, B.; Simantov, R.; Kelley, S. Discovery and development of sorafenib: a multikinase inhibitor for treating cancer. *Nat Rev Drug Discov,* **2007,** *6* (2).
149. Fong, T. A. T.; Shawver, L. K.; Sun, L.; Tang, C.; App, H.; Powell, T. J.; Kim, Y. H.; Schreck, R.; Wang, X.; Risau, W.et al. SU5416 Is a Potent and Selective Inhibitor of the Vascular Endothelial Growth Factor Receptor (Flk-1/KDR) That Inhibits Tyrosine Kinase Catalysis, Tumor Vascularization, and Growth of Multiple Tumor Types. *Cancer Research,* **1999,** *59* (1), 99.
150. Laird, A. D.; Vajkoczy, P.; Shawver, L. K.; Thurnher, A.; Liang, C.; Mohammadi, M.; Schlessinger, J.; Ullrich, A.; Hubbard, S. R.; Blake, R. A. SU6668 is a potent antiangiogenic and antitumor agent that induces regression of established tumors. *Cancer Research,* **2000,** *60* (15), 4152.
151. Chuma, M.; Terashita, K.; Sakamoto, N. New molecularly targeted therapies against advanced hepatocellular carcinoma: From molecular pathogenesis to clinical trials and future directions. *Hepatology Research,* **2015,** *45* (10).

152. Stone, E. L.; Citossi, F.; Singh, R.; Kaur, B.; Gaskell, M.; Farmer, P. B.; Monks, A.; Hose, C.; Stevens, M. F. G.; Leong, C.-O.et al. Antitumour benzothiazoles. Part 32: DNA adducts and double strand breaks correlate with activity; synthesis of 5F203 hydrogels for local delivery. *Bioorganic & Medicinal Chemistry,* **2015,** *23* (21), 6891.

153. Shen, X.; Jiao, T.; Zhang, Q.; Guo, H.; Lv, Y.; Zhou, J.; Gao, F. Nanostructures and self-assembly of organogels via benzimidazole/benzothiazole imide derivatives with different alkyl substituent chains. *Journal of Nanomaterials,* **2013,** *2013,* 2.

154. Raeburn, J.; Mendoza-Cuenca, C.; Cattoz, B. N.; Little, M. A.; Terry, A. E.; Cardoso, A. Z.; Griffiths, P. C.; Adams, D. J. The effect of solvent choice on the gelation and final hydrogel properties of Fmoc–diphenylalanine. *Soft Matter,* **2015,** *11* (5), 927.

155. Rowe, R. C.; Sheskey, P. J.; Weller, P. J. *Handbook of pharmaceutical excipients*; Pharmaceutical press London, **2006**.

156. Grunt, T. W.; Somay, C.; Pavelka, M.; Ellinger, A.; Dittrich, E.; Dittrich, C. The effects of dimethyl sulfoxide and retinoic acid on the cell growth and the phenotype of ovarian cancer cells. *Journal of cell science,* **1991,** *100* (3), 657.

157. McIntyre, L. J.; Kim, Y. S. Effects of sodium butyrate and dimethylsulfoxide on human pancreatic tumor cell lines. *European Journal of Cancer and Clinical Oncology,* **1984,** *20* (2), 265.

158. Gupta, J. K.; Adams, D. J.; Berry, N. G. Will it gel? Successful computational prediction of peptide gelators using physicochemical properties and molecular fingerprints. *Chemical Science,* **2016,** *7* (7), 4713.

159. Remko, M.; Boháč, A.; Kováčiková, L. Molecular structure, pKa, lipophilicity, solubility, absorption, polar surface area, and blood brain barrier penetration of some antiangiogenic agents. *Structural Chemistry,* **2011,** *22* (3), 635.

160. Steed, J. W. Anion-tuned supramolecular gels: a natural evolution from urea supramolecular chemistry. *Chemical Society Reviews,* **2010,** *39* (10), 3686.

161. George, M.; Tan, G.; John, V. T.; Weiss, R. G. Urea and Thiourea Derivatives as Low Molecular-Mass Organogelators. *Chemistry–A European Journal*, **2005,** *11* (11), 3243.
162. Arai, S.; Imazu, K.; Kusuda, S.; Yoshihama, I.; Tonegawa, M.; Nishimura, Y.; Kitahara, K.-i.; Oishi, S.; Takemura, T. Organogel formation by self-assembly of Ag (I) and mono-urea derivatives containing pyridyl group. *Chemistry Letters*, **2006,** *35* (6), 634.
163. Bajaj, N.; Hart, L. R.; Greenland, B. W.; Hayes, W. Macromolecular Symposia, 2013; p 118.
164. Van Esch, J.; De Feyter, S.; Kellogg, R. M.; De Schryver, F.; Feringa, B. L. Self-assembly of bisurea compounds in organic solvents and on solid substrates. *Chemistry–A European Journal*, **1997,** *3* (8), 1238.
165. Brinksma, J.; Feringa, B. L.; Kellogg, R. M.; Vreeker, R.; van Esch, J. Rheology and thermotropic properties of bis-urea-based organogels in various primary alcohols. *Langmuir*, **2000,** *16* (24), 9249.
166. Jeong, Y.; Hanabusa, K.; Masunaga, H.; Akiba, I.; Miyoshi, K.; Sakurai, S.; Sakurai, K. Solvent/gelator interactions and supramolecular structure of gel fibers in cyclic bis-urea/primary alcohol organogels. *Langmuir*, **2005,** *21* (2), 586.
167. Schoonbeek, F. S.; van Esch, J. H.; Hulst, R.; Kellogg, R. M.; Feringa, B. L. Geminal Bis-ureas as Gelators for Organic Solvents: Gelation Properties and Structural Studies in Solution and in the Gel State. *Chemistry–A European Journal*, **2000,** *6* (14), 2633.
168. Yabuuchi, K.; Marfo-Owusu, E.; Kato, T. A new urea gelator: incorporation of intra-and intermolecular hydrogen bonding for stable 1D self-assembly. *Organic & biomolecular chemistry*, **2003,** *1* (19), 3464.
169. de Loos, M.; Ligtenbarg, A. G.; van Esch, J.; Kooijman, H.; Spek, A. L.; Hage, R.; Kellogg, R. M.; Feringa, B. L. Tripodal tris-urea derivatives as gelators for organic solvents. *European Journal of Organic Chemistry*, **2000**, 3675.
170. Linifanib. *Drugs R D*, **2010,** *10* (2), 111.
171. Aversa, C.; Leone, F.; Zucchini, G.; Serini, G.; Geuna, E.; Milani, A.; Valdembri, D.; Martinello, R.; Montemurro, F. Linifanib: current status

and future potential in cancer therapy. *Expert review of anticancer therapy,* **2015,** *15* (6), 677.

172. Yancopoulos, G. D.; Davis, S.; Gale, N. W.; Rudge, J. S.; Wiegand, S. J.; Holash, J. Vascular-specific growth factors and blood vessel formation. *Nature,* **2000,** *407* (6801), 242.
173. Adams, J.; Huang, P.; Patrick, D. A strategy for the design of multiplex inhibitors for kinase-mediated signalling in angiogenesis. *Current opinion in chemical biology,* **2002,** *6* (4), 486.
174. Arteaga, C. L. Molecular Therapeutics Is One Promiscuous Drug against Multiple Targets Better than Combinations of Molecule-specific Drugs? *Clinical Cancer Research,* **2003,** *9* (4), 1231.
175. Dai, Y.; Guo, Y.; Frey, R. R.; Ji, Z.; Curtin, M. L.; Ahmed, A. A.; Albert, D. H.; Arnold, L.; Arries, S. S.; Barlozzari, T. Thienopyrimidine ureas as novel and potent multitargeted receptor tyrosine kinase inhibitors. *Journal of Medicinal Chemistry,* **2005,** *48* (19), 6066.
176. Garuti, L.; Roberti, M.; Bottegoni, G.; Ferraro, M. Diaryl Urea: A Privileged Structure in Anticancer Agents. *Current medicinal chemistry,* **2016,** *23* (15), 1528.
177. Dai, Y.; Hartandi, K.; Ji, Z.; Ahmed, A. A.; Albert, D. H.; Bauch, J. L.; Bouska, J. J.; Bousquet, P. F.; Cunha, G. A.; Glaser, K. B. Discovery of N-(4-(3-Amino-1 H-indazol-4-yl) phenyl)-N'-(2-fluoro-5-methylphenyl) urea (ABT-869), a 3-Aminoindazole-Based Orally Active Multitargeted Receptor Tyrosine Kinase Inhibitor. *Journal of Medicinal Chemistry,* **2007,** *50* (7), 1584.
178. Albert, D. H.; Tapang, P.; Magoc, T. J.; Pease, L. J.; Reuter, D. R.; Wei, R.-Q.; Li, J.; Guo, J.; Bousquet, P. F.; Ghoreishi-Haack, N. S. Preclinical activity of ABT-869, a multitargeted receptor tyrosine kinase inhibitor. *Molecular cancer therapeutics,* **2006,** *5* (4), 995.
179. Zhou, J.; Goh, B.-C.; Albert, D. H.; Chen, C.-S. ABT-869, a promising multi-targeted tyrosine kinase inhibitor: from bench to bedside. *Journal of hematology & oncology,* **2009,** *2* (1), 1.
180. Tan, E.-H.; Goss, G. D.; Salgia, R.; Besse, B.; Gandara, D. R.; Hanna, N. H.; Yang, J. C.-H.; Thertulien, R.; Wertheim, M.; Mazieres, J. Phase

2 trial of Linifanib (ABT-869) in patients with advanced non-small cell lung cancer. *Journal of Thoracic Oncology*, **2011,** *6* (8), 1418.

181. Tannir, N. M.; Wong, Y.-N.; Kollmannsberger, C. K.; Ernstoff, M. S.; Perry, D. J.; Appleman, L. J.; Posadas, E. M.; Cho, D.; Choueiri, T. K.; Coates, A. Phase 2 trial of linifanib (ABT-869) in patients with advanced renal cell cancer after sunitinib failure. *European Journal of Cancer*, **2011,** *47* (18), 2706.
182. O'Neil, B. H.; Cainap, C.; Van Cutsem, E.; Gorbunova, V.; Karapetis, C. S.; Berlin, J.; Goldberg, R. M.; Qin, Q.; Qian, J.; Ricker, J. L. Randomized phase II open-label study of mFOLFOX6 in combination with linifanib or bevacizumab for metastatic colorectal cancer. *Clinical colorectal cancer*, **2014,** *13* (3), 156.
183. Palmer, D. H.; Johnson, P. J. Evaluating the role of treatment-related toxicities in the challenges facing targeted therapies for advanced hepatocellular carcinoma. *Cancer and Metastasis Reviews*, **2015,** *34* (3), 497.
184. Cainap, C.; Qin, S.; Huang, W.-T.; Chung, I. J.; Pan, H.; Cheng, Y.; Kudo, M.; Kang, Y.-K.; Chen, P.-J.; Toh, H.-C. Linifanib versus Sorafenib in patients with advanced hepatocellular carcinoma: results of a randomized phase III trial. *Journal of Clinical Oncology*, **2014**, JCO. 2013.54. 3298.
185. Rodriguez-Llansola, F.; Hermida-Merino, D.; Nieto-Ortega, B.; Ramirez, F. J.; Navarrete, J. T.; Casado, J.; Hamley, I. W.; Escuder, B.; Hayes, W.; Miravet, J. F. Self-assembly studies of a chiral bisurea-based superhydrogelator. *Chemistry*, **2012,** *18* (46), 14725.
186. Qi, Z.; de Molina, P. M.; Jiang, W.; Wang, Q.; Nowosinski, K.; Schulz, A.; Gradzielski, M.; Schalley, C. A. Systems chemistry: logic gates based on the stimuli-responsive gel–sol transition of a crown ether-functionalized bis (urea) gelator. *Chemical Science*, **2012,** *3* (6), 2073.
187. Ryan, D. M.; Anderson, S. B.; Nilsson, B. L. The influence of side-chain halogenation on the self-assembly and hydrogelation of Fmoc-phenylalanine derivatives. *Soft Matter*, **2010,** *6* (14), 3220.

188. Miyaura, N.; Yamada, K.; Suzuki, A. A new stereospecific cross-coupling by the palladium-catalyzed reaction of 1-alkenylboranes with 1-alkenyl or 1-alkynyl halides. *Tetrahedron Letters,* **1979,** *20* (36), 3437.
189. Miyaura, N.; Suzuki, A. Stereoselective synthesis of arylated (E)-alkenes by the reaction of alk-1-enylboranes with aryl halides in the presence of palladium catalyst. *Journal of the Chemical Society, Chemical Communications,* **1979,** (19), 866.
190. Miyaura, N.; Suzuki, A. Palladium-Catalyzed Cross-Coupling Reactions of Organoboron Compounds. *Chemical Reviews,* **1995,** *95* (7), 2457.
191. Amatore, C.; Jutand, A.; Le Duc, G. Kinetic Data for the Transmetalation/Reductive Elimination in Palladium-Catalyzed Suzuki–Miyaura Reactions: Unexpected Triple Role of Hydroxide Ions Used as Base. *Chemistry – A European Journal,* **2011,** *17* (8), 2492.
192. Raeburn, J.; Pont, G.; Chen, L.; Cesbron, Y.; Lévy, R.; Adams, D. J. Fmoc-diphenylalanine hydrogels: understanding the variability in reported mechanical properties. *Soft Matter,* **2012,** *8* (4), 1168.
193. Rodrigues, M.; Calpena, A. C.; Amabilino, D. B.; Garduño-Ramírez, M. L.; Pérez-García, L. Supramolecular gels based on a gemini imidazolium amphiphile as molecular material for drug delivery. *Journal of Materials Chemistry B,* **2014,** *2* (33), 5419.
194. Metrangolo, P.; Meyer, F.; Pilati, T.; Resnati, G.; Terraneo, G. Halogen bonding in supramolecular chemistry. *Angew Chem Int Ed Engl,* **2008,** *47* (33), 6114.
195. Priimagi, A.; Cavallo, G.; Metrangolo, P.; Resnati, G. The halogen bond in the design of functional supramolecular materials: recent advances. *Accounts of chemical research,* **2013,** *46* (11), 2686.
196. Wang, Y.; Zhang, Z.; Xu, L.; Li, X.; Chen, H. Hydrogels of halogenated Fmoc-short peptides for potential application in tissue engineering. *Colloids and Surfaces B: Biointerfaces,* **2013,** *104*, 163.
197. Meazza, L.; Foster, J. A.; Fucke, K.; Metrangolo, P.; Resnati, G.; Steed, J. W. Halogen-bonding-triggered supramolecular gel formation. *Nature Chemistry,* **2013,** *5* (1), 42.

198. Loo, Y.; Zhang, S.; Hauser, C. A. From short peptides to nanofibers to macromolecular assemblies in biomedicine. *Biotechnology advances,* **2012,** *30* (3), 593.

199. Dudukovic, N. A.; Zukoski, C. F. Evidence for equilibrium gels of valence-limited particles. *Soft Matter,* **2014,** *10* (39), 7849.

200. Mezger, T. G. *The rheology handbook: for users of rotational and oscillatory rheometers*; Vincentz Network GmbH & Co KG, **2006**.

201. Sáez, J. A.; Escuder, B.; Miravet, J. F. Supramolecular hydrogels for enzymatically triggered self-immolative drug delivery. *Tetrahedron,* **2010,** *66* (14), 2614.

202. Kleinsmann, A. J.; Weckenmann, N. M.; Nachtsheim, B. J. Phosphate-Triggered Self-Assembly of N-[(Uracil-5-yl) methyl] urea: A Minimalistic Urea-Derived Hydrogelator. *Chemistry–A European Journal,* **2014,** *20* (31), 9753.

203. Ren, C.; Xu, C.; Li, D.; Ren, H.; Hao, J.; Yang, Z. Gemcitabine induced supramolecular hydrogelations of aldehyde-containing short peptides. *RSC Advances,* **2014,** *4* (66), 34729.

204. Rodríguez-Llansola, F.; Hermida-Merino, D.; Nieto-Ortega, B.; Ramírez, F. J.; Navarrete, J. T. L.; Casado, J.; Hamley, I. W.; Escuder, B.; Hayes, W.; Miravet, J. F. Self-Assembly Studies of a Chiral Bisurea-Based Superhydrogelator. *Chemistry–A European Journal,* **2012,** *18* (46), 14725.

205. Mears, L. L. E.; Draper, E. R.; Castilla, A. M.; Su, H.; Zhuola; Dietrich, B.; Nolan, M. C.; Smith, G. N.; Doutch, J.; Rogers, S.et al. Drying Affects the Fiber Network in Low Molecular Weight Hydrogels. *Biomacromolecules,* **2017**, DOI:10.1021/acs.biomac.7b00823 10.1021/acs.biomac.7b00823.

206. Cicchi, S.; Ghini, G.; Lascialfari, L.; Brandi, A.; Betti, F.; Berti, D.; Baglioni, P.; Di Bari, L.; Pescitelli, G.; Mannini, M. Self-sorting chiral organogels from a long chain carbamate of 1-benzyl-pyrrolidine-3, 4-diol. *Soft Matter,* **2010,** *6* (8), 1655.

207. Moffat, J. R.; Smith, D. K. Controlled self-sorting in the assembly of 'multi-gelator'gels. *Chemical Communications,* **2009,** (3), 316.

208. Moniruzzaman, M.; Sundararajan, P. R. Low molecular weight organogels based on long-chain carbamates. *Langmuir*, **2005,** *21* (9), 3802.

209. Mannhold, R.; Kubinyi, H.; Folkers, G.; Rautio, J. *Prodrugs and targeted delivery: towards better ADME properties*; John Wiley & Sons, **2011**.

210. Redasani, V. K.; Bari, S. B. *Prodrug Design: Perspectives, Approaches and Applications in Medicinal Chemistry*; Academic Press, **2015**.

211. Wang, G.; Cheuk, S.; Yang, H.; Goyal, N.; Reddy, P. N.; Hopkinson, B. Synthesis and Characterization of Monosaccharide-Derived Carbamates as Low-Molecular-Weight Gelators†. *Langmuir*, **2009,** *25* (15), 8696.

212. Rautio, J.; Kumpulainen, H.; Heimbach, T.; Oliyai, R.; Oh, D.; Järvinen, T.; Savolainen, J. Prodrugs: design and clinical applications. *Nature Reviews Drug Discovery*, **2008,** *7* (3), 255.

213. Simplício, A. L.; Clancy, J. M.; Gilmer, J. F. Prodrugs for amines. *Molecules*, **2008,** *13* (3), 519.

214. Alexander, J.; Cargill, R.; Michelson, S. R.; Schwam, H. (Acyloxy) alkyl carbamates as novel bioreversible prodrugs for amines: increased permeation through biological membranes. *Journal of medicinal chemistry*, **1988,** *31* (2), 318.

215. Gogate, U.; Repta, A.; Alexander, J. N-(Acyloxyalkoxycarbonyl) derivatives as potential prodrugs of amines. I. Kinetics and mechanism of degradation in aqueous solutions. *International journal of pharmaceutics*, **1987,** *40* (3), 235.

216. Alexander, J.; Fromtling, R. A.; Bland, J. A.; Pelak, B. A.; Gilfillan, E. C. (Acyloxy) alkyl carbamate prodrugs of norfloxacin. *Journal of medicinal chemistry*, **1991,** *34* (1), 78.

217. Cundy, K. C.; Annamalai, T.; Bu, L.; De Vera, J.; Estrela, J.; Luo, W.; Shirsat, P.; Torneros, A.; Yao, F.; Zou, J. XP13512 [(±)-1-([(α-isobutanoyloxyethoxy) carbonyl] aminomethyl)-1-cyclohexane acetic acid], a novel gabapentin prodrug: II. Improved oral bioavailability, dose proportionality, and colonic absorption compared with gabapentin in rats and monkeys. *Journal of Pharmacology and Experimental Therapeutics*, **2004,** *311* (1), 324.

218. Cundy, K. C.; Branch, R.; Chernov-Rogan, T.; Dias, T.; Estrada, T.; Hold, K.; Koller, K.; Liu, X.; Mann, A.; Panuwat, M. XP13512 [(±)-1-([(α-Isobutanoyloxyethoxy) carbonyl] aminomethyl)-1-cyclohexane acetic acid], a novel gabapentin prodrug: I. Design, synthesis, enzymatic conversion to gabapentin, and transport by intestinal solute transporters. *Journal of Pharmacology and Experimental Therapeutics,* **2004,** *311* (1), 315.

219. Meng, Q.; Luo, H.; Liu, Y.; Li, W.; Zhang, W.; Yao, Q. Synthesis and evaluation of carbamate prodrugs of SQ109 as antituberculosis agents. *Bioorganic & medicinal chemistry letters,* **2009,** *19* (10), 2808.

220. Fages, F.; Vögtle, F.; Žinic, M. In *Low Molecular Mass Gelator*; Springer, 2005.

221. Vig, B. S.; Huttunen, K. M.; Laine, K.; Rautio, J. Amino acids as promoieties in prodrug design and development. *Advanced drug delivery reviews,* **2013,** *65* (10), 1370.

222. Beginn, U.; Sheiko, S.; Möller, M. Self-organization of 3, 4, 5-tris (octyloxy) benzamide in solution and embedding of the aggregates into methacrylate resins. *Macromolecular Chemistry and Physics,* **2000,** *201* (10), 1008.

223. George, M.; Snyder, S. L.; Terech, P.; Glinka, C. J.; Weiss, R. G. N-alkyl perfluoroalkanamides as low molecular-mass organogelators. *Journal of the American Chemical Society*, **2003,** *125* (34), 10275.

224. Maitra, U.; Potluri, V. K.; Sangeetha, N.; Babu, P.; Raju, A. Helical aggregates from a chiral organogelator. *Tetrahedron: Asymmetry,* **2001,** *12* (3), 477.

225. Babu, P.; Sangeetha, N.; Vijaykumar, P.; Maitra, U.; Rissanen, K.; Raju, A. Pyrene-Derived Novel One-and Two-Component Organogelators. *Chemistry–A European Journal,* **2003,** *9* (9), 1922.

226. de Vries, E. J.; Kellogg, R. M. Small depsipeptides as solvent gelators. *Journal of the Chemical Society, Chemical Communications,* **1993,** (3), 238.

227. Crisp, G. T.; Gore, J. Biotin derivatives as gelators of organic solvents. *Synthetic communications,* **1997,** *27* (13), 2203.

228. Diaz-Padilla, I.; Siu, L. L. Brivanib alaninate for cancer. *Expert opinion on investigational drugs,* **2011,** *20* (4), 577.

229. Huynh, H.; Fargnoli, J. Brivanib alaninate. *Drugs of The Future,* **2009,** *34*, 881.

230. Soul-Lawton, J.; Seaber, E.; On, N.; Wootton, R.; Rolan, P.; Posner, J. Absolute bioavailability and metabolic disposition of valaciclovir, the L-valyl ester of acyclovir, following oral administration to humans. *Antimicrobial agents and chemotherapy*, **1995,** *39* (12), 2759.

231. de Miranda, P.; Blum, M. R. Pharmacokinetics of acyclovir after intravenous and oral administration. *Journal of Antimicrobial Chemotherapy,* **1983,** *12* (suppl B), 29.

232. Vergin, H.; Kikuta, C.; Mascher, H.; Metz, R. Pharmacokinetics and bioavailability of different formulations of aciclovir. *Arzneimittel-Forschung,* **1995,** *45* (4), 508.

233. Kim, I.; Chu, X.-y.; Kim, S.; Provoda, C. J.; Lee, K.-D.; Amidon, G. L. Identification of a human valacyclovirase biphenyl hydrolase-like protein as valacyclovir hydrolase. *Journal of Biological Chemistry,* **2003,** *278* (28), 25348.

234. Miller, W.; Miller, R. Phosphorylation of acyclovir (acycloguanosine) monophosphate by GMP kinase. *Journal of Biological Chemistry,* **1980,** *255* (15), 7204.

235. Song, X.; Lorenzi, P. L.; Landowski, C. P.; Vig, B. S.; Hilfinger, J. M.; Amidon, G. L. Amino acid ester prodrugs of the anticancer agent gemcitabine: synthesis, bioconversion, metabolic bioevasion, and hPEPT1-mediated transport. *Molecular pharmaceutics*, **2005,** *2* (2), 157.

236. Landowski, C. P.; Vig, B. S.; Song, X.; Amidon, G. L. Targeted delivery to PEPT1-overexpressing cells: acidic, basic, and secondary floxuridine amino acid ester prodrugs. *Molecular cancer therapeutics,* **2005,** *4* (4), 659.

237. Wu, Z.; Shah, A.; Patel, N.; Yuan, X. Development of methotrexate proline prodrug to overcome resistance by MDA-MB-231 cells. *Bioorganic & medicinal chemistry letters,* **2010,** *20* (17), 5108.

238. Gomes, P.; Vale, N.; Moreira, R. Cyclization-activated prodrugs. *Molecules,* **2007,** *12* (11), 2484.

239. Santos, C.; Mateus, M. L.; dos Santos, A. P.; Moreira, R.; de Oliveira, E.; Gomes, P. Cyclization-activated prodrugs. Synthesis, reactivity and toxicity of dipeptide esters of paracetamol. *Bioorganic & medicinal chemistry letters,* **2005,** *15* (6), 1595.

240. Johnson, E. K.; Adams, D. J.; Cameron, P. J. Peptide based low molecular weight gelators. *Journal of Materials Chemistry,* **2011,** *21* (7), 2024.

241. Tomasini, C.; Castellucci, N. Peptides and peptidomimetics that behave as low molecular weight gelators. *Chemical Society Reviews,* **2013,** *42* (1), 156.

242. Zanna, N.; Merlettini, A.; Tatulli, G.; Milli, L.; Focarete, M. L.; Tomasini, C. Hydrogelation Induced by Fmoc-Protected Peptidomimetics. *Langmuir,* **2015,** *31* (44), 12240.

243. Suzuki, M.; Hanabusa, K. L-Lysine-based low-molecular-weight gelators. *Chemical Society Reviews,* **2009,** *38* (4), 967.

244. Hanabusa, K.; Nakayama, H.; Kimura, M.; Shirai, H. Easy Preparation and Prominent Gelation of New Gelator Based on L-Lysine. *Chemistry Letters,* **2000,** (9), 1070.

245. Suzuki, M.; Yumoto, M.; Kimura, M.; Shirai, H.; Hanabusa, K. A Family of Low-Molecular-Weight Hydrogelators Based on L-Lysine Derivatives with a Positively Charged Terminal Group. *Chemistry–A European Journal,* **2003,** *9* (1), 348.

246. Suzuki, M.; Yumoto, M.; Kimura, M.; Shirai, H.; Hanabusa, K. Hydrogel Formation Using New L-Lysine-Based Low-Molecular-Weight Compounds with Positively Charged Pendant Chains. *Helvetica chimica acta,* **2003,** *86* (6), 2228.

247. Reches, M.; Gazit, E. Controlled patterning of aligned self-assembled peptide nanotubes. *Nature nanotechnology,* **2006,** *1* (3), 195.

248. Demirel, G. k.; Malvadkar, N.; Demirel, M. C. Control of Protein Adsorption onto Core− Shell Tubular and Vesicular Structures of Diphenylalanine/Parylene. *Langmuir,* **2009,** *26* (3), 1460.

249. Yan, X.; Cui, Y.; He, Q.; Wang, K.; Li, J. Organogels based on self-assembly of diphenylalanine peptide and their application to immobilize quantum dots. *Chemistry of Materials,* **2008,** *20* (4), 1522.

250. Xu, H.; Das, A. K.; Horie, M.; Shaik, M. S.; Smith, A. M.; Luo, Y.; Lu, X.; Collins, R.; Liem, S. Y.; Song, A. An investigation of the conductivity of peptide nanotube networks prepared by enzyme-triggered self-assembly. *Nanoscale*, **2010,** *2* (6), 960.
251. Cheng, G.; Castelletto, V.; Moulton, C.; Newby, G.; Hamley, I. Hydrogelation and self-assembly of Fmoc-tripeptides: unexpected influence of sequence on self-assembled fibril structure, and hydrogel modulus and anisotropy. *Langmuir*, **2010,** *26* (7), 4990.
252. Adams, D. J.; Butler, M. F.; Frith, W. J.; Kirkland, M.; Mullen, L.; Sanderson, P. A new method for maintaining homogeneity during liquid–hydrogel transitions using low molecular weight hydrogelators. *Soft Matter*, **2009,** *5* (9), 1856.
253. Chen, L.; Revel, S.; Morris, K.; C. Serpell, L.; Adams, D. J. Effect of molecular structure on the properties of naphthalene− dipeptide hydrogelators. *Langmuir*, **2010,** *26* (16), 13466.
254. Conte, M. P.; Singh, N.; Sasselli, I. R.; Escuder, B.; Ulijn, R. V. Metastable hydrogels from aromatic dipeptides. *Chemical Communications*, **2016,** *52* (96), 13889.
255. Kuang, Y.; Gao, Y.; Xu, B. Supramolecular hydrogelators of N-terminated dipeptides selectively inhibit cancer cells. *Chemical Communications*, **2011,** *47* (47), 12625.
256. Lan, Y.; Corradini, M. G.; Liu, X.; May, T. E.; Borondics, F.; Weiss, R. G.; Rogers, M. A. Comparing and correlating solubility parameters governing the self-assembly of molecular gels using 1, 3: 2, 4-dibenzylidene sorbitol as the gelator. *Langmuir*, **2014,** *30* (47), 14128.
257. Das, R. K.; Kandanelli, R.; Linnanto, J.; Bose, K.; Maitra, U. Supramolecular chirality in organogels: A detailed spectroscopic, morphological, and rheological investigation of gels (and xerogels) derived from alkyl pyrenyl urethanes. *Langmuir*, **2010,** *26* (20), 16141.
258. Tang, C.; Ulijn, R. V.; Saiani, A. Self-assembly and gelation properties of glycine/leucine Fmoc-dipeptides. *The European Physical Journal E*, **2013,** *36* (10), 111.

259. Goolcharran, C.; Borchardt, R. T. Kinetics of diketopiperazine formation using model peptides. *Journal of pharmaceutical sciences,* **1998,** *87* (3), 283.

260. Bruice, P. Y. *Organic Chemistry*; Pearson Education, Limited, **2016**.

261. Pierra, C.; Amador, A.; Benzaria, S.; Cretton-Scott, E.; D'Amours, M.; Mao, J.; Mathieu, S.; Moussa, A.; Bridges, E. G.; Standring, D. N. Synthesis and pharmacokinetics of valopicitabine (NM283), an efficient prodrug of the potent anti-HCV agent 2 '-C-methylcytidine. *Journal of medicinal chemistry,* **2006,** *49* (22), 6614.

262. Henderson, L. J. Concerning the relationship between the strength of acids and their capacity to preserve neutrality. *Survey of Anesthesiology,* **1964,** *8* (5), 504.

263. Milanesi, L.; Hunter, C. A.; Tzokova, N.; Waltho, J. P.; Tomas, S. Versatile Low-Molecular-Weight Hydrogelators: Achieving Multiresponsiveness through a Modular Design. *Chemistry–A European Journal,* **2011,** *17* (35), 9753.

264. O'Lenick, T. G.; Jin, N.; Woodcock, J. W.; Zhao, B. Rheological properties of aqueous micellar gels of a thermo-and pH-sensitive ABA triblock copolymer. *The Journal of Physical Chemistry B,* **2011,** *115* (12), 2870.

265. D'Aléo, A.; Pozzo, J.-L.; Fages, F.; Schmutz, M.; Mieden-Gundert, G.; Vögtle, F.; Caplar, V.; Zinic, M. 11-Aminoundecanoic acid: a versatile unit for the generation of low molecular weight gelators for water and organic solvents. *Chemical communications,* **2004,** (2), 190.

266. Tang, C.; Ulijn, R. V.; Saiani, A. Effect of Glycine Substitution on Fmoc–Diphenylalanine Self-Assembly and Gelation Properties. *Langmuir,* **2011,** *27* (23), 14438.

267. Manchun, S.; Dass, C. R.; Sriamornsak, P. Targeted therapy for cancer using pH-responsive nanocarrier systems. *Life sciences,* **2012,** *90* (11), 381.

268. Wike-Hooley, J.; Haveman, J.; Reinhold, H. The relevance of tumour pH to the treatment of malignant disease. *Radiotherapy and Oncology,* **1984,** *2* (4), 343.

269. Suzuki, M.; Yumoto, M.; Shirai, H.; Hanabusa, K. Supramolecular Gels Formed by Amphiphilic Low-Molecular-Weight Gelators of Nα, Nε-Diacyl-L-Lysine Derivatives. *Chemistry-a European Journal,* **2008,** *14* (7), 2133.

270. Yang, M.; Zhang, Z.; Yuan, F.; Wang, W.; Hess, S.; Lienkamp, K.; Lieberwirth, I.; Wegner, G. Self-Assembled Structures in Organogels of Amphiphilic Diblock Codendrimers. *Chemistry-A European Journal,* **2008,** *14* (11), 3330.

271. Chen, L.; Raeburn, J.; Sutton, S.; Spiller, D. G.; Williams, J.; Sharp, J. S.; Griffiths, P. C.; Heenan, R. K.; King, S. M.; Paul, A. Tuneable mechanical properties in low molecular weight gels. *Soft Matter,* **2011,** *7* (20), 9721.

272. Park, S. M.; Shen, Y.; Kim, B. H. Water gelation abilities of alkylbenzyltriazole-appended 2′-deoxyribonucleoside and ribonucleoside. *Organic & biomolecular chemistry,* **2007,** *5* (4), 610.

273. Yang, Y.-h.; Aloysius, H.; Inoyama, D.; Chen, Y.; Hu, L.-q. Enzyme-mediated hydrolytic activation of prodrugs. *Acta Pharmaceutica Sinica B,* **2011,** *1* (3), 143.

274. Singh, Y.; Palombo, M.; Sinko, P. J. Recent trends in targeted anticancer prodrug and conjugate design. *Current medicinal chemistry,* **2008,** *15* (18), 1802.

275. Vacondio, F.; Bassi, M.; Silva, C.; Castelli, R.; Carmi, C.; Scalvini, L.; Lodola, A.; Vivo, V.; Flammini, L.; Barocelli, E. Amino acid derivatives as palmitoylethanolamide prodrugs: synthesis, in vitro metabolism and in vivo plasma profile in rats. *PloS one,* **2015,** *10* (6), e0128699.